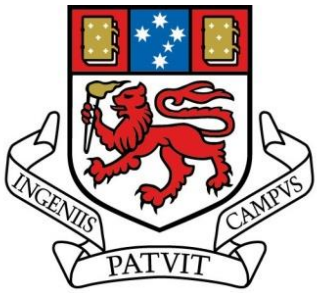

UNIVERSITY
OF TASMANIA

Examination of Catalytically Relevant Palladium *N*-Heterocyclic Carbene Complexes

By

Catriona R. Vanston, BSc(Hons)

A thesis submitted in partial fulfilment of the requirements

for the degree of Doctor of Philosophy at the University of Tasmania

School of Physical Sciences-Chemistry

University of Tasmania

March 2016

Declaration

This thesis contains no material which has been accepted for a degree or diploma by the University or any other institution, except by way of background information and duly acknowledged in the thesis, and to the best of my knowledge and belief no material previously published or written by another person except where due acknowledgement is made in the text of the thesis, nor does the thesis contain any material that infringes copyright.

Catriona R. Vanston

March 2016

Acknowledgements

I would first like to express my great gratitude to my primary supervisor Assoc. Prof. Michael Gardiner for the constant encouragement and guidance throughout this project for the hours of valuable discussions, immense transfer of knowledge and patience. I am also grateful to my co-supervisors Dr. Alison Edwards for her many hours of invaluable instruction and experiments in crystallography and neutron sciences and Dr. David McGuinness for his support and guidance when needed.

Thanks must also be given to Prof. Gordon Kearley and Dr. Nicolas De Souza at the Bragg Institute, Australian Nuclear Science and Technology Organisation (ANSTO) for enlightening me to the world of neutron spectroscopy and computational simulations, and for the many hours of advice, assistance and experimentation provided to further my knowledge and understanding. Thanks must also be given to Dr. Tamim Darwish of the National Deuteration Facility (NDF) for his contributions, and to beamline scientists Dr. Sax Mason and Dr. Anibal Ramirez-Cuesta for their invaluable assistance and expertise at the Institut Laue-Langevin (ILL) and ISIS facilities, respectively. I would also like to thank Dr. Thomas Rodemann and Dr. James Horne for their services in elemental microanalysis and NMR spectroscopy, respectively.

I would like to express immense gratitude to Dr. Adele Wilson for her support throughout my candidature, Dr. Curtis Ho for his constant aid, guidance, and patience with my questions, and the other members of the Gardiner Research Group and Synthesis Supergroup for advice and assistance.

I would like to acknowledge ANSTO, NDF, ILL, the ISIS facility and the Australian Synchrotron for access and beam time *via* the respective merit allocation rounds, and also thank the AMRFP (International Science Linkages Program) and the Austrailian Institute of Nuclear Science and Engineering (AINSE) for travel funding. I would also like to thank AINSE for a 2011 Research Award and a Posgraduate Research Award throughout the duration of my candidature.

Finally I wish to express my immense gratitude to my parents Annette and Myles Vanston and my brother Conor Vanston, and my many friends for their constant, loving support throughout my life and research.

Abstract

Palladium complexes bearing *N*-heterocyclic carbene (NHC) ligands, and their applications in catalysis have remained topical in the literature for the past two decades. Their versatility is due to a vast array of structural modifications possible that afford influences on metal complex geometry and reactivity, and alternative ligand binding modes. These have been extensively developed due to the wide range of catalytic applications for palladium NHC complexes and continue to remain of interest. This thesis describes investigations into several aspects of palladium NHC complexes with potential or known catalytic applications.

The synthesis of the novel bis(NHC) dipalladium(I) hydride complex $[\mu\text{-}\{(MesIm)_2CH_2\}_2Pd_2H][PF_6]$ has been reported. ^{1}H NMR spectroscopic studies and preliminary single crystal X-ray and neutron diffraction studies on a THF solvate of this complex were indicative of possible solid state hydride dynamics. This hypothesis was probed by further variable temperature and low temperature single crystal neutron diffraction experiments, and by incoherent inelastic neutron scattering (IINS) experiments coupled with DFT-MD simulations. The simulations allowed us to approximate the rate of hydride transfer in the solid state. Laue single crystal neutron diffraction was also employed to examine the propylene-linked bis(NHC) complexes $[\mu\text{-}\{(MesIm)_2(CH_2)_3\}_2Pd_2H][PF_6]$ and $[\mu\text{-}\{(MesIm)_2(CH_2)_3\}\{(PdH)(MesIm)_2(CH_2)_3\}_2][PF_6]_2$.

The synthesis of chelated bis(NHC) palladium(II) dihalide complexes has been established to proceed *via* a pendant imidazolium mono(NHC) palladium(II) dihalide acetate intermediate. This intermediate was isolable for the *t*-butyl *N*-substituent and a series of complexes sharing the motif $[\{(tBuIm)(tBuImH)CH_2\}PdX_2CO_2R]$ were

prepared with variations to the ancillary halide ligands and acetate substituent. The hydrogen bonding between the imidazolium C-2 proton and the acetate ligand was examined in solution by ^{1}H NMR spectroscopy and in the solid state by single crystal X-ray and Laue neutron diffraction. The *N*-mesityl pendant imidazolium mono(NHC) palladium(II) trihalide complexes of the motif [{(MesIm)(MesImH)$(CH_2)_n$}PdX_3] were prepared and used to access the mono(NHC) palladium dihalide acetate intermediates of the form [{(MesIm)(MesImH)$(CH_2)_n$}PdX_2CO_2R].

We expanded previous studies on chelated bis(NHC) palladium(II) complexes to include saturated NHC species through the preparation of complexes [{(^{S}MesIm)$_2CH_2$}$PdBr_2$] and [{(^{S}MesIm)$_2CH_2$}$Pd(NCMe)_2$][PF_6]$_2$, and examined the catalytic activity of the latter towards ethylene and carbon monoxide copolymerisation, similar to studies undertaken on the unsaturated analogue. The reactivity towards formation of the dipalladium(I) hydride complex from the dicationic palladium(II) precursor under basic conditions was also examined.

Expansion of these saturated NHC complexes to include extended alkyl linkers was limited by the formation solely of the pendant imidazolinium mono(NHC) palladium(II) tribromide complexes [{(^{S}MesIm)(^{S}MesImH)$(CH_2)_n$}$PdBr_3$] upon reaction of the diimidazolinium salts with palladium acetate. The bis(NHC) disilver(I) complexes [{(^{S}MesIm)$_2(CH_2)_n$}$_2Ag_2$][PF_6]$_2$ bearing methylene and propylene-linked imidazoline ligands were prepared, though transmetallation *via* PdBrMe(COD) to form reactive palladium(II) complexes for catalysis was not successful.

There has been growing interest in the study of abnormal or remote NHC ligands (aNHCs and rNHCs, respectively) due to their apparent increase in σ-donor strength

and reported improvement in catalytic activity *cf.* their normal NHC (nNHC) counterparts. We prepared an aNHC ligand precursor containing a 5-(4-pyridinium) substituent which, if aligned coplanar to the NHC ring, could allow conjugation through the biaryl C-C bond, and show varying contributions from aNHC and "partially normalised" NHC resonance forms. The complexes of the motif [{1,2,3-trimethyl-5-(*N*-methylpyridinium)Im}PdL_n][PF_6]$_y$ were prepared by oxidative addition of the 4-brominated ligand precursor to palladium(0) and structurally characterised by X-ray crystallography. The degree of contribution from the desired resonance form was probed by examination of key C-C bond lengths and by the angle between the NHC and pyridinium ring planes.

Table of Contents

Abbreviations

^{1}H	hydrogen-1
^{2}H	hydrogen-2, deuterium
Å	Ångström
aNHC	abnormal *N*-heterocyclic carbene
ANSTO	Australian Nuclear Science and Technology Organisation
Ar	Aryl
aq	aqueous
bd	broad doublet (NMR)
bipy	2,2′-bipyridine
bs	broad singlet (NMR)
CD_3OD	deuterated methanol
$CDCl_3$	deuterated chloroform
COD	1,5-cyclooctadiene
d	doublet (NMR)
DCM	dichloromethane
DFT	density functional theory
dipp	2,6-diisopropylphenyl
DMSO	dimethyl sulfoxide

DMSO-d_6	deuterated dimethyl sulfoxide
fs	femto second, 10^{-15} s
ILL	Institut Laue-Langevin
INS	inelastic neutron scattering
ISIS	neutron scattering facility, Chilcot, England.
L	ligand
m-	meta
m	multiplet (NMR)
M	metal
meV	milli electron volt
MD	molecular dynamics
Me	methyl
Mes	mesityl; 2,4,6-trimethylphenyl
NCA	normal coordinate analysis
NHC	*N*-heterocyclic carbene
NMR	nuclear magnetic resonance
nNHC	normal *N*-heterocyclic carbene
o-	ortho
p-	para

Ph	phenyl
ppm	parts per million
ps	picoseconds, 10^{-12} s
QENS	quasi-elastic neutron scattering
R	alkyl, aryl
rNHC	remote *N*-heterocyclic carbene
s	singlet (NMR)
t-Bu	tertiary butyl
THF	tetrahydrofuran
THF-d_8	deuterated tetrahydrofuran
TOSCA	time of flight neutron spectroscopy instrument
UV	ultra-violet
VT	variable temperature

Chapter 1: Introduction

1.1 *N*-Heterocyclic Carbenes

Carbenes are defined as neutral compounds containing a divalent carbon atom with a six-electron valence shell.[1] The first free carbene was isolated in 1988 by Bertrand *et al.* which utilised interactions with adjacent phosphorous and silicon atoms to stabilise the inherently unstable carbene.[2] In 1991 Arduengo *et al.* reported the first isolable carbene stabilised by adjacent nitrogen atoms contained in an aromatic heterocycle.[3] Referred to as *N*-heterocyclic carbenes (NHCs), this family of compounds have a wide range of uses in areas such as medicinal chemistry, physical and surface chemistry and, most commonly, catalysis.[4-9]

Carbenes can have either singlet or triplet ground states. In the former case the non-bonding electrons are paired in bent systems and both occupy the same sp^2-orbital, leaving an empty *p*-orbital, which aids stabilisation. In the latter case the non-bonding electrons are unpaired and adopt a diradical structure, which is inherently less stable than the ground state singlet carbene arrangement (Figure 1.1).

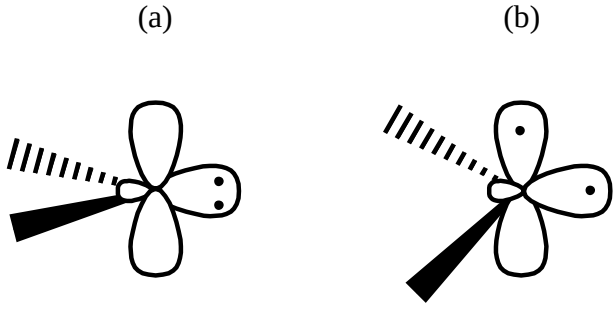

Figure 1.1. (a) Singlet and (b) triplet state carbene orbitals for bent geometries.

NHCs generally display singlet ground state electron configuration.[7] Electronic stabilisation is provided by the adjacent heteroatoms which have both σ-electron withdrawing and π-electron donating properties. The former inductively lowers the energy of the σ-orbital while the latter donation into the vacant *p*-orbital increases the mesomeric effect of the system (Figure 1.2). This results in the widening of the σ-p_π energy gap, which helps maintain the preferred sp^2 hybridised geometry for the singlet carbene.

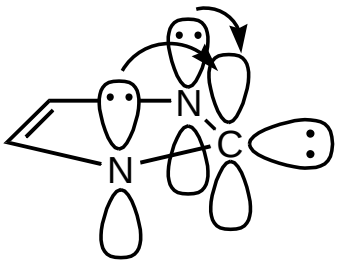

Figure 1.2. Carbene stabilisation *via* electron donation from flanking heteroatoms.

NHCs cover a broad spectrum of species, with variation of the number, type and positioning of the heteroatom(s), ring size and aromaticity, and ring and *N*-substitution, some examples of which are shown in Figure 1.3.

As well as impacting somewhat on the electronic stabilisation of the carbene the *N*-substituents play a significant role in the steric effects of the NHC, while alterations to the backbone of the NHC such as substitution or saturation, as well as varied heteroatoms can have a significant effect on the electronic properties.

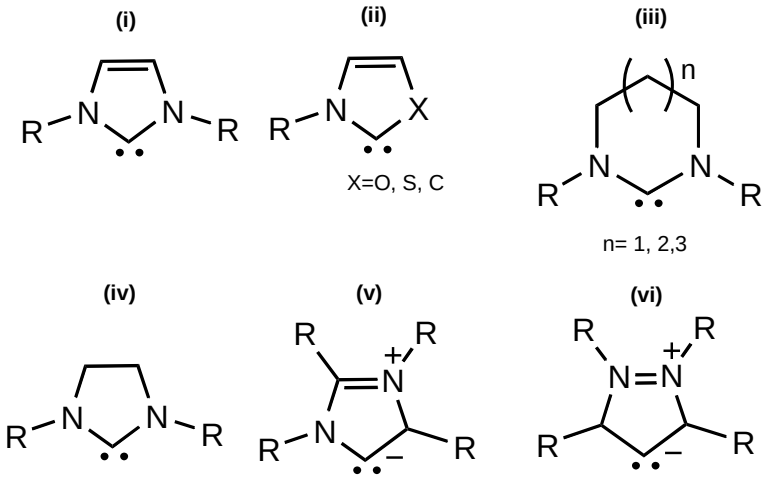

Figure 1.3. General motifs of some NHC classes.

The first reported free NHC by Aruengo *et al.* was a symmetrically substituted imidazol-2-ylidine type NHC (**i**) which used bulky adamantyl *N*-substituents to further stablilise the carbene kinetically.[3]

NHCs containing alternative heteroatoms (**ii**) such as thiazolylidines or oxazolylidines are accessible and can provide useful alternative binding modes through the non-nitrogen heteroatom. The varied heteroatoms also offer expanded potential for biological applications. NHCs containing a single heteroatom have also been reported.[10,11]

NHCs containing 6, 7 and 8 atom rings have been reported (**iii**). It has been noted that the increased ring size can have significant effects on the electronic and steric stability of the NHC. [12,13]

Saturated NHCs (**iv**) lack the added stability of aromaticity that most other NHC classes have.[1] However the increased electron density in the vicinity of the carbene results in greater sigma donating properties of these ligands in comparison to their unsaturated analogues[14] making them useful in a range of applications.[11,15]

Recently there has been a lot of interest in abnormal NHCs (**v**) and remote NHCs (**vi**), denoted aNHCs and rNHCs herein, respectively. These compounds are called such as the carbene site is generally not adjacent to both heteroatoms and the ring system often requires the assignment of formal charge.[16] All aNHCs and some rNHCs have no neutral resonance form. This enhances the carbanionic character of the carbene site, resulting in greater σ-donating power compared to normal NHC analogues.[16]

1.2 **Metal Complexes of NHCs**

NHCs have found use in a wide range of applications including organocatalysis[17] and medicinal chemistry[4], though the most explored field is as ligands in organometallic complexes. The majority of NHC complexes involve coordination to transition metals, though there are also examples of main-group and *f*-block NHC complexes.[1]

NHCs are often compared to phosphine ligands as they share similar activity and purpose.[5] However NHCs provide some benefits in the form of generally greater σ-donating and π-accepting properties, resulting in stronger M-L bonds and therefore more stable complexes, as well as greater range of structure activity relationships due to the ligand *N*-substituents being directed more towards the metal centre. They also allow separate tuning of the steric and electronic properties of the ligand by modification of the *N*-substituents and backbone of the NHC, respectively.

Several methods are used to describe and compare the steric and electronic properties of NHCs. Buried volume (%V_{bur}) is often used as a measure to quantify the steric properties of a range of ligands, including NHCs. Developed by Cavallo and Nolan the value of %V_{bur} refers to the area of a sphere centred on the metal

coordinated to the ligand covered or 'buried' by the ligand (Figure 1.4).[11] Generally a radius (r) of 3.5 Å and a distance (d) of 2 Å is used to ensure valid comparison between various ligands.

Nolan and Clavier provide an extensive collection of $\%V_{bur}$ values for a range of coinage metal NHC complexes.[18] They observe that while this is a useful method in understanding how the steric bulk of the ligand can affect reactivity (and therefore activity of the metal complexes they form) it does require a consistent method of calculation to be used to obtain good comparison between NHCs. It also may not provide an accurate measure for flexible ligands whose conformation is subject to change.

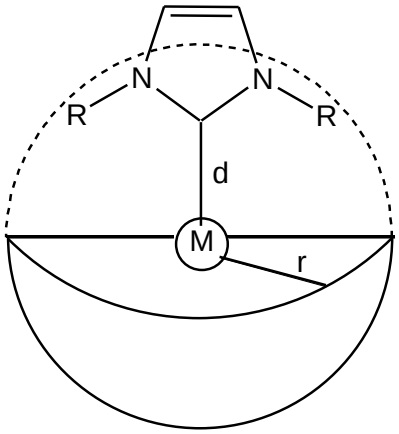

Figure 1.4. $\%V_{bur}$ representation for NHC steric bulk measurements.

The electronic properties of NHCs as well as some other ligands are most commonly described by the Tolman electronic parameter (TEP). The electron donating effect of the ligand is directly measured by the IR stretching frequency of a trans carbonyl ligand coordinated to a suitable metal. Comparison to some 'standard' complexes allows for the measure of the electron donating effect to be determined based on the frequency shift of the IR band for CO.

However the TEP method is lacking in several ways: Firstly it requires the ability to produce a suitable metal complex containing a CO ligand *trans* to the NHC. Secondly the solvent of measurement can greatly affect the experimentally determined IR stretch values, which for NHCs are generally only within a narrow range (~ 10 cm^{-1} variance). Lastly, the TEP is a good measure of the π-donating ability of the metal centre, but does not necessarily take into account the entire electron density at the metal centre.[14] As such, ligands which differ in the nature of their M-L bonding might be misrepresented. This is important when comparing the electronic properties of 'normal' NHCs with saturated NHCs or aNHCs, for example. In a recent review Nolan and Nelson collate an extensive range of NHCs with their respective observed υ_{CO} and TEP values.[14]

Another method of quantifying the nature of the M-L bonding is the shift of the carbene carbon resonance in NMR spectroscopy. The frequency shifts measured by ^{13}C NMR (or ^{31}P NMR in the case of phosphine ligands) can be compared with the free ligand precursor or with other analogous complexes, where an increase in electron density at the metal centre is indicated by a subsequent downfield shift of the coordinated carbene ^{13}C NMR signal.

In a similar manner, X-ray crystallography can prove a useful tool for considering the strength of the M-L interaction by comparing the bond length to similar examples. The *trans* influence of NHCs can also be interpreted somewhat by the lengthening or shortening of the bond between the metal and the relevant other ligand.[19] This is especially useful when a series of analogues are considered, or when the *trans* ligand is common to a range of literature examples.

NHCs are most commonly used as monodentate ligands, with a wide range of applications in both homogeneous and heterogeneous catalysis as well as medicinal chemistry. Transition metal-NHC catalysts have received much recognition in the last decade, with part of the 2005 Nobel Prize being awarded to Grubbs for ruthenium NHCs in the development of metathesis methods.[20] The 2010 Nobel Prize was shared by Heck, Suzuki and Negishi for their work on palladium catalysed C-C cross-coupling reactions in organic synthesis, many examples of which use palladium-NHC complexes.[21]

As mentioned above a good example of NHCs in catalysis is Grubbs' catalysts for olefin metathesis, which have gone through several generations of development.[22] The first generation Grubbs' catalyst was reported in 1995 (Figure 1.5).[23] The second generation catalyst (1999) replaced one of the phosphine ligands with a saturated NHC, which showed greater catalytic activity as well as increased thermal stability and reduced catalyst degradation.[24] Other generations of these catalysts have followed with modifications to the *N*-substituents and various substitutions of the NHC backbone in order to optimise the system.

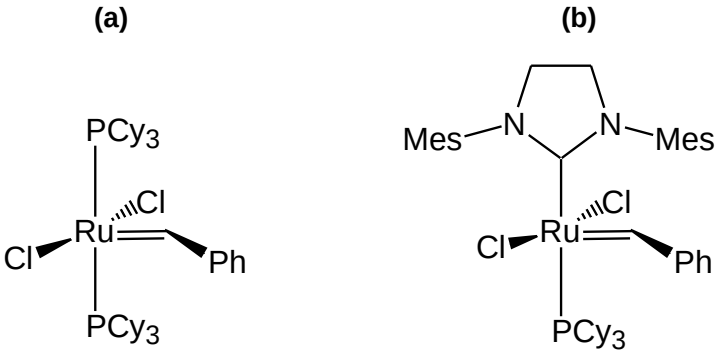

Figure 1.5. Examples of Grubbs' catalyst for olefin metathesis; (a) first generation[23] and (b) second generation[24].

Other metal-NHC complexes introduce supports which allow the tethering of the catalyst to a polymer or silica surface. These heterogeneous systems allow for easier recycling of catalysts and reduced decomposition, though it does require additional synthesis steps to create these tethers and can limit the steric bulk of the system used.[5]

Figure 1.6 shows two examples of heterogeneous catalysts tethered to solid surfaces using one of the *N*-substituents as a linker unit. Lee *et al.* reported a palladium-NHC catalyst tethered to a polystyrene support (Figure 1.6(a)).[25] This species showed good activity for various Suzuki coupling reactions. They indicate that the polymer support aids in catalyst recyclability for multiple uses.

Thieulex and co-workers reported a silica tethered iridium-NHC species designed to line a tubular structure which showed some C-H bond activating properties useful for H/D exchange (Figure 1.6(b)).[26]

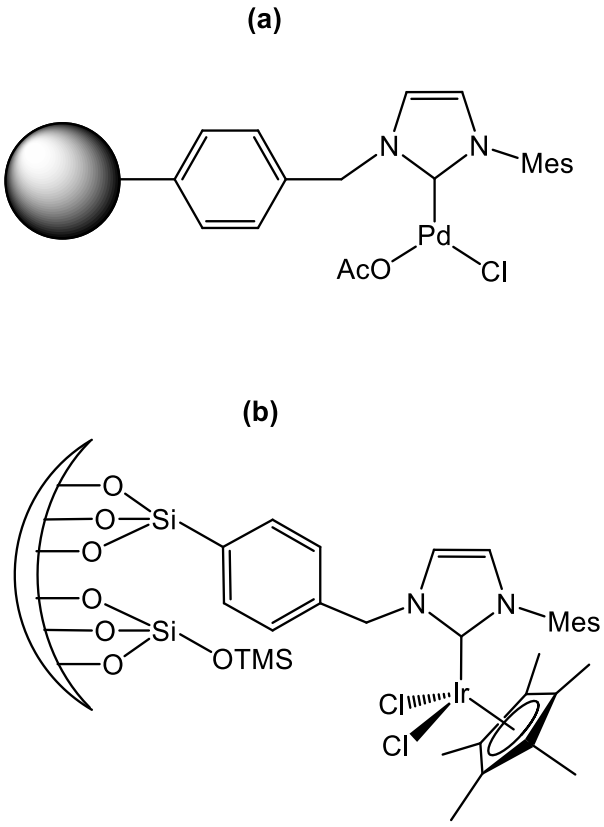

Figure 1.6. Examples of supported transition metal-NHC complexes used in catalysis.[25,26]

As mentioned previously, there is also some use of metal-NHC complexes in the field of medicinal chemistry. Roland and Jolivalt *et al.* reported on a series of silver NHC complexes (such as complex (a) in Figure 1.7) which showed significant activity against antibiotic resistant strains of both *E. Coli* and *S. Aureus*.[27]

Complex (b) in Figure 1.7 is an example of a series of platinum NHC complexes reported by Mailliet and Marinetti *et al.* based on the well-known anti-cancer drug cisplatin.[28] They report that these NHC complexes provide a new avenue to explore in reducing the toxicity and increasing the effectiveness and direct targeting properties of such drugs. Specific mention is given to the useful variety in

substitution of NHCs as a scaffold to build upon for modular design changes to target specific sites.

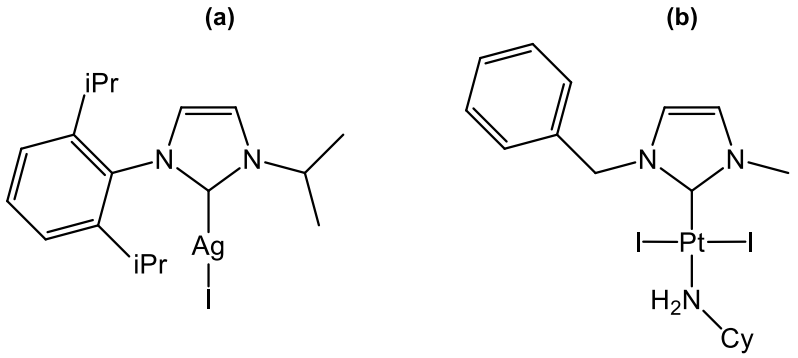

Figure 1.7. Examples of metal-NHC complexes used in medicinal chemistry.[27,28]

Bidentate NHCs are an important subclass of NHCs. Complexes of these ligands benefit from the increased rigidity of the chelating ligand to help maintain a suitable coordination geometry for specific catalytic processes as well as reduced complex degradation from M-C bond cleavage. Figure 1.8 shows some examples of bidentate NHCs used for (a) C-C bond formation from alcohols[29], (b) transfer hydrogenation,[30] and (c) carbon monoxide-ethylene copolymerisation.[31]

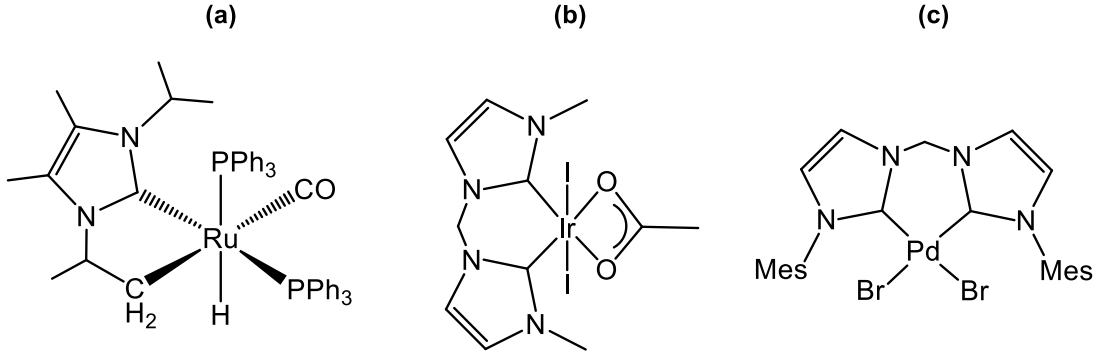

Figure 1.8. Various bidentate NHC catalysts/precatalysts.[29-31]

Recently the potential of abnormal NHC complexes has been explored for catalytic applications. The greater σ-donating power of aNHCs has been observed to result in enhanced catalytic activity when directly compared to their nNHC analogues (Figure 1.9).[32] However it was also observed that the Pd-C bonds in the aNHC metal complexes were more prone to cleavage under conditions where the nNHC analogue remained stable. An in-depth discussion of this interesting class of NHCs is provided in Chapter 5.

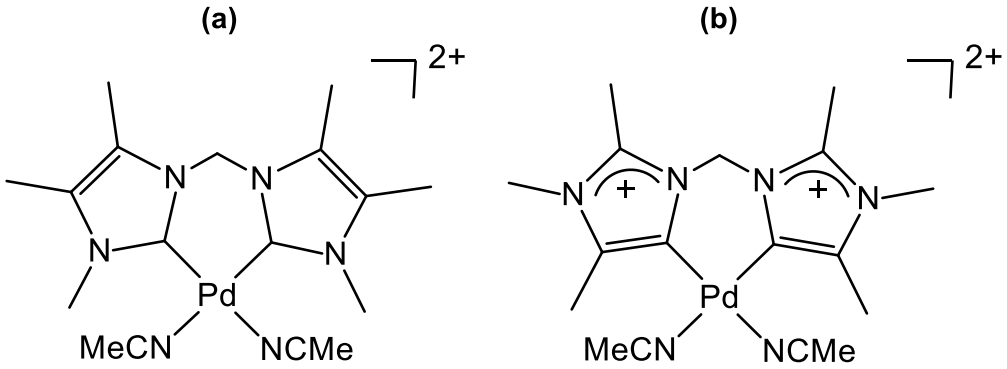

Figure 1.9. Dicationic nNHC and aNHC palladium complexes bearing identical steric bulk for studies in catalytic activity.[32]

Many of the catalytic applications for which transition metal NHC complexes are used invoke metal hydride intermediates. However due to the frequent instability of such intermediates, these species are rarely isolated, and there have been few in-depth studies to provide full structural characterisation of these important complexes. This is in part due to the limitations of X-ray crystallography in determining hydride locations, especially in systems where multiple hydrides are present.

1.3 Neutron Scattering Techniques for the Examination of Hydrides

Neutron techniques have been used to probe structural and dynamic properties of compounds since the 1950s.[33] Often these techniques are used to study hydrogen-containing materials due to the uniquely high incoherent scattering cross section of the ^{1}H isotope.[34] However these techniques are not widely available and the added expense results in them being used only when other more common analysis and characterisation methods have failed to provide the necessary information.

Neutron sources are either reactor based or non-reactor based, such as spallation.[35] Reactor sources provide both thermal and cold neutrons in a constant flow, and are termed 'steady state' sources.[36] Spallation sources use a particle accelerator to collide a proton beam with a heavy metal source to produce a short burst of hot neutrons. These neutron pulses are moderated by materials containing large amounts of hydrogen, such as water or hydrocarbons, and provide hot, thermal, and cold neutrons depending upon the temperature of the moderator.[36]

Neutron scattering techniques target the interactions between the neutron beam and the nuclei of atoms in the molecule, unlike photon-based techniques which interact with the electron density surrounding each atom.[37] Broadly, there are two types of scattering: elastic scattering, in which a neutron is scattered with no loss of energy, and inelastic scattering, where there is some energy exchange between the sample and the scattered neutron.

The latter of these interactions can further be considered in terms of the grouping of inelastic and quasielastic scattering. Inelastic neutron scattering (INS) arises from

molecular motions of an oscillatory nature such as vibrations, while quasi-elastic neutron scattering (QENS) occurs as a result of diffusive processes. These can be considered in terms of a function of P and t, where P is the probability of a given atom being in a particular spatial location, and t is time. Thus a diffusive process typically results in an exponentially decreasing function as the atom moves continually away from its initial location. In contrast, molecular vibrations involve atoms moving away from and then returning to their initial spatial location, appearing as an oscillatory process as the probability first decreases and then increases as the atom returns.

There is also the effect of incoherent and coherent scattering of the neutrons, where the neutrons are considered as plane waves. Coherent scattering occurs when the molecular array of the target contains only particles in a regular array. In the case of elastic scattering this results in each lattice point producing identical spherical waves upon interaction with neutrons. These form patterns of constructive and destructive interference known as nodal lines, which create diffraction patterns. In the case of inelastic scattering, each identical lattice point can be considered to identically scatter portions of the neutron energy, resulting in simultaneous motions.[37]

Incoherent scattering is a result of interactions with non-identical lattice points. This includes disordered crystalline structures and materials where the natural abundance of isotopes are present, as two isotopes can have very different scattering cross sections.[34] In this case, the plane wave is scattered spherically, but differently by each lattice point, with no interference pattern produced. This allows the dynamics local to the irregularity to be measured by spectroscopic methods.[38]

Compounds produce a combination of coherent and incoherent scattering.[39] Atomic scattering cross sections are the sum of the coherent and incoherent scattering cross sections for each atomic species. These can be vastly different between similar elements and isotopes of an element, with no specific correlation with atomic size or number. For example, ^{1}H has an incoherent scattering cross section of 80 barn and coherent scattering cross section of 2 barn, with an overall scattering cross section of 82 barn, while ^{2}H has an incoherent, coherent and overall scattering cross section of 2, 6 and 8 barn respectivly. In comparison, ^{12}C and ^{14}N have overall scattering cross sections of 6 and 11 barn, respectively.[34]

1.4 **Neutron Diffraction**

Neutron diffraction relies on coherent elastic neutron scattering to produce diffraction from crystalline materials.[40] Diffraction instruments with reactor based sources can be either Laue (white beam) diffractometers which use a band of wavelengths, or monochromated diffractometers, which select a narrow band centred upon a particular chosen wavelength.[36] The wavelength distribution from a constant flow (reactor) neutron source appears as a Boltzmann distribution such as that in Figure 1.10. The neutron flux which interacts with the sample can be calculated by integrating the region under the Boltzmann distribution between the minimum and maximum wavelengths incident on the sample.

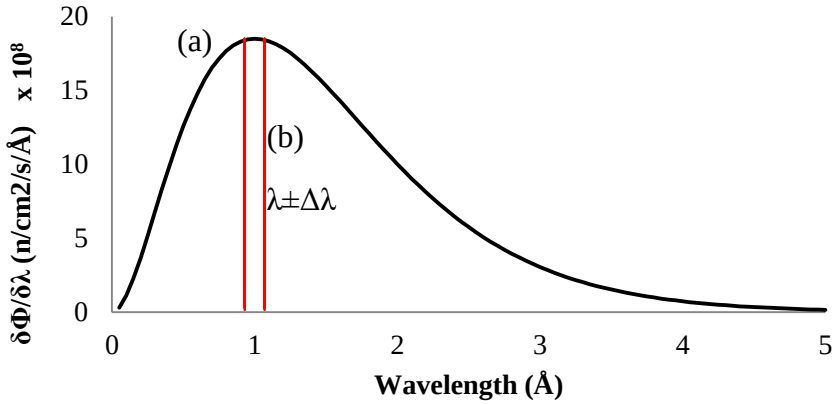

Figure 1.10. Boltzmann distribution of the wavelength range used for (a) Laue and (b) monochromated neutron diffraction experiments.

Laue diffraction exploits the vastly enhanced neutron flux incident on the sample compared with monochromatic methods, though the technique is of reduced precision compared to monochromatic methods. A consequential limitation of Laue diffraction is the smaller unit cell sizes that are amenable to study owing to the non-monochromatic source, which physically limits detection resolution. However, the crystal volume required for monochromated instruments is orders of magnitude greater than for Laue instruments due to comparatively lower flux.[36] Thus Laue neutron diffraction provides a crystallographic technique applicable to crystalline compounds as small as 0.1 mm^3 and unit cell lengths up to *ca.* 42 Å and cell volumes up to *ca.* 15000 $Å^3$,[41,42] and this is a major advantage.

1.5 **Inelastic Neutron Scattering (INS)**

Inelastic neutron scattering, or neutron spectroscopy, probes the dynamics of a system using incoherent elastic and incoherent inelastic scattering. Experimental spectra are recorded in the frequency domain, where the exponential diffusive function in time appears as a single Lorentzian peak at a low frequency (elastic line).

The oscillatory functions produce a series of peaks based upon the particular properties of each oscillation from inelastic interactions (Figure 1.11).

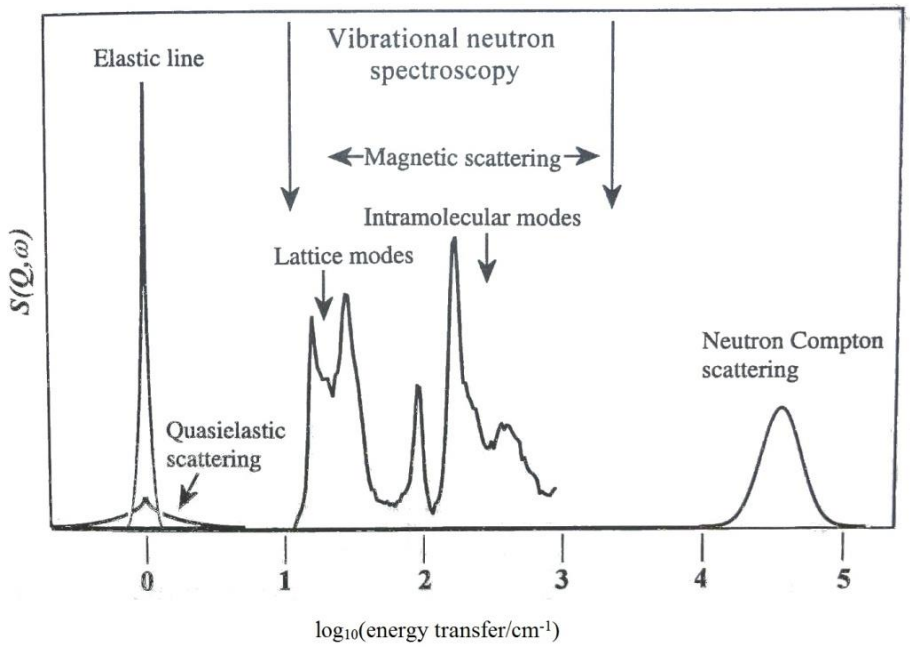

Figure 1.11. Frequency regions for each scattering process. Reproduced from Vibrational Spectroscopy with Neutrons (2005).[43]

Neutron spectroscopy can be considered analogous to other types of vibrational spectroscopy such as IR and Raman spectroscopy. However, neutron spectroscopy has several key advantages for the study of hydrides: Firstly, neutron spectroscopy is not limited by selection rules which prevent certain vibrations from being active in photon-based methods.[37] Therefore all vibrations corresponding to all motions undertaken by the molecule will appear in the spectrum. As detection of ^{1}H by neutron techniques is vastly enhanced compared to other elements, the additional vibrations involving only non-hydrogen atoms contribute relatively less to the overall signal and this allows a clear view of the entire dynamics of the hydrogen atoms present.[44] This almost constitutes a "hydrogen selection rule".

Another key advantage of neutron spectroscopy is the ability to measure the very low energy (low frequency) region which is often inaccessible by photon-based techniques. Some instruments are capable of measuring vibrations occurring at fractions of a wavenumber, with most instruments at least able to reach as low as 20 cm^{-1}.[37] This provides a method of studying diffusive processes, which are generally seen below 50 cm^{-1}.

Finally, specific hydrogen atoms in a substance can be targeted with this technique by selective deuteration of the molecule. The incoherent scattering cross section of deuterium is approximately 2.5% of that for hydrogen,[34] reducing the contributions of any bands involving D-labelled atoms to the overall spectrum.

Experimental spectra are most easily analysed by performing computational simulations. These allow calculated spectra to be produced, which can be compared with the experimental spectra. This allows each fundamental normal vibrational mode to be traced back to the specific molecular motion that gives rise to the signal. From this we can infer the possible mechanism by which fluxional processes occur.

1.6 **Project Scope**

It is evident from the above discussions that the field of NHC metal complexes has been diversely studied, especially in relation to catalytic applications. Furthermore it is evident that neutron diffraction and neutron spectroscopy are useful tools to examine the metal hydride species which are necessary intermediates or interesting byproducts in many catalytically relevant reactions.

The scope of this project is to probe several gaps in these fields:

1. The examination of a previously reported dipalladium(I) hydride species produced under catalytically relevant conditions using neutron techniques to probe for solid state hydride dynamics. We will also expand our study to an extended linker analogue of this complex which was recently synthesised in our group. Preliminary analysis of this complex has been previously reported and we will provide more complete structural analysis.
2. The preparation and examination of a series of NHC palladium(II) dihalide acetate reaction intermediates as precursors to a range of bis(NHC) palladium(II) catalysts. These intermediates involve hydrogen bonding in the formation of the chelate ring which we will probe in solution by NMR spectroscopy and in the solid state by neutron diffraction.
3. The preparation of saturated bis(NHC) palladium(II) complexes, the unsaturated analogues of which have been previously examined for catalysis. The reactivity of the saturated palladium(II) complex under basic conditions towards the synthesis of a dipalladium(I) hydride will also be explored.
4. The preparation of a series of unusual aNHC metal complexes in which the ligand may fall outside of the conventional definitions of aNHC and nNHC.

1.7 References

[1] Hopkinson, M. N.; Richter, C.; Schedler, M.; Glorius, F. *Nature* **2014**, *510*, 485.

[2] Igau, A.; Grutzmacher, H.; Baceiredo, A.; Bertrand, G. *J. Am. Chem. Soc.* **1988**, *110*, 6463.

[3] Arduengo, A. J.; Harlow, R. L.; Kline, M. *J. Am. Chem. Soc.* **1991**, *113*, 361.

[4] Oehninger, L.; Rubbiani, R.; Ott, I. *Dalton Trans.* **2013**, *42*, 3269.

[5] Ranganath, K. V. S.; Onitsuka, S.; Kumar, A. K.; Inanaga, J. *Catal. Sci. Tech.* **2013**, *3*, 2161.

[6] Gaillard, S.; Renaud, J. L. *Dalton Trans.* **2013**, *42*, 7255.

[7] Fevre, M.; Pinaud, J.; Gnanou, Y.; Vignolle, J.; Taton, D. *Chem. Soc. Rev.* **2013**, *42*, 2142.

[8] Champness, N. R. *Dalton Trans.* **2011**, *40*, 10311.

[9] Fortman, G. C.; Nolan, S. P. *Chem. Soc. Rev.* **2011**, *40*, 5151.

[10] Lavallo, V.; Canac, Y.; Prasang, C.; Donnadieu, B.; Bertrand, G. *Angew. Chem. Int. Ed.* **2005**, *44*, 5705.

[11] Hillier, A. C.; Sommer, W. J.; Yong, B. S.; Petersen, J. L.; Cavallo, L.; Nolan, S. P. *Organometallics* **2003**, *22*, 4322.

[12] Iglesias, M.; Beetstra, D. J.; Knight, J. C.; Ooi, L.-L.; Stasch, A.; Coles, S.; Male, L.; Hursthouse, M. B.; Cavell, K. J.; Dervisi, A.; Fallis, I. A. *Organometallics* **2008**, *27*, 3279.

[13] Lu, W. Y.; Cavell, K. J.; Wixey, J. S.; Kariuki, B. *Organometallics* **2011**, *30*, 5649.

[14] Nelson, D. J.; Nolan, S. P. *Chem. Soc. Rev.* **2013**, *42*, 6723.

[15] Arnold, P. L.; Casely, I. J.; Turner, Z. R.; Bellabarba, R.; Tooze, R. B. *Dalton Trans.* **2009**, 7236.

[16] Crabtree, R. H. *Coord. Chem. Rev.* **2013**, *257*, 755.

[17] Flanigan, D. M.; Romanov-Michailidis, F.; White, N. A.; Rovis, T. *Chem. Rev.* **2015**, *115*, 9307.

[18] Clavier, H.; Nolan, S. P. *Chem. Commun.* **2010**, *46*, 841.

[19] Pinter, B.; Van Speybroeck, V.; Waroquier, M.; Geerlings, P.; De Proft, F. *Phys. Chem. Chem. Phys.* **2013**, *15*, 17354.

[20] Casey, C. P. *J. Chem. Educ.* **2006**, *83*, 192.

[21] Colacot, T. J. *Platin. Met. Rev.* **2011**, *55*, 84.

[22] Vougioukalakis, G. C.; Grubbs, R. H. *Chem. Rev.* **2010**, *110*, 1746.

[23] Schwab, P.; France, M. B.; Ziller, J. W.; Grubbs, R. H. *Angew. Chem. Int. Ed.* **1995**, *34*, 2039.

[24] Scholl, M.; Ding, S.; Lee, C. W.; Grubbs, R. H. *Org. Lett.* **1999**, *1*, 953.

[25] Lee, D. H.; Kim, J. H.; Jun, B. H.; Kang, H.; Park, J.; Lee, Y. S. *Org. Lett.* **2008**, *10*, 1609.

[26] Maishal, T. K.; Alauzun, J.; Basset, J. M.; Coperet, C.; Corriu, R. J.; Jeanneau, E.; Mehdi, A.; Reye, C.; Veyre, L.; Thieuleux, C. *Angew. Chem. Int. Ed.* **2008**, *47*, 8654.

[27] Roland, S.; Jolivalt, C.; Cresteil, T.; Eloy, L.; Bouhours, P.; Hequet, A.; Mansuy, V.; Vanucci, C.; Paris, J.-M. *Chem. Eur. J.* **2011**, *17*, 1442.

[28] Skander, M.; Retailleau, P.; Bourrie, B.; Schio, L.; Mailliet, P.; Marinetti, A. *J. Med. Chem.* **2010**, *53*,

[29] Burling, S.; Paine, B. M.; Nama, D.; Brown, V. S.; Mahon, M. F.; Prior, T. J.; Pregosin, P. S.; Whittlesey, M. K.; Williams, J. M. J. *J. Am. Chem. Soc* **2007**, *129*, 1987.

[30] Albrecht, M.; Miecznikowski, J. R.; Samuel, A.; Faller, J. W.; Crabtree, R. H. *Organometallics* **2002**, *21*, 3596.

[31] Gardiner, M. G.; Herrmann, W. A.; Reisinger, C.-P.; Schwarz, J.; Spiegler, M. *J. Organomet. Chem.* **1999**, *572*, 239.

[32] Heckenroth, M.; Neels, A.; Garnier, M. G.; Aebi, P.; Ehlers, A. W.; Albrecht, M. *Chem. Eur. J.* **2009**, *15*, 9375.

[33] Levi, B. G. *Physics Today* **1994**, *42*, 17.

[34] http://www.ncnr.nist.gov/resources/n-lengths/, accessed October 20, **2011**.

[35] Ullmaier, H.; Carsughi, F. *Nucl. Instr. Meth. Phys. Res.* **1995**, *101*, 406.

[36] Wilson, C. C. *Z. Kristallogr.* **2005**, *220*, 385.

[37] Mitchell, P. C. H.; Parker, S. F.; Ramirez-Cuesta, A. J.; Tomkinson, J., in *Vibrational Spectroscopy with Neutrons With Applications in Chemistry, Biology, Materials Science and Catalysis*, *Vol. 3*, World Scientific Publishing Co. Pte. Ltd., Singapore, **2005**, pp. 1-10.

[38] Suzuki, K., Neutron scattering in Price, D. L.; Sköld, K. (Ed), *Methods of Experimental Physics*, *Vol. 23*, Academic Press, San Diego, **1987**.

[39] Quasielastic Neutron Scattering: Principles and Applications in Solid State Chemistry, Biology and Materials Science in Bee, M. (Ed), *Vol.* IOP Publishing Ltd, Bristol, **1988**.

[40] Wilson, C. C., in *Single Crystal Neutron Diffraction from Molecular Materials*, *Vol.* World Scientific Publishing, Singapore, **2000**, pp. 32-34.

[41] Edwards, A. J. *Aust. J. Chem* **2011**, *64*, 869.

[42] Edwards, A. J., Personal Communication, February 16, 2016.

[43] Mitchell, P. C. H.; Parker, S. F.; Ramirez-Cuesta, A. J.; Tomkinson, J., in *Vibrational Spectroscopy with Neutrons With Applications in Chemistry, Biology, Materials Science and Catalysis*, *Vol. 3*, World Scientific Publishing Co. Pte. Ltd., Singapore, **2005**, pp. 5.

[44] Parker, S. F.; Williams, K. P. J.; Smith, T.; Bortz, M.; Berthevillec, B.; Yvon, K. *Phys. Chem. Chem. Phys.* **2002**, *4*, 1732.

Chapter 2: Examination of Catalytically Relevant Palladium(I) Hydride Complexes

2.1 Introduction

Transition metal hydride complexes are used or invoked as intermediates in a wide range of roles in catalysis, molecular hydrogen activation and storage. Complexes range from mononuclear species with single hydride ligands to large catalyst clusters or surfaces designed for hydrogen capture.[1-9] As well as providing an alternative to traditional catalytic cycles based on mononuclear complexes, some clusters are known to act as reservoirs for active mononuclear species.[10]

One important aspect of metal hydride chemistry is the ability of hydride ligands to undergo fluxional processes while remaining coordinated to the metal centre, a property that is useful to some catalyst activity and selectivity. Catalysts of this type may range from long established systems such as Wilkinson's catalyst for alkene hydrogenation[11] to multinuclear clusters with known or potential use for the catalytic hydrogen transfer reactions.[12,13]

Palladium hydride complexes in particular are often invoked as key participants in a range of catalytic processes. One example of this is the Mizoroki-Heck reaction which was first described in 1971 for the coupling of aryl halides to alkenes using a palladium catalyst.[14,15] The β-hydride elimination step to release the coupled product requires the formation of a palladium hydride species, which is then involved in reductive elimination to restore the palladium(0) catalyst (Scheme 2.1).

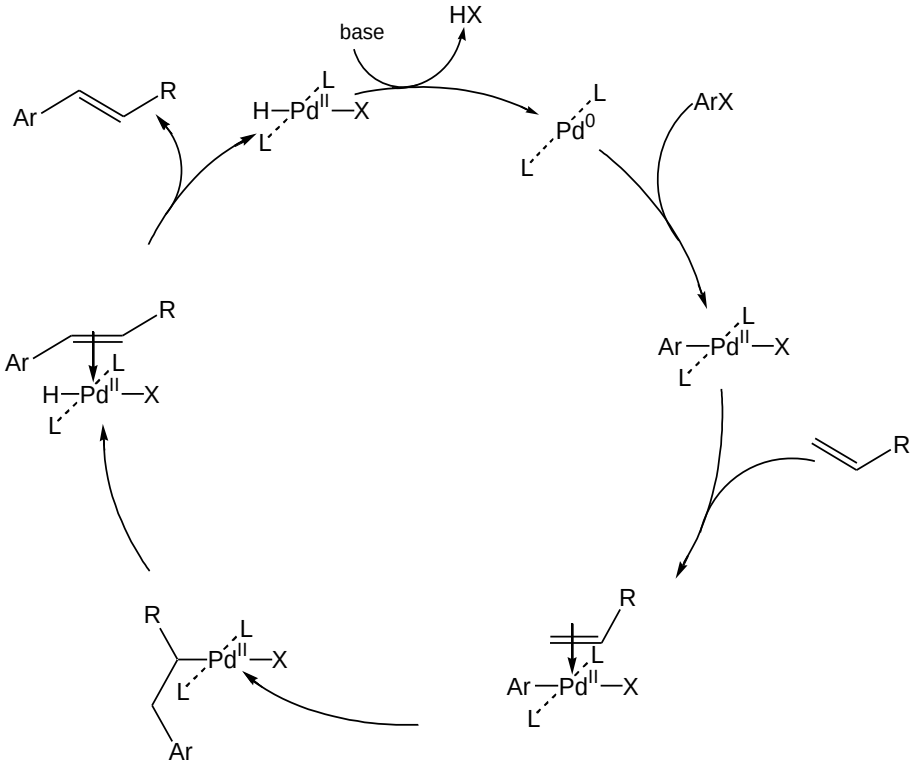

Scheme 2.1. Generalised catalytic cycle for the Mizoroki-Heck reaction.

The deliberate synthesis of palladium hydride species can be achieved through a range of conditions such as reaction with a strong reducing agent, oxidative addition of acids, as well as the aforementioned β-hydride elimination.[16] It is interesting to note that while a number of stable platinum hydride species are reported in the literature, their palladium analogues are rarely seen, or found to be highly unstable hence often unisolable.[16]

Brooks and Glockling reported the first isolated palladium hydride species in 1965 (Figure 2.1(a)),[17,18] which was structurally characterised in 1973 by Shearer.[19] Single crystal X-ray crystallographic analysis confirmed that the complex displayed square planar geometry with a T-shaped arrangement of ligands, with the remaining site presumed to be occupied by the hydride ligand. The presence of the palladium-bound hydride ligand was confirmed by ^{1}H NMR and IR spectroscopy.

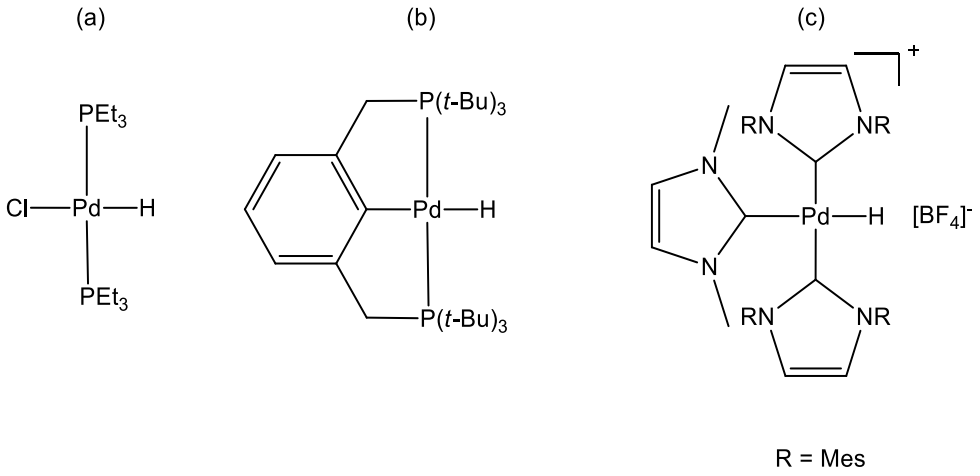

Figure 2.1. Examples of mononuclear palladium hydride species reported by Brooks (a)[17], Shaw (b)[20] and Cavell (c).[21]

Shaw reported the preparation of a range of transition metal-hydrides stabilised by a bulky PCP pincer ligand.[20] The palladium hydride species was formed by reaction of the palladium halide precursor with sodium borohydride, with initial structural characterisation by ^{1}H NMR spectroscopy and IR spectroscopy (Figure 2.1(b)). Confirmation of the molecular structure by X-ray crystallography was obtained by Wendt and co-workers in 2007.[22]

Cavell reported a tris(NHC) palladium hydride complex formed through the oxidative addition of an imidazolium C-H moiety to a bis(NHC) palladium(0) complex (Figure 2.1(c)).[21] In this case the molecular geometry was elucidated *via* X-ray crystallography, where the hydride ligand was reported with a Pd-H bond length of 1.57(3) Å.

Dipalladium hydride complexes have also been observed from a range of synthetic methods including the dimerisation of mononuclear palladium hydride complexes, reactions with various reducing agents and oxidative addition.[16] These complexes

can display a variety of hydride bonding modes, some of which will be discussed below.

The first unequivocally characterised dipalladium complex featuring bridging hydrides were reported by Fryzuk and co-workers in 1991.[23] The reduction of a bidentate phosphine palladium dihalide complex with a strong so-called "superhydride" produced a binuclear palladium complex with two bridging hydride ligands shown in Figure 2.2(a). A similar species was reported by Milstein, featuring a carbonyl alongside a hydride bridge, which was formed under catalytically relevant conditions for the reaction of aryl halides (Figure 2.2(b)).[24]

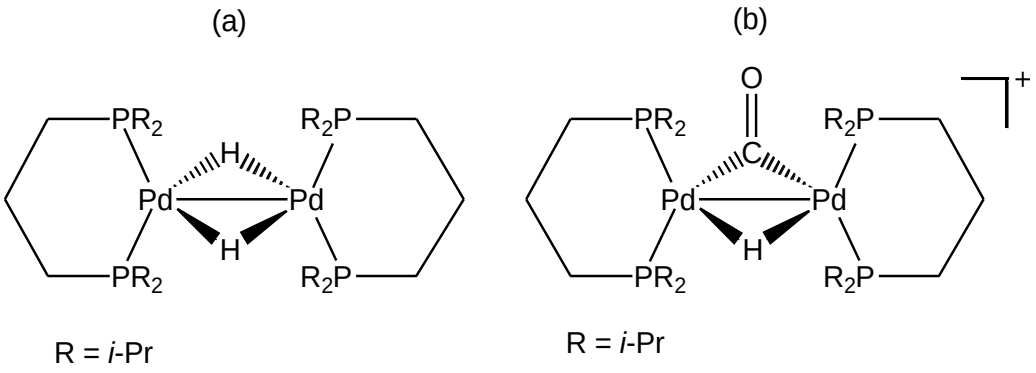

Figure 2.2. Examples of binuclear palladium complexes with bridging hydrides reported by Fryzuk (a)[23] and Milstein (b). [24]

Both of these complexes were structurally characterised using X-ray crystallography in which the hydride ligands were located and refined. The Pd-Pd distances of 2.8245(8) and 2.767(4) Å for (a) and (b), respectively indicated weak metal-metal interactions. The bridging hydrides in (a) were asymmetrical with Pd-H bond lengths ranging from 1.67(3)-2.13(4) Å. In the second complex reported by Milstein the Pd-H distances were indistinguishable, ranging from 1.531(11)-1.540(10) Å, and of

a similar length to Pd-H distances observed in terminal mononuclear Pd-H complexes.[21,25]

Milstein provided a proposed mechanism of the formation of the carbonyl- and hydride-bridged complex, in which the chloride ligand of the initial complex was exchanged by methoxide formed *in situ* in methanol under basic or neutral conditions. Rearrangement and β-hydride elimination of the methoxy ligand, concomitant with reductive elimination of benzene would result in a zero-valent palladium formaldehyde complex. This complex could undergo two reaction pathways, with oxidative addition of formaldehyde followed by hydride migration and H_2 elimination to form a monopalladium carbonyl complex, while dissociation of formaldehyde and subsequent protonation would result in a cationic monopalladium hydride complex. The combination of these two species would result in the observed cationic dipalladium complex.

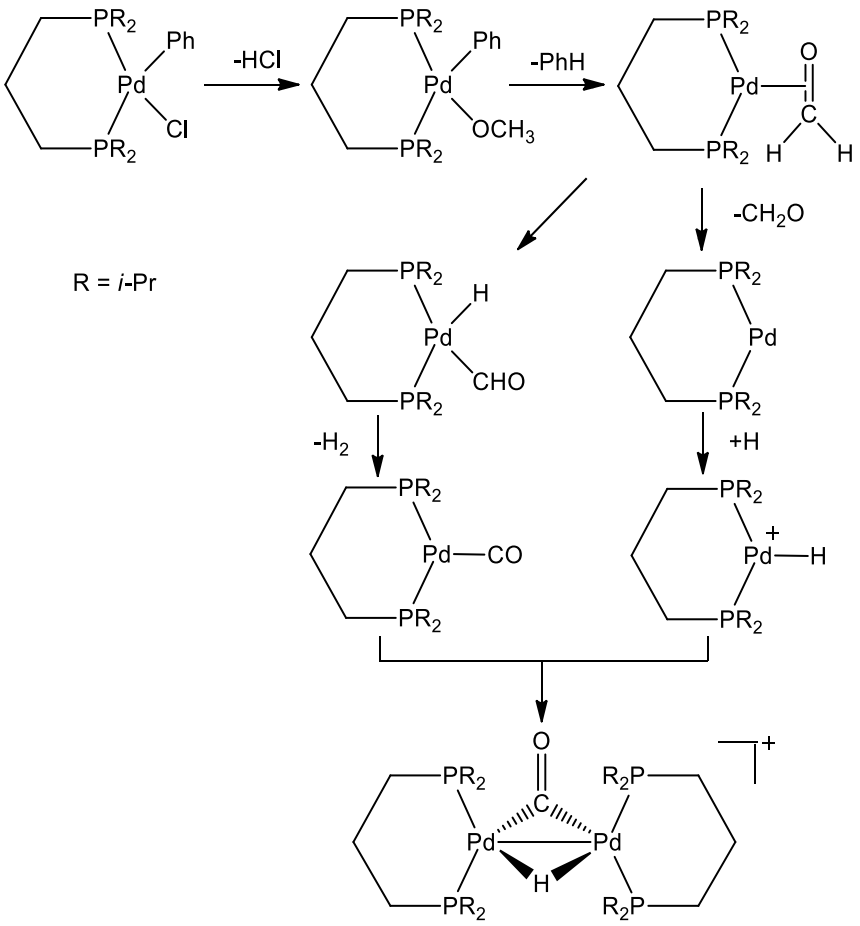

Scheme 2.2. Proposed mechanism for the formation of the dipalladium complex with bridging hydride and carbonyl ligands reported by Milstein.[24]

Rimml and Venanzi proposed the formation of an interesting binuclear palladium hydride complex with a single bridging hydride ligand between two palladium(II) centres, in which the mononuclear palladium hydride was formed first *via* decarboxylation of a precursor and subsequently coordinated to an unreacted mononuclear palladium unit to form the binuclear complex (Figure 2.3).[26] The complex lacked a Pd-Pd bond and was proposed to be linearly bridged by only a single ligand consistent with the preferred square planar geometry of the d^8 palladium(II) centres.

The complex was stable with suitable counteranions, though decomposed to palladium metal if these were exchanged. However, like many palladium hydride complexes, there was no unequivocal crystallographic characterisation of the hydride location for this complex.

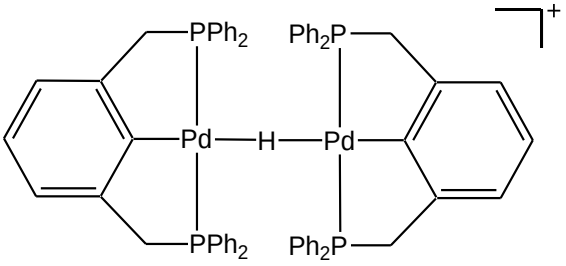

Figure 2.3. Proposed structure of the binuclear palladium complex with a single bridging hydride ligand reported by Rimml and Venanzi.[26]

In 2011 Ozerov reported two hydride bridged binuclear palladium complexes supported by a pincer ligand with alkyl linkers of varying length. The bridging hydride ligands were formed under reductive conditions by the addition of sodium isopropoxide (Figure 2.4).[27]

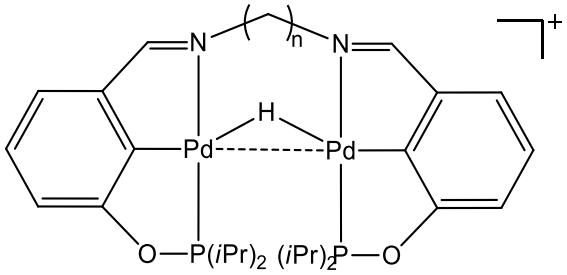

Figure 2.4. Examples of bridging pincer ligand supported binuclear palladium hydride complexes reported by Ozerov.[27]

The Pd-Pd distances in these two complexes were 3.2612(12) and 2.9602(8) Å, for the ethylene and butylene linked analogues, respectively. Again, the palladium

coordination sphere adopted a square planar geometric configuration expected for Pd d^8 metal complexes. It was noted that the increased flexibility of the longer linker enabled a closer Pd-Pd interaction, though neither complex had Pd-Pd distances in the range of an unambiguous metal-metal bond. The hydride ligands were located by X-ray crystallography for both complexes and shared a similar non-linear bridging arrangement.

An unusual binuclear palladium hydride complex was reported by Stille and co-workers in which the hydride ligand is bound in a terminal position while the palladium centres are bridged by a chloride ligand (Figure 2.5).[25] This structure was confirmed by X-ray crystallographic structural determination, where the hydride ligand was located and refined (Pd-H 1.53(5) Å). Stille discussed the formation and reactivity of the binuclear palladium complex, inferring that the hydride could bridge the palladium centres under certain conditions. This complex rearranged to a more favourable arrangement in this particular analogue when crystallised.

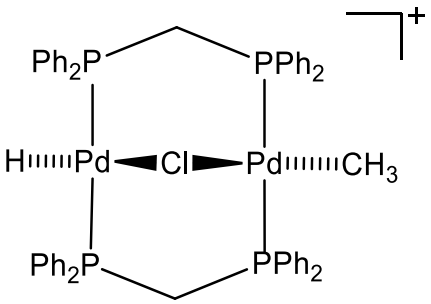

Figure 2.5. Binuclear palladium hydride complex reported by Stille.[25]

Multinuclear palladium hydride clusters have also been reported, such as those shown in Figure 2.6. Baya and co-workers[10] investigated the reactivity of a palladium(II) precatalyst for hydroformylation under various catalytic conditions and discussed several binuclear palladium complexes formed, including one which

shares a similar bridging hydride/carbonyl core to that reported by Milstein.[24] The tripalladium cluster (Figure 2.6(a) below) was formed when the precatalyst was reduced by hydrogen gas and was structurally characterised by X-ray crystallography. The presence of two hydride ligands was confirmed by ^{1}H NMR spectroscopy despite not being located in the crystal structure.

Harvey and co-workers report a tetranuclear palladium cluster formed from a catalytically relevant precursor, in which the presence of a hydride was confirmed through ^{1}H NMR and ^{31}P NMR spectroscopic analysis (Figure 2.6(b)).[28] Again, this cluster was structurally characterised by X-ray diffraction, with the hydride not located in the crystal structure. They infer that the central bridging position of the hydride between the four palladium atoms was most probable as the Pd-H distances would be consistent with other literature examples.[16]

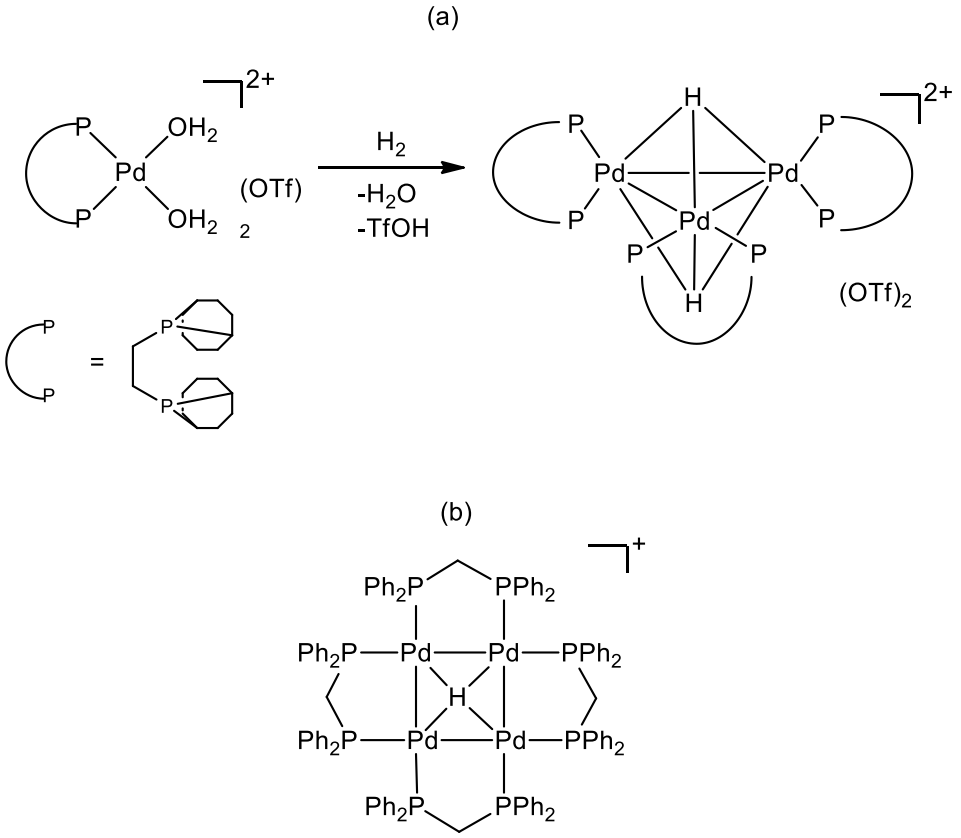

Figure 2.6. Examples of multinuclear palladium hydride clusters reported by (a) Baya[10] and (b) Harvey.[12]

Binuclear, multinuclear and cluster complexes such as those discussed above are of great importance in understanding catalytic systems. By elucidating active catalytic species, and the location, binding modes and possible dynamics of hydride ligands will allow for improved systems to yield greater activity. Understanding decomposition routes of these species will aid the design of more stable systems that will ultimately afford more economically viable catalytic processes.

Our group has reported the synthesis of a binuclear palladium(I) hydride complex which is produced under catalytic conditions from a bis(NHC) palladium(II) precursor (Scheme 2.3).[29]

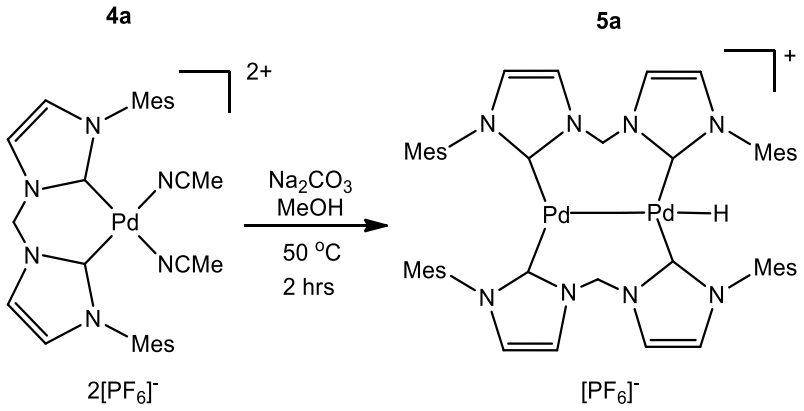

Scheme 2.3. Synthesis of dipalladium(I) hydride complex **5a** from the catalyst precursor **4a**.

The mechanism of this reaction has been probed by DFT calculations, which suggested that **4a** underwent initial methoxide ligand substitution, followed by loss of solvent and ligand rearrangement. Subsequent β-hydride elimination *via* agostic transition states resulted in a palladium(II) hydride formaldehyde adduct, which, after loss of formaldehyde, formed the three-coordinate palladium(II) hydride **A** (Scheme 2.4).[30]

The latter steps of the transformation were explored briefly by DFT, where it was assumed that two monomeric units of **A** underwent bis(NHC) chelate ring opening which facilitated the change in binding mode from chelating to bridging. This interaction between two mononuclear palladium units to form a dipalladium complex was similar to that proposed by Milstein (Scheme 2.2). Methoxide-assisted proton abstraction from **D** would have resulted in the observed reduction of the metal centre and **5a** is obtained after rearrangement of the hydride ligand from the calculated energy minimum **G**, which contains a linear bridging hydride, to the terminal position determined by single crystal neutron diffraction.[29]

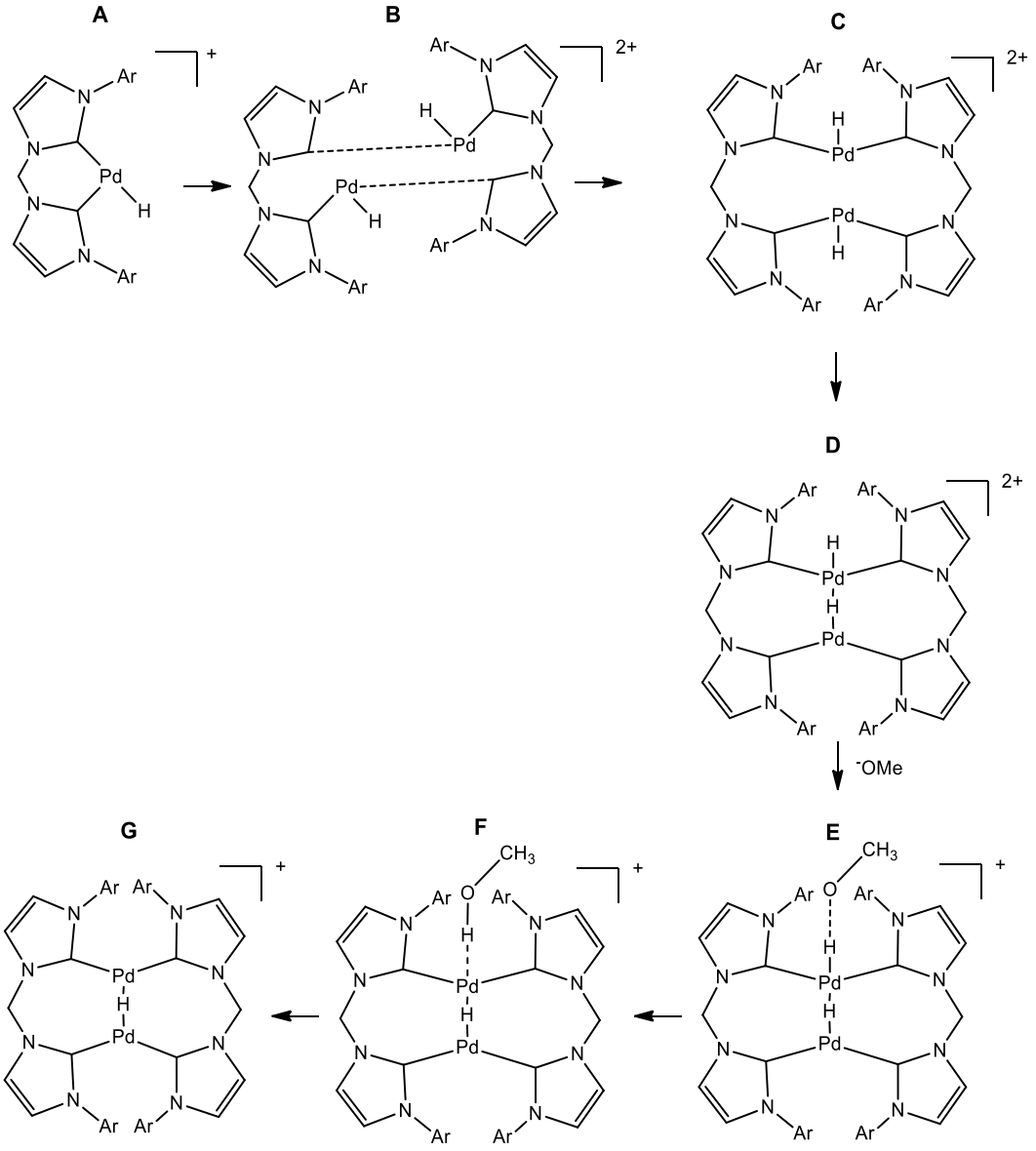

Scheme 2.4. Calculated reaction pathway for latter stage transformations in the synthesis of **5a** using B3LYP/Pd-LANL2TZ, C, H, O, N-6-31G(d) DFT level of theory.

Solution ^{1}H NMR spectroscopic studies of **5a** suggested the occurrence of a fluxional process, which was thought to involve the hydride ligand migration between the palladium centres (Figure 2.7).

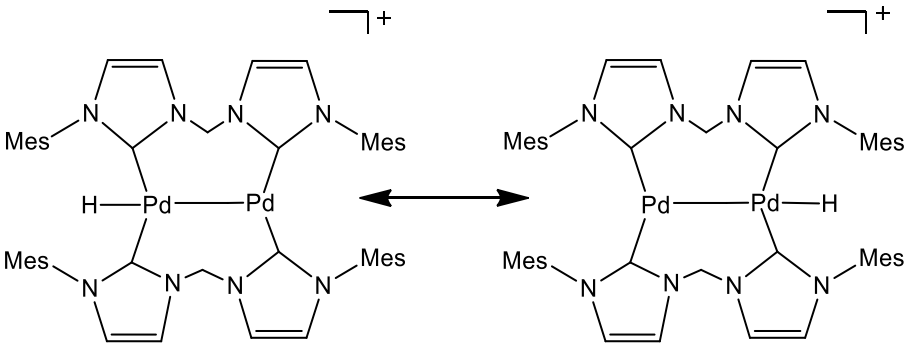

Figure 2.7. Proposed solution phase dynamics of hydride transfer in $[\{(MesIm)_2CH_2\}_2Pd_2H][PF_6]$ **5a**.

An analogue of this complex was also prepared containing the bulkier 2,6-diisopropylphenyl (dipp) *N*-substituent. X-ray crystallographic analysis of this structure showed a significantly greater Pd-Pd distance in this complex, suggesting that this analogue contained the computationally proposed linear Pd-H-Pd core arrangement. Confirmation of the hydride location has not yet been obtained, however.

Three different crystalline forms of **5a** were observed, dependant on the solvent of recrystallisation. An unsolvated crystal form was produced from methanol as red needles or blocks and the block form was used for single crystal neutron diffraction to confirm the terminal hydride position.[29] Recrystallisation from THF produced the solvate as large red blocks, in which two THF molecules per unit of **5a** were incorporated into the crystal lattice. This THF solvate of **5a** underwent a phase change at *ca.* 110 K, observed by X-ray and neutron diffraction, in which each spot appeared multiply twinned at or below this temperature (measured to *ca.* 90 K). At 150 K, Laue single crystal neutron diffraction was used to resolve a structure in which the hydride was disordered with 50 % occupancy at each of the palladium centres.

We were interested to see if this apparent phase change was due to solid state hydride dynamics, in which the hydride ligand was assumed to be transitioning between metal centres similarly to the observed solution phase dynamics. As discussed in Chapter 1, neutron techniques are well suited to probing hydrogen atom location and interactions, especially in complexes containing heavy metals due to the enhanced neutron scattering coefficient of ^{1}H, in comparison to X-ray methods.

We were also interested in examining a recently obtained analogue of **5a**, in which the alkylene linker was extended to propylene.[30] We will probe whether this analogue shares similar structural properties, hydride position and dynamics.

2.2 Results and Discussion

2.2.1. Neutron Scattering Experiments of Isotopomers of 5a

Previous experimental studies on palladium hydride clusters have suggested that hydride transfer processes between metal centres can occur either with the Pd–Pd bond remaining intact, or with cleavage of the Pd–Pd via a Pd–H–Pd geometry.[13] These studies were mostly based on the interpretation of solution phase fluxionality investigated by variable temperature ^{1}H NMR spectroscopy. However, in this investigation of hydride transfer in the solid state, the more significant changes to the cluster core thought to accompany Pd-Pd bond cleavage to the linear Pd-H-Pd bridged arrangement would likely be disfavoured due to crystal packing effects.

Computational investigations into the possible solid state hydride transfer were undertaken by Prof. Gordon Kearley and Dr. Nicolas De Souza at the Bragg institute, ANSTO. Initial calculations on H-transfer in **5a** revealed that it would be too slow to observe the H-transfer process directly, using for example quasielastic neutron

scattering. Simulation at high temperatures seemed to be a possible way forward as, presuming the model was confirmed to remain valid at this increased temperature, the frequency of transfer processes would increase and there would be a significant decrease in the required simulation timeframe.

Using DFT-MD, it was observed that the dynamics of the H-ligand in **5a** were largely determined by the time-dependent free-energy landscape of neighbouring molecular groups. These dynamics could be scaled up by increasing the nominal temperature, and probed at an energy of 1500 K, where a hydride transfer event could just be seen, within 8 ps, though higher temperatures and longer times lead to rupture of the model. It was noted that the amplitude of the fluctuations in the hydride transfer free-energy surface increased with temperature rather than a new process being activated. In this case validation of the model at low temperature still applied reasonably well at high temperature.

However there were three key difficulties to overcome with applying this method: Firstly, **5a**, particularly in the full crystal structure, had a formidable number of degrees of freedom, though only those that involved the hydride ligand were of interest for this study. The associated vibrational dynamics of the hydride ligand in **5a** were conveniently studied almost in isolation by the use of inelastic neutron scattering (INS). The hydrogen ^{1}H nucleus has a uniquely high incoherent neutron scattering cross-section, hence selective deuteration of all hydrogen atoms, except the hydride ligand, would make the hydride vibrations more pronounced in the INS spectrum. Secondly, due to the transfer process involved in bond-making and breaking, and the general lack of a suitable force-field for **5a**, it was necessary to use DFT-MD. This method has the advantage of removing ambiguity, but is vastly more computationally expensive than empirical force-field methods, and consequently the

size of the model and the time-scale covered was rather limited. Finally, the unit-cell of the crystal was large and it was important to establish how the crystal forces might distort the gas-phase molecular conformation. We observed in this case that the calculated vibrational dynamics of the isolated molecule and the full periodic crystal were very similar.

Two deuterated isotopomers of **5a** were prepared to aid in our investigation. As previously discussed in Chapter 1 there is a significant difference in the neutron scattering cross-section between ^{1}H and ^{2}H of approximately an order of magnitude.[31] By substituting all NHC ligand hydrogens for deuterium atoms we were theoretically able to minimise the vibrational contributions from all non-hydride bending and stretching modes for IINS experiments and simulations of the spectra.

To this end, we provided 20 g of *N*-mesityl imidazole **1a** to the National Deuteration Facility (NDF) at ANSTO for chemical deuteration. The compound was heated at 150 °C for 3 days under pressure in deuterium oxide in the presence of a mixture of Pt/C and Pd/C catalysts and using 20 % v/v THF as a co-solvent.[32] The hydrothermal reaction mixture was purified using silica column chromatography to give the deuterated *N*-mesityl imidazole **1b** in 96 % yield, where the two mesityl *m*-CH protons remained essentially un-exchanged. Conversion to the deuterated diimidazolium salt **2b** was also undertaken at the NDF using a modified literature procedure[33] with deuterated dibromomethane (99 % D) and resulted in an overall molecule deuteration of 84 ± 2 %. The deuteration percentages at each location of the molecule were calculated by ^{1}H and $^{13}C\{^{1}H,^{2}H\}$ NMR spectroscopy, along with mass spectrometry and isotopic distribution analysis to confirm the specific site, as well as the overall isotopic purity, respectively.

The synthesis of the deuterated chelating bis(NHC) palladium(II) dibromide complex **3b**, ligand exchange to form the deuterated palladium(II) bis(acetonitrile) adduct **4b** and conversion to the deuterated bridging bis(NHC) dipalladium(I) hydride **5b** were completed *via* literature methods (Scheme 2.5).[29,33]

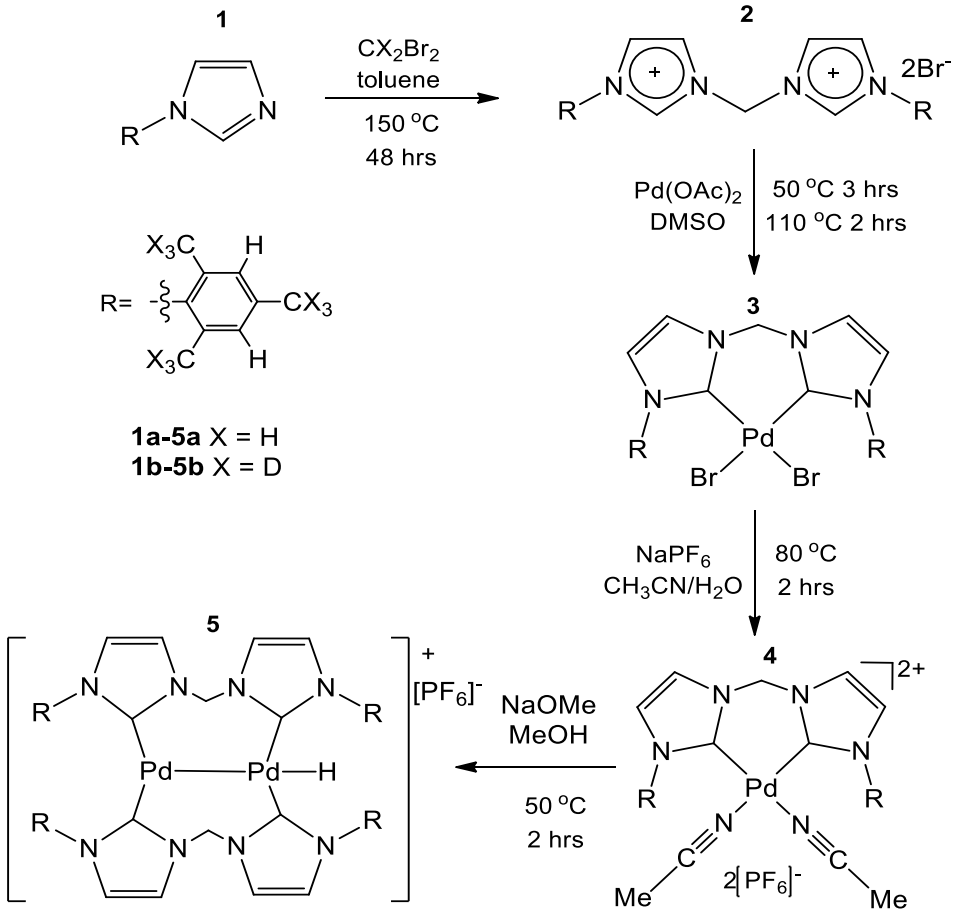

Scheme 2.5. Synthesis of dipalladium hydride complexes [{(MesIm)$_2$CH$_2$}$_2$Pd$_2$H][PF$_6$] **5a** and [{(^{D}MesIm)$_2$CD$_2$}$_2$Pd$_2$H][PF$_6$] **5b** .

A portion of the deuterated dipalladium hydride complex **5b** was dissolved in CD_3OD and heated at 50 °C for 48 hours to undergo H/D exchange of the hydride ligand and form the deuterated isotopomer **5c**. The overall deuterated structures of the three isotopomers **5a-c** are shown in Figure 2.8 below**.**

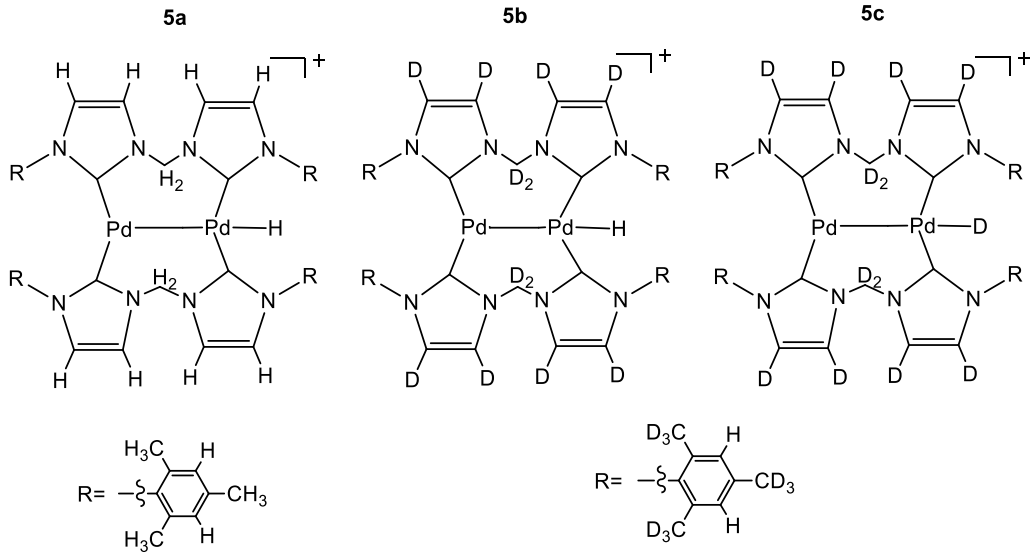

Figure 2.8. Deuterated isotopomers of $[\{(MesIm)_2CH_2\}_2Pd_2H][PF_6]$: **5a** , **5b**, and **5c**. The ring H-atoms of the R groups could not be deuterated, but these are the same in **1b** and **1c** and contributed equally to the INS spectra.

The vibrational spectra of the isotopomers **5a**, **5b** and **5c** were collected on the TOSCA instrument at the ISIS facility in Oxford, England, and were interpreted using two different standard approaches. This provided a validation of the MD approach and some justification for being able to extend this to much higher temperatures, and therefore gave access to the H transfer process that was observed a single time in the high-temperature DFT-MD simulation. The accessible free-energy profile was then analysed and extended to include the H-transfer. The experimental INS spectra of **5b** and **5c** were remarkably similar, as illustrated in Figure 2.9.

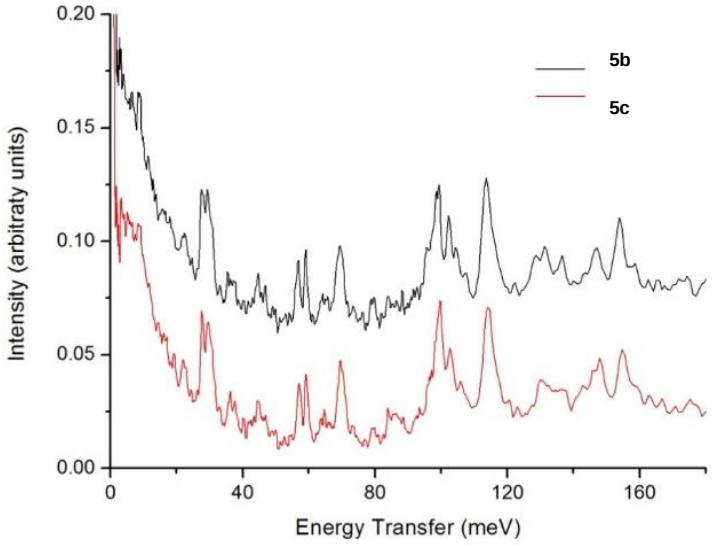

Figure 2.9. Comparison of INS spectra for **5b** and **5c** obtained on TOSCA. Relative intensity of **5b** shifted 0.1 arbitrary units to aid comparison.

It was expected from the matrix-method calculation that the hydride ligand present in **5b** would produce a strong feature in the 50 meV region corresponding to an out-of-plane wagging (H–Pd–Pd deformation), that would be absent in the spectrum of **5c**, as shown in the lower part of Figure 2.10. It is worth noting that in both analogues there were 2 un-exchanged hydrogen atoms on each mesityl unit (see Figure 2.8) and these contributed additional peaks from vibrations of the NHC ligands, but these were identical for both analogues.

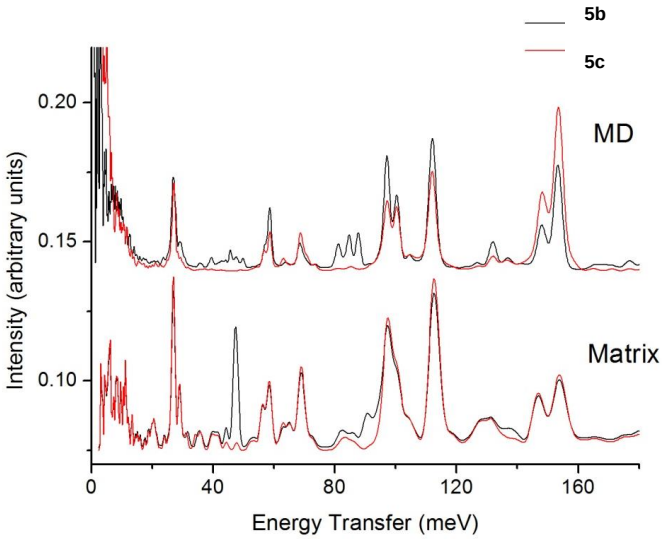

Figure 2.10. Comparison of the calculated spectra of **5b** and **5c** by MD and Matrix simulation methods. Relative intensity of MD spectra shifted 0.1 arbitrary units to aid comparison.

The absence of the strong peak at around 50 meV predicted by the matrix method was due to a breakdown of the harmonic approximation for modes of the hydride ligand. This was easily demonstrated by using the alternative MD method to produce the calculated INS spectrum. Whilst DFT-MD lacks proper treatment of overtones and combinations, it has the advantage that it makes no assumption about the form of the vibrational potential, or other potentials that may be involved. It was observed from the MD spectrum (shown in the upper part of Figure 2.10) that the strong peak at 50 meV was indeed absent in the calculated spectrum, and casual examination of the MD trajectories for the hydride ligand showed the dynamics to be locally diffusive rather than oscillatory. This was unusual as the difference between the INS spectra calculated by the two methods is usually small, and even the differences in Figure 2.10 between 80 and 100 meV that were in part due to the lack of overtones and combinations in the MD, would be considered as significant. To the best of our

knowledge, the difference at around 50 meV in the current example is much larger than any reported so far.[34]

The purpose of the INS was to validate that DFT-MD could at least reproduce the dynamics measured on the low-frequency part of the vibrational spectrum. The general agreement between the experimentally observed and calculated spectra of **5b** and **5c** by comparison of Figure 2.9 and Figure 2.10, and in particular the correct prediction of the non-oscillatory H-ligand dynamics, was taken as sufficient validation of the method.

Computationally based energy-barrier calculations are generally performed by mapping the potential energy of the system as a function of some pre-defined reaction coordinate, taking no account of thermal motion. Even in better defined systems such as linear hydrogen bonds the involvement of many degrees of freedom can play a crucial role.[35] In **5a**, where the hydrogen atom was weakly bound and surrounded by molecular groups, each with many degrees of freedom, the choice of reaction coordinate was not obvious. MD was used to sample the free energy surface in a systematic and physically meaningful way, albeit at lower precision and greater computational expense, though the amplitudes sampled were limited by the available kinetic energy (simulation temperature). Thus the MD simulation temperature was increased, and was considered to be a more realistic approach than mapping potential-energies along pre-determined coordinates (at 0 K).

The simulation temperature was increased until a transfer process occurred once within the timescale of the simulation (8 ps). The crucial coordinate for the transfer process was identified as the dihedral angle between the plane of one heterocyclic ring and the Pd–H vector, which approximated to an extension of the mode that was

predicted, but not observed, by the harmonic approximation at 50 meV in the INS. The actual definition used is shown in Figure 2.11(a), but for convenience this will be referred to as the Pd–Pd–H angle, which it approximates.

(a)

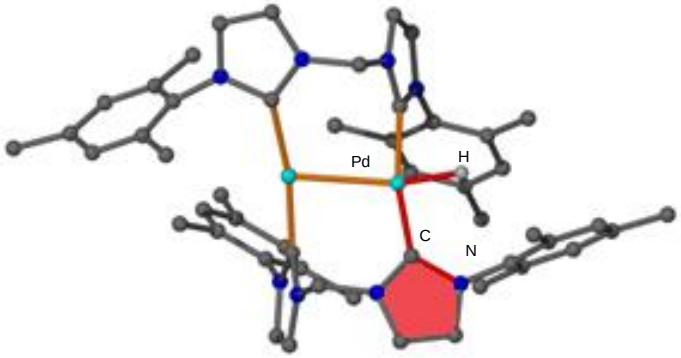

(b)

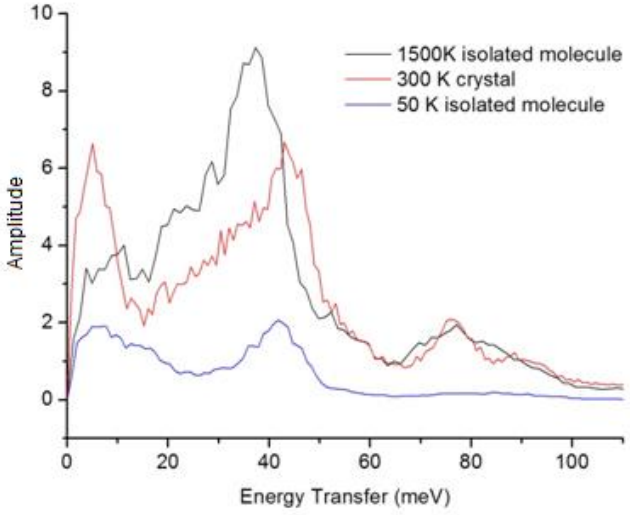

Figure 2.11. (a) Structure of the cation of **5a** indicating the plane used to define the dihedral torsion coordinate. The Pd–Pd–H angle was not actually used, although it is denoted this way in the text as that axis includes motion of both Pd atoms. (b) Frequency spectra of the hydride torsion showing comparison between the isolated molecule at 1500 K and 50 K, as well as with the periodic structure calculation.

Clearly, this coordinate was not a normal coordinate of the system and so has a distributed spectral profile, which is shown (from the MD simulations) in Figure 2.11(b). The crucial point illustrated in this figure is that this frequency distribution does not change significantly between 50 K, where this was validated against experiment, and 1500 K where the transfer was seen in the MD, although there was a large increase in amplitude. A limited MD simulation for the periodic crystal at 300 K showed a very similar profile in Figure 2.11(b) to those of the isolated molecule. This indicated that the vibrational dynamics were not only dominated by intra-molecular interactions, but also the H-transfer mechanism.

The actual transfer process was assumed to be terminal hydride at one palladium centre, to bridging hydride between the two palladium centres to terminal hydride at the second palladium centre. Neither this whole process, nor the alternative "bridge and return" process was observed, however.

The resources for the longer simulations required for this were not available for this work, and further increase in the simulation temperature destroyed the model before any transfer process was seen. Consequently, our analysis was based on the dihedral angle shown in Figure 2.11(a).

The temporal evolution of this Pd–Pd–H coordinate contained the resultant of the dynamics of the neighbouring ligands to which it was strongly coupled. To estimate the barrier to the transfer process the free energy was calculated from the frequency distribution of this angle during the 8 ps simulation at 1500 K as:

$$FE_{(Pd\text{-}Pd\text{-}H)} = kT\ln\left(\frac{P_{(Pd\text{-}Pd\text{-}H)}}{P_{(max)}}\right) \qquad (1)$$

where T was the temperature of the simulation, $P_{(Pd–Pd–H)}$ was the time average population of a particular value of the angle, and $P_{(max)}$ was the maximum value of $P_{(Pd–Pd–H)}$. This energy function is shown in Figure 2.12. Because only a single partial transfer was seen during the simulation, there were no data points around the peak of the barrier, and it would take an extremely long simulation to obtain these. In the absence of a known functional form, the angle-dependent data was fitted with a sinusoidal function which resulted in an estimate for the energy barrier between 19 and 23 kcal mol^{-1}. By using the Arrhenius equation:

$$k = Ae^{\frac{-E_a}{RT}} \qquad (2)$$

where k was the rate constant, A was the frequency factor determined using the observed single transfer in the MD as the rate at 1500 K, E_a was the activation energy, R was the universal gas constant 1.986 x 10^{-3} kcal $mol^{-1}K^{-1}$ and T was the temperature, a room temperature transfer rate of one transfer per 5.3 seconds was calculated. However, because the error in the barrier transformed exponentially to the rate, the limiting values were 360 ms and 77 s.

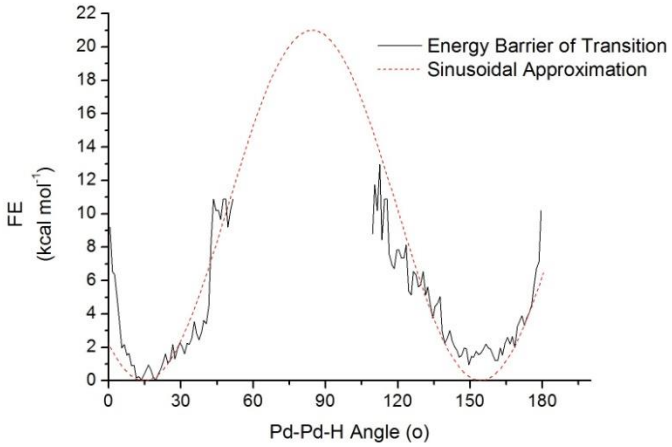

Figure 2.12. Free energy from the frequency distribution of the Pd-Pd-H angle approximated with a sinusoidal function to estimate the energy barrier.

No attempt has been made at this stage to analyse the correlations between torsional motions of the methyl groups, whole-body torsions of the ligands and the hydride transfer process. These are clearly central to the hydride transfer process and could be chemically tailored to either increase or decrease the rate, or indeed to trap the H-ligand in a bridging or terminal position. To date we do not have an ideal experiment for measuring transitions at the proposed rate of 360 ms-77 s, and therefore have no way of observing whether the hydride transition we proposed is occurring.

A low temperature neutron diffraction study of the THF solvate of **5a** was undertaken at the ILL facility in Grenoble, France using the monochromated single crystal diffractometer D19. Successful data reduction of the crystal as a two-component twin was produced, however the lack of a starting X-ray crystallographic model for the structure has prevented further progress on the

analysis of the data. Numerous attempts to obtain a suitable low temperature X-ray crystal structure of the THF solvate of **5a** have been attempted, however multiple twinning of the sample below *ca*. 110 K has, to date, prevented data reduction.

2.2.2. Variable Temperature Neutron Diffraction of 5a

As discussed previously, three crystal forms of **5a** were observed dependant on the solvent of recrystallisation. The X-ray and neutron crystal structure of the unsolvated block form of **5a** at 100 and 150 K did not show any of the apparent phase change behaviour seen in the THF solvate.[29] We endeavoured to probe whether, over a range of temperatures approaching room temperature, any structural changes or signs of solid state hydride dynamics were observed in this unsolvated form.

A variable temperature single crystal neutron diffraction study was performed on solvent-free crystals of **5a** using the Laue diffractometer KOALA at the ANSTO facility in Lucas Heights, Australia. Data were obtained at temperatures of 100, 200, 260 and 300 K, with structure refinement by a least squares fit to the data using CRYSTALS.[36]

The molecular structures did not show any variation in the hydride position over the 200 K temperature range. Most of the isotropic displacement parameters of the atoms (including the hydrogen atoms) refined on a per atom basis showed a general increasing trend with temperature as expected. This necessitated the modelling some of the methyl hydrogen atoms as toroids to represent the C-C bond torsion disorder above 100K, though it was not possible to determine whether this was a static or dynamic disorder. The methyl and methylene hydrogen atoms nearest the three-coordinate palladium centre (Pd1) had more limited increase in the

displacement parameters with respect to the other atoms. This less distributed nuclear density at higher temperatures suggested the possibility of a significant interaction with the three-coordinated palladium centre (Figure 2.13).

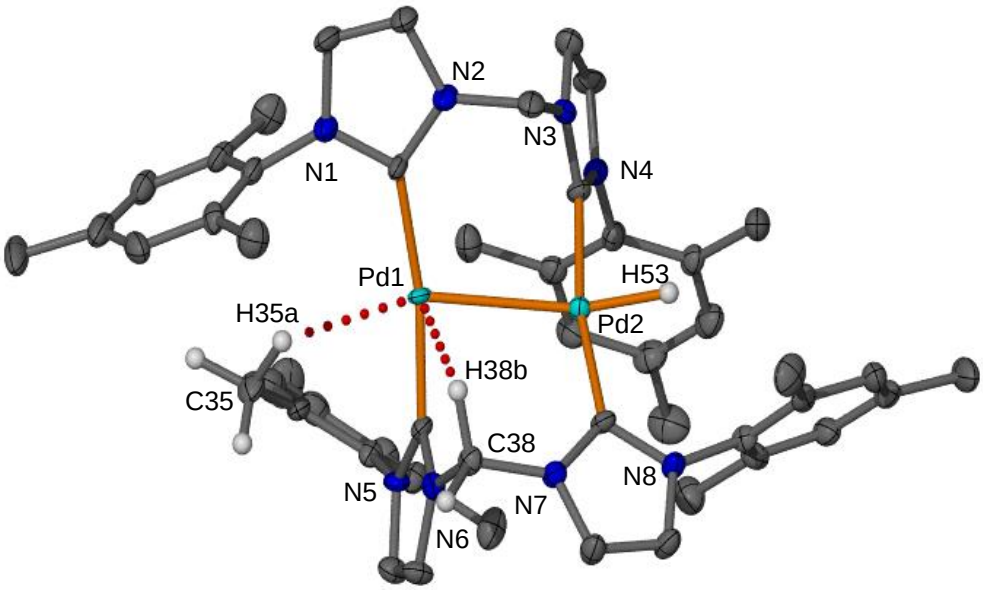

Figure 2.13. Molecular structure of the cation of $[\{(MesIm)_2CH_2\}_2Pd_2H][PF_6]$ **5a** in the unsolvated form at 100 K from neutron diffraction. Displacement ellipsoids are shown at the 50 % probability level. Counter anion $[PF_6]^-$ and hydrogen atoms except H35a, H38b and H53 are omitted for clarity. Selected bond lengths (Å) and angles (°): Pd1-Pd2 2.725(6), Pd2-H53 1.536(10), Pd1···H35a 2.589(13), Pd1···H38b 2.638(11), Pd1-Pd2-H53 152.5(9), C35-H35a···Pd1 144.0(9), C38-H38b···Pd1 116.7(7).

An agostic interaction is observed between the non-hydridic palladium and one of the mesityl methyl protons, with a Pd1···H35a distance of 2.589(13) Å. The Pd1···H38b distance and bond angle is comparable to anagostic Pd···H interactions reported by Dyker *et al.* who observed particularly notable interactions occurring where the complex geometry allowed the relevant hydrogen atom(s) to position in

roughly axial positions compared to the directly coordinated M-L plane (Figure 2.17).[37] We compared the similar angles and distances between Dyker's complex showing the greatest agostic interactions and the anagostic Pd···H38b interaction in complex **5a** in Table 1 below. The Pd···H distances and bond angles for these interactions are within the range of other reported agostic and anagostic M···H interactions.[38,39] The θ angles approximate 90 ° as would be necessary for pseudo-square pyramidal geometry.

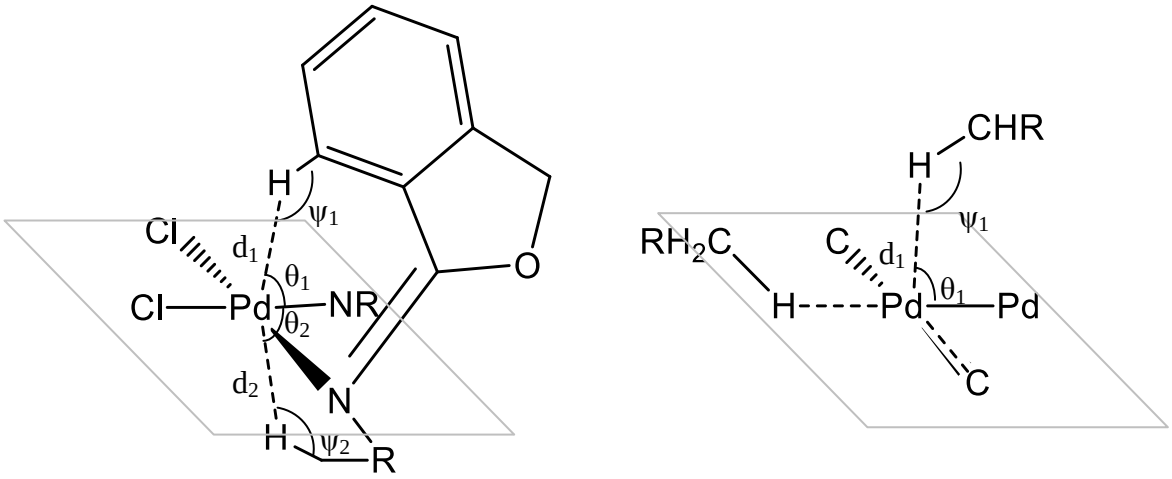

Figure 2.14. Partial representations of (a) Dyker complex[37] and (b) [{$(MesIm)_2CH_2$}$_2$$Pd_2H$][$PF_6$] **5a** showing the axial positioning of H38b against the square planar palladium centre.

Table 1. Contact length and angles from the palladium atom to the interacting protons in Dyker's literature example[37] and **5a**.

Compound	d_1	ψ_1	θ_1	d_2	ψ_2	θ_2
Dyker	2.581	128.83	82.55	2.299	119.14	70.40
5a	2.638(11)	116.7(7)	71.8(3)	-	-	-

ψ_1 = Pd1···H38b-C38 [°]; θ_1 = Pd2-Pd1···H38b [°]; d_1, d_2 [Å].

The interaction between the methylene linker proton H38b and the palladium was also observed by ^{1}H NMR spectroscopy, with a significant downfield shift of the proton from 5.98 ppm for the non-interacting methylene protons to 7.89 ppm (Δ 1.91 ppm). This is also consistent with observations from Dyker, who noted that the interaction is defined as the more electrostatic anagostic rather than agostic as the proton shift is downfield not upfield, though they reported significantly greater (Δ 3.35 and 4.10 ppm) downfield shifts for these anagostic interactions.

It is likely that the anagostic interactions prevent the hydride from undergoing any fluxional process in the solid state as the partially filled coordination sites on the non-hydridic palladium obstruct any hydride transfer in the solid state.

2.2.3. Examination of an Extended Linker Analogue of 5a

Synthesis of an extended linker analogue of **5a,** [μ-{(MesIm)$_2$(CH$_2$)$_3$}$_2$Pd$_2$H][PF$_6$] **7** was achieved in our research group in 2014 by Dr. Curtis Ho.[30] Compound **7** showed similar structural transformations from a chelating bis(NHC) mononuclear palladium(II) complex to a bridging bis(NHC) dinuclear palladium(I) hydride complex under reducing conditions.

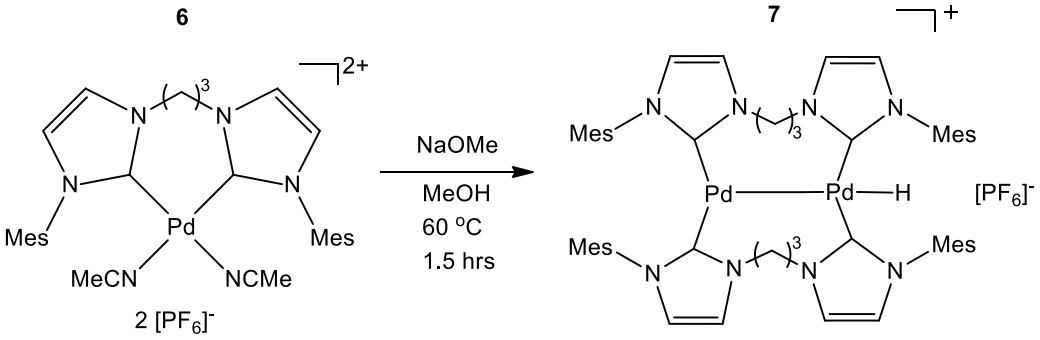

Scheme 2.6. Synthesis of dipalladium(I) hydride complex [{(MesIm)$_2$(CH$_2$)$_3$}$_2$Pd$_2$H][PF$_6$] **7**.

The X-ray crystal structure of **7** is shown in Figure 2.15 and displayed a greatly reduced Pd-Pd distance of 2.7058(3) Å compared to both the unsolvated and THF solvate forms of **5a** (ranging from 2.7530(4)–2.8757(6) Å)[29], potentially influenced by the helical twist of the ligand alkyl linker groups. However, like the unsolvated form of **5a**, one palladium site (Pd2) was more sterically shielded by the interactions with the mesityl methyl and methylene groups of the nearby NHC ligands, resulting in agostic and anagostic interactions that would effectively block one palladium centre and cause the hydride to preferentially bind at Pd1. The relatively short Pd···C distances between Pd1 and the nearest linker methylene carbons (3.291(3) and 3.307(3) Å) was consistent with these proposed anagostic interactions.

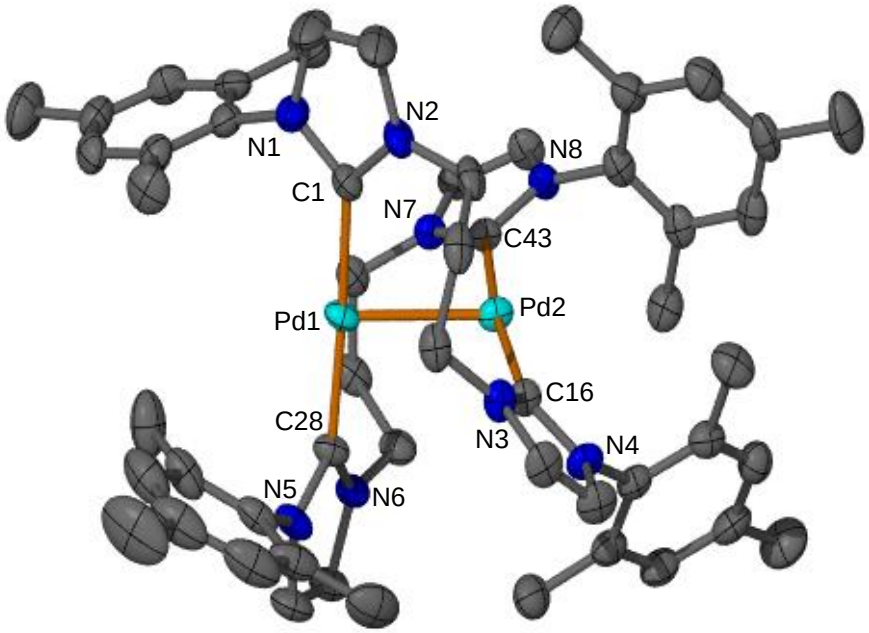

Figure 2.15. Molecular structure of the cation of [μ-{(MesIm)$_2$(CH$_2$)$_3$}$_2$Pd$_2$H][PF$_6$] **7** determined by X-ray crystallography. Displacement ellipsoids are shown at the 50 % probability level. Counter anion [PF$_6$] and hydrogen atoms omitted for clarity. Selected bond lengths (Å) and angles (°): Pd1-Pd2 2.7058(3), Pd1-C1,C28 2.034(3), 2.025(3), Pd2-C16,C43 2.037(3),2.038(3), Pd1-C1-N1,N2 124.2(2),132.7(2), Pd1-C28-N5,N6 124.8(2),132.6(2), Pd2-C16-N3,N4 132.5(2),123.8(2), Pd2-C43-N7,N8 133.2(2),123.5(2).

The ^{1}H NMR spectrum of **7** at 20 °C has been reported, though was incorrectly assigned, with an inseparable coproduct also observed (discussed *vide infra*). The hydride resonance of **7** was observed at -15.58 ppm.[30]

Previous studies of the methylene linked analogue **5a** showed key signs of hydride fluxionality in solution. In the spectra of **5a**, desymmetrisation of the NHC ligands at low temperatures was observed by the eight unique resonances for the *N*-mesityl *o*-Me hydrogen atoms below -30 °C, followed by coalescence while warming above this temperature.[29] There was also a shift of the hydride signal, where the initial

resonance at -16.2 ppm began broadening around -30 °C and rapidly sharpened below that temperature again to a single hydride peak at -16.5 ppm. This was consistent with the proposed solid state dynamics in which the hydride ligand was fluxional at higher temperatures (as shown by the equivalent ligand signals), but was "frozen out" at lower temperatures to a single site, which resulted in a desymmetrised complex structure consistent with the proposed hydride fluxionality.

A variable temperature (VT) ^{1}H NMR spectroscopy study was conducted on **7** in CD_3OD, with spectra obtained for the temperature range -50 - 50 °C. The hydride region showed only a progression of the signal downfield from -15.37 ppm at -50 °C to -15.66 ppm at 50 °C. The aliphatic and aromatic regions also showed little variation across the temperature range examined, though analysis was difficult due to overlapping signals and the presence of the aforementioned coproduct. The clear indications of solution phase hydride fluxionality that were seen in **5a** were not observed for complex **7**, however.

Neutron diffraction was performed on a single crystal of **7** as an unsolvated sample. A yellow plate crystal measuring 0.70 x 0.70 x 0.15 mm^3 was grown from a saturated methanol solution under an inert atmosphere. The structure was refined isotropically with an R_1 of 9.94 and the disorder in the $[PF_6]^-$ counteranion was modelled with a ring containing four fluorine atoms.

Neutron structure analysis indicated a terminal positioning of the hydride ligand similar to that observed in the methylene linked analogue **5a**, situated on Pd2 as expected due to the interactions with the mesityl methyl and methylene groups of the NHC ligands with Pd1. The Pd-H bond length of 1.53(6) Å is typical of terminal hydrides and similar (within error) to that of **5a**.[21]

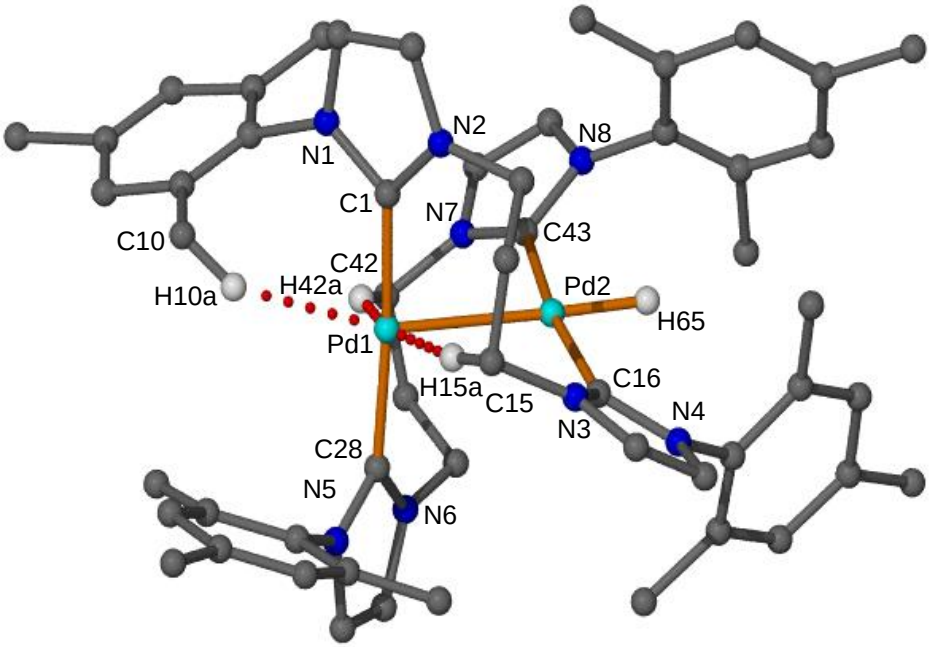

Figure 2.16. Molecular structure of the cation of [μ-{(MesIm)$_2$(CH$_2$)$_3$}$_2$Pd$_2$H][PF$_6$] **7** from neutron diffraction. The structure was refined isotropically with spheres shown with an arbitrarily fixed radius of 0.2 Å. Counter anion [PF$_6$]$^-$ and all hydrogen atoms except H10a, H15a, H42a and H65 are omitted for clarity. Selected bond lengths (Å) and angles (°): Pd2-H65 1.53(6), Pd1···H10a 2.84(6), Pd1···H15a 2.32(6), Pd1···H42a 2.33(5), Pd1-Pd2-H65 178(2), Pd1···H15a-C15 149(3), Pd1···H42a-C42 164(4).

Similar to **5a**, **7** also shows significant anagostic interactions between the non-hydridic palladium atom and the linker CH$_2$ protons H15a and H42a of 2.32(6) and 2.33(5) Å, respectively. These are again comparable to those reported by Dyker (Figure 2.17),[37] and we compare the similar angles and distances between the Dyker complex showing the greatest agostic interactions and our complex **7** in Table 2. A weaker agostic interaction between the non-hydridic palladium atom and one of the

mesityl methylene protons was also observed with a Pd1···H10a distance of 2.84(6) Å

The ^{1}H NMR spectroscopic downfield shift of one of the propylene linker CH_2 protons from *ca.* 3.6 ppm to 6.20 ppm (Δ *ca.* 2.60 ppm) was consistent with the observed anagostic interaction between these protons and three-coordinate palladium site.[37] This is again a smaller downfield shift observed by Dyker for anagostic interactions (Δ 3.35 and 4.10 ppm),[37] though the different steric environments may account for this.

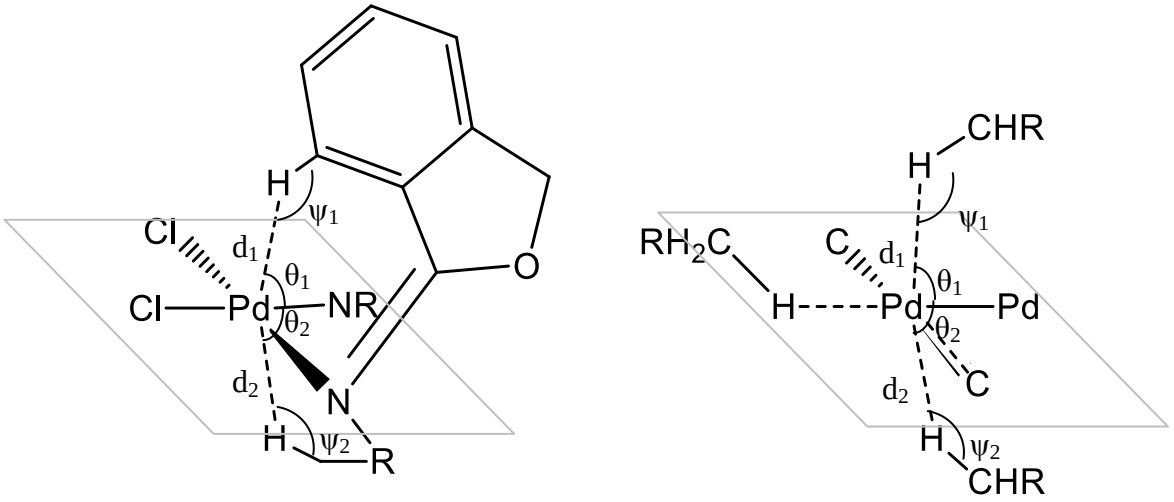

Figure 2.17. Partial representations of (a) Dyker's complex[37] and (b) [{(MesIm)$_2$(CH$_2$)$_3$}$_2$Pd$_2$H][PF$_6$] **7** showing the axial positioning of the hydride against the square planar palladium centre.

Table 2. Contact length and angles from the palladium atom to the anagostic interacting protons in Dyker's literature example and **7**.

Compound	d_1	ψ_1	θ_1	d_2	ψ_2	θ_2
Dyker	2.581	128.83	82.55	2.299	119.14	70.40
7	2.32(6)	164(4)	80.9(13)	2.33(5)	149(3)	83.0(13)

ψ_1 Pd1···H42a-C42 [°];= ψ_2 = Pd1···H15a-C15 [°];θ_1 = Pd2-Pd1···H42a [°]; θ_2 = Pd2-Pd1···H15a [°];d_1, d_2, [Å].

The θ angles again show a similar range close to the 90 ° angle to the palladium-NHC plane, which would be expected for the pseudo-octahedral geometry of the Pd1 site and these relatively short anagostic interactions likely play a significant role in preventing any hydride dynamics in this extended linker complex.

2.2.4. Examination of a Trapped Intermediate of 7

While undertaking the recrystallisation necessary to produce suitable crystals of **7** for neutron diffraction, a second product was obtained (Scheme 2.7). $[\mu\text{-}\{(MesIm)_2(CH_2)_3\}\{(PdH)(MesIm)_2(CH_2)_3\}_2][PF_6]_2$ **8** was produced as large colourless crystals from methanol. Often the products **7** and **8** were observed to intergrow with a crystal of one acting as a nucleation site for the other, leading to an impure solid. Several crystals mostly free of contamination from **7** were isolated on this occasion and examined by ^{1}H NMR spectroscopy, X-ray crystallography, and neutron diffraction.

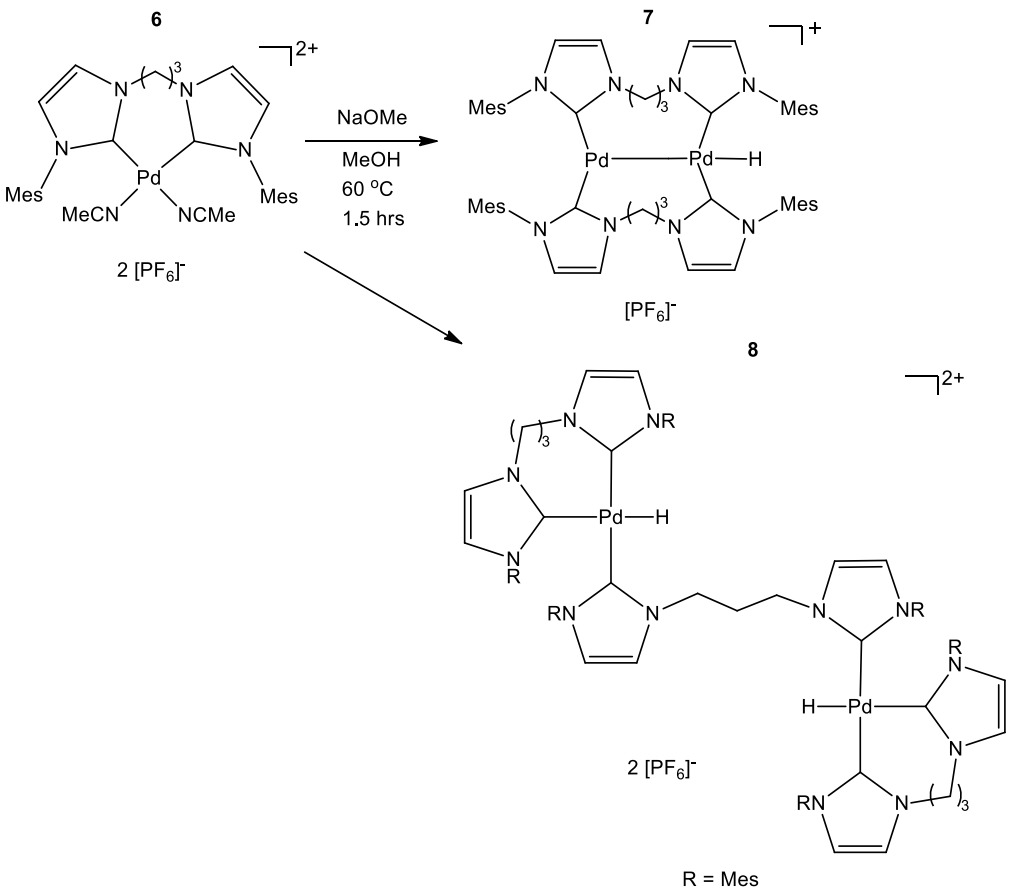

Scheme 2.7. Synthesis of complex **8** formed alongside **7** under basic reaction conditions.

X-ray crystallographic analysis on a colourless crystal of **8** from methanol determined the mixed chelate/bridged structure as well as the likely hydride ligand, inferred from the T-shaped palladium(II) centre and the dicationic nature of the overall unit (Figure 2.18). The complex has C_2 symmetry with the rotation axis centred on the disordered bridging propylene linker.

This tricarbene palladium(II) hydride shares a similar palladium coordination environment to that observed by Cavell (Figure 2.1(c)),[21] with the Pd-C bond *trans* to the hydride lengthened compared to the NHCs *cis* to the hydride. In complex **8**, the Pd1-C1 bond *trans* to the hydride was observed to be 2.096(4) Å. The chelating NHC Pd1-C16 bond *cis* to the hydride was 2.060(4) Å (Δ 0.036Å compared to the

trans Pd-C) while the bridging NHC Pd1-C28 bond was 2.025(4) Å (Δ 0.071 Å). In the tricarbene complex reported by Cavell, the Pd-C bond *trans* to the hydride was 2.111(2) Å, while the Pd-C bonds *cis* to the hydride were 2.030(2) and 2.031(2) Å (Δ 0.081 and 0.080 Å compared to the *trans* Pd-C, respectively). It is important to note, however that the complex reported by Cavell contained only monodentate NHC ligands, and that the NHC *trans* to the hydride had considerably less steric bulk than those *cis* to the hydride. In complex **8**, the bridging NHC shows a similar bond lengthening effect to that reported by Cavell, though the reduced flexibility of the chelate ring forced extension of the Pd1-C16 bond.

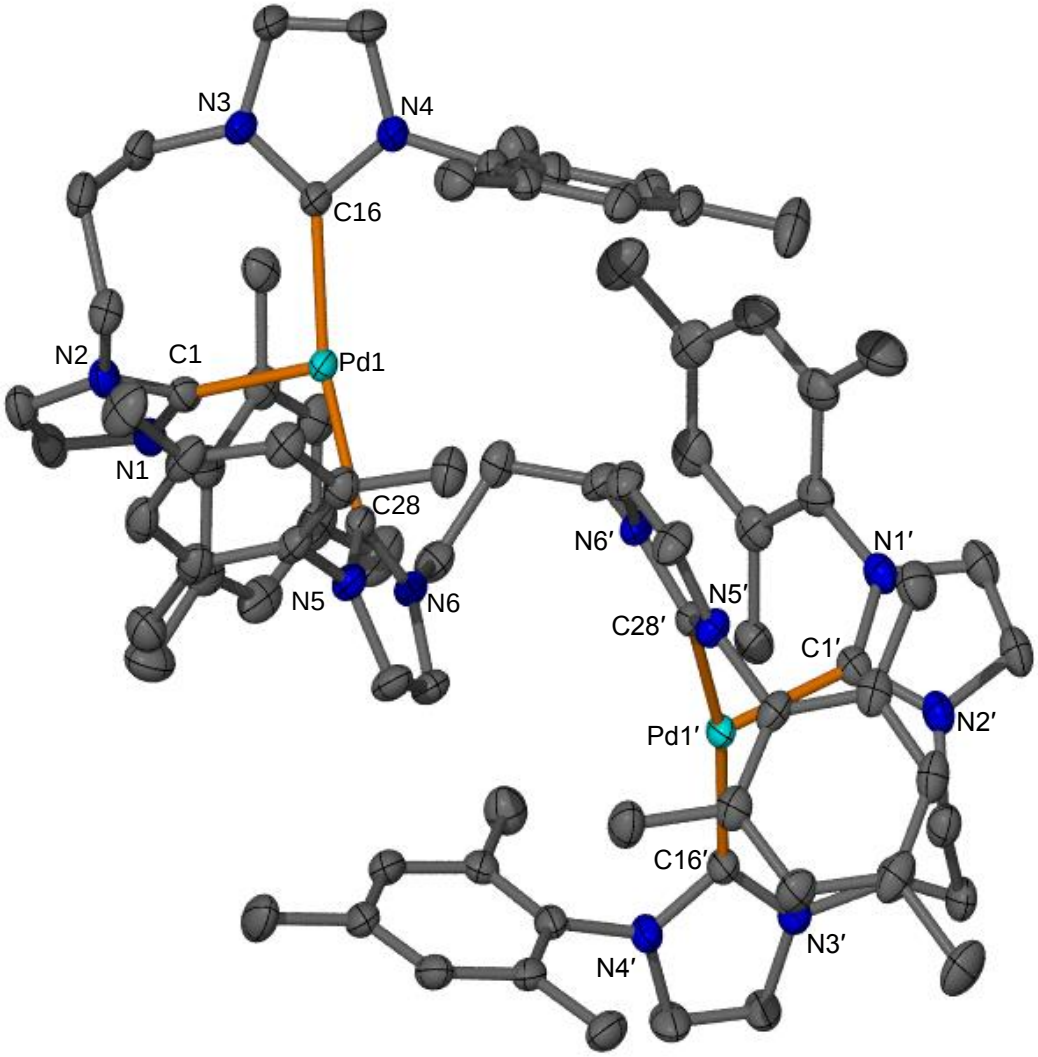

Figure 2.18. Molecular structure of the dication of [μ-{$(MesIm)_2(CH_2)_3$}{$(PdH)(MesIm)_2(CH_2)_3$}$_2$][PF_6]$_2$ **8** from X-ray crystallography. Displacement ellipsoids are shown at the 50 % probability level. Lattice solvent methanol, $[PF_6]^-$ counter anions, one of two equally disordered CH_2 linker atoms and hydrogen atoms are omitted for clarity. Selected bond lengths (Å) and angles (°): Pd1-C1,C16,C28 2.096(4),2.060(4),2.025(4), Pd1-C1-C16,C28 98.03(17),96.18(17), Pd1-C1-N1,N2, 133.8(3),122.2(3), Pd1-C16-N3,N4 132.9(3),123.8(3), Pd1-C28-N5,N6 125.2(3),129.9(3).

^{1}H NMR spectroscopy of **8** in CD_3OD indicated the presence of the hydride with two signals at -10.14 and -10.12 ppm. The spectrum also contained numerous

inequivalent signals consistent with the mixture of chelating and bridging ligands, as well as the two diastereomers which would occur due to slow chelate ring-flipping on the NMR timescale. A small amount of the dipalladium hydride species **7** was observed (^{1}H NMR spectroscopic hydride signal at -15.45 ppm) as an impurity, though the compound visually appeared free of the yellow contaminant.

Neither heating of the ^{1}H NMR sample of **8** or addition of sodium methoxide to the sample resulted in noticeable conversion of **8** towards the dipalladium hydride **7**, suggesting that this is a trapped reaction intermediate. Such an intermediate was suggested in the computational study for the methylene analogue **5a** (Scheme 2.4) as an early step transitioning from the chelate to bridging NHC binding modes. This mechanistic pathway also involved methoxide in a later step to reduce the palladium, though this reactivity is clearly not observed here.

Neutron diffraction was performed on a single crystal of **8** grown from methanol measuring 2.0 x 1.0 x 0.8 mm^3. Data was collected from two orientations of the crystal, where the sample was manually rotated 90 ° with respect to the instrument φ axis, to provide an enhanced sampling of the asymmetric volume of reciprocal space. The refined structure (Figure 2.19) confirmed the presence of the expected terminal hydride ligands.

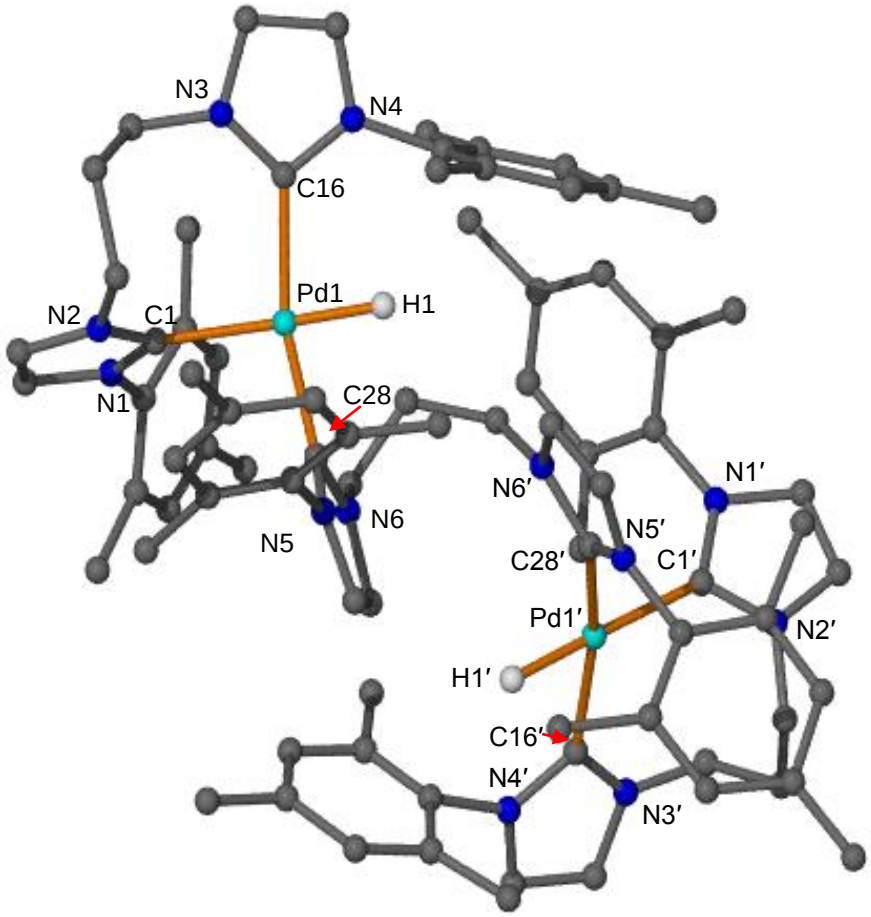

Figure 2.19. Molecular structure of the dication of $[\mu\text{-}\{(MesIm)_2(CH_2)_3\}\{(PdH)(MesIm)_2(CH_2)_3\}_2][PF_6]_2$ **8** from neutron diffraction. Structure was refined isotropically with spheres shown at an arbitrarily fixed radius of 0.2 Å. Lattice solvent methanol, $[PF_6]^-$ counter anions, disordered propylene linker atoms and all hydrogen atoms except H1 are omitted for clarity. Pd1-H1 1.59(3) Å.

The Pd-H distance of 1.59(3) Å is similar to that reported for the terminal Pd(II) hydride reported by Cavell (Figure 2.1(c)). The ^{1}H NMR hydride signal reported by Cavell at -10.17 ppm is also consistent with those of **8** at -10.14 and -10.12 ppm. Interestingly, Cavell reported a minor product with a hydride signal at -15.84 ppm, which was consistent with values observed for Pd(I) hydrides such as **5a** and **7**,

though they reported no success in this complex being isolated or characterised. As the triscarbene palladium hydride reported by Cavell was prepared by oxidative addition of palladium(0) rather than by reduction of palladium(II), the mechanism of the formation of any palladium(I) hydride species would likely involve markedly different mechanistic pathways.

2.3 Conclusion

The dipalladium(I) hydride species **5a**, produced under catalytically relevant conditions, has been shown to undergo solution hydride dynamics and was examined for possible solid state hydride dynamics.

Using simulations of possible solid state hydride dynamics we have shown it is difficult to determine barriers to slow transfer processes in complex systems that have many degrees of freedom. We have attempted to circumvent this by using approximations that may not be general, but have been demonstrated to be suitable for the system under study. In particular, we have used an MD simulation at a temperature that is high enough to yield the proposed hydride transfer process within our resource-limited time, but even though this is above the decomposition temperature, it is low enough that this does not occur within the simulation period. In this way the MD probes physically meaningful coordinates and takes account of the dynamics of the whole system, albeit somewhat limited close to the actual transfer barrier. Additional MD simulations show that it is not the amplitude of the dynamics that lead to hydride transfer, but rather a change in their geometry, or the onset of a new process. At least for these transfer-coordinates it is reasonable to extrapolate the low-temperature INS validation to the higher temperature dynamics.

Our examination of dipalladium(I) hydride analogues **5a** and **7** by neutron diffraction clearly show agostic and anagostic interactions that potentially limit any solid state hydride dynamics. Our discovery of the dipalladium(II) dihydride complex **8** as an apparent trapped intermediate is partially consistent with those proposed from DFT calculations probing the mechanism of the formation of the dipalladium(I) complexes as an example of the transition between chelating and bridging NHC ligand binding modes.

2.4 Experimental

2.4.1 General Conditions

All syntheses of imidazolium salts and the ligand exchange reactions for the formation of metal complexes **4a-b** were carried out in air, while the syntheses of the palladium complexes were conducted under an inert atmosphere of high purity argon (BOC gases) using standard Schlenk techniques. Compounds **1a-5a**[29] and **6**[30] were synthesised using literature methods. Handling of air-sensitive chemicals was carried out in a dry glove box (Innovative Technologies) under a nitrogen atmosphere with Schlenk type glassware. Anhydrous solvents used were obtained by passage through columns on an Innovative Technologies Solvent Purifier. All other reagents were purchased from Sigma-Aldrich and used as received. For non-air-sensitive syntheses, solvents were analytical grade and used as received.

2.4.2 Instrumentation

NMR spectroscopic studies were carried out on a 300 MHz Varian Gemini Mercury Plus spectrometer or a 400 MHz Bruker Avance 3 HD 400 MHz Wide Bore spectrometer with a 5 mm BBFO probe in CD_3OD, THF-d_8 or DMSO-d_6. NMR

spectral data were obtained at room temperature (293 K) unless specified otherwise. DMSO-d_6 and THF-d_8 was used as received, while CD_3OD was freeze-dried and stored over activated 4 Å molecular sieves.

^{1}H NMR and ^{13}C NMR spectra were obtained at 299.89 or 399.58 MHz and 100.48 MHz, respectively. ^{1}H NMR spectra were referenced to the ^{1}H resonance of the residual solvent peaks, while ^{13}C NMR spectra were referenced to the deuterated ^{13}C resonance. Elemental analysis was conducted by the Central Science Laboratory at the University of Tasmania using a Carlo Erba EA1108 Elemental Analyser.

Inelastic neutron scattering spectroscopy was performed using the time-of-flight spectrometer TOSCA at the ISIS facility in Chilton, UK.[40] Approximately 1 g of the samples of the isotopomers shown in Figure 2.8 were placed in an aluminium sachet, which was cooled in a standard closed-cycle cryostat. Spectral data were accumulated until an acceptable statistical quality was obtained at sample temperatures of 80 and 7 K. Data correction and transformation to the energy spectrum were made using standard local algorithms.

2.4.3 **X-ray Crystallography**

Data for **7** and **8** were collected at -123 and -173 °C, respectively, on a single crystal mounted on a Hampton Scientific cryoloop using a Bruker D8 Quest diffractometer with copper microfocused tube (λ= 1.54178 Å) with a nominal crystal to detector distance of 40 mm. The structures were solved by direct methods with SHELXS-97,[41] refined using full-matrix least-squares routines against F^2 with SHELXL-97, and visualised using X-SEED.[42] All non-hydrogen atoms were refined anisotropically. All hydrogen atoms were placed in calculated positions and refined using a riding model with fixed C-H distances of 0.95 Å (sp^2CH), 0.99 Å (CH_2),

0.98 Å (CH_3). The displacement parameters of all hydrogen atoms were estimated as $U_{iso}(H) = 1.2U_{eq}(C)$ except for CH_3 where $U_{iso}(H) = 1.5U_{eq}(C)$. CIF files for X-ray crystallographic analysis can be provided upon request.

2.4.4 **Neutron Diffraction**

KOALA VT Experiment of 5a

Variable temperature single crystal neutron diffraction studies were performed on a crystal of the dipalladium(I) hydride complex **5a** (unsolvated form from methanol) on the Laue diffractometer KOALA at ANSTO, New South Wales. The single flawless crystal measuring approximately 2x1x1 mm^3 was supported on an aluminium stand mounted in fluorinated silicon oil. The sample was cooled using a Cobra open flow nitrogen cooling system and diffraction data collected using Nimura special neutron image plate detectors.[43] Data sets were collected at 100, 200, 260 and 300 K and structure models comprising positional and isotropic displacement parameters for all atoms were refined by full-matrix least-squares in the CRYSTALS[36] program suite.

KOALA Experiments of 7 and 8

Single crystal neutron diffraction studies were performed on crystals of dipalladium hydride complexes $[\{(MesIm)_2(CH_2)_3\}Pd_2H][PF_6]$ **7** (unsolvated form from methanol) and $[\mu\text{-}\{(MesIm)_2(CH_2)_3\}\{(PdH)(MesIm)_2(CH_2)_3\}_2][PF_6]_2$ **8** on the Laue diffractometer KOALA at ANSTO, New South Wales. The single flawless crystals measuring approximately 0.70 x 0.70 x 0.15 mm^3 (**7**) and 2.0 x 1.0 x 0.8 mm^3 (**8**) were supported on an aluminium stand mounted in fluorinated silicon oil. The sample was cooled using a Cobra open flow nitrogen cooling system and diffraction data collected using Nimura special neutron image plate detectors.[43] Data sets were

collected at 150 K (**7**) and 100 K (**8**) and structure models comprising positional and isotropic displacement parameters for all atoms were refined by full-matrix least-squares in the CRYSTALS[36] program suite. CIF files for neutron crystallographic analysis can be provided upon request.

2.4.5 **Synthesis**

Preparation of selectively deuterated samples for TOSCA

20 g of *N*-mesitylimidazole **1a** was provided to the National Deuteration Facility at ANSTO for chemical deuteration. This was achieved by heating the compound at 150 °C for 3 days under pressure in deuterium oxide in the presence of a mixture of Pt/C and Pd/C catalysts and using 20 % v/v THF as a co-solvent.[32] The hydrothermal reaction mixture was purified using silica column chromatography to give deuterated MesIm (96 % yield) where the two *m*-phenyl protons remained essentially un-exchanged. Conversion to the deuterated diimidazolium salt using literature procedures[33] with deuterated dibromomethane (99 % D) resulted in an overall molecule deuteration of 84 ± 2 %. The deuteration percentages at each location of the molecule were calculated by ^{1}H and $^{13}C\{^{1}H,^{2}H\}$ NMR spectroscopy, along with mass spectrometry and isotopic distribution analysis to confirm the specific site, as well as the overall isotopic purity, respectively. **1b** (5.00 g, 25.21 mmol) was then reacted with CD_2Br_2 (4.44 g, 25.3 mmol) in identical conditions described earlier for **2**, to give **d-2** (7.91 g, 91%). This resulted in overall 84 ± 2 % deuteration, with individual position percentages calculated by mass spectrometry and ^{1}H and ^{2}H decoupled ^{13}C NMR spectroscopy.

^{1}H NMR (299.89 MHz, DMSO-d_6): δ 2.03 (0.39H, s, *o*-Me), 2.32 (0.24H, s, *p*-Me), 6.92 (0.05H, s, CH_2), 7.16 (3.72H, s, *m*-CH(mesityl)), 7.96 (0.10H, s,

CH(imidazolium)), 8.43 (0.05H, s, CH(imidazolium)), 9.96 (0.29H, s, CH(imidazolium)).

Synthesis of [{(^{D}MesIm)$_2$CDH$_2$}PdBr$_2$] 3b

In a modified literature procedure,[33] a Schlenk flask was loaded with deuterated imidazolium **2b** (2.56 g, 4.48 mmol) and palladium acetate (1.00 g, 4.47 mmol) and dried *in vacuo* at 70 °C. The solids were dissolved in DMSO (20 mL) and heated at 50 °C for 3 hours, then 110 °C for 2 hours. The solvent was removed *in vacuo* and the residue washed with DCM and collected by filtration as a pale yellow solid (2.80 g, 93 % yield).

^{1}H NMR (399.58 MHz, CD_3OD): 2.02 (~0.29H, bs, *o*-CH_3), 2.23 (~0.28H, bs, *p*-CH_3), 6.91 (~4H, d, J = 19.2 Hz, *m*-CH(mesityl)), 7.29 (~0.08H, bs, 2 x CH(imidazolium)), 7.83 (~0.08H, bs, 2 x CH(imidazolium)) (methylene linker protons not observed).

Synthesis of [{(^{D}MesIm)$_2$CD$_2$}Pd(NCMe)$_2$][PF$_6$]$_2$ 4b

In a modified literature procedure, complex **3b** (1.50 g, 2.22 mmol) and an excess of sodium hexafluorophosphate (2.96 g, 17.3 mmol) were dissolved in a 1:1 mixture of acetonitrile:water (200 mL each) and heated at 80 °C for 2 hours. The solution was cooled and acetonitrile removed *in vacuo*, and the resultant white precipitate was collected by filtration. The crude solid was dissolved in a minimal volume of acetonitrile and recrystallised by slow diffusion of diethyl ether to produce **4b** as a pure colourless crystalline solid (1.24 g, 63 % yield).

^{1}H NMR (299.89 MHz, DMSO-d_6): 7.12 (~ 4 x *m*-CH). All remaining signals were indistinguishable from baseline.

Synthesis of [{(^{D}MesIm)$_2$CD$_2$}$_2$Pd$_2$H][PF$_6$] 5b and [{(^{D}MesIm)$_2$CD$_2$}$_2$Pd$_2$H][PF$_6$] 5c

In a modified literature procedure, a Schlenk flask was charged with **4b** (0.60 g, 0.67 mmol) and an excess of sodium methoxide (0.13 g, 2.46 mmol). The solids were dissolved in methanol (20 mL) and the solution was heated at 50 °C for 2.5 hours. The red solution was filtered into a secondary Schlenk flask, the solution volume reduced *in vacuo* to *ca.* 10 mL and the solution cooled at -30 °C overnight. The resultant red crystalline solid was collected as pure **5b** in the desolvated form (0.34 g, 43 % yield). The fully deuterated isotopomer **5c** was prepared by dissolving a portion of **5b** in CD_3OD and heating at 50 °C for 48 hours to exchange the hydride ligand for deuteride.

Isotopomers **5a-5c** were recrystallised from THF-d_8 to form the deuterated THF solvate crystals suitable for the IINS experiment.

5b:

^{1}H NMR (299.89 MHz, THF-d_8): -14.48 (1H, s, Pd-H), 8.72 (~ 8H, bs, *m*-CH). All remaining signals were indistinguishable from baseline.

5c:

^{1}H NMR (299.89 MHz, THF-d_8): 8.72 (~ 8H, bs, *m*-CH). All remaining signals were indistinguishable from baseline.

Synthesis of [{(MesIm)$_2$(CH$_2$)$_3$}$_2$Pd$_2$H][PF$_6$] 7 and [μ-{(MesIm)$_2$(CH$_2$)$_3$}{(PdH)(MesIm)$_2$(CH$_2$)$_3$}$_2$][PF$_6$]$_2$ 8

In a modified literature procedure,[30] **6** (135.7 mg, 0.15 mmol) and sodium methoxide (20 mg, 0.37 mnol) were dried *in vacuo* and dissolved in methanol (10 mL). The solution was heated at 60 °C for 1.5 hours, where it took on a deep yellow colour. The solution was filtered and reduced *in vacuo* to 5 mL, yielding yellow crystals of **7** after slow cooling at – 30 °C which were spectroscopically identical to literature. The crystals of **7** were isolated by filtration and recrystallised from a freshly prepared methanol solution to produce large crystals suitable for neutron diffraction. (32 mg, 18 % yield).

The mother liquor was filtered again and reduced *in vacuo* further, and after resting at room temperature for *ca.* 1 week produced a mixture of small yellow crystals of **7** and large colourless crystals of **8** suitable for neutron diffraction.

While pure crystals of **7** and **8** suitable for diffraction were selected, the bulk of both products contained minor impurities of the other, preventing any ^{1}H NMR spectroscopic assignment besides the hydride and partial alkyl linker region. ^{13}C NMR spectroscopic data and reliable elemental microanalysis were also not obtained due to the inseparable mixture of products and diastereoisomers of **8**.

[μ-{(MesIm)$_2$(CH$_2$)$_3$}$_2$Pd$_2$H][PF$_6$] 7

^{1}H NMR (399.58 MHz, CD_3OD, partial assignment): δ -15.58 (1H, s, Pd-H), 3.67-4.04 (4H, m, 2 x *N*-CH_2), 6.20 (2H, t, *J* = 12 Hz, CH_2).

[μ-{(MesIm)$_2$(CH$_2$)$_3$}{(PdH)(MesIm)$_2$(CH$_2$)$_3$}$_2$][PF$_6$]$_2$ 8

^{1}H NMR (399.58 MHz, CD_3OD, partial assignment): δ -10.14 (1H, s, Pd-H), -10.12 (1H, s, Pd-H), 3.18 (2H, t, J = 13.4 Hz, CH_2).

Found: C, 55.80; N, 8.40; H, 6.30. Calc. for $C_{81}H_{98}N_{12}Pd_2P_2F_{12}.(CH_3OH)_4$: C, 54.57; N, 8.94; H, 6.14.

2.4.6 **Computational conditions**

DFT calculations

DFT calculations were undertaken by collaboration with Prof. Gordon Kearley and Dr. Nicolas de Souza at the Bragg Institute, ANSTO. All DFT calculations were carried out using plane-wave code, Vienna *ab initio* Simulation Package (VASP).[44-46] Isolated (or gas phase) molecule calculations were performed on an isolated $[\{(MesIm)_2CH_2\}_2Pd_2H]^+$ cation composed of 117 atoms contained in a periodic cell of dimensions 25 x 18 x 18 Å. This cell is large enough to avoid fictive intermolecular interactions. Geometry optimisation, vibrational dynamics, and MD simulations were made using the Projector Augmented Wave (PAW) potential [47] and the Perdew–Burke–Ernzerhof (PBE) exchange-correlation functional.[48] In all cases a single *k*-point was used (Γ-point) and for accurate calculations a 400 eV energy cut-off, with an electronic-energy convergence of 1.0 x 10^{-5} eV. For all MD simulations the energy cut-off was reduced to 300 eV and the electronic convergence to 1.0 x 10^{-4} eV, with a time step of 1 fs being used. The crystallographic unit cell volume is almost 7000 Å^3 and contains over 700 atoms so only a limited number of calculations was possible, and then only at low precision to obtain an estimate of the solid state effects on the H ligand dynamics.

Geometry optimisation

Geometry optimisation was achieved by allowing the atoms to relax to their minimum energy positions. For the crystal simulation the values of the cell constants were constrained to the experimental values and the full symmetry of the crystal structure was maintained during this optimisation. For the isolated molecule optimisation the initial conformation was taken from the crystal and relaxed with no symmetry constraints. The final molecular structure was very similar to the initial structure, illustrating that the crystal forces only play a minor role in determining the molecular conformation. An energy convergence criterion of 1.0×10^{-4} eV was used for the isolated molecule and 1.0×10^{-3} eV for the crystal.

Matrix method molecular vibrations

Normal mode vibrational frequencies and amplitudes were calculated for the molecule by obtaining the Hessian matrix using VASP with the same criteria as for the geometry optimisation. Atoms were displaced in positive and negative Cartesian directions from the minimum energy positions by 0.03 Å to determine the second derivatives of the energy. The INS spectrum was calculated from the frequencies and amplitudes using CLIMAX[49] applying the instrumental parameters from the TOSCA spectrometer. Spectra for all isotopomers were calculated using the same force constants, but with the appropriate atomic masses being used in the corresponding inverse kinetic energy matrix.

DFT-MD simulations

The matrix method used the harmonic approximation, which turned out to be a poor model for vibrations of the hydride ligand. *Ab initio* MD allowed exploration of the

form and origin of anharmonicity taking finite temperature of the sample into account, which is required not only for spectral agreement, but more importantly for the study of the H-transfer process. For all simulations a 4 ps equilibration on the energy minimised structure in the isokinetic ensemble at the target temperature was performed to distribute the kinetic energy within the system. For the periodic crystal model this was followed by 4.2 ps production run in the microcanonical ensemble. For the isolated molecule models, an additional 4 ps equilibration in the microcanonical ensemble was made followed by an 8.5 ps production run.

The MD trajectories from the low temperature runs were used to calculate the INS spectrum using nMoldyn.[50] This was achieved via the incoherent intermediate scattering function F(Q,t) that was calculated on a regular grid in both momentum transfer, Q, and time, t, which was then Fourier transformed to obtain the scattering function S(Q,u). The appropriate cut in Q,u was taken to coincide with the experimental INS spectrum on TOSCA. This spectrum was then convoluted with the instrumental resolution function to obtain the calculated INS spectrum.

2.5 References

[1] Nag, N. K. *J. Phys. Chem. B* **2001**, *105*, 5945.

[2] Hagen, C. M.; Vieille-Petit, L.; Laurenczy, G.; Suss-Fink, G.; Finke, R. G. *Organometallics* **2005**, *24*, 1819.

[3] Brayshaw, S. K.; Harrison, A.; McIndoe, J. S.; Marken, F.; Raithby, P. R.; Warren, J. E.; Weller, A. S. *J. Am. Chem. Soc.* **2007**, *129*, 1793.

[4] Chaudhuri, S.; Graetz, J.; Ignatov, A.; Reilly, J. J.; Muckerman, J. T. *J. Am. Chem. Soc.* **2006**, *128* 11404.

[5] Pérez Jigato, M.; Coussens, B.; King, D. A. *J. Chem. Phys.* **2003**, *118*, 5623.

[6] Ozawa, F.; Okamoto, H.; Kawagishi, S.; Yamamoto, S.; Minami, T.; Yoshifuji, M. *J. Am. Chem. Soc.* **2002**, *124*, 10968.

[7] Viciu, M. S.; Grasa, G. A.; Nolan, S. P. *Organometallics* **2001**, *20*, 3607.

[8] Zuideveld, M. A.; Kamer, P. C. J.; Leeuwen, P. W. N. M. v.; Klusener, P. A. A.; Stil, H. A.; Roobeek, C. F. *J. Am. Chem. Soc.* **1998**, *120*, 7977.

[9] Duan, Y.; Li, L.; Chen, M.; Yu, C.; Fan, H.; Zhou, Y. *J. Am. Chem. Soc.* **2014**, *136*, 7688.

[10] Baya, M.; Houghton, J.; Konya, D.; Champouret, Y.; Daran, J.-C.; Leñero, K. Q. A.; Schoon, L.; Mul, W. P.; Oort, A. B. v.; Meijboom, N.; Drent, E.; Orpen, A. G.; Poli, R. *J. Am. Chem. Soc.* **2008** *130* 10612.

[11] Duckett, S. B.; Newell, C. L.; Eisenberg, R. *J. Am. Chem. Soc.* **1994**, *116*, 10548.

[12] Evrard, D.; Groison, K.; Mugnier, Y.; Harvey, P. D. *Inorg. Chem.* **2004**, *43*, 790.

[13] Cugnet, C.; Lucas, D.; Collange, E.; Hanquet, B.; Vallat, A.; Mugnier, Y.; Soldera, A.; Harvey, P. D. *Chem. Eur. J.* **2007**, *13*, 5338.

[14] Mizoroki, T.; Mori, K.; Ozaki, A. *Bull. Chem. Soc. Jpn.* **1971**, *44*, 581.

[15] Heck, R. F.; Nolley, J. P. *J. Org. Chem.* **1972**, *37*, 2320.

[16] Grushin, V. V. *Chem. Rev.* **1996**, *96*, 2011.

[17] Brooks, E. H.; Glockling, F. *Chem. Commun.* **1965**, 510.

[18] Brooks, E. H.; Glockling, F. *J. Chem. Soc. (A)* **1967**, 1030.

[19] Schneider, M. L.; Shearer, H. M. M. *J. Chem. Soc., Dalton Trans.* **1973**, 354.

[20] Moulton, C. J.; Shaw, B. L. *J. Chem. Soc., Dalton Trans.* **1976**, 1020.

[21] Clement, N. D.; Cavell, K. J.; Jones, C.; Elsevier, C. J. *Angew. Chem. Int. Ed.* **2004**, *43*, 1277.

[22] Johansson, R.; Wendt, O. F. *Organometallics* **2007**, *26*, 2426.

[23] Fryzuk, M. D.; Lloyd, B. R.; Clentsmith, G. K. B.; Rettig, S. J. *J. Am. Chem. Soc.* **1994**, *116*, 3804.

[24] Portnoy, M.; Frolow, F.; Milstein, D. *Organometallics* **1991**, *10*, 3960.

[25] Young, S. J.; Kellenberger, B.; Reibenspies, J. H.; Himmel, S. E.; Manning, M.; Anderson, O. P.; Stille, J. K. *J. Am. Chem. Soc.* **1988**, *110*, 5744.

[26] Rimml, H.; Venanzi, L. M. *J. Organomet. Chem.* **1984**, *260*, C52.

[27] Herbert, D. E.; Ozerov, O. V. *Organometallics* **2011**, *30*, 6641.

[28] Evrarda, D.; Meilleura, D.; Drouina, M.; Mugnierb, Y.; Harvey, P. D. *Z. Anorg. Allg. Chem.* **2002**, *628*, 2286.

[29] Boyd, P. D. W.; Edwards, A. J.; Gardiner, M. G.; Ho, C. C.; Lemee-Cailleau, M.-H.; McGuinness, D. S.; Riapanitra, A.; Steed, J. W.; Stringer, D. N.; Yates, B. F. *Angew. Chem. Int. Ed.* **2010**, *49*, 6315

[30] Ho, C. C. Structural and Mechanistic Investigations of Systematically Modified Bis(NHC) Palladium Complexes (PhD Thesis), University of Tasmania, Hobart, **2015**.

[31] http://www.ncnr.nist.gov/resources/n-lengths/, accessed October 20, **2011**.

[32] Darwish, T. A.; Smith, A. R. G.; Gentle, I. R.; Burn, P. L.; Luks, E.; Moraes, G.; Gillon, M.; Holden, P. J.; James, M. *Tetrahedron Lett.* **2012**, *53*, 931.

[33] Gardiner, M. G.; Herrmann, W. A.; Reisinger, C.; Schwarz, J.; Spiegler, M. *J. Organomet. Chem.* **1999**, *572*, 239.

[34] Johnson, M. R.; Kearley, G. J., in *Neutron Scattering-Fundamentals, Vol. 44*, Academic Press, San Diego, **2013**, pp. 419-420.

[35] Plazanet, M.; Fukushima, N.; Johnson, M. R.; Horsewill, A. J.; Trommsdorff, H. P. *J. Chem. Phys.* **2001**, *115*, 3241.

[36] Betteridge, P. W.; Carruthers, J. R.; Cooper, R. I.; Prout, K.; Watkin, D. J. *J. Appl. Cryst.* **2003**, *36*, 1487.

[37] Scholer, S.; Wahl, M. H.; Wurster, N. I.; Puls, A.; Hattig, C.; Dyker, G. *Chem. Commun.* **2014**, *50*, 5909.

[38] Braga, D.; Grepioni, F.; Tedesco, E.; Biradha, K.; Desiraju, G. R. *Organometallics* **1997**, *16*, 1846.

[39] Brookhart, M.; Green, M. L. H. *J. Organomet. Chem.* **1983**, *250*, 395.

[40] Ramirez-Cuesta, A. J.; Parker, S. F.; Tomkinson, J., in *TOSCA User Guide*,

[41] Sheldrick, G. M., *SHELX97*, Programs for Crystal Structure Analysis, Universität Göttingen, Germany, **1998**.

[42] Barbour, L. J. *J. Supramol. Chem.* **2001**, *1*, 189.

[43] Shaikh, A. M. **2012**, Applications of various imaging techniques in neutron radiography at BARC, Trombay, in *18th World Conference on Nondestructive Testing*, Durban, South Africa.

[44] Kresse, G.; Furthmuller, J. *Comput. Mater. Sci.* **1996**, *6*, 15.

[45] Kresse, G.; Hafner, J. *Phys. Rev. B: Condens. Matter Mater. Phys.* **1993**, *47*, 558.

[46] Kresse, G.; Joubert, D. *Phys. Rev. B: Condens. Matter Mater. Phys.* **1999**, *59*, 1758.

[47] Blochl, P. E. *Phys. Rev. B: Condens. Matter Mater. Phys.* **1994**, *50*, 17953.

[48] Perdew, J. P.; Burke, K.; Ernzerhof, M. *Phys. Rev. Lett.* **1996**, *77*, 3865.

[49] Kearley, G. J. *Nucl. Instr. Meth. Phys. Res.* **1995**, *354*, 53.

[50] Kneller, G. R.; Keiner, V.; Kneller, M.; Schiller, M. *Comput. Phys. Commun.* **1995**, *91*, 191.

Chapter 3: Investigation of Intermediates in the Formation of Chelating Palladium(II) Complexes

3.1 Introduction

As discussed briefly in Chapter 1, transition metal complexes bearing NHC ligands are used in a wide range of applications. The formation of these complexes can be achieved *via* a range of methods, which are often tailored to suit the particular system (Scheme 3.1). The most common method involves the deprotonation of an azolium precursor with an appropriate base to form a free carbene, which can then coordinate to the metal.

Frequently the free carbene is formed *in situ* upon reaction with an appropriate metal salt containing, or in the presence of base, such as palladium acetate.[1] This increased atom economy leads to more efficient syntheses (Scheme 3.1(a)). Strong bases such as potassium bis(trimethylsilyl)amide or potassium *t*-butoxide have also been used to deprotonate the azolium, where the free carbene is isolated or used *in situ* and coordinated to a suitable metal in a subsequent reaction (Scheme 3.1(b)).[2,3]

Free carbenes are, however, often unstable and frequently necessitate low temperatures or inert conditions for the reaction to proceed without decomposition. Even when the deprotonation of the azolium occurs *in situ* the free carbene must be transiently stable. Should a more acidic proton be present in the azolium ligand precursor, it is possible that multiple sites apart from the targeted carbene site can be deprotonated, resulting in various products.

On-metal assembly (Scheme 3.1(c)) of NHC-metal complexes is achieved *via* the reaction of a suitable nucleophile with a metal-coordinated isonitrile.[4] This can limit the scope of substituents present on the final NHC species.

Oxidative addition of a halogenated azolium to low valent metal precursors has been used for a range of systems, though this does require additional synthesis to form the halogen-substituted compound (Scheme 3.1(d)).[5] C-H oxidative addition has also been shown as a potentially viable method for some select systems.[6]

Synthesis *via* transmetallation from a silver NHC complex (Scheme 3.1(e)), is especially useful for systems where the free carbene is transiently unstable as the silver coordination is thought to occur in a base-mediated proton abstraction.[7] The silver is displaced easily upon reaction with a transition metal precursor to form the desired transition metal NHC complex, however reactions and complexes involving silver are frequently photosensitive and there is poor atom economy in the transmetallation reaction.

Preparation of bidentate bis(NHC) complexes in particular can be more difficult than mono carbene complexes. Often the linker groups joining the azolium moiety can contain acidic protons which may exclude the use of some base deprotonation methods. On-metal templating is also not generally suitable for chelating ligands, while transmetallation *via* a silver NHC complex is often used to produce chelating complexes, there are stoichiometry issues for some systems that can result in poor atom economy and low yields.

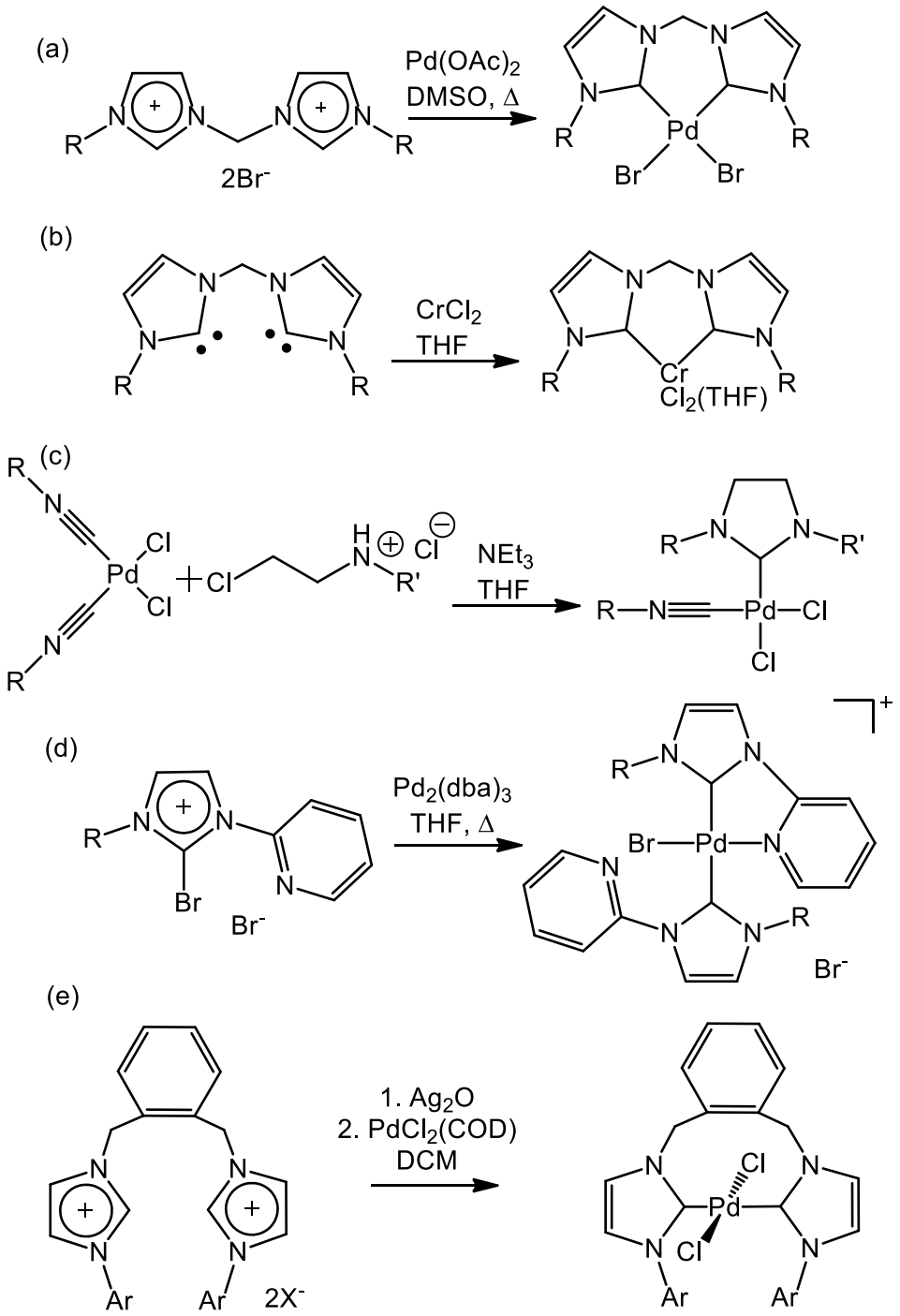

Scheme 3.1. *In situ* deprotonation of azolium salt precursors **(a)**,[1] free carbene complex synthesis **(b)**,[2] on-metal template synthesis **(c)**,[4] C-X oxidative addition to low-valent metal precursors **(d)**,[6] and transmetallation *via* a silver NHC complex **(e)**.[7]

While the majority of NHC complexes used for catalytic applications have monodentate ligand systems, a range of bidentate or multidentate NHC complexes have been reported.[6,7] It has been generally noted that the these bidentate ligands offer increased complex stability and disfavour the cleavage of the NHC carbon-metal bond.[8] The bidentate coordination mode is ideal for many catalytic procedures as it helps minimise catalyst decomposition where harsh reaction conditions are necessary.

One system of particular interest to us are the *N*,*N′*-disubstituted methylene linked chelated bis(NHC) palladium(II) dihalide complexes first prepared by Herrmann and co-workers as catalysts for the copolymerisation of CO and ethylene, and carbon-carbon coupling reactions.[1,9] These complexes were formed *via* the *in situ* deprotonation of the diimidazolium salt with palladium acetate using a multistage heating regime (Scheme 3.2) which was shown to produce significantly higher yields of the desired product and reduced decomposition of palladium than utilising a single stage heating step.

For the *N*-*t*-butyl substituted bis(NHC) palladium complex, our research group confirmed that the reaction proceeded *via* the formation of a pendant imidazolium mono(NHC) palladium dihalide acetate complex, where this intermediate could be isolated prior to the secondary heating stage. Hydrogen bonding between the imidazolium C-2 proton and the acetate oxygen in the pendant imidazolium mono(NHC) palladium dibromide acetate complex was inferred by the significant downfield shift of the C-2 proton at 11.16 and 11.41 ppm for the bromide and iodide analogues, respectively. It was also observed that longer reaction times (> *ca.* 12 hours) at this first heating stage to form the mono(NHC) complex could result in the substitution of the acetate group with a third halide to form a

non-reactive mono(NHC) palladium trihalide complex alongside other decomposition products.

Other analogues containing bulkier substituents such as *N*-mesityl were also investigated and showed better activity in the aforementioned catalytic applications, though no pendant imidazolium mono(NHC) intermediates for these were observed.[9]

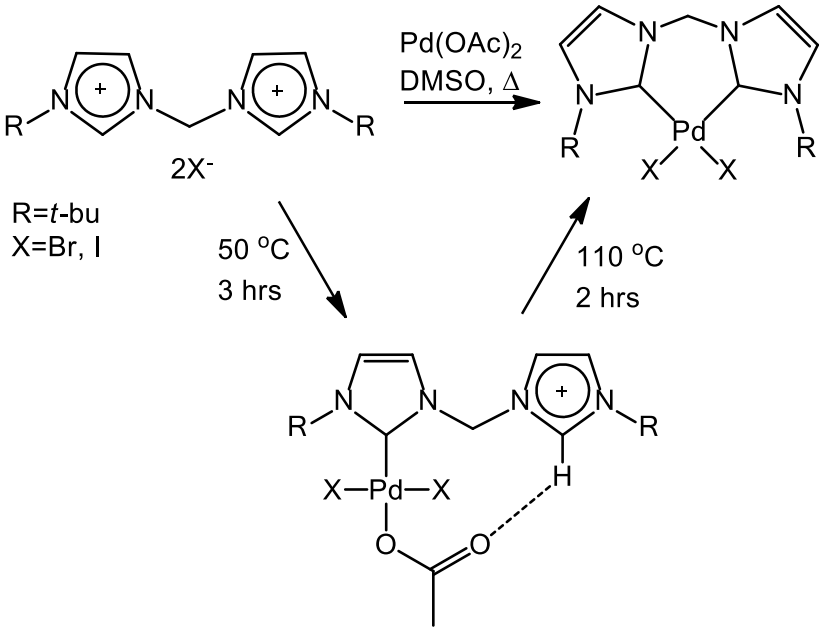

Scheme 3.2. Synthesis of chelated bis(NHC) palladium dihalide complex *via* pendant imidazolium mono(NHC) palladium dihalide acetate intermediate.

Recent work in our group has expanded on this ligand motif, focusing especially on extending the alkyl linker. In the case of the ethylene linked *N*-mesityl substituted analogue an unexpected secondary reaction pathway was observed. The pendant imidazolium mono(NHC) palladium complex was initially formed, however progression to the second heating stage resulted in the formation of two products (Scheme 3.3). In some instances the expected chelated bis(NHC) complex was isolated, however repetitions under similar conditions resulted in an unusual rearrangement of the imidazolium to form an isolable mono(NHC) palladium

tribromide complex (denoted **I** throughout). This complex featured bis(NHC) coupling through the C-4 position, resulting in a tricyclic mono(NHC) palladium tribromide arrangement. Both the chelated bis(NHC) palladium dibromide and the rearranged mono(NHC) palladium tribromide complexes were isolated in yields of <15 %.[10]

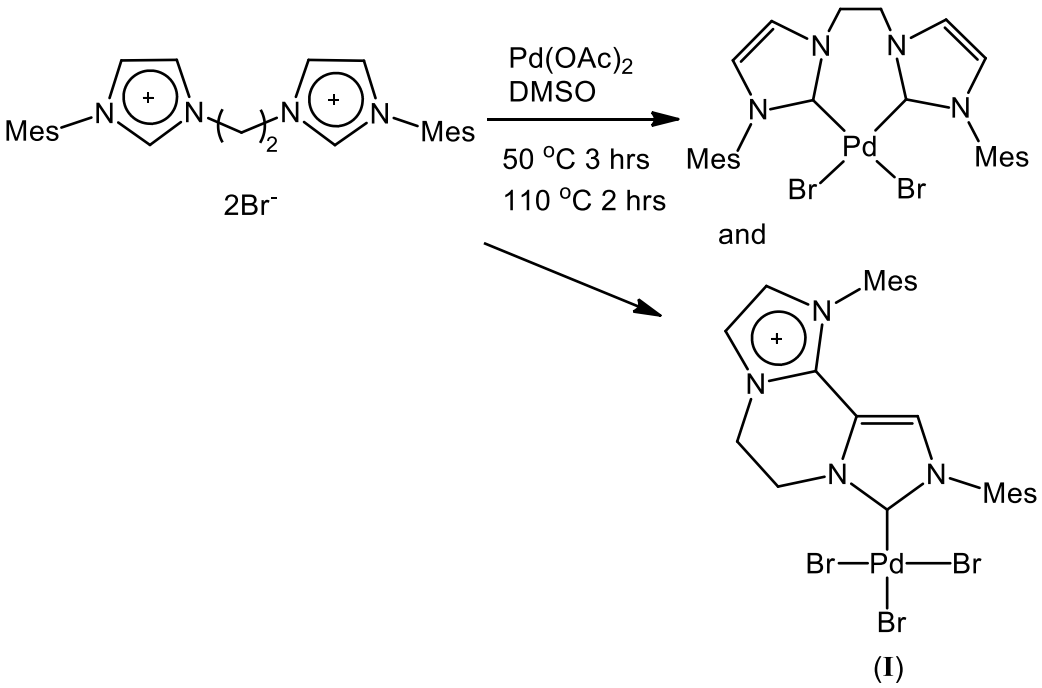

Scheme 3.3. Synthesis of conventional *N*-mesityl ethylene linked chelated bis(NHC) palladium(II) dibromide and the unexpected mono(NHC) palladium(II) tribromide complexes.[10]

The relatively low yields of extended alkyl linker bis(NHC) palladium(II) complexes with bulky *N*-substituents,[9,10] and the variability in synthetic outcome for the *N*-mesityl ethylene linked analogue[10] led us to probe the intermediate obtained after the initial heating stage. We sought to examine whether isolation and modification of the pendant imidazolium mono(NHC) palladium dihalide acetate species could help increase the yields and direct the reaction favourably towards the desired product.

For the initial study we used the *N*-*t*-butyl methylene linked diimidazolium analogues as they have been shown to be isolable under moderate conditions.[1] We proposed modifications to the ancillary halides, and to the basicity of the acetate group to investigate whether there were improvements in the hydrogen bonding interaction between the acetate oxygen and the imidazolium C-2 proton (Scheme 3.4). These modifications may improve yields for this catalytically relevant class of compounds, and will allow us to examine a wider range of analogues with further variations in the *N*-substituents and linkers, which may otherwise not be accessible.

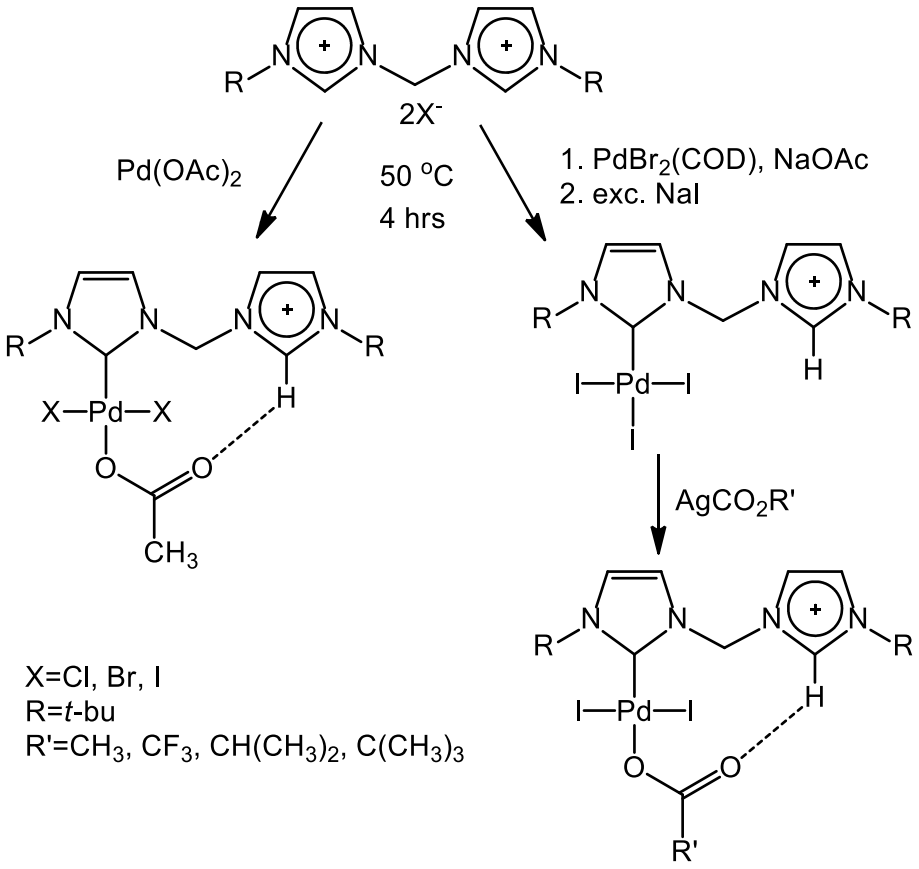

Scheme 3.4. Proposed variations of pendant imidazolium mono(NHC) palladium dihalide acetate intermediate motif.

3.2 Results and Discussion

3.2.1 Effect of Different Halides in Mono(NHC) Pendant Intermediates

Herrmann and coworkers have previously reported the synthesis of the palladium dihalide acetate complexes [{(tBuIm)(tBuImH)CH_2}$PdBr_2CO_2CH_3$] **11b** and [{(tBuIm)(tBuImH)CH_2}$PdI_2CO_2CH_3$] **11c**.[1] Both complexes were characterised, by ^1H and ^{13}C NMR spectroscopy, elemental analysis and, in the case of the iodide analogue **11c**, X-ray crystallography. No X-ray crystallographic characterisation has been reported for the bromide analogue **11b**, however.

The dibromide acetate complex **11b** was prepared *via* the literature procedure, with the reaction of palladium acetate and the diimidazolium dibromide salt **9a** in DMSO at 50 °C for 4 hours (Scheme 3.5). DMSO was removed *in vacuo*, and the yellow residue was dissolved in a 1:1 mixture of acetonitrile and water at 50 °C. The acetonitrile was then removed *in vacuo* to produce **11b** as a yellow precipitate which was collected by filtration.

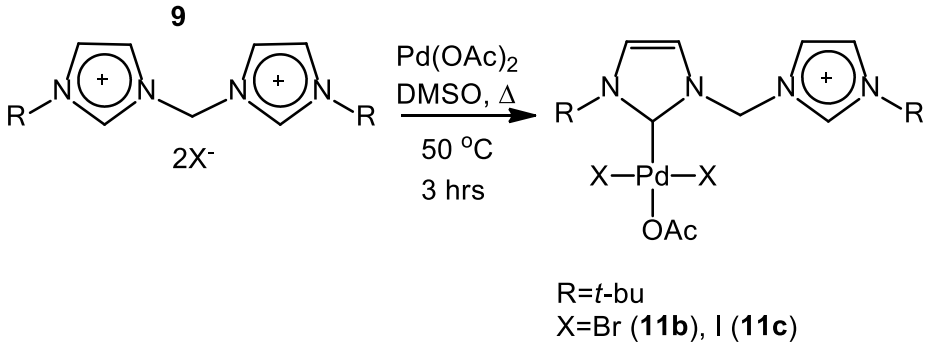

Scheme 3.5. Synthesis of pendant imidazolium mono(NHC) palladium dihalide acetate complexes reported by Herrmann.[1]

^{1}H NMR spectroscopy was used to confirm the product was consistent with literature[1] and crystals suitable for X-ray diffraction studies were produced by slow evaporation of a concentrated acetonitrile solution (Figure 3.1).

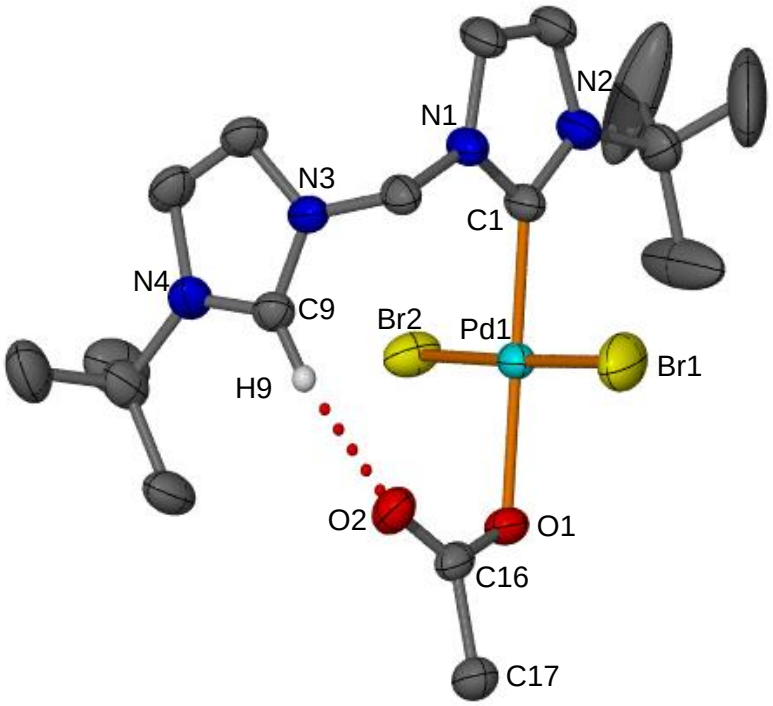

Figure 3.1. Molecular structure of [{(tBuIm)(tBuImH)CH_2}$PdBr_2CO_2CH_3$] **11b**. Displacement ellipsoids are shown at the 50 % probability level. All hydrogen atoms except H16 are omitted for clarity. Selected bond lengths (Å) and angles (°): Pd1-C1 1.972(5), Pd1-Br1,Br2 2.4311(10),2.4430(9) , Pd1-O1 2.067(4), C9···O2 3.103(7), C1-Pd1-Br1,Br2 86.9(2),91.5(2), O1-Pd1-Br1,Br2 89.15(13),92.45(13), Pd1-C1-N1,N2 120.1(4),134.6(5).

X-ray crystallography confirmed that the structures of **11b** and the iodide analogue **11c** previously reported by Herrmann were isostructural with the palladium centre adopting the expected square planar geometry alongside the pendant imidazolium mono(NHC) arrangement of the ligand. Large displacement parameters were

observed due to the C-C torsional disorder on one of the *t*-butyl groups, however attempts to model these atoms as a two-site disorder did not improve the refinement. The acetate ligand showed the expected η^1 terminal bonding arrangement which allowed the non-bound oxygen to interact with the C-2 proton on the pendant imidazolium. As the hydrogen positions were calculated in the X-ray structure, it is not possible to accurately determine the O2-H9 distance as a measure of the hydrogen bonding from this method. We can however compare the C9···O2 distance of the various analogues to provide some measure of the strength of the interaction. A comparison of the C9···O2 distances for all the complexes is provided at the end of this section.

Preparation of a dichloride analogue of the imidazolium salt **9a** was not achieved. The pendant imidazolium mono(NHC) trichloride complex **10a** was prepared by heating imidazolium **9a**, palladium chloride and one equivalent of sodium acetate at 50 °C for 4 hours. An excess of sodium chloride was added and the suspension was heated for a further hour, after which the solvent was removed *in vacuo* (Scheme 3.6). The complex was isolated by dissolving the residue in a 1:1 mixture of acetonitrile:water and heating for 10 minutes at 80 °C, after which the acetonitrile was removed *in vacuo* and the yellow precipitate was collected by filtration.

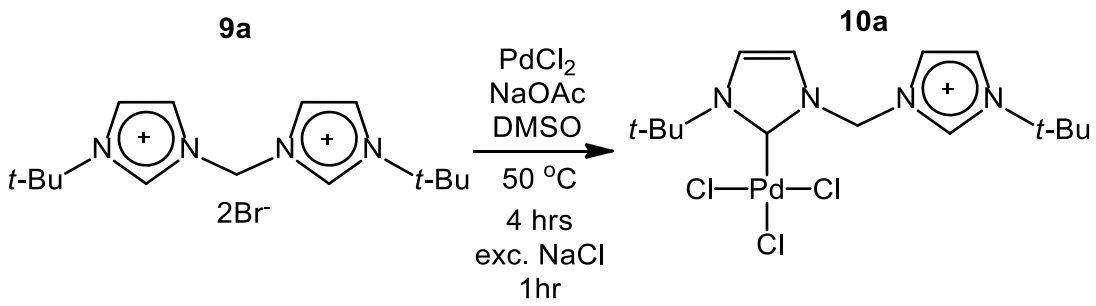

Scheme 3.6. Synthesis of pendant imidazolium mono(NHC) palladium trichloride complex **10a**.

^{1}H NMR spectroscopic analysis indicated the presence of one major product and multiple similar compounds in smaller amounts, presumably with various arrangements of Br/Cl scrambling. X-ray crystallography corroborated this mixture with crystals grown from slow evaporation of acetonitrile. The halide ligands *cis* to the NHC were modelled as an approximate 1:1 mixture of bromides and chlorides, while the halide *trans* to the carbene refined well as a chloride (Figure 3.2).

An alternative route to procure the pure chloride complex was attempted by counteranion exchange of **9a** from bromide to hexafluorophosphate and subsequent reaction of this imidazolium salt under the conditions shown in Scheme 3.6. The counteranion exchange of imidazolium **9a** was successful, though attempts to procure the pure trichloride complex *via* subsequent reaction with palladium chloride, sodium acetate and an excess of sodium chloride was unsuccessful, with only minute yields (< 1 %) of impure product produced.

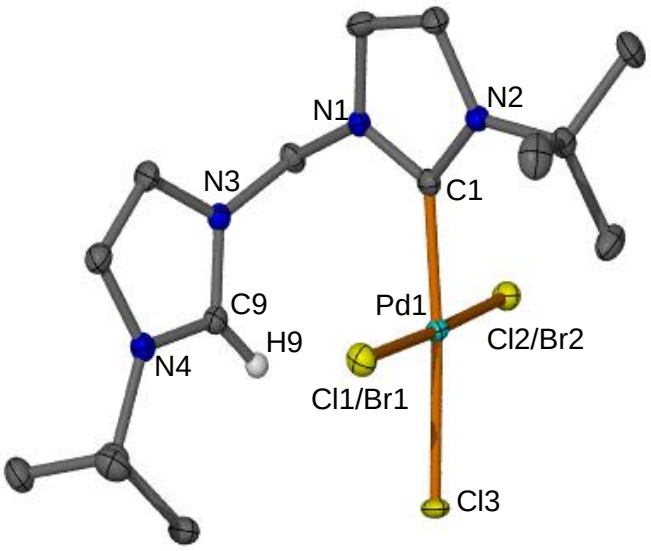

Figure 3.2. Molecular structure of [{(tBuIm)(tBuImH)CH_2}$PdCl_xBr_y$] **10a**. Displacement ellipsoids are shown at the 50 % probability level. All hydrogen atoms except H9 are omitted for clarity. Selected bond lengths (Å) and angles (°): Pd1-C1 1.960(3), Pd1-Cl1/Br1,Cl2/Br2,Cl3 2.3924(6),2.3899(6),2.3773(7), C1-Pd1-Cl1/Br1,Cl2/Br2 86.94(8),91.12(8), Cl3-Pd1-Cl1/Br1,Cl2/Br2 92.00(2),89.87(2), Pd1-C1-N1,N2 122.2(2),132.1(2).

The minor products formed alongside **10a** were not separable by recrystallisation so the mixture was used to prepare the acetate species **11a** using silver acetate, resulting in a yellow solid which again was an impure mix of the expected dichloride acetate **11a** and some minor products with Br/Cl scrambling. Consistent microanalysis was not obtained for the halide scrambled products **10a** and **11a** as the Cl:Br ratios of the *cis* halides, while close to 1:1, had minor variations between batches.

Crystals of **11a** suitable for single crystal X-ray diffraction were produced by slow evaporation of a concentrated acetonitrile solution and a single crystal containing essentially pure **11a** was used for structural characterisation (Figure 3.3). The

structure is isomorphic to the dibromide acetate analogue **11b** and isostructural to the other acetate analogues as expected, including the C-C torsional disorder on one of the *t*-butyl ligands shows some disorder of the free-rotating methyl groups. Attempts to model these atoms as a two-site disorder did not improve the refinement.

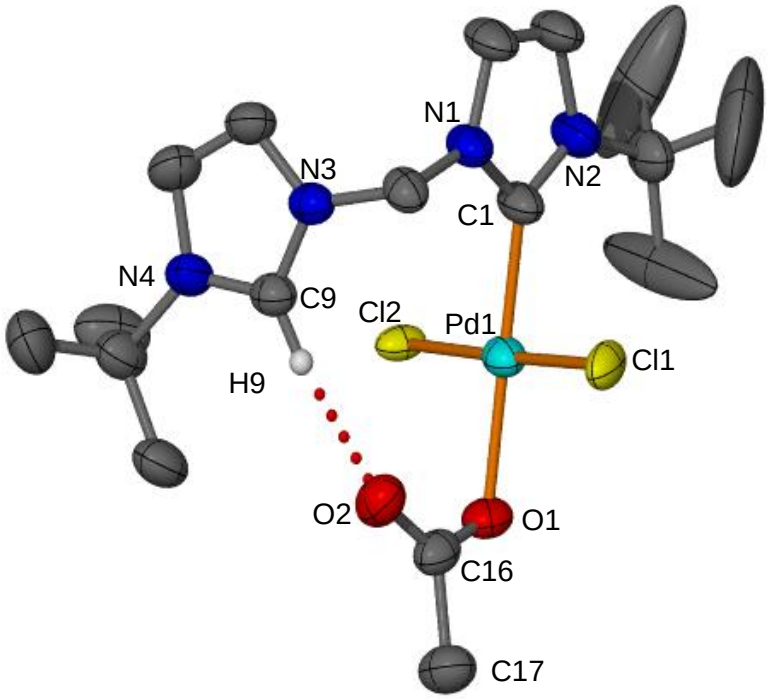

Figure 3.3. Molecular structure of [{(tBuIm)(tBuImH)CH_2}$PdCl_2CO_2CH_3$] **11a**. Displacement ellipsoids are shown at the 50 % probability level. All hydrogen atoms except H9 are omitted for clarity. Selected bond lengths (Å) and angles (°): Pd1-C1 1.967(6), Pd1-Cl1,Cl2 2.3337(16),2.3686(15), Pd1-O1 2.066(5), C9···O2 3.098(9), C1-Pd1-Cl1,Cl2 86.8(2),91.7(2), O1-Pd1-Cl1,Cl2 89.91(15),91.60(15), Pd1-C1-N1,N2 119.5(5),134.6(5).

The ^{1}H NMR chemical shift of the C-2 protons and the C9···O2 distances from the X-ray crystal structures of the various halide analogues **11a**, **11b** and **11c** are summarised in Table 1.

Table 1. Comparison of ^{1}H NMR chemical shift of the imidazolium C-2 proton and C9···O2 distances of analogues **11a**, **11b** and **11c**.

Compound	Halide	^{1}H NMR shift (ppm)	C9···O2 (Å)
11a	Cl	11.59	3.098(9)
11b	Br	11.44	3.103(7)
11c	I	11.17	3.067(6)

There is a significant increase in the downfield shift of the C-2 proton as the halide size is reduced, though the C···O distances display no obvious trend. This suggests that while the smaller halides appear to favour hydrogen bonding in solution, this trend is not observed in the solid state structures.

3.2.2 Effect of Different Acetate Substituents in Pendant Mono(NHC) Intermediates

The pendant imidazolium mono(NHC) palladium diiodide acetate complex **11c** was previously isolated and characterised by X-ray crystallography.[1] For convenience, the pendant imidazolium mono(NHC) triiodide complex **10c** was prepared by the reaction of **9a**, $PdBr_2$(COD), and one equivalent of sodium acetate in DMSO at 50 °C for 4 hours, followed by addition of an excess of sodium iodide and further heating for 1 hour. The DMSO was removed *in vacuo* and the residue dissolved in a 1:1 mixture of acetonitrile:water and heated at 80 °C for 10 minutes. Acetonitrile was removed *in vacuo* and the red precipitate collected and dried as pure [{(tBuIm)(tBuImH)CH_2}PdI_3] **10c**. This method had the added advantage of being amenable to higher temperatures than the literature method, allowing for easier isolation and purification of the triiodide complex.

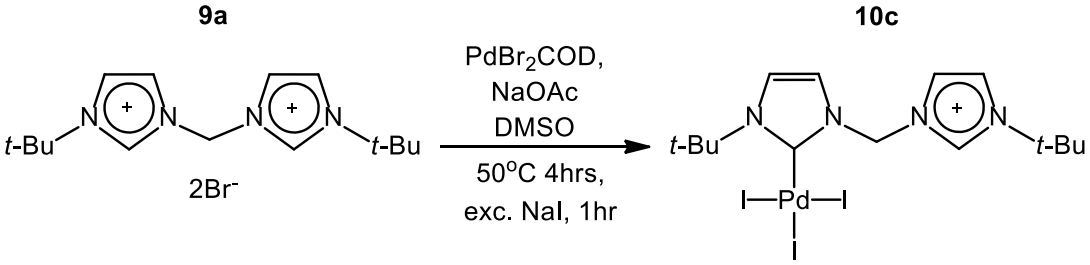

Scheme 3.7. Synthesis of [{(tBuIm)(tBuImH)CH_2}PdI_3] **10c.**

Complex **10c** was reacted with a range of silver acetate species to form the series of palladium dihalide acetate complexes **11c-11f**. The triiodide analogue was used in this case due to the increased lability of iodide compared to bromide ligands, which helped promote formation of the acetate complex.

Preparation of [{(tBuIm)(tBuImH)CH_2}PdI_2CO_2R] analogues **11c-11f** was achieved by reacting the triiodide species **10c** with one equivalent of the appropriate silver acetate salt in methanol. The solution was stirred for 4 hours with the exclusion of light and the resultant silver halide precipitate was removed by filtration. Complexes **11c-11f** were then isolated by removal of solvent *in vacuo* and crystals of each suitable for X-ray diffraction were produced by slow evaporation of a concentrated acetonitrile solution. The crystals for the isomers **11c-11f** were similar in appearance, growing as thin rectangular orange prisms. All four isomers displayed dichroic behaviour with a colour change from orange to yellow observed when an individual crystal was rotated 90 ° under a polarised microscope.

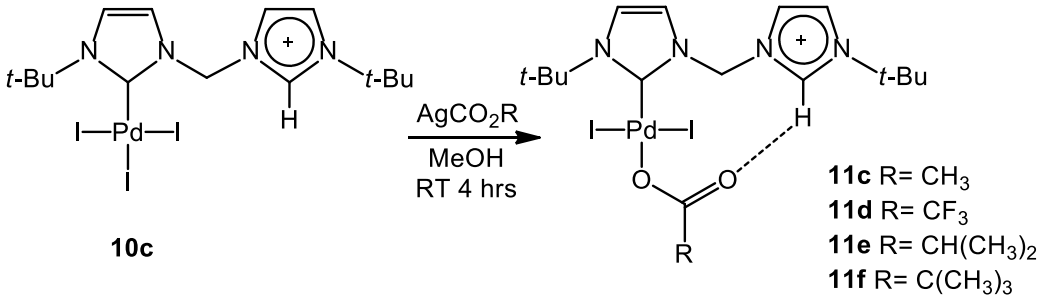

Scheme 3.8. Synthesis of pendant imidazolium mono(NHC) palladium dihalide acetate analogues **11c-11f**.

The dihalide acetate complex [{(tBuIm)(tBuImH)CH_2}$PdI_2CO_2CH_3$] **11c** was produced in moderate yield as an orange solid. ^{1}H NMR spectroscopy of **11c** was consistent with literature,[1] where the unsymmetrical pendant imidazolium mono(NHC) ligand arrangement was confirmed *via* retention of the five inequivalent NHC/imidazolium C-4/5 hydrogens and the inequivalent *t*-butyl groups. The previously noted downfield shift of the C-2 proton on the pendant imidazolium from 9.63 ppm in the triiodide complex **10c** to 11.17 ppm was also observed. X-ray crystallographic data was collected on orange crystals of **11c** and confirmed the structure matched that previously reported (Figure 3.4).[1]

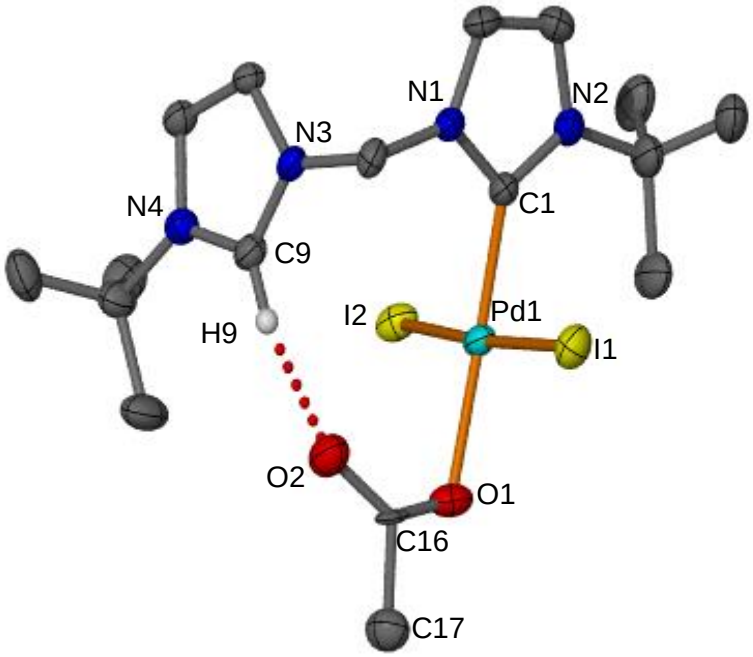

Figure 3.4. Molecular structure of [{(tBuIm)(tBuImH)CH_2}$PdI_2CO_2CH_3$] **11c**. Displacement ellipsoids are shown at the 50 % probability level. All hydrogen atoms except H9 are omitted for clarity. Selected bond lengths (Å) and angles (°): Pd1-C1 1.959(5), Pd1-I1,I2 2.6082(7),2.6335(7), Pd1-O1 2.091(4), C9···O2 3.067(6), C1-Pd1-I1,I2 85.86(16),90.20(16), O1-Pd1-I1,I2 89.41(11),94.80(11), Pd1-C1-N1,N2 119.2(3),135.3(4).

The analogue with a less basic acetate substituent, [{(tBuIm)(tBuImH)CH_2}$PdI_2CO_2CF_3$] **11d** was produced from **10c** and silver trifluoroacetate in moderate yield as an orange solid. ^{1}H NMR spectroscopy of **11d** was consistent with the expected structure. The unsymmetrical pendant imidazolium mono(NHC) ligand arrangement was confirmed *via* retention of the five inequivalent NHC/imidazolium C-4/5 hydrogens and the inequivalent *t*-butyl groups. The downfield shift of the C-2 proton on the pendant imidazolium from 9.63 ppm in **10c** to 9.76 ppm in **11d** is significantly less than the shift observed for the more basic

acetate **11c**. ^{13}C NMR spectroscopy showed the resonance for the C-2 carbon was at 136.6 ppm. X-ray crystallographic data was collected on orange crystals of **11d** for structural characterisation, shown in Figure 3.5.

Structural analysis showed the palladium adopting the expected square planar geometry with essentially isostructural carbene and acetate bonding arrangements to the acetate complex **11c**. One of the *N*-*t*-butyl groups displayed large displacement parameters due to the C-C torsional disorder, however attempts to model these atoms as a two-site disorder did not improve the refinement. The Pd1-C1 distance was identical within error between the analogues, while Pd1-I1 and Pd1-I2 distances were shorter in **11d**. The Pd1-O1 distance in **11d** appeared to be elongated to 2.116(4) Å (Δ0.025 Å increase compared to **11c**), though this was not a statistically significant increase. Surprisingly the C9···O2 distance was reduced in **11d** by 0.07 Å, contrary to our expectation that the less basic acetate species would decrease the hydrogen bonding interaction. It appeared that the Pd1-O1 and C9···O2 distances were affected by a combination of electronic and steric effects. Thus the Pd1-O1 bond was elongated. The shorter C···O distance might imply greater hydrogen bonding interaction, which was unexpected for this less basic acetate. A comparison of the C9···O2 distances for all the complexes with varied acetate substitients will be summarised at the end of this section.

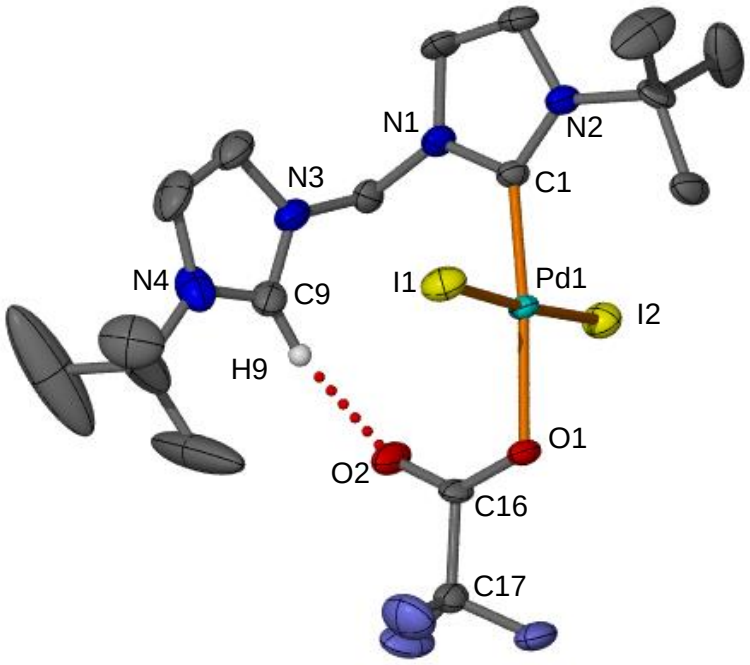

Figure 3.5. Molecular structure of [{(tBuIm)(tBuImH)CH_2}$PdI_2CO_2CF_3$] **11d**. Displacement ellipsoids are shown at the 50 % probability level. All hydrogen atoms except H9 are omitted for clarity. Selected bond lengths (Å) and angles (°): Pd1-C1 1.956(5), Pd1-I1,I2 2.5997(7),2.6229(7), Pd1-O1 2.116(4), C9···O2 2.998(8), C1-Pd1-I1,I2 88.85(18),88.03(18), O1-Pd1-I1,I2 91.60(12),91.51(12), Pd1-C1-N1,N2 119.2(4),134.5(4).

A more basic analogue [{(tBuIm)(tBuImH)CH_2}$PdI_2CO_2CH(CH_3)_2$] **11e** was produced from **10c** and silver dimethylacetate in moderate yield as an orange solid. ^{1}H NMR spectroscopy of **11e** was consistent with the expected structure. The unsymmetrical mono(NHC) pendant ligand arrangement was again confirmed to be retained from the five inequivalent NHC/imidazolium C-4/5 hydrogens and the inequivalent *t*-butyl groups. The downfield shift of the C-2 proton on the pendant imidazolium was increased from 9.63 ppm in the trihalide **10c** to 11.36 ppm, a

further downfield shift in comparison to that of **11c**. The presence of the dimethylacetate ligand was confirmed by the appearance of two CH_3 resonances at 0.93 and 0.95 ppm, and a methylene proton at 2.15 ppm. ^{13}C NMR spectroscopy showed the downfield chemical shift for the C-2 carbon at 140.0 ppm. X-ray crystallographic data was collected on orange crystals of **11e** for structural characterisation shown in Figure 3.6.

Compound **11e** contained two molecules in the asymmetric unit in which the palladium atoms shared near-identical square planar geometries with similar carbene and acetate bonding arrangements to the previous analogues. The Pd1-C1 distances of the two molecules were identical within error to analogues **11c-d** and the Pd1-O1 distance in both molecules of **11e** was identical to the shorter distance observed in **11c**. The Pd1-O1 bond was similar in length to **11c**. The C9···O2 distances in **11e** were 2.999(9) and 3.015(9) Å, on average 0.067 Å shorter than that observed in the original acetate complex **11c** and identical within error to that observed in **11d**.

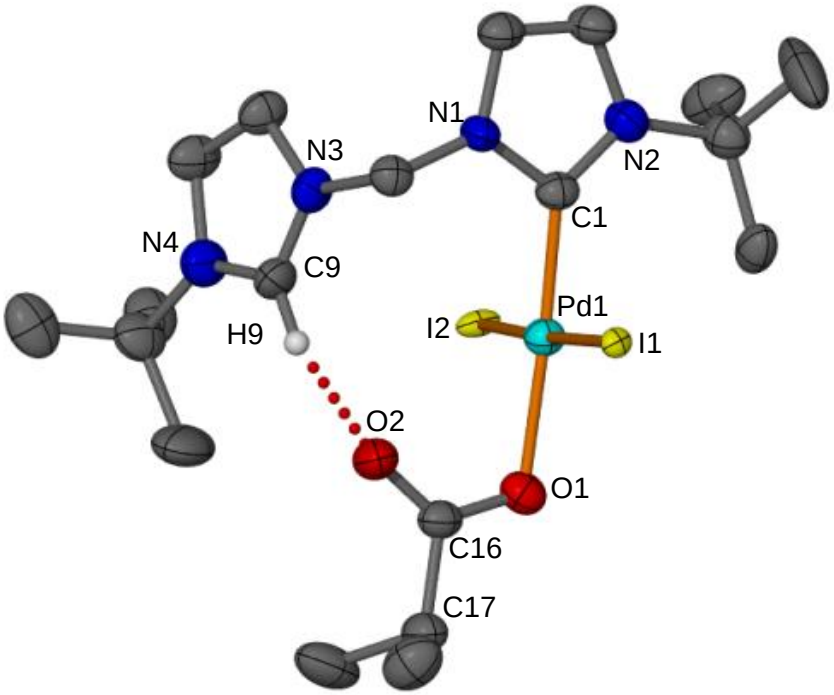

Figure 3.6. Molecular structure of one of the two crystallographically independent molecules of [{(tBuIm)(tBuImH)CH_2}$PdI_2CO_2CH(CH_3)_2$] **11e**. Displacement ellipsoids are shown at the 50 % probability level. All hydrogen atoms except H9 and lattice acetonitrile and water solvent molecules are omitted for clarity. Selected bond lengths (Å) and angles (°) of the above molecule (values for the second molecule provided in brackets): Pd1-C1 1.953(6) (1.950(7)), Pd1-I1,I2 2.5944(8) (2.5989(8)),2.6190(8) (2.6207(8)), Pd1-O1 2.089(5) (2.090(5)), C9···O2 3.015(9) (2.999(9)), C1-Pd1-I1,I2 87.67(17) (87.99(17)),89.86(17) (89.22(17)), O1-Pd1-I1,I2 90.40(13) (89.70(12)),92.19(13) (93.13(12)), Pd1-C1-N1,N2 119.8(4) (119.4(4)),135.6(5) (136.1(5)).

The most basic analogue [{(tBuIm)(tBuImH)CH_2}$PdI_2CO_2C(CH_3)_3$] **11f** was produced from **10c** and silver trimethylacetate in poor yield as an orange solid. ^{1}H NMR spectroscopy of **11f** was again consistent with the expected structure. The

unsymmetrical mono(NHC) pendant ligand arrangement was confirmed *via* retention of the five inequivalent NHC/imidazolium C-4/5 hydrogens and the inequivalent *t*-butyl groups. The downfield shift of the C-2 proton on the pendant imidazolium was increased from 9.63 ppm in the triiodide **10c** to 11.42 ppm, a further downfield shift compared to the other analogues consistent with the increased basicity. The presence of the trimethylacetate ligand was confirmed by the CH_3 resonance at 0.99 ppm which integrated for the expected nine protons. ^{13}C NMR spectroscopy showed the resonance for the C-2 carbon was similar to **11e** at 140.2 ppm. Isolation of crystals suitable for X-ray crystallographic analysis was difficult as the orange crystalline solid formed from both slow diffusion of diethyl ether into and slow evaporation of a saturated acetonitrile solution of **11f** contained solvent in the crystalline lattice and the crystals were prone to rapid desolvation which impacted sample crystal quality. Multiple attempts at recrystallisation and isolation resulted in a single dataset of moderate quality for structural confirmation (Figure 3.7).

Compound **11f** was essentially isostructural with **11c-d**, with the palladium in the expected square planar geometry and similar carbene and acetate bonding arrangements to the previous analogues. The low data quality and the C-C torsional disorder of the three *t*-butyl groups resulted in large anisotropic displacement parameters, though attempts to model the *t*-butyl torsions as two site disorders did not improve the structure refinement. The lattice solvent was severely disordered and the SQUEEZE program was used to remove the electron density in the solvent voids.[11] The Pd1-C1 distance of **11f** (1.968(7) Å) was increased slightly compared to analogues **11c-e**. Conversely there was a small decrease in the Pd1-O1 distance to 2.063(6) Å, a change of *ca.* 0.026 Å from analogues **11c** and **11e**. The C9···O2 distance in **11f** was increased (3.130(14) Å) compared to **11c-e**, an increase of

0.063 Å from **11c** and *ca.* 0.123 Å compared to **11e**, which only differs by an additional methyl group on the acetate substituent.

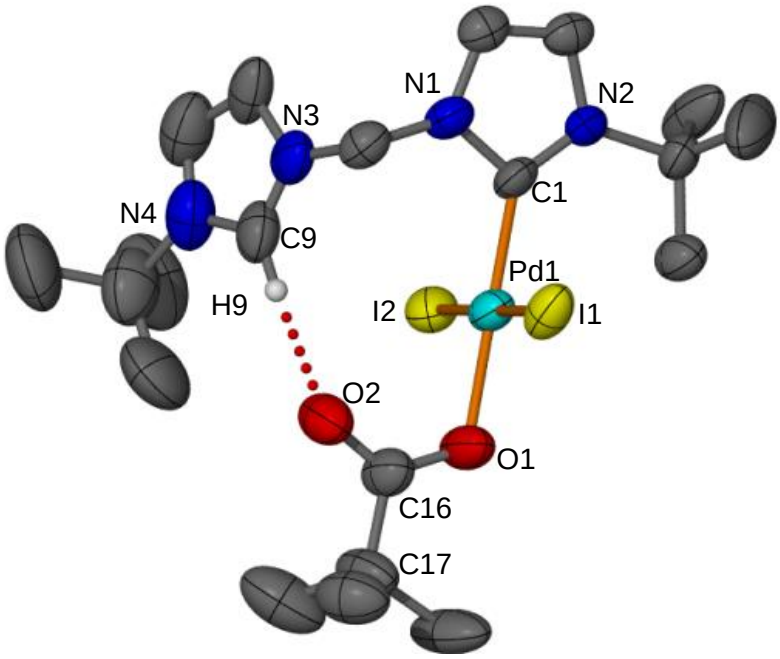

Figure 3.7. Molecular structure of [{(tBuIm)(tBuImH)CH_2}$PdI_2CO_2C(CH_3)_3$] **11f**. Displacement ellipsoids are shown at the 50 % probability level. All hydrogen atoms except H9 are omitted for clarity. Selected bond lengths (Å) and angles (°): Pd1-C1 1.968(7), Pd1-I1,I2 2.6159(10),2.6408(10), Pd1-O1 2.063(6), C9···O2 3.130(14), C1-Pd1-I1,I2 87.9(2),92.3(2) O1-Pd1-I1,I2 91.0(2),88.8(2), Pd1-C1-N1,N2 120.2(5),135.3(5).

A summary of the various acetate species comparing the pK_a of the conjugate acetate acids, the ^{1}H NMR chemical shift of the pendant imidazolium C-2 proton and the C9···O2 distances is provided in Table 2. There was good correlation between the pK_a values and the downfield shift of the C-2 proton, which suggested that the more basic acetate analogues were affecting the strength of the hydrogen bonding O···H interaction in solution. In the solid state the differences in C···O distances were not consistent with the basicity trend, though we are unsure whether this is due to the

C9···O2 distances not necessarily providing a good a measure of the hydrogen bonding, or whether external effects such as crystal packing, lattice solvent interactions and disorder and (in the case of **11f**) poor data impacted this measure.

Table 2. Comparison of pK_a values of the conjugate acids of the acetates, ^{1}H NMR chemical shift and C9···O2 distances of analogues **11c-f**.

Compound	pK_a	^{1}H NMR chemical shift (ppm)	C9···O2 (Å)
11d	0.23	9.76	2.998(8)
11c	4.76	11.17	3.067(6)
11e	4.86	11.36	2.999(9)/3.015(9)
11f	5.03	11.42	3.130(14)

A limiting factor in this study was the lack of acetate species with significantly increased basicity, with a pK_a increase of only 0.27 between the unsubstituted acetate and the trimethyl analogue. Furthermore, the various acetate derivatives added increased steric bulk in the vicinity of the hydrogen bonding interaction which potentially has affected the solid state comparison of C···O distances.

Observation of ^{1}H NMR samples of complexes **11c-f** in DMSO-d_6 saw slow conversion of **11c**, **11e** and **11f** to the chelated bis(NHC) complex at room temperature over *ca.* 5 days. Complex **11d**, which contained the less basic acetate group, underwent this conversion at a much slower rate. The pendant imidazolium diiodide trifluoroacetate species remained the major product even after 2 weeks in solution. This shows that while the slight increase in acetate basicity does not obviously increase the rate of reaction from the mono(NHC) intermediate to the

chelated bis(NHC) palladium complex, the significantly less basic trifluoroacetate does aid the stabilisation of the mono(NHC) pendant diiodide acetate intermediate.

3.2.3 Neutron Diffraction Studies of Hydrogen Bonding

We sought to examine the extent of the hydrogen bonding in some of these acetate species *via* single crystal neutron diffraction where feasible depending on sample availability. As discussed in Chapter 2, neutron techniques are uniquely suited to the study of hydrogen due to the relatively high neutron scattering cross section of the ^{1}H nucleus. However this technique requires significantly larger crystals than X-ray crystallography, which can limit the scope of compounds that can be studied.

Crystals of the pendant imidazolium mono(NHC) palladium triiodide complex **10c** were produced from a saturated acetonitrile solution over *ca.* 3 days. Single crystal neutron diffraction was performed on a large crystal (measuring 1.2 x 0.8 x 0.2 mm^3) of **10c** in order to establish the C-H distance of the C-2 proton in the non-hydrogen bonding species as a benchmark for comparison to the acetate analogues (Figure 3.8). After approximately half the collection time the crystal was manually rotated 90 ° to ensure sufficient sampling of reciprocal space. The structure was refined with all non-hydrogen atoms and H9 anisotropic, while the remaining hydrogen atoms were refined isotropically. A weak intermolecular H9-I3 interaction (*ca*. 2.78 Å) likely contributed to the orientation of the pendant imidazolium group.

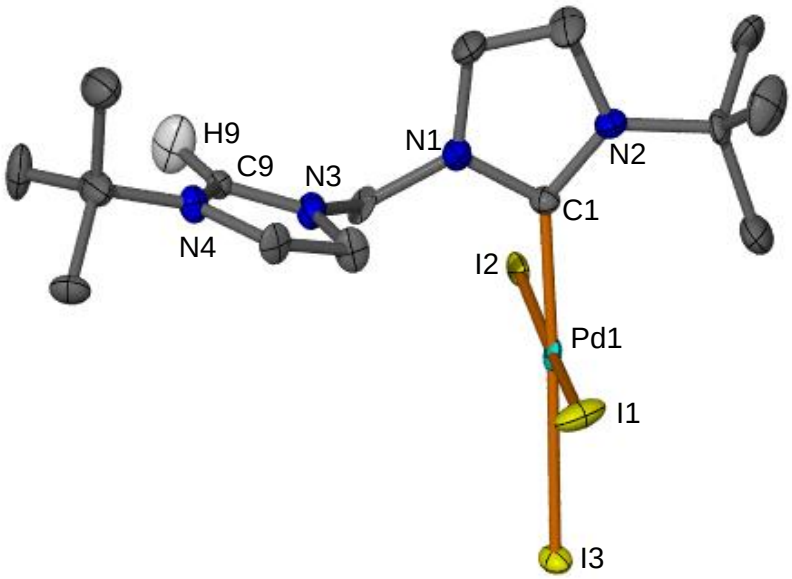

Figure 3.8. Molecular structure of [{(tBuIm)(tBuImH)CH_2}PdI_3] **10c** from single crystal neutron diffraction. All non-hydrogen atoms and H9 were refined anisotropically with displacement ellipsoids shown at the 50 % probability level, while all remaining hydrogen atoms are refined isotropically. Lattice solvent water and all hydrogen atoms except H9 are omitted for clarity. C9-H9 1.02(4) Å.

Crystals of the pendant palladium diiodide trifluoroactate complex **11d** of suitable size and quality for single crystal Laue neutron diffraction were grown from a saturated solution of acetonitrile in a sealed vessel over *ca.* 1 week. Initial neutron diffraction was performed on a single orange crystal measuring 1.0 x 1.0 x 0.3 mm^3, however the experiment was stopped prematurely due to instrument failure, with insufficient data collected. A second crystal measuring 1.5 x 0.6 x 0.2 mm^3 was procured and data collected at a later date, during which the crystal was manually rotated 90 ° to ensure sufficient sampling of reciprocal space. This provided an opportunity to explore a recent advancement in the instrument data processing software designed to merge datasets for different crystals. The software also enabled the comparison of the orientation matrices for the two crystals to ensure sufficient

rotation so that more unique reflections were obtained. The structure was refined with all non-hydrogen atoms and H9 anisotropic, while the remaining hydrogen atoms were refined isotropically (Figure 3.9).

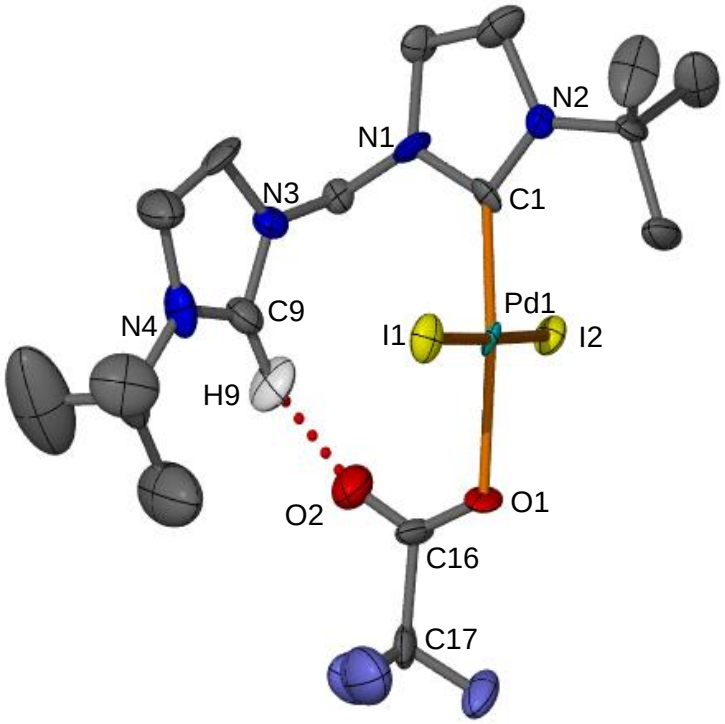

Figure 3.9. Molecular structure of [{(tBuIm)(tBuImH)CH_2}$PdI_2CO_2CF_3$] **11d** from single crystal neutron diffraction. All non-hydrogen atoms and H9 were refined anisotropically with displacement ellipsoids shown at the 50 % probability level, while all remaining hydrogen atoms were refined isotropically. All hydrogen atoms except H9 are omitted for clarity. Selected bond lengths (Å) and angles (°): C9-H9 1.08(5), O2···H9 1.98(4), C9···O2 3.04(3), C9-H9···O2 165(2).

Comparison of the C9-H16 distance between **10c** and **11d** shows a small, but statistically insignificant increase of 0.06 Å which would be consistent with hydrogen bonding, though the high error margins prevent definitive comment.

Due to the propensity of other acetate analogues **11c**, **11e**, and **11f** to grow as thin stacked plates we have not yet been able to produce crystals of suitable size and quality for neutron diffraction.

3.2.4 Synthesis of *N*-Mesityl Pendant Imidazolium Palladium(II) Complexes

We expanded our study to include the *N,N'*-dimesityl substituent analogues. The chelated *N*-mesityl methylene-linked bis(NHC) palladium(II) complexes have better catalytic activity for the copolymerisation of CO and ethylene than the *N*-*t*-butyl analogue[9] and an examination of intermediates, which may improve these syntheses, is therefore of interest. As previously discussed, the ethylene-linked *N*-mesityl analogue showed variability in synthetic products and access to the pendant imidazolium mono(NHC) complex might allow improved yields of, and influence the reaction pathway towards the preferred chelated bis(NHC) complex.

The *N*-mesityl palladium dihalide acetate complexes were not accessible *via* the direct synthesis route with palladium acetate due to the increased reactivity of the complexes with the bulky *N*-aryl substituent. Monitored reactions showed that the reaction of the methylene linked *N*-mesityl imidazolium salt with palladium acetate proceeded to the chelating product upon stirring in DMSO at room temperature for 1 hour. This is noticeably different to the *N*-*t*-butyl analogue, which forms only the mono(NHC) pendant palladium complex after heating at 50 °C for 3 hours and requires additional heating at 110 °C for 1-2 hours to metallate, then coordinate the second carbene.

Thus an alternative synthetic method was used to form the pendant imidazolium mono(NHC) palladium trihalide complexes [{(MesIm)(MesImH)CH_2}$PdBr_3$] **12a** and [{(MesIm)(MesImH)CH_2}PdI_3] **12b**. These were prepared from the reaction of

N-mesityl diimidazolium salt **9b**, $PdBr_2(COD)$ and one equivalent of sodium acetate in DMSO, which was heated for 4 hours at 50 °C (Scheme 3.9). For the iodide analogue **12b**, sodium iodide was added and the solution was heated for an additional hour. The solvent was removed *in vacuo* and the residue was dissolved in acetonitrile, and filtered (for **12a**) or dissolved in a 1:1 mixture of acetonitrile: water and the mixture heated at 80 °C for 10 minutes (for **12b**). Acetonitrile was then removed *in vacuo* to produce **12a** or **12b** as a yellow or red precipitates, respectively.

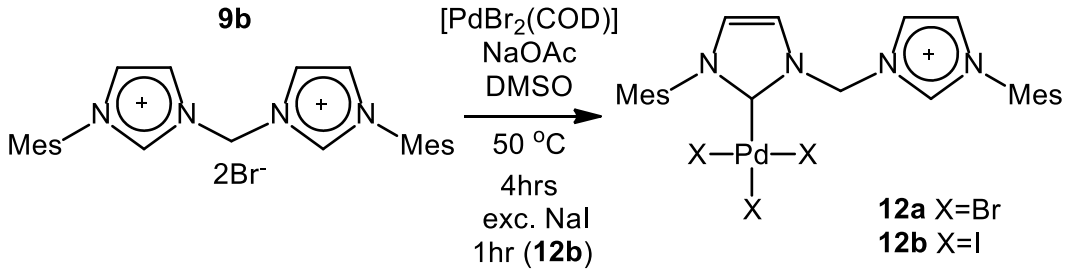

Scheme 3.9. Synthesis of *N*-mesityl pendant palladium trihalide complexes **12a** and **12b**.

^{1}H NMR spectroscopy confirmed the successful synthesis of both analogues, showing the desymmetrisation of the ligand with inequivalent mesityl *o*-methyl and *m*-CH protons, as well as the five inequivalent NHC/imidazolium protons. The presence of a single resonance which integrates for one hydrogen for each of the C-2 protons (9.75 and 9.81 ppm in **12a** and **12b** respectively) is also consistent with the pendant imidazolium mono(NHC) arrangement. Crystals of **12a** and **12b** suitable for X-ray diffraction were grown by slow evaporation of a concentrated acetonitrile solution with the structures of each shown in Figure 3.10.

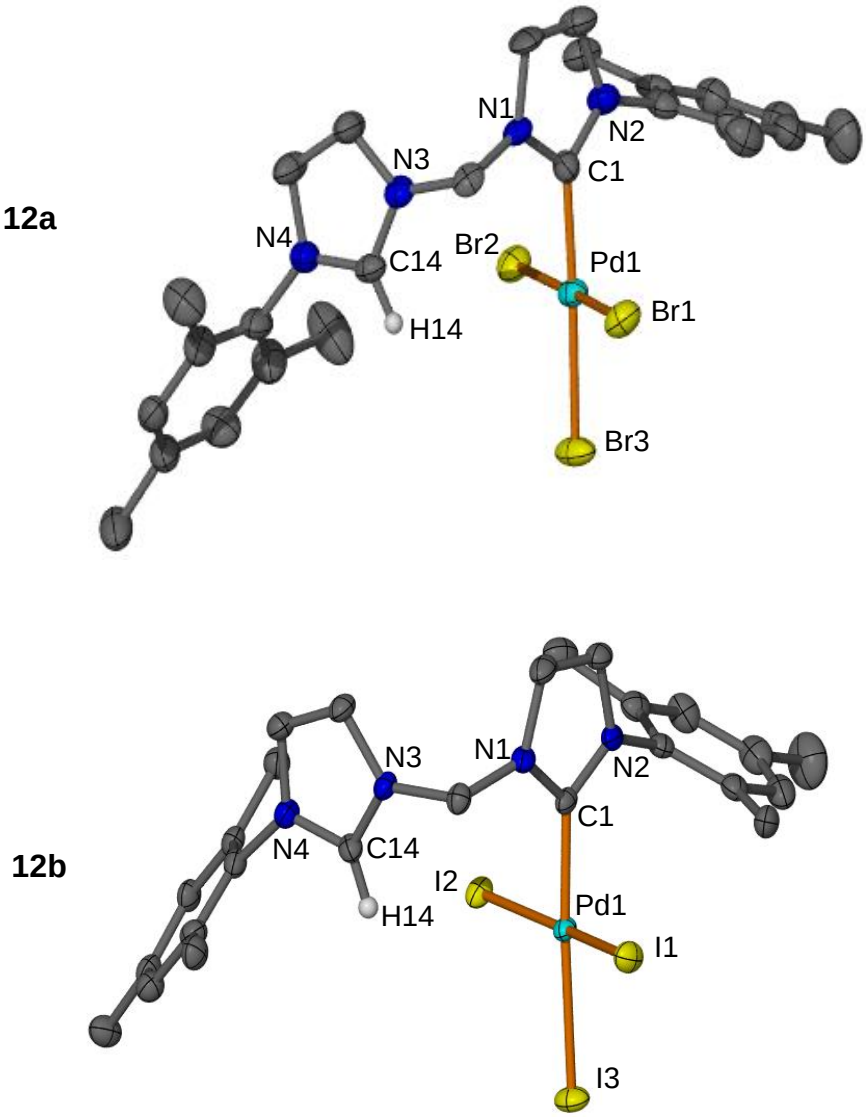

Figure 3.10. Molecular structures of [{(MesIm)(MesImH)CH_2}$PdBr_3$] **12a** and [{(MesIm)(MesImH)CH_2}PdI_3] **12b**. Displacement ellipsoids are shown at the 50 % probability level. All hydrogen atoms except H14 and lattice acetonitrile solvent molecules are omitted for clarity. Selected bond lengths (Å) and angles (°): Pd1-C1 1.978(9), Pd1-Br1,2,3 2.4296(15),2.4338(14),2.4749(13), C1-Pd1-Br1,Br2 90.2(3),88.3(3), Br3-Pd1-Br1,Br2 90.00(5),91.30(5), Pd1-C1-N1,N2 123.7(7),130.4(7) for **12a** and Pd1-C1 1.984(4), Pd1-I1,2,3 2.6166(5),2.6024(6),2.6510(7), C1-Pd1-I1,I2 88.20(11),87.83(11), I3-Pd1-I1,I2 92.11(2),92.496(19), Pd1-C1-N1,N2 126.0(3),128.7(3) for **12b**.

The reaction of compounds **12a** and **12b** with silver acetate to produce dihalide acetate species analogous to **11b-c** was unsuccessful. The chelated bis(NHC) palladium dihalide complex was the only product observed by ^{1}H NMR spectroscopy after isolation, following the stirring of the trihalide and silver acetate in methanol at room temperature for as little as 30 minutes. A mixture of unreacted trihalide and the chelated complex were observed for reaction times shorter than this.

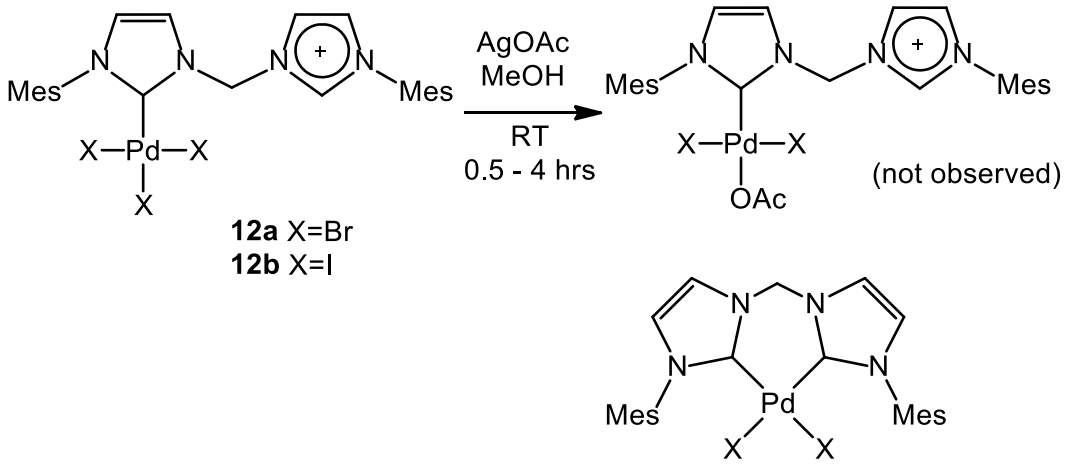

Scheme 3.10. Attempted synthesis of *N*-mesityl pendant imidazolium mono(NHC) palladium dihalide acetate complexes.

High reactivity was also noted when an excess of sodium acetate was added to a ^{1}H NMR sample of **12a**, whereupon there was an immediate disappearance of the downfield C-2 proton and the originally desymmetrised mesityl *o*-methyl signals were observed as a single resonance. This is consistent with the unsuccessful initial attempt to isolate the acetate intermediate from the reaction with palladium acetate at room temperature.

A pendant imidazolium mono(NHC) palladium dihalide intermediate was observed upon addition of an excess of the less basic sodium trifluoroacetate to a fresh ^{1}H NMR sample of **12a**. In our previous investigation of the *t*-butyl analogues it was

noted that the trifluoroacetate analogue showed the least reactivity to C-2 deprotonation as indicated by ^{1}H NMR spectroscopy, and we suspect this lesser reactivity allowed us to observe this intermediate. The spectrum was consistent with the pendant imidazolium mono(NHC) palladium dibromide acetate arrangement featuring hydrogen bonding between the imidazolium C-2 proton and the acetate oxygen, with a downfield shift of the C-2 proton to a broad singlet at 10.29 ppm (Δ 0.5 ppm) observed, as well as small shifts in the four remaining NHC/imidazolium C-4/5 proton signals. The mesityl methyl groups remained desymmetrised. Isolation of this product was attempted by removal of the NMR solvent *in vacuo* followed by extraction of the yellow residue in dichloromethane to separate the complex from any excess sodium trifluoroacetate. The yellow solid obtained from evaporation of dichloromethane was shown to be a mixture of the trihalide complex **12a** and the trifluoroacetate complex [{(MesIm)(MesImH)CH_2}$PdBr_2CO_2CF_3$] **13**. The products could not be separated by recrystallisation from vapour diffusion of diethyl ether into a saturated dichloromethane solution, though a single crystal of **13** was selected for structural characterisation by X-ray diffraction (Figure 3.11).

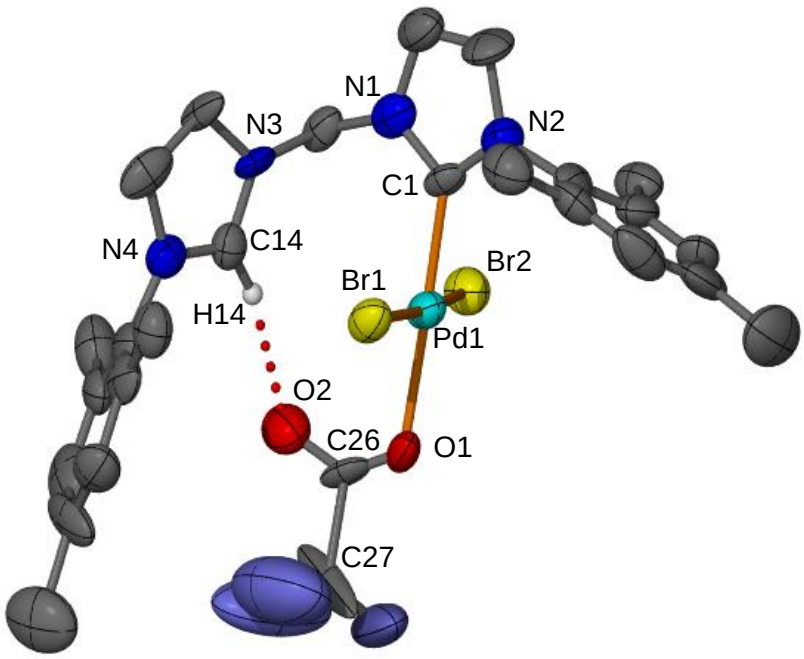

Figure 3.11. Molecular structure of [{(MesIm)(MesImH)CH_2}$PdBr_2CO_2CF_3$] **13**. Displacement ellipsoids are shown at the 50 % probability level. Lattice dichloromethane solvent atom and all hydrogen atoms except H14 are omitted for clarity. Selected bond lengths (Å) and angles (°): Pd1-C1 1.97(2), Pd1-Br1,Br2 2.425(3),2.418(3), Pd1-O1 2.132(16), C14···O2 3.04(3), C1-Pd1-Br1,Br2 86.6(5),91.6(5), O1-Pd1-Br1,Br2 89.0(4),92.6(4), Pd1-C1-N1,N2 121.5(17),130.9(15).

The structure of **13** is similar to the *t*-butyl palladium dihalide acetate complexes **11a-f**, with the C-2 proton oriented towards the acetate ligand to assist with hydrogen bonding. The X-ray crystallography data was low quality, with an R_{int} of 0.16 however further attempts to isolate the complex were unsuccessful and attempted modelling of the trifluoroacetate fluoride and carbon atoms as disordered did not improve the refinement. The C14···O2 distance of 3.04(3) Å is consistent with the range found for the *N*-*t*-butyl substituted series. Synthesis of **13** *via* our

previous silver trifluoroacetate method was unsuccessful, with only the initial material **12a** recovered from the reaction.

The synthesis of the ethylene linked mono(NHC) pendant palladium trihalide complex **14** from the imidazolium salt **9c** has been previously reported (Scheme 3.11).[10]

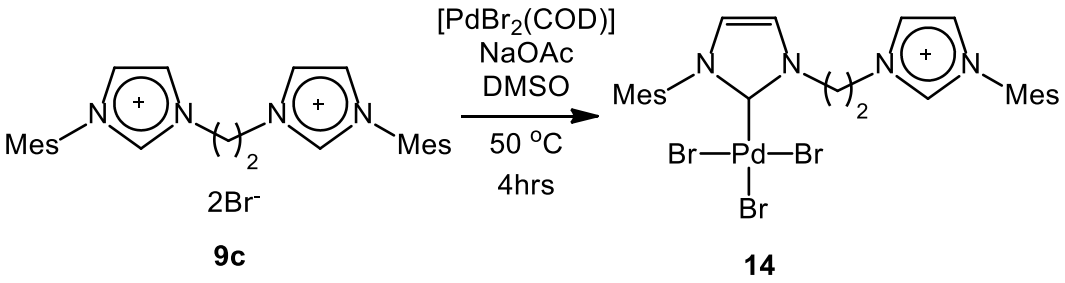

Scheme 3.11. Synthesis of *N*-mesityl ethylene linked pendant imidazolium palladium tribromide complex **14**.[10]

It was observed by Herrmann and coworkers that for the *N*-*t*-butyl methylene linked trihalide analogues, the addition of sodium acetate to a ^{1}H NMR sample of the pure trihalide resulted in clean conversion to the dihalide acetate complex, with only the *trans*-halide exchanging.[1] Addition of an excess of sodium acetate to the ^{1}H NMR sample of **14** appeared to result in an immediate conversion to a new product. In particular there was a small downfield shift of the pendant imidazolium C-2 proton from 9.37 ppm to 9.65 ppm (Figure 3.12) consistent with previously observed hydrogen bonding between the imidazolium C-2 proton and the acetate oxygen, albeit a smaller shift than seen between the *N*-*t*-butyl triiodide and acetate analogues **10c** and **11c**. There was also a downfield shift of a similar magnitude for one of the pendant imidazolium backbone protons from 8.04 ppm to 8.37 ppm; this is noteworthy as the *N*-*t*-butyl analogue series had essentially no shift of the

NHC/imidazolium backbone protons between the trihalide and dihalide acetate species.

This shift was suggestive of the acetate group showing hydrogen bonding interactions with both the C-2 position traditionally involved in carbene formation and a C-4/5 imidazolium backbone proton, which could then facilitate reactivity towards the coupled complex **I** (Scheme 3.3) discussed previously. The fact that interactions with two different protons were observed potentially implies the formation of two isomers containing different hydrogen-bonding arrangements, which might be rapidly exchanging in solution.

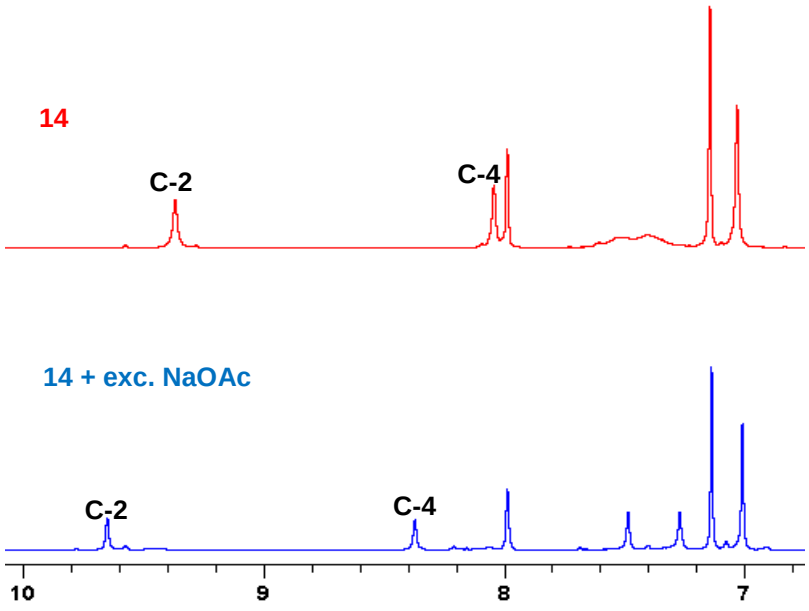

Figure 3.12. Comparison of the ^{1}H NMR spectra of **14** before and after the addition of sodium acetate (7-10 ppm region).

Albrecht and co-workers discuss similar acetate O···H interactions involving the C-4 proton being a factor in the formation of abnormal carbene complexes.[12] They prepared an asymmetric imidazolium salt which had one C-2 position blocked by a methyl group to prevent the normal bis(NHC) formation. Reaction of this species

with palladium acetate produced a pendant imidazolium mono(NHC) palladium diiodide acetate complex which, during workup underwent anion metathesis and formed the triiodide complex (Scheme 3.12).

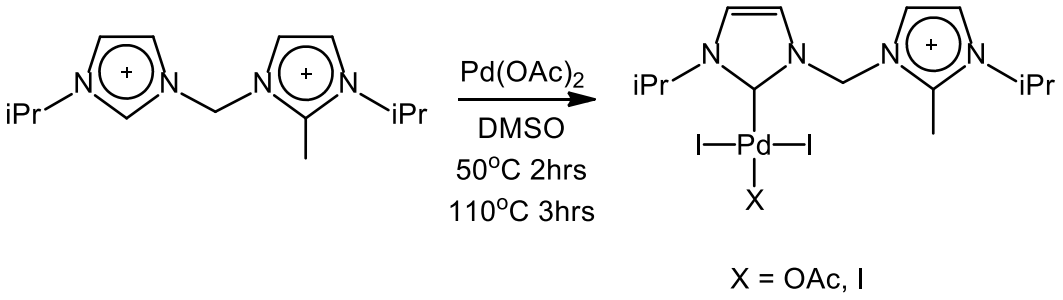

Scheme 3.12. Synthesis of pendant imidazolium mono(NHC) palladium complexes reported by Albrecht.[12]

The diiodide acetate complex reported by Albrecht presumably showed hydrogen bonding between the acetate and C-4 bound proton, however no NMR spectroscopic or X-ray crystallographic data was available for comparison to our similar species.

Reaction of **14** with one equivalent of silver acetate under similar conditions used to prepare the *N*-*t*-butyl palladium acetate complex **11c** produced a yellow solid in poor yield which was shown by ^{1}H NMR to contain one major product and several minor products. The major product was identical to that produced by the addition of excess sodium acetate to **14** and was assumed to be the dihalide acetate complex **15** (Scheme 3.13). The complex appears inseparable from the minor products however and we have yet been unsuccessful in obtaining crystallographic confirmation of the structure.

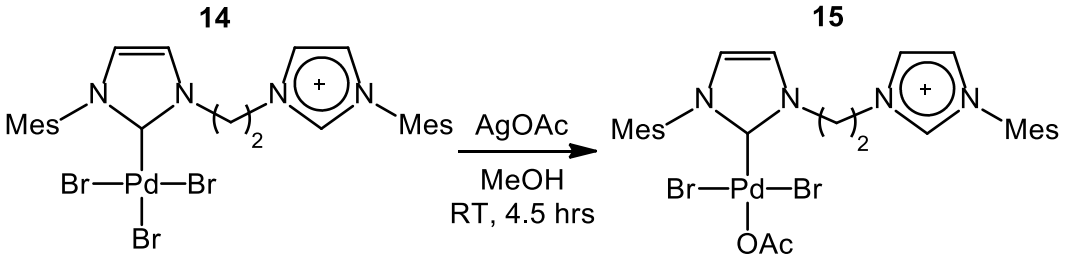

Scheme 3.13. Synthesis of the pendant imidazolium mono(NHC) ethylene linked palladium dibromide acetate complex **15**.

3.3 Conclusion

A series of *N*-*t*-butyl pendant imidazolium palladium dihalide acetate complexes **11a-f** were prepared to examine the hydrogen bonding effects influencing formation of the chelating bis(NHC) palladium complexes. Variations were made to the basicity of the acetate group and the type of ancillary halide, and the acetate-imidazolium O···H interactions were probed by ^{1}H NMR spectroscopy and X-ray diffraction. It was observed that in solution there was a notable downfield shift of the pendant imidazolium C-2 proton dependant on halide. A less significant downfield shift of the pendant imidazolium C-2 proton was observed dependant on acetate basicity. X-ray diffraction provided little differentiation in the solid state structures between complexes based on O···C2 distances involving the H-bonding interaction. No significant increases in conversion from the pendant imidazolium mono(NHC) diiodide acetate complexes **11c**, **11e** or **11f** to the chelated bis(NHC) palladium diiodide complex were observed. The significantly less basic trifluoroacetate analogue **11d** did show a greatly reduced conversion rate to the chelated species, however.

Neutron diffraction was used to directly probe the C-H bond length of the triiodide complex **10c** and the O···H bonding for the trifluoroacetate analogue **11d**. There

appeared to be little difference in C-H distance between these two species and to date we have not been able to prepare suitably large single crystals of the other acetate analogues to compare O···H distances.

The *N*-mesityl pendant imidazolium palladium trihalide complexes **12a** and **12b** were also prepared and it was observed that reaction of these complexes with silver acetate under identical reaction conditions used to prepare the *t*-butyl analogues resulted in immediate formation of the chelated bis(NHC) palladium dihalide complexes. Addition of the less basic sodium trifluoroacetate to an NMR sample of the tribromide complex **12a** did produce the pendant imidazolium palladium dibromide trifluoroacetate complex **13**, which was structurally authenticated by X-ray crystallography.

^{1}H NMR spectroscopic studies of the reaction of the ethylene-linked *N*-mesityl pendant imidazolium palladium tribromide complex **14** with sodium acetate indicated possible O···H interactions between the acetate group and the C-4/5 imidazolium backbone protons which may facilitate the secondary reaction pathway invoked in the formation of the self-coupled palladium complex **I**. Attempts to isolate and structurally authenticate the acetate intermediate **15** are ongoing.

3.4 Experimental

3.4.1 **General Conditions**

All syntheses of imidazolium salts and ligand exchange reactions of metal trihalide complexes to dihalide acetate complexes were carried out in air, while the syntheses of the mono(NHC) palladium complexes were conducted under an inert atmosphere of high purity argon (BOC gases) using standard Schlenk techniques. Anhydrous DMSO was purchased from Sigma-Aldrich and stored over activated 3 Å molecular

sieves. Other anhydrous solvents used were obtained by passage through columns on an Innovative Technologies Solvent Purifier.

Palladium(II) acetate was purchased from Precious Metals Online and used as received. Silver acetate, silver dimethylacetate and silver trimethylacetate were prepared by treating their respective sodium salts with aqueous silver nitrate solution and collecting the resultant precipitate by filtration, while silver trifluoroacetate was prepared from a literature procedure.[13] Imidazolium salts **9a**,[1] **9b**,[9] and **9c**[10] and palladium complex **14**[10] were prepared according to their cited literature procedure. All other reagents were purchased from Sigma-Aldrich and used as received. For non-air-sensitive syntheses, solvents were analytical grade and used as received.

3.4.2 **Instrumentation**

NMR spectroscopic studies were carried out on a 400 MHz Bruker Avance 3 HD Wide Bore spectrometer with a 5 mm BBFO probe in DMSO-d_6. NMR spectral data was obtained at room temperature (293 K) unless specified otherwise. DMSO-d_6 was distilled over CaH_2 and stored over 4 Å molecular sieves.

^{1}H NMR spectra were obtained at 399.58 MHz while ^{13}C NMR spectra were recorded at 100.47 MHz. ^{1}H NMR spectra were referenced to the ^{1}H resonance of the residual solvent peaks, while ^{13}C NMR spectra were referenced to the deuterated ^{13}C resonance. Elemental analyses were conducted by the Central Science Laboratory at the University of Tasmania using a Carlo Erba EA1108 Elemental Analyser. X-ray crystallographic studies were conducted at the Australian Synchrotron using the MX1 and MX2 beamlines.

3.4.3 **X-ray Crystallography**

Data for **10a-14** were collected at -173 °C on crystal mounted on a Hampton Scientific cryoloop at the MX1 or MX2 beamline of the Australian Synchrotron.[14,15] Data completeness is limited by the single axis goniometer on the MX beamlines at the Australian Synchrotron. The structures were solved by direct methods with SHELXS-97,[16] refined using full-matrix least-squares routines against F^2 with SHELXL-97, and visualised using X-SEED or OLEX2.[17,18] All non-hydrogen atoms were refined anisotropically. All hydrogen atoms were placed in calculated positions and refined using a riding model with fixed C-H distances of 0.95 Å (sp^2CH), 0.99 Å (CH_2), 0.98 Å (CH_3). The displacement parameters of all hydrogen atoms were estimated as $U_{iso}(H) = 1.2U_{eq}(C)$ except for CH_3 where $U_{iso}(H) = 1.5U_{eq}(C)$. Two-site atom disorder was modelled in OLEX2. Where solvent disorder was unable to be modelled the electron density was removed with PLATON SQUEEZE.[11] CIF files for X-ray crystallographic analysis can be provided upon request.

3.4.4 **Neutron Diffraction**

KOALA Experiments of 10c and 11d

Single crystal neutron diffraction studies were performed on crystals of pendant imidazolium mono(NHC) palladium(II) complexes [{(tBuIm)(tBuImH)CH_2}PdI_3] **10c** and [{(tBuIm)(tBuImH)CH_2}$PdI_2CO_2CF_3$] **11d** on the Laue diffractometer KOALA at ANSTO, New South Wales. The single flawless crystals measuring approximately 1.2 x 0.8 x 0.2 mm^3 (**10c**) and 1.0 x 1.0 x 0.3 mm^3 and 1.5 x 0.6 x 0.2 mm^3 (**11d**) were supported on an aluminium stand mounted in fluorinated silicon oil. The sample was cooled using a Cobra open flow nitrogen cooling system and diffraction data collected using Nimura special neutron image plate detectors.[19] Data sets were collected at 100 K and structure models comprising positional and

isotropic displacement parameters for all atoms were refined by full-matrix least-squares in the CRYSTALS[20] program suite. CIF files for neutron crystallographic analysis can be provided upon request.

3.4.5 **Synthesis**

Preparation of [{(tBuIm)(tBuImH)CH_2}$PdCl_3$] 10a

9a (218.7 mg, 0.52 mmol), palladium chloride (91.9 mg, 0.52 mmol) and sodium acetate (42.8 mg, 0.52 mmol) were dried in a Schlenk flask at *ca.* 70 °C. DMSO (10 mL) was added and the orange solution heated at 50 °C for 4 hours. Sodium chloride (0.99 g, 16.94 mmol) was added and the orange solution heated for a further 1 hour. The solvent was removed *in vacuo* and the yellow solid dissolved in a mixture of acetonitrile and water (20 mL/20 mL) and heated at 80 °C for 15 minutes. Acetonitrile was removed *in vacuo*, the resulting yellow precipitate collected by filtration, washed with water (5 mL) and dried *in vacuo* to produce a yellow solid that was an inseparable mixture of **10a** (major product) and various halide scrambled Cl/Br products (minor) (69.7 mg, ~ 22 % yield). Consistent elemental microanalysis was not obtained due to the indeterminate mixture of halides. m.p. 284 °C (dec).

^{1}H NMR (major product only, 399.58 MHz, DMSO-d_6): δ 1.62 (9H, s, C(CH_3)$_3$), 1.92 (9H, m, C(CH_3)$_3$), 6.99 (2H, s, CH_2) 7.73 (1H, bs, ImCH), 7.88 (1H, bs, ImCH), 8.05 (1H, m, ImCH), 8.09 (1H, bs, ImCH), 9.89 (1H, m, ImCH).

^{13}C NMR (major product only, 100.5 MHz, DMSO-d_6): δ 28.7 (C(*C*H_3)$_3$), 31.2 (C(*C*H_3)$_3$), 61.3 (CH_2), 120.8 (CH), 121.9 (CH), 122.3 (CH), 123.0 (CH), 136.2 (CH), 136.6 (C-Pd).

Preparation of [{(tBuIm)(tBuImH)CH_2}PdI_3] 10c

From a literature procedure[1] **9a** (0.193 g, 0.45 mmol) and palladium acetate (0.103 g, 0.45 mmol) were dried in a Schlenk flask at *ca.* 70 °C. DMSO (15 mL) was added and the orange solution heated at 50 °C for 4 hours. Sodium iodide (3.9 g, 26 mmol) was added and the red-orange solution heated for a further 1 hour. The solvent was removed *in vacuo* and the red solid dissolved in a mixture of acetonitrile and water (20 mL/20 mL) and heated at 80 °C for 15 minutes. Acetonitrile was removed *in vacuo*, the resulting red precipitate collected by filtration, washed with water (5 mL) and DCM (10 mL) and dried *in vacuo* to produce a red solid that is spectroscopically identical to literature (0.136 g, 40 % yield).

^{1}H NMR (399.58 MHz, DMSO-d_6): δ 1.59 (9H, s, CH_3), 1.83 (9H, s, CH_3), 6.81 (2H, s, CH_2) 7.75 (1H, s, ImCH), 7.88 (1H, s, ImCH), 7.96 (1H, s, ImCH), 8.06 (1H, s, ImCH), 9.63(1H, s, ImCH).

Preparation of[{(tBuIm)(tBuImH)CH_2}$PdCl_2$OAc] 11a

10a (24.0 mg, 0.05 mmol) and silver acetate (8.1 mg, 0.05 mmol) were dissolved in methanol (10 mL). The solution was excluded from light and stirred for four hours. The precipitated silver halide was removed by filtration through celite and the solvent was removed *in vacuo* to produce a yellow solid (6.2 mg, ~31% yield) that was an inseparable mix of complex and a minor byproduct of the Cl/Br halide scrambled acetate species. Consistent elemental microanalysis was not obtained due to an inconsistent mixture of halides.

^{1}H NMR (major product only, 399.58 MHz, DMSO-d_6): δ 1.59 (9H, s, CH_3), 1.67 (3H, s, CO_2CH_3), 1.91 (9H, m, CH_3), 7.15 (2H, s, CH_2) 7.57-7.60 (1H, m, ImCH), 7.91 (1H, bs, ImCH), 7.99-8.02 (2H, m, 2 x ImCH), 11.52-11.59 (1H, m, ImCH).

^{13}C NMR (major product only, 100.5 MHz, DMSO-d_6): δ 24.1 (CO_2CH_3), 28.5 (CH_3), 30.8 (CH_3), 58.8 ($C(CH_3)_3$), 59.2 ($C(CH_3)_3$), 60.8 (CH_2), 120.4 (CH), 120.9 (CH), 121.4 (CH), 123.0 (CH), 139.3 (CH), 175.1 (CO_2CH_3), Pd-C not observed.

Preparation of [{(tBuIm)(tBuImH)CH_2}$PdBr_2$OAc] 11b

From a literature procedure[1] **9a** (187.0 mg, 0.44 mmol) and palladium acetate (98.5 mg, 0.44 mmol) were dried in a Schlenk flask at *ca.* 70 °C. DMSO (5 mL) was added and the orange solution heated at 50 °C for 4 hours. The solvent was removed *in vacuo* and the yellow solid dissolved in a mixture of acetonitrile and water (20 mL/20 mL) and heated at 80 °C for 15 minutes. Acetonitrile was removed *in vacuo*, the resulting yellow precipitate collected by filtration, washed with water (5 mL) and DCM (10 mL) and dried *in vacuo* to produce a yellow solid that is spectroscopically identical to literature (108.7 mg, 42 % yield).

^{1}H NMR (399.58 MHz, DMSO-d_6): δ 1.62 (9H, s, *t*-Bu), 1.66 (3H, s, CH_3), 1.87 (9H, s, *t*-Bu), 7.01 (2H, s, CH_2) 7.71 (1H, s, ImCH), 7.98 (1H, s, ImCH), 7.99 (1H, s, ImCH), 8.04 (1H, s, ImCH), 11.17 (1H, s, ImCH).

General procedure for preparation of [{(tBuIm)(tBuImH)CH_2}PdI_2R] 11c-f

10c was dissolved in methanol, and the relevant silver salt added. The solution was excluded from light and stirred for four hours. The precipitated silver iodide was removed by filtration through celite and the solvent was removed *in vacuo* to produce the pure complex.

Preparation of [{(tBuIm)(tBuImH)CH_2}PdI_2OAc] 11c

From **10c** (136.2 mg, 0.18 mmol) and silver acetate (30.4 mg, 0.18 mmol) in methanol (35 mL), product was obtained as an orange solid that could be recrystallised from slow evaporation of acetonitrile that is spectroscopically identical to literature[1] (76.6 mg, 62 % yield).

^{1}H NMR (399.58 MHz, DMSO-d_6): δ 1.62 (9H, s, CH_3), 1.66 (3H, s, CH_3), 1.87 (9H, s, *t*-Bu), 7.01 (2H, s, CH_2) 7.71 (1H, s, ImCH), 7.98 (1H, s, ImCH), 7.99 (1H, s, ImCH), 8.04 (1H, s, ImCH), 11.17 (1H, s, ImCH).

Preparation of [{(tBuIm)(tBuImH)CH_2}$PdI_2CO_2CF_3$] 11d

From **10c** (138.0 mg, 0.18 mmol) and silver trifluoroacetate (40.8 mg, 0.18 mmol) in methanol (25 mL), product was obtained as an orange solid that could be recrystallised from slow evaporation of acetonitrile (85.1 mg, 63 % yield). m.p. 250 °C (dec).

^{1}H NMR (299.89 MHz, DMSO-d_6): δ 1.61 (9H, s, CH_3), 1.85 (9H, s, CH_3), 6.81 (2H, s, CH_2), 7.98 (1H, s, ImCH), 8.02 (1H, s, ImCH), 8.03 (1H, s, ImCH), 8.12 (1H, s, ImCH), 9.76 (1H, s, ImCH).

^{13}C NMR (100.48 MHz, DMSO-d_6): δ 28.8 (CH_3), 31.1 (CH_3), 59.4 ($C(CH_3)_3$), 60.0 ($C(CH_3)_3$), 62.3 (CH_2), 121.2 (CH), 121.9 (CH), 123.5 (CH), 124.4 (CH), 136.6 (CH), 158.1 (Pd-C),185.6 (OC=O) (CF_3 carbon not observed).

^{19}F NMR (375.94 MHz, DMSO-d_6): -73.52 (s, CF_3)

Found: C, 28.02; N, 7.78; H, 3.40. Calc. for $C_{17}H_{25}N_4O_2PdF_3I_2$: C, 27.79; N, 7.63; H, 3.43.

Preparation of [{(tBuIm)(tBuImH)CH_2}$PdI_2CO_2CH(CH_3)_2$] 11e

From **10c** (99.6 mg, 0.13 mmol) and silver dimethylacetate (25.9 mg, 0.13 mmol) in methanol (30 mL), product was obtained as an orange solid that could be recrystallised from slow evaporation of acetonitrile (45.4 mg, 48 % yield). m.p. 272 °C (dec).

^{1}H NMR (399.58 MHz, DMSO-d_6): δ 0.94 (6H, d, J = 7.0 Hz, 2 x $CO_2CH(CH_3)$), 1.62 (9H, s, *t*-Bu), 1.87 (9H, s, *t*-Bu), 2.15 (1H, sep. J = 6.9 Hz, $CO_2CH(CH_3)_2$), 7.03 (2H, s, CH_2), 7.71 (1H, s, ImCH), 7.98 (2H, s, 2 x ImCH), 8.03 (1H, s, ImCH), 11.36 (1H, s, ImCH).

^{13}C NMR (100.48 MHz, DMSO-d_6): δ 20.2 (2 x CH_3), 28.9 (CH_3), 31.2 (CH_3), 35.1 ($CH(CH_3)_2$), 58.7 ($C(CH_3)_3$), 59.7 ($C(CH_3)_3$), 62.0 (CH_2), 120.7 (CH), 121.3 (CH), 122.3 (CH), 123.4 (CH), 140.0 (CH), 148.3 (C-Pd), 181.0 (OC=O).

Found: C, 30.91; N, 7.48; H, 4.63. Calc. for $C_{19}H_{32}N_4O_2PdI_2.(H_2O)_2$: C, 30.64; N, 7.52; H, 4.87.

Preparation of [{(tBuIm)(tBuImH)CH_2}$PdI_2CO_2C(CH_3)_3$] 11f

From **10c** (99.9 mg, 0.13 mmol) and silver trimethylacetate (27.9 mg, 0.13 mmol) in methanol (30 mL), product was obtained as an orange solid that could be recrystallised from slow evaporation of acetonitrile (26.3 mg, 27 % yield). m.p. 247 °C (dec).

^{1}H NMR (399.58 MHz, DMSO-d_6): δ 0.99 (9H, s, $CO_2C(CH_3)$), 1.62 (9H, s, $C(CH_3)_3$), 1.88 (9H, s, $C(CH_3)_3$), 7.04 (2H, s, CH_2) 7.70 (1H, s, ImCH), 7.96 (2H, s, 2 x ImCH), 8.02 (1H, s, ImCH), 11.42 (1H, s, ImCH).

^{13}C NMR (100.48 MHz, DMSO-d_6): δ 28.4 ($CO_2C(CH_3)$, 28.9 ($C(CH_3)_3$), 30.7 ($C(CH_3)_3$), 38.2 (CO_2CCH_3), 58.7 (CCH_3), 59.7 (CCH_3), 61.9 (CH_2), 120.6 (CH), 121.3 (CH), 122.3 (CH), 123.4 (CH), 140.2 (CH), 148.3 (C-Pd), 182.3 (OC=O).

Found: C, 33.34; N, 7.27; H, 4.56. Calc. for $C_{20}H_{34}N_4O_2PdI_2$: C, 33.24; N, 7.75; H, 4.56.

Preparation of [{(MesIm)(MesImH)CH$_2$}PdBr$_3$] 12a

A Schlenk flask was loaded with **9b** (0.226 g, 0.41 mmol), $PdBr_2$(COD) (0.155 g, 0.41 mmol) and sodium acetate (0.034 g, 0.41 mmol) and dried *in vacuo* at 70 °C. DMSO (8 mL) was added and the solution heated at 50 ^{o}C for 4 hours. The solvent was removed *in vacuo* and the residue was dissolved in a 1:1 mixture of water and acetonitrile (20 mL /20 mL) and heated at 80 °C for 15 minutes. The solvent mixture was reduced *in vacuo* to remove the acetonitrile, and the resultant yellow precipitate was collected by filtration and washed with a further 10 mL water, then dried *in vacuo*. **12a** was produced as a yellow solid (0.173 g, 57 % yield) which could be recrystallised for X-ray diffraction by slow evaporation of a saturated solution of acetonitrile. m.p. 267 °C(dec).

^{1}H NMR (399.58 MHz, DMSO-d_6): δ 2.07 (6H, s, *o*-CH_3), 2.13 (6H, s, *o*-CH_3), 2.33 (6H, s, 2 x *p*-CH_3), 7.06 (2H, s, *m*-CH), 7.15 (2H, s, *m*-CH), 7.17 (2H, s, CH_2), 7.62 (1H, s, ImCH), 8.06 (1H, s, ImCH), 8.11 (1H, s, ImCH), 8.39 (1H, s, ImCH), 9.81 (1H, s, ImCH).

^{13}C NMR (100.48 MHz, DMSO-d_6): δ 17.2 (*o*-CH_3), 19.2 (*o*-CH_3), 20.6 (2 x *p*-CH_3), 61.5 (CH_2), 122.4 (ImCH), 123.2 (ImCH), 124.5 (ImCH), 127.0 (ImCH), 129.0

(*m*-CH), 129.3 (*m*-CH), 130.9 (C), 134.3 (C) 134.4 (C), 135.5 (C), 138.4 (Pd-C), 138.8 (ImCH), 140.5 (2 x C overlaid).

Found: C,40.68; N, 8.28; H, 4.07. Calc. for $C_{25}H_{28}N_4PdBr_3.NCMe.(H_2O)_2$: C, 40.15; N, 8.67; H, 4.37.

Preparation of [{(MesIm)(MesImH)CH_2}PdI_3] 12b

A Schlenk flask was loaded with **9b** (99.7 mg, 0.18 mmol), $PdBr_2$ (48.6 mg, 0.18 mmol) and sodium acetate (15.2 mg, 0.18 mmol) and dried *in vacuo* at 70 °C. DMSO (15 mL) was added and the solution heated at 50 ^oC for 4 hours. Sodium iodide (550 mg, 366 mmol) was added and the solution was heated for a further 1 hour. The solvent was removed *in vacuo* and the residue was dissolved in a 1:1 mixture of water and acetonitrile (25 mL /25 mL) and heated at 80 °C for 15 minutes. The solvent mixture was reduced *in vacuo* to remove the acetonitrile, and the resultant red precipitate was collected by filtration and washed with further 10 mL water, then dried *in vacuo*. **12b** was produced as a red solid (64.8 mg, 41 % yield) which could be recrystallised for X-ray diffraction by slow evaporation of a saturated solution of acetonitrile. m.p. 274 °C(dec).

^{1}H NMR (399.58 MHz, DMSO-d_6): δ 2.09 (6H, s, *o*-CH_3), 2.22 (6H, s, *o*-CH_3), 2.32 (3H, s, *p*-CH_3), 2.34 (3H, s, *p*-CH_3), 7.04 (2H, s, *m*-CH), 7.12 (2H, s, CH_2), 7.16 (2H, s, *m*-CH), 7.65 (1H, s, ImCH), 8.07 (2H, s, 2 x ImCH), 8.33 (1H, s, ImCH), 9.75 (1H, s, ImCH).

^{13}C NMR (100.48 MHz, DMSO-d_6): δ 17.2 (*o*-CH_3), 20.54 (*o*-CH_3), 20.55 (*p*-CH_3), 21.1 (*p*-CH_3), 62.4 (CH_2), 122.6 (ImCH), 122.8 (ImCH), 124.5 (ImCH), 127.9

(ImCH), 129.1 (*m*-CH), 129.3 (*m*-CH), 130.8 (C), 130.9(C), 134.1 (C), 134.3 (C), 135.3 (C), 138.6 (ImCH), 138.8 (Pd-C), 140.4 (C).

Found: C, 34.47; N, 6.56; H, 3.28. Calc. for $C_{25}H_{28}N_4PdI_3$: C, 34.45; N, 6.43; H, 3.24.

Preparation of [{(MesIm)(MesImH)CH_2}$PdBr_2CO_2CF_3$] 13

12a (*ca.* 5 mg) was dissolved in DMSO-d_6 in an NMR tube. An excess of sodium trifluoroacetate (*ca.* 10 mg) was added and the sample was agitated to ensure mixing. Following confirmation of conversion by ^{1}H NMR, the sample was transferred into a Schlenk flask, where the solvent was removed *in vacuo* and the resultant yellow glass extracted with dichloromethane (5 mL). The solution was filtered through fibreglass and dried under vacuum to produce a mixture of **13** and **12a** (*ca.* 2 mg). Crystals suitable for X-ray diffraction were produced by slow diffusion of diethyl ether into a concentrated DCM solution. Insufficient pure product was isolated to obtain ^{13}C NMR spectroscopic data or elemental microanalysis.

^{1}H NMR (*in situ* from addition of $NaCO_2CF_3$, 399.58 MHz, DMSO-d_6): δ 2.07 (6H, s, *o*-CH_3), 2.12 (6H, s, *o*-CH_3), 2.31 (3H, s, *p*-CH_3), 2.32 (3H, s, *p*-CH_3), 7.04 (2H, s, *m*-CH), 7.12 (2H, s, *m*-CH), 7.23 (2H, s, CH_2), 7.59 (1H, s, ImCH), 8.05 (1H, s, ImCH), 8.20 (1H, s, ImCH), 8.56 (1H, bs, ImCH), 10.29 (1H, bs, ImCH).

Preparation of [{(MesIm)(MesImH)$(CH_2)_2$}$PdBr_2CO_2CH_3$] 15

14 (45.2 mg, 0.06 mmol) and silver acetate (10.5 mg, 0.06 mmol) were dissolved in methanol (25 mL) and stirred with exclusion from light for 4.5 hours at room temperature. The resultant pale yellow solution was filtered through celite to remove the grey precipitate and the solvent removed *in vacuo* to produce a pale yellow solid

which was a mixture of **15** and some inseparable minor products (15.6 mg, ~36% yield). Elemental microanalysis was not obtained as the compound was not successfully isolated as a pure product.

^{1}H NMR (major product only, 399.58 MHz, DMSO-d_6): δ 1.63 (3H, s, $OCCH_3$), 2.03 (6H, s, 2 x *o*-CH_3), 2.10 (6H, s, 2 x *o*-CH_3), 2.50 (6H, s, 2 x *p*-CH_3), 5.20 (2H, t, J = 6.6 Hz, CH_2), 5.65 (2H, t, J = 6.2 Hz, CH_2), 7.01 (2H, s, *m*-CH), 7.13 (2H, s, *m*-CH), 7.27 (1H, s, ImCH), 7.45 (1H, s, ImCH), 7.99 (1H, s, ImCH), 8.38 (1H, s, ImCH), 9.63 (1H, s, ImCH).

^{13}C NMR (partial assignment due to mixed products, 100.5 MHz, DMSO-d_6): δ 10.8 (CO_2CH_3), 16.9 (CH_3), 19.2 (CH_3), 20.5 (CH_3), 48.6 (2 x CH_2), 123.3 (C), 124.1 (C), 124.3 (C), 128.9 (CH), 129.2 (CH), 129.3 (CH), 134.1 (C), 134.2 (C), 140.4 (C), 168.7 (CO_2CH_3).

3.5 References

[1] Herrmann, W. A.; Schwarz, J.; Gardiner, M. G. *Organometallics* **1999**, *18*, 4082.

[2] Kreisel, K. A.; Yap, G. P.; Theopold, K. H. *Chem. Commun.* **2007**, 1510.

[3] Douthwaite, R. E.; ssinger, D. H.; Green, M. L. H.; Silcock, P. J. *Organometallics* **1999**, *18*, 4584.

[4] Hashmi, A. S. K.; Lothschütz, C.; Böhling, C.; Rominger, F. *Organometallics* **2011**, *30*, 2411.

[5] McGuinness, D. S.; Cavell, K. J.; Yates, B. F.; Skelton, B. W.; White, A. H. *J. Am. Chem. Soc.* **2001**, *123*, 8317.

[6] Gründemann, S.; Albrecht, M.; Kovacevic, A.; Faller, J. W.; Crabtree, R. H. *J. Chem. Soc., Dalton Trans.* **2002**, 2163.

[7] Danopoulos, A. A.; Tulloch, A. A. D.; Winston, S.; Eastham, G.; Hursthouse, M. B. *Dalton Trans.* **2003**, 1009.

[8] Liao, C.-Y.; Chan, K.-T.; Zeng, J.-Y.; Hu, C.-H.; Tu, C.-Y.; Lee, H. M. *Organometallics* **2007**, *26*, 1692.

[9] Gardiner, M. G.; Herrmann, W. A.; Reisinger, C.-P.; Schwarz, J.; Spiegler, M. *J. Organomet. Chem.* **1999**, *572*, 239.

[10] Ho, C. C. Structural and Mechanistic Investigations of Systematically Modified Bis(NHC) Palladium Complexes (PhD Thesis), University of Tasmania, Hobart, **2015**.

[11] Spek, A. L. *Acta Cryst. C71* **2015**,

[12] Heckenroth, M.; Kluser, E.; Neels, A.; Albrecht, M. *Dalton Trans.* **2008**, 6242.

[13] Fox, C. M. J. Synthetic uses of β-ketothiosters **1985**, from Sel. Org. React. Database (SORD), accessed 2nd May 2012.

[14] Cowieson, N. P.; Aragao, D.; Clift, M.; Ericsson, D. J.; Gee, C.; Harrop, S. J.; Mudie, N.; Panjikar, S.; Price, J. R.; Riboldi-Tunnicliffe, A.; Williamson, R.; Caradoc-Davies, T. *J. Synchrotron Radiat.* **2015**, *22*, 187.

[15] Kuhn, P.; McPhillips, T. M.; McPhillips, S. E.; Chiu, H.-J.; Cohen, A. E.; Deacon, A. M.; Ellis, P. J.; Garman, E.; Gonzalez, A.; N. K. Sauter; 2002 *J. Synchrotron Radiat.* **2002**, *179*, 401.

[16] Sheldrick, G. M., *SHELX97*, Programs for Crystal Structure Analysis, Universität Göttingen, Germany, **1998**.

[17] Barbour, L. J. *J. Supramol. Chem.* **2001**, *1*, 189.

[18] Dolomanov, O. V.; Bourhis, L. J.; Gildea, R. J.; Howard, J. A. K.; Puschmann, H. *J. Appl. Cryst.* **2009**, *42*, 339.

[19] Shaikh, A. M. **2012**, Applications of various imaging techniques in neutron radiography at BARC, Trombay, in *18th World Conference on Nondestructive Testing*, Durban, South Africa.

[20] Betteridge, P. W.; Carruthers, J. R.; Cooper, R. I.; Prout, K.; Watkin, D. J. *J. Appl. Cryst.* **2003**, *36*, 1487.

Chapter 4: Synthesis of Saturated bis(NHC) Palladium(II) Complexes

4.1 Introduction

As discussed briefly in Chapter 1, there are several classes of NHCs with differing electronic properties.[1,2] Saturated NHC ligands lack the added stability of aromaticity compared to their unsaturated counterparts, but generally have increased electron density in the vicinity of the carbene.[2,3] This results in increased σ-donating properties for saturated carbenes, which in turn provides stronger M-C interactions and therefore more stable complexes.

Complexes containing saturated NHCs have been used for a variety of catalytic applications, with some examples shown in Figure 4.1. Liu and co-workers reported a benzyl-linked saturated NHC diiridium complex which showed good catalytic activity for *N*,*N*′-dialkylation of diamines with alcohols.[4] Arnold and co-workers prepared a series of magnesium and zinc complexes bearing asymmetrically substituted saturated NHC ligands, in which the *N*-substituents provided additional bidentate binding modes.[5] While these metals are not commonly associated with catalysis it was reported by Arnold that these complexes showed good activity for lactide polymerisation.

Grubbs' second generation catalyst for olefin metathesis utilises a saturated *N*,*N*′-dimesityl NHC ligand. Variations of this general moiety have been reported by several groups with a range of ligand modifications, and many of these studies note

the improved catalytic performance of the saturated carbene in comparison to unsaturated analogues bearing identical substitution.[6-8]

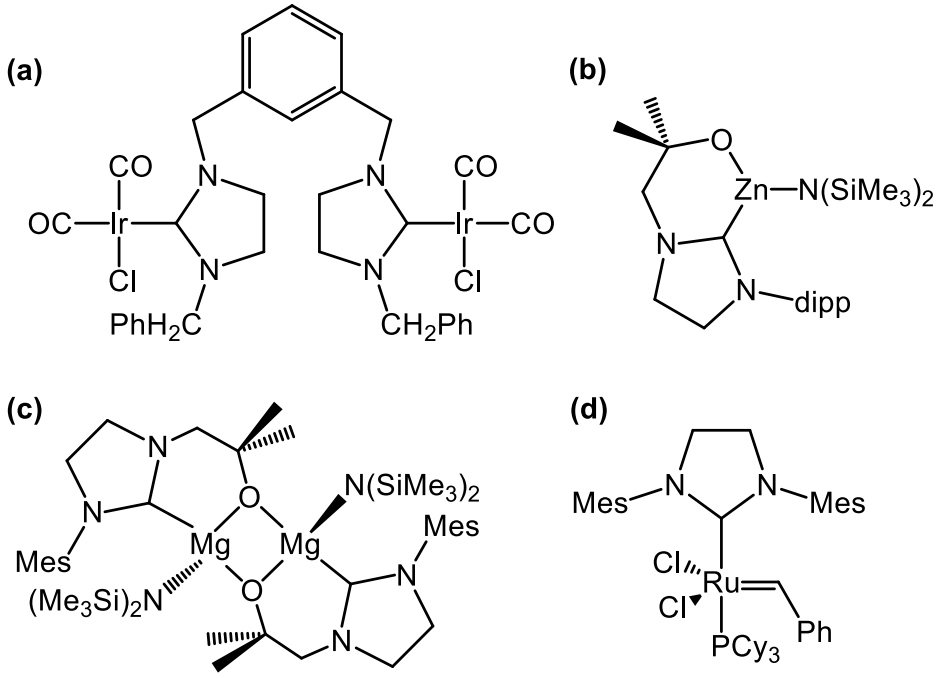

Figure 4.1. Examples of various saturated NHC complexes used for catalysis.[4-6]

Chen and co-workers compared bis(NHC) palladium dichloride complexes with identically substituted saturated and unsaturated carbene ligands to directly examine the differences in structure, stability and catalytic activity (Figure 4.2).[9] They observed that the saturated analogue showed better catalytic activity for Suzuki-Miayaura coupling of a range of aryl chlorides than the unsaturated analogue, as well as better complex stability in both acidic and iodic conditions. This is consistent with the hypothesis that the increased donating ability of saturated NHCs may positively influence metal complexes for catalytic uses.

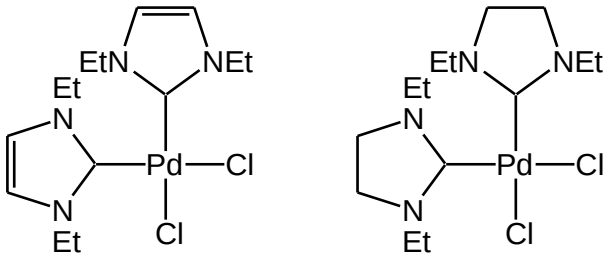

Figure 4.2. Unsaturated and saturated analogues of bis(NHC) palladium complexes reported by Chen and co-workers for comparison of activity and stability.[9]

There have been remarkably few reports of saturated bis(NHC) species which contain a linker between the NHC ligands and, to the best of our knowledge, no chelating saturated bis(NHC) complexes have been isolated and fully structurally characterised.

Straub and co-workers prepared a propylene linked diimidazolinium dihalide salt which, *via* an unisolated silver intermediate was successfully transmetallated to form a bridging dicopper(I) complex.[10] This was structurally authenticated by X-ray crystallography, forming a coordination polymer through Cu-Br interactions, though no potential applications of this species were discussed.

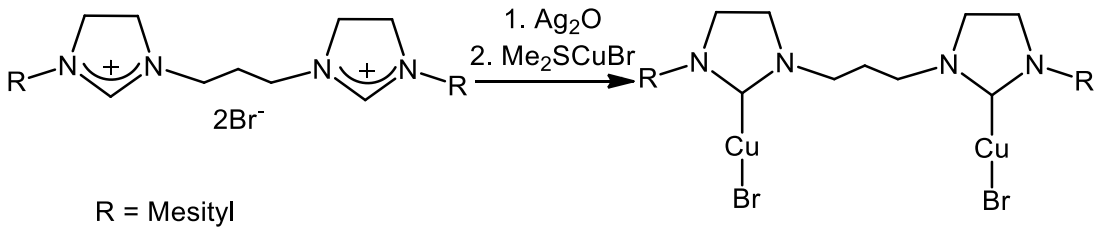

Scheme 4.1. Synthesis of saturated bis(NHC) dicopper(I) complex *via* a silver intermediate reported by Straub and co-workers.[10]

Özdemir and co-workers prepared a series of saturated diimidazolinium dibromide salts with alkylene linkers ranging from methylene to butylene (Figure 4.3).[11] These

showed good activity with palladium acetate for the Suzuki cross coupling of aryl chlorides, though the palladium complexes of the diimidazolinium salts were assumed to form *in situ* and never isolated for structural confirmation.

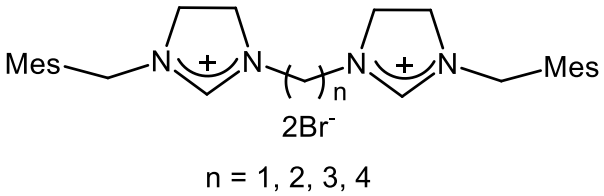

Figure 4.3. Diimidazolinium salts produced by Özdemir and co-workers for *in situ* formation of palladium Suzuki cross-coupling catalysts.[11]

Herein we present the first synthesis of a chelated saturated bis(NHC) palladium complex. The unsaturated analogue has previously been reported[12,13] for catalytic applications and we sought to determine whether the increased activity and stability of saturated NHC metal complexes observed for monodentate species translates to the bidentate system. We also sought to examine whether the reactivity towards the formation of a dipalladium(I) hydride species under basic conditions would occur as reported for the unsaturated analogue.[14]

4.2 Results and Discussion

4.2.1 **Saturated bis(NHC) Palladium(II) Complex**

N-mesityl imidazoline **16** (denoted ^{S}MesIm throughout) was produced *via* literature methods[15] and subsequent conversion to the bis(imidazolinium) salt $[(^{S}MesIm)_2CH_2]Br_2$ **17a** utilised our standard conditions for the unsaturated analogue.[13] The imidazoline **16** and 1.5 equivalents of dibromomethane were dissolved in toluene and the solution heated at 130 °C for 48 hours. The resultant white precipitate was collected by filtration, however ^{1}H NMR spectroscopy

indicated a mixture of the desired imidazolinium salt **17a** and the hydrobromide salt of **16**, **16a** (Scheme 4.2). These were easily separated by washing the white solid with chloroform and drying the precipitate *in vacuo* as pure **17a** free from the salt **16a**. The successful synthesis of **17a** was confirmed by ^{1}H NMR spectroscopy, which showed the expected *para*- and *ortho*-methyl resonances at 2.29 and 2.34 ppm, respectively. The eight imidazolinium backbone protons resolved as overlapping resonances at 4.31 ppm and the linker was confirmed by the resonance at 5.50 ppm. ^{13}C NMR spectroscopy and microanalysis were also consistent with the intended product.

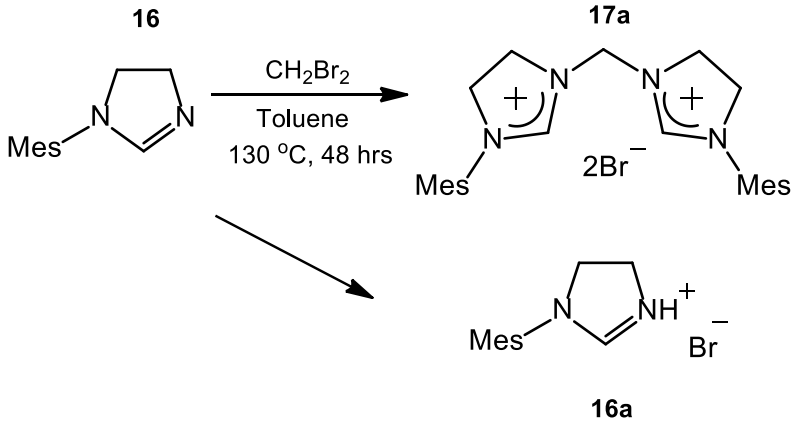

Scheme 4.2. Synthesis of saturated diimidazolinium salt **17a**.

Our standard method[13] for the formation of chelated (bis)NHC palladium(II) complexes was applied to prepare the chelated bis(NHC) palladium dibromide complex [{(^{S}MesIm)$_2$CH$_2$}PdBr$_2$] **18a**. The diimidazolinium salt **17a** and palladium acetate were dried *in vacuo* and dissolved in DMSO. Stirring at 50 °C for 3 hours and 110 °C for 2 hours under an atmosphere of argon and subsequent removal of the solvent *in vacuo* at 110 °C resulted in an orange glass which was washed with dichloromethane and the resultant grey precipitate collected by filtration (Scheme 4.3).

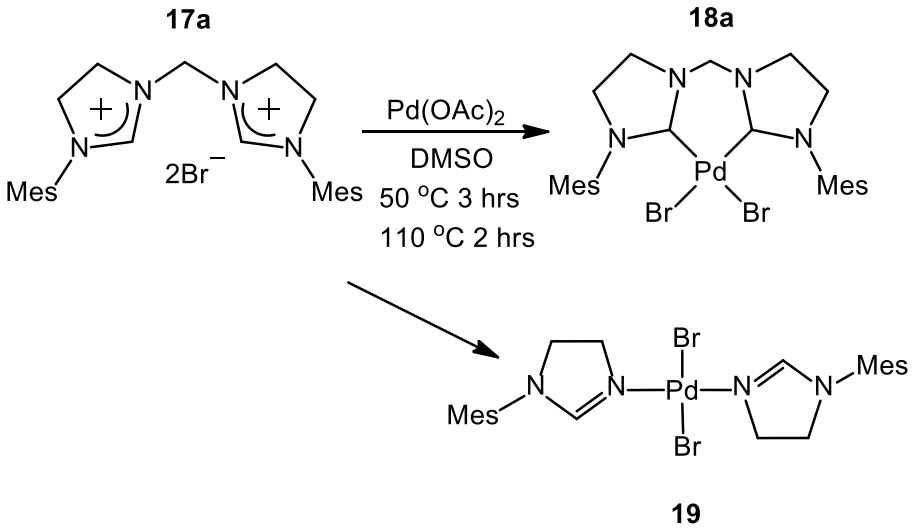

Scheme 4.3. Synthesis of the saturated analogue of the chelated (bis)NHC palladium dibromide complex.

Successful synthesis of the chelated bis(NHC) palladium complex **18a** was confirmed by ^{1}H NMR spectroscopy. The absence of the C-2 proton resonances supported carbene formation and the inequivalence of the ligand backbone protons showed a desymmetrisation in chemical environment when compared to the imidazolinium salt precursor. The spectrum showed significant broadening of all peaks and the methylene linker protons were observed as separate broad resonances at 4.89 and 5.34 ppm, indicative of a fluxional ring-flipping which coalesces at room temperature. ^{13}C NMR spectroscopy and elemental composition microanalysis were also consistent with the proposed structure of **18a**. Recrystallisation from slow diffusion of diethyl ether into a saturated acetonitrile solution produced colourless crystals of **18a** suitable for X-ray diffraction (Figure 4.4).

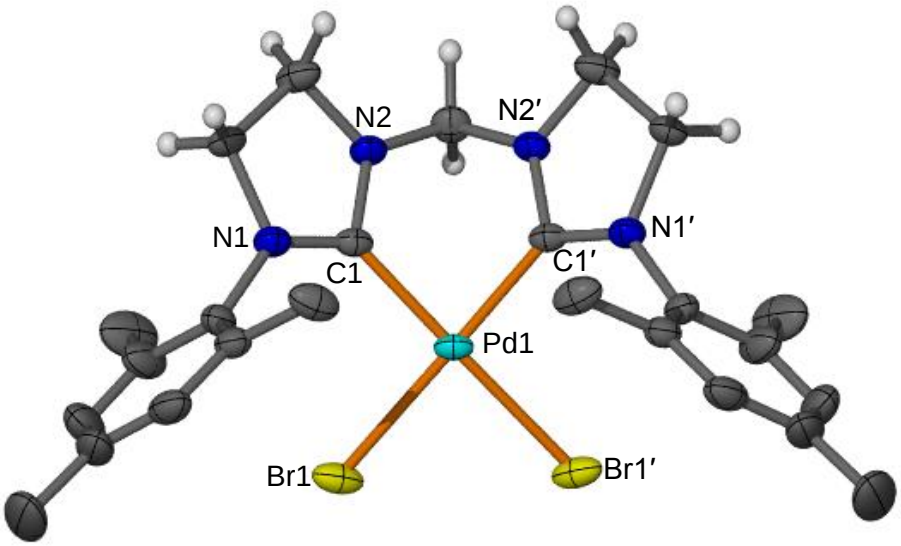

Figure 4.4. Molecular structure of [{(^{S}MesIm)$_2$CH$_2$}PdBr$_2$] **18a**. Displacement ellipsoids are shown at the 50 % probability level. All *N*-substituent hydrogen atoms are omitted for clarity. Selected bond lengths (Å) and angles (°): Pd1-C1 2.014(3), Pd1-Br1 2.4790(6), C1-Pd1-Br1 91.55(9), Pd1-C1-N1,N2 133.7(2),118.5(2).

The complex featured square planar geometry expected for palladium(II) complexes, and consistent with the previously reported unsaturated analogue.[12] The increased donor ability of the saturated NHCs was displayed in the slight (Δ 0.023(8) Å) decrease in the Pd1-C1 distance in **18a** compared to its unsaturated analogue, though the average Pd1-Br1 distances were identical within error between the saturated and unsaturated analogues.

On some occasions however a secondary orange product was observed which was identified by X-ray crystallography as **19**, a coordination complex containing the imidazoline **16** as *N*-bound ligands. We are uncertain whether this is due to the methylene linker of the imidazolinium having decomposed to reform the original imidazoline **16**, which was then bound through the unsubstituted nitrogen to

palladium (Figure 4.5), or whether minor impurities of the imidazoline **16** remained in the synthesis of the diimidazolinium salt **17a**.

Complex **19** could be deliberately synthesised by stirring two equivalents of **16** with $PdBr_2(COD)$ in tetrahydrofuran at room temperature for 16 hours. The solvent was removed and the product precipitated out of acetonitrile as an orange crystalline solid suitable for X-ray diffraction. ^{1}H NMR spectroscopy of complex **19** was consistent with the X-ray structure, where the presence of the C-2 protons at 7.41 ppm indicated that carbene formation had not occurred.

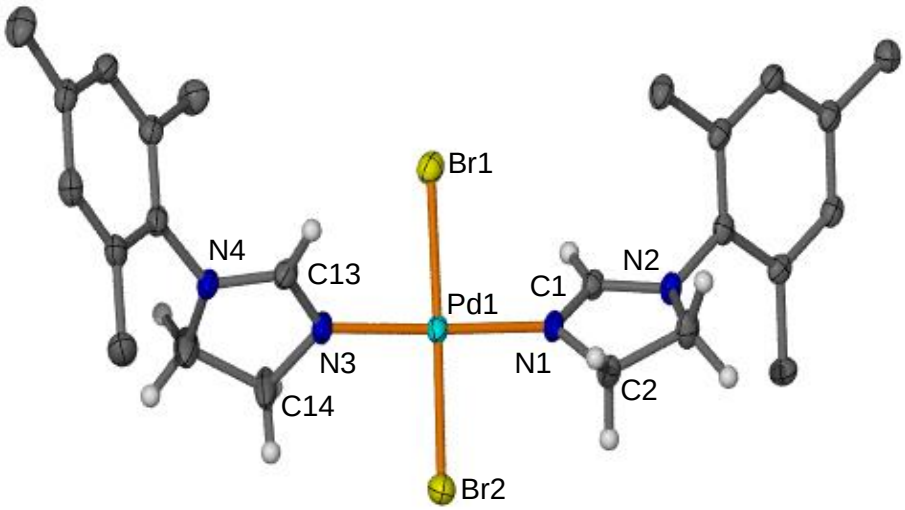

Figure 4.5. Molecular structure of [(^{S}MesImH)$_2$PdBr$_2$] **19**. Displacement ellipsoids are shown at the 50 % probability level. All *N*-substituent hydrogen atoms are omitted for clarity. Selected bond lengths (Å) and angles (°): Pd1-N1,N3 2.009(2),2.003(3), Pd1-Br1,Br2 2.4409(6),2.4370(6), N1-Pd1-Br1,Br2 90.53(8),90.85(8), N3-Pd1-Br1,Br2 88.14(8),90.44(8), Pd1-N1-C1,C2 126.6(2),125.6(2), Pd1-N3-C13,C14 123.7(2),127.7(2).

Conversion of the bis(NHC) palladium dibromide complex **18a** to the dicationic acetonitrile adduct [{(^{S}MesIm)$_2$CH$_2$}Pd(NCMe)$_2$][PF$_6$]$_2$ **20a** was achieved under

identical conditions to the unsaturated analogue.[13] Complex **18a** and a twenty-fold excess of sodium hexafluorophosphate were dissolved in a 1:1 mixture of acetonitrile and water. The solution was stirred at 80 °C for 1.5 hours and subsequent removal of the acetonitrile *in vacuo* produced **20a** as an off-white precipitate which was collected *via* filtration and dried *in vacuo* (Scheme 4.4). The compound was recrystallised by slow diffusion of diethyl ether into a saturated acetonitrile solution to produce large colourless crystals of pure **20a** suitable for catalysis, further reaction and X-ray diffraction.

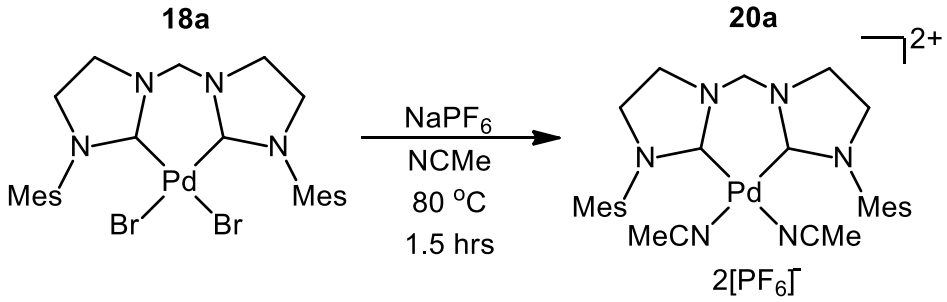

Scheme 4.4. Synthesis of the dicationic bis(NHC) palladium complex $[\{(^{S}MesIm)_2CH_2\}Pd(NCMe)_2][PF_6]_2$ **20a**.

Synthesis of the dication **20a** was confirmed by ^{1}H and ^{13}C NMR spectroscopy, and elemental microanalysis. The symmetrical nature of the species was preserved, with the *ortho*- and *para*-mesityl methyl groups appearing as singlets at 2.26 and 2.28 ppm. The NHC ring protons appeared as two multiplets centred at 3.98 and 4.11 ppm, and the methylene linker and mesityl *meta*-CH protons were observed as singlets at 5.21 and 7.00 ppm, respectively. The signal broadness of the linker protons observed in complex **18a** was not seen in complex **20a**, consistent with other previously reported unsaturated analogues, indicating rapid chelate ring flipping on the NMR timescale at room temperature.[13,16] The coordinating acetonitrile ligands

were observed as a single resonance of suitable integration at 2.07 ppm. The carbene carbon was observed by ^{13}C NMR at 175.3 ppm.

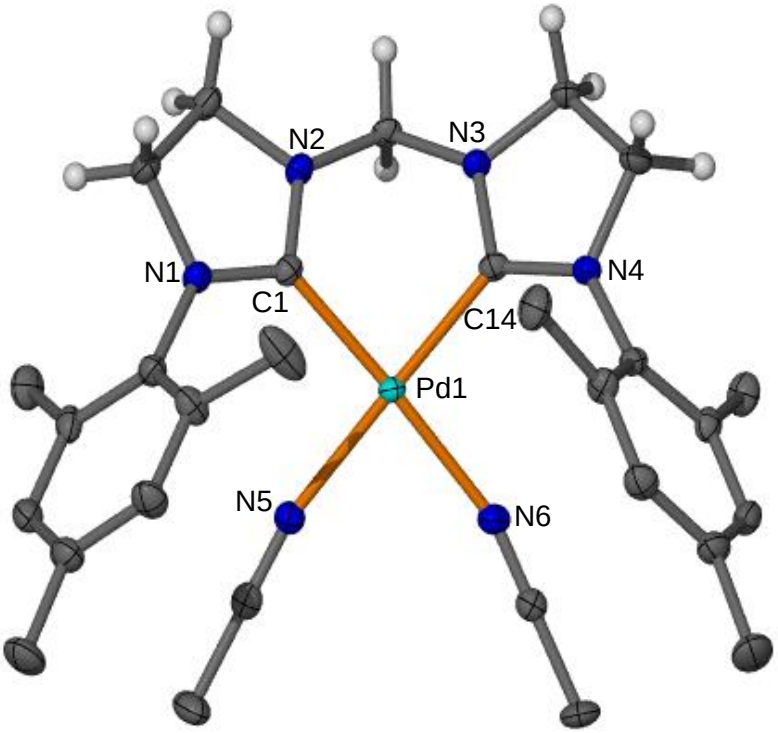

Figure 4.6. Molecular structure of the dication of [{(^{S}MesIm)$_2$CH$_2$}Pd(NCMe)$_2$][PF$_6$]$_2$ **20a**. Displacement ellipsoids are shown at the 50 % probability level. All [PF$_6$]$^-$ counteranions, lattice solvent acetonitrile molecule, *N*-substituent and coordinated acetonitrile hydrogen atoms are omitted for clarity. Selected bond lengths (Å) and angles (°): Pd1-C1,C14, 1.987(4),1.996(4), Pd1-N5,N6, 2.053(4),2.062(4), C1-Pd1-N5,C14, 93.90(17),87.18(18), C14-Pd1-N6, 95.68(17), Pd1-C1-N1,N2, 128.1(3),122.9(3), Pd1-C14-N3,N4 122.6(3),128.7(3).

The solid state structure of **20a** was confirmed by X-ray crystallography, in which the palladium had the expected square planar geometry, consistent with the unsaturated analogue (Figure 4.6).[17] The Pd-C bonds are slightly lengthened in **20a**

compared to the unsaturated analogue (Δ 0.014(4) Å), though the Pd-N bonds are identical within error.

As discussed briefly in Chapter 3, chelated bis(NHC) palladium complexes with bulky *N*-substituents have been studied for catalytic applications.[13] The analogous unsaturated dicationic *N*-mesityl palladium(II) diacetonitrile complexes of varying linker lengths were in particular examined for catalytic activity in the copolymerisation of ethylene and carbon monoxide.[16]

Identical conditions from these trials were used to examine the catalytic activity of **20a**, in which 20.1 mg of **20a** was dissolved in 50 mL of methanol under inert atmosphere and transferred to a Parr reactor. The reactor was charged with carbon monoxide and ethylene (10 bar/10 bar) and stirred at 70 °C for 2 hours. The reactor was allowed to cool and the black precipitate (a mixture of assumed copolymer and co-precipitated palladium black decomposition)[13] was collected by filtration to yield 8.0 mg of solid, or 0.348 g/ mmol Pd used. This is less than the 0.698 g/mmol Pd recorded for the unsaturated analogue, and an indication that the increased electron density on the metal from the saturated carbene does not necessarily translate to increased catalytic yield for this reaction. It is possible that the reduced activity could be due to increased reactivity towards decomposition products compared to the unsaturated analogue.

As previously discussed in Chapter 2, it has been shown that unsaturated *N*-mesityl bis(NHC) palladium(II) diacetonitrile complexes undergo unusual reactivity under catalytic conditions to form dipalladium(I) hydride complexes.[14,16] We sought to examine whether this reactivity was also observed for the saturated complex **20a**.

In a modified literature procedure,[14] a 10 mg sample of the saturated bis(NHC) palladium dication **20a** was dissolved in deuterated methanol in a Young's NMR tube. Sodium carbonate was added and the suspension was heated at 60 °C. ^{1}H NMR spectroscopic data was collected prior to and immediately after the addition of sodium carbonate, and after 2 and 4.5 hours of heating, during which time the solution turned orange and upfield shifts of all resonances were observed in the ^{1}H NMR spectrum.

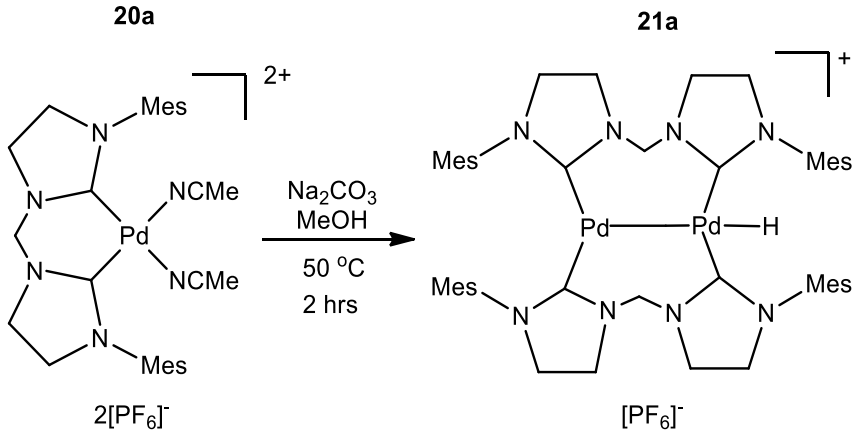

Scheme 4.5. Proposed synthesis of dipalladium(I) hydride complex **21a**.

The solution volume was concentrated to facilitate crystallisation of compound **21a**, however only precipitation of palladium black was observed. The reaction was repeated on an increased scale under Schlenk conditions but similar decomposition to palladium black was observed and the complex, to date, has not been successfully isolated.

4.2.2 **Extended Linker Analogues of 18a**

The synthesis of the propylene-linked imidazolinium salt analogue of **17a** has previously been reported.[10] The ethylene- and propylene-linked imidazolinium salts $[(^{S}MesIm)_2C_2H_4]Br_2$ **17b** and $[(^{S}MesIm)_2C_3H_6]Br_2$ **17c** were prepared by a neat

reaction of the imidazoline **16** with 0.5 equivalents of the appropriate dibromoalkane at 100 °C for 2 hours. The resultant orange glass was dissolved in a minimal volume of dichloromethane and diethyl ether was added to precipitate out the product as a white solid which was collected by filtration (Scheme 4.6).

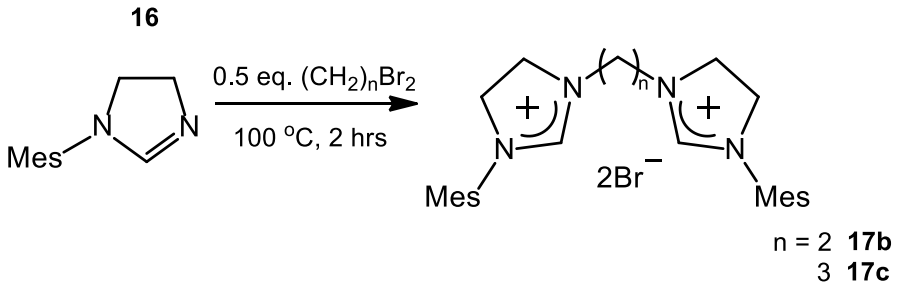

Scheme 4.6. Synthesis of ethylene- and propylene-linked imidazolinium salts **17b** and **17c**.[10]

The propylene-linked imidazolinium salt **17c** was produced in good yield as previously reported and was spectroscopically identical to literature.[10] The ethylene- linked imidazolinium salt **17b** was only produced in 24 % yield however, and attempts to prepare it in a method analogous to that of **17a** resulted in lower yields of approximately 5-10 %, with greatly increased formation of the hydrobromide salt **16a**. The successful synthesis of **17b** was confirmed by ^{1}H and ^{13}C NMR spectroscopic analysis. The expected symmetry of the signals was observed with the linker appearing as a single resonance at 4.48 ppm and the C-2 protons identifiable by their significant downfield shift at 10.34 ppm.

Synthesis of the chelated bis(NHC) palladium dibromide analogues with the extended linker imidazolinium salts **17b-c** was attempted under identical conditions to the methylene linked analogue **18a**. The relevant imidazolinium salt and palladium acetate were dried *in vacuo* and dissolved in DMSO. Stirring at 50 °C for

3 hours and 110 °C for two hours under an atmosphere of argon and subsequent removal of the solvent *in vacuo* at 110 °C resulted in an orange glass (Scheme 4.7). This was dissolved in dichloromethane, the orange solution filtered through Celite and the solvent allowed to evaporate slowly over 16 hours to produce a small amount of a yellow-orange solid which did not redissolve in dichloromethane and was collected by filtration.

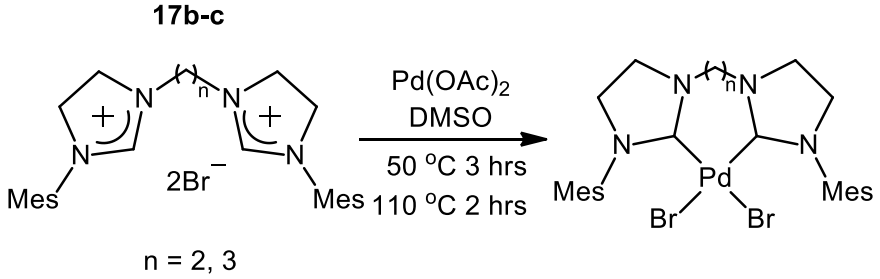

Scheme 4.7. Proposed synthesis of extended linker analogues of chelated bis(NHC) palladium dibromide **18a**.

^{1}H NMR spectroscopy of these yellow solids was not consistent with the proposed chelate structure, however. In both cases there was a downfield resonance which integrated for a single proton at 8.87 and 8.88 ppm for the two complexes, respectively. Both complexes also showed visible desymmetrisation of the mesityl methyl groups; in the ethylene-linked analogue this appeared to be inequivalent *ortho*-methyl groups on each mesityl group, while the ^{1}H NMR spectrum of the propylene-linked analogue was consistent with inequivalent *N*-substituents. This data was consistent with a pendant imidazolinium mono(NHC) palladium trihalide complex similar to those discussed in Chapter 3. The proposed structures of the ethylene- and propylene-linked complexes **22b** and **22c** are shown in Figure 4.7 below.

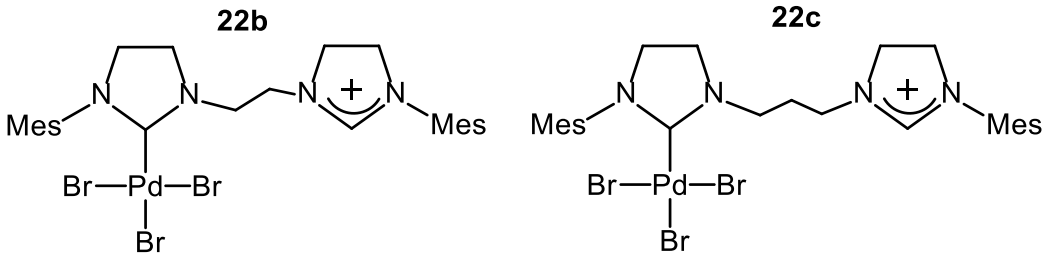

Figure 4.7. Proposed structures of the products formed by the reaction of imidazolinium salts **17b** and **17c** with palladium acetate.

4.2.3 **Saturated NHC Palladium(II) Pendant Imidazolium Complexes**

In order to further understand the extended linker complexes **22b-c** the saturated NHC palladium(II) trihalide complexes were prepared in an identical fashion to the unsaturated analogues described in Chapter 3. The methylene-linked pendant imidazolium mono(NHC) palladium triiodide complex [{(^{S}MesIm)(^{S}MesImH)CH_2}PdI_3] **22a** was also prepared for direct comparison to the unsaturated analogue **12b**. For complex **22a**, imidazolinium salt **17a**, $PdBr_2$(COD) and sodium acetate were dried *in vacuo* and dissolved in DMSO. The solution was stirred at 50 °C for 4 hours, an excess of sodium iodide was added and the solution was heated for an additional hour, after which the solvent was removed *in vacuo* at 110 °C and the red-brown glass redissolved in a 1:1 mixture of acetonitrile and water. This solution was heated at 80 °C for 10 minutes after which the acetonitrile was removed *in vacuo* to produce **22a** as a dark red precipitate which was collected by filtration (Scheme 4.8).

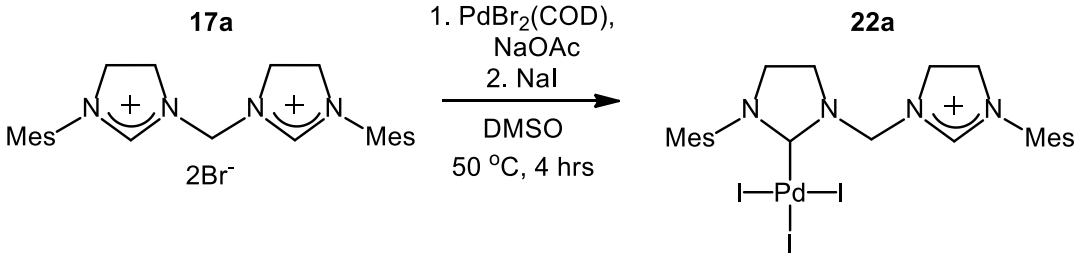

Scheme 4.8. Synthesis of pendant imidazolinium methylene linked palladium triiodide complex **22a**.

Successful synthesis of **22a** was confirmed by ^{1}H and ^{13}C NMR spectroscopy and elemental analysis. The desymmetrisation of the mesityl groups was indicated by two distinct resonances for the mesityl *ortho*-methyl protons at 2.28 and 2.30 ppm, the separation of the C4/5 NHC/imidazolinium backbone protons at 3.94 and 4.32 ppm and the two separate resonances of the mesityl *meta*-CH protons at 6.98 and 7.07 ppm. The pendant imidazolinium C-2 proton appeared as a single proton downfield resonance at 8.93 ppm. ^{13}C NMR spectroscopy showed the imidazolinium C-H and carbene C-Pd resonances at 140.1 and 160.5 ppm, respectively.

Multiple recrystallisations were attempted using slow diffusion of diethyl ether into and slow evaporation of saturated acetonitrile, methanol and dichloromethane solutions of **22a** whereupon orange crystals were frequently produced. X-ray crystallographic analysis of the majority of these crystals showed them to be the iodide analogue of the diimidazole dihalide palladium coordination complex **19**, which was not further characterised. The presence of this coordination complex was observed despite ^{1}H NMR spectroscopy indicating pure material of the complex **22a** immediately prior to recrystallization without imidazoline **16** being present, which suggested that the acidic linker CH_2 group was moderately prone to decomposition in solution. Crystals of **22a** suitable for X-ray diffraction were only produced after

multiple repetitions by slow evaporation of a saturated acetonitrile solution, alongside crystals of the diiodide coordination complex **19a** analogue (Figure 4.8).

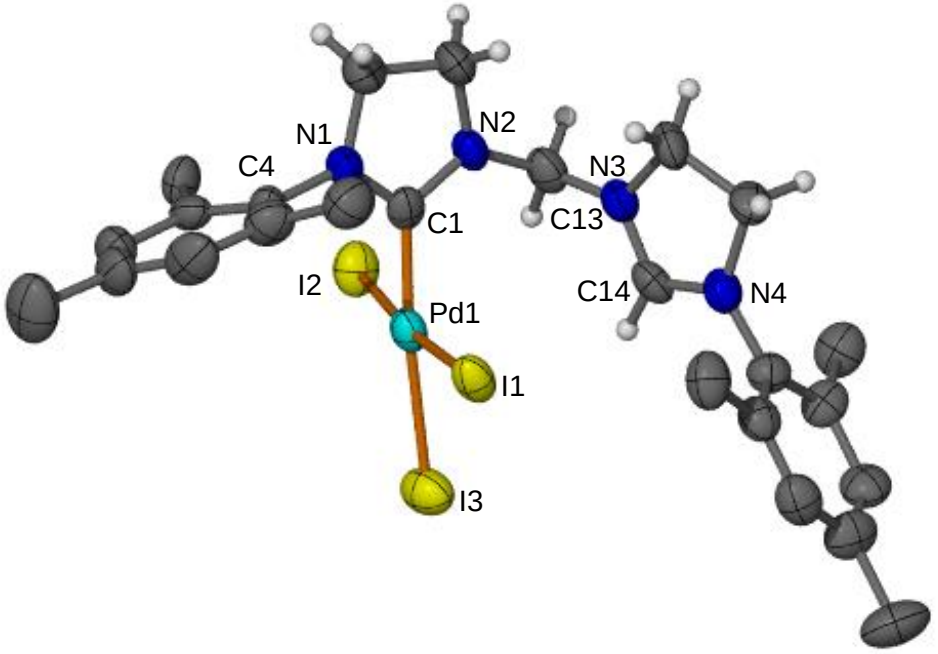

Figure 4.8. Molecular structure of [{(^{S}MesIm)(^{S}MesImH)CH_2}PdI_3], **22a**. All *N*-substituent hydrogen atoms, lattice acetonitrile and diethyl ether solvent molecules are omitted for clarity. Selected bond lengths (Å) and angles (°): Pd1-C1 1.981(12), Pd1-I1,I2,I3 2.6179(13),2.6080(13),2.6622(14), C1-Pd1-I1,I2 89.1(3),87.1(3), I3-Pd1-I1,I2 91.16(4),92.21(4), Pd1-C1-N1,N2 121.2(8),130.9(8).

The pendant imidazolinium moiety of **22a** and the presence of the three ancillary iodide ligands was confirmed by X-ray crystallography. The palladium coordination plane displayed a slightly distorted square planar geometry with the palladium atom sitting *ca.* 0.1 Å above the C1,I1,I2,I3 mean plane. The Pd1-C1 bond length was identical within error to the unsaturated analogue **12b**.

An overlay of the X-ray crystallographic structures of the saturated pendant complex **22a** with its unsaturated analogue **12b** showed that there appear to be noticeable

effects of the different imidazolinium backbone (Figure 4.9), although crystal packing effects and H-I interactions between adjacent molecules may cause some of these differences.

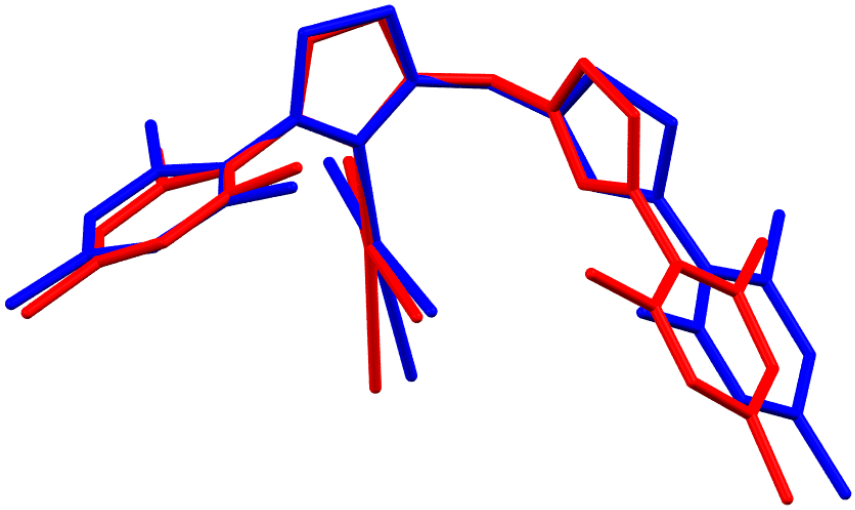

Figure 4.9. Overlay of the pendant imidazolinium methylene-linked mono(NHC) palladium triiodide complexes with unsaturated (**12b**, red) and saturated (**22a**, blue) imidazolium backbones (atoms Pd1, C4, N1, C1, N2, C13 overlaid).

The ethylene- and propylene-linked pendant imidazolinium mono(NHC) palladium tribromide complexes [{(^{S}MesIm)(^{S}MesImH)C_2H_4}$PdBr_3$] **22b** and [{(^{S}MesIm)(^{S}MesImH)C_3H_6}$PdBr_3$] **22c** were directly prepared. The relevant imidazolium salt **17b** or **17c**, $PdBr_2$(COD) and sodium acetate were dried *in vacuo* and dissolved in DMSO. The solution was stirred at 50 °C for 4 hours, after which the solvent was removed *in vacuo* at 110 °C and the orange glass redissolved in dichloromethane. The solution was filtered through Celite and allowed to concentrate over 16 hours to produce a yellow precipitate. This was collected by filtration as pure product in yields of 6 % and 9 % for **22b** and **22c**, respectively (Scheme 4.9).

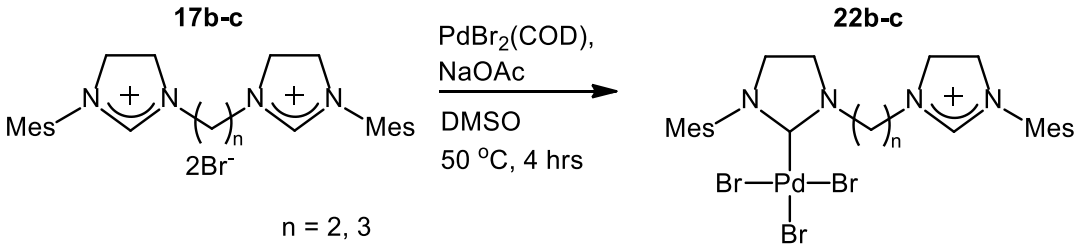

Scheme 4.9. Synthesis of pendant imidazolinium extended linker palladium tribromide complexes **22b** and **22c**.

Successful synthesis of the pendant imidazolinium mono(NHC) palladium tribromide complexes was supported by ^{1}H NMR spectroscopy. For the ethylene-linked complex **22b** the desymmetrisation of the mesityl *ortho*-methyl groups was evident in their appearance as overlapping resonances of correct integration in the region 2.26-2.32 ppm rather than as a single resonance. The C4/5 NHC/imidazolinium protons had distinct separations as broad singlets at 3.87 and 4.46 ppm and the ethylene linker protons were observed as multiplets at 4.05 and 4.21 ppm. The imidazolinium C-2 proton appeared as a single resonance at 8.87 ppm, consistent with the proposed pendant imidazolinium monocarbene structure.

The propylene-linked compound **22c** showed similar signs of desymmetrisation, with the splitting of the *ortho*- and *para*- mesityl methyl protons as four resonances at 2.26, 2.27, 2.30, and 2.37 ppm. The *N*-CH_2 linker protons were observed as a broad resonance at 3.76 ppm and a multiplet spanning 4.30-4.39 ppm, while the resonance of the central CH_2 linker group overlapped the mesityl *ortho*-CH_3 resonance at 2.30 ppm. The imidazolinium C-2 proton resonance was observed at the expected downfield position at 8.88 ppm as a single proton to further confirm the pendant arrangement of the ligand. ^{13}C NMR spectroscopy was also in agreement with the proposed desymmetrised products **22b** and **22c** with the pendant

imidazolinium C-2 peaks observed at 159.5 and 159.9 ppm, respectively. Elemental composition microanalysis of compounds **22b** and **22c** was also consistent with the proposed monocarbene pendant imidazolinium palladium tribromide products.

The ^{1}H NMR spectra of complexes **22b** and **22c** were identical to those observed from the products obtained from the reaction between the extended linker imidazolinium salts with palladium acetate, confirming that the standard synthesis for the chelating bis(NHC) palladium complexes does indeed produce monocarbene pendant imidazolinium products for the saturated analogues.

Recrystallisations of complexes **22b** and **22c** were attempted with both slow diffusion of diethyl ether into and slow evaporation of saturated solutions of acetonitrile and methanol. In all cases where orange crystals were produced, X-ray diffraction showed them to be the coordination complex **19**. As with the methylene-linked pendant analogue, it appears that these compounds undergo partial decomposition under the recrystallisation conditions as ^{1}H NMR spectroscopic data of the specific samples indicated pure product immediately prior to recrystallisation and only baseline impurities consistent with the ^{1}H NMR spectra of **19** after recrystallisation.

The addition of excess sodium acetate to ^{1}H NMR samples of both **22b** and **22c** resulted in the formation of multiple species by NMR spectroscopic analysis. After 24 hours it was observed that the imidazolinium C-2 proton resonances had been significantly reduced in proportion to the other resonances. No significant downfield chemical shifts appeared for the ethylene-linked analogue **22b**, though a small peak was observed at 10.19 ppm for the propylene-linked analogue **22c**. This was consistent with the downfield shift in the C-2 proton due to hydrogen bonding

observed in the conversion of the unsaturated palladium trihalide complexes to the dihalide acetate intermediates discussed in Chapter 2. This suggests that future efforts to form saturated extended linker chelating bis(NHC) palladium complexes may be possible with modifications to the standard methods utilising additions of base. It is worth noting that the low yields and alternative reaction products observed for the extended linker unsaturated analogues may also occur in attempts to prepare these saturated chelated bis(NHC) palladium dibromide complexes.

4.2.4 **Disilver Complexes with Saturated NHC Ligands**

The formation of both saturated and unsaturated NHC complexes by transmetallation with silver NHC species is well established.[10,18,19] Hahn and co-workers recently reported a high-yielding synthesis of bridging disilver dicarbene complexes using a modified literature procedure to other reported methods.[20] This method has previously been used by our group to access the unsaturated *N*-mesityl methylene linked disilver complex, of which analogues with different counteranions had been prepared prior in poorer yields (Scheme 4.10).[16] The subsequent reaction of the unsaturated disilver complex $[\{(MesIm)_2CH_2\}_2Ag_2][PF_6]_2$ with PdBrMe(COD) resulted in the formation of a chelated bis(NHC) palladium complex which was active in the polymerisation of ethylene and carbon monoxide.[16] We sought to use this methodology to prepare the saturated analogue of this highly active species, and to prepare the extended linker chelated palladium complexes *via* reaction of the disilver species with $PdBr_2$(COD) that were not accessible by our conventional procedure.

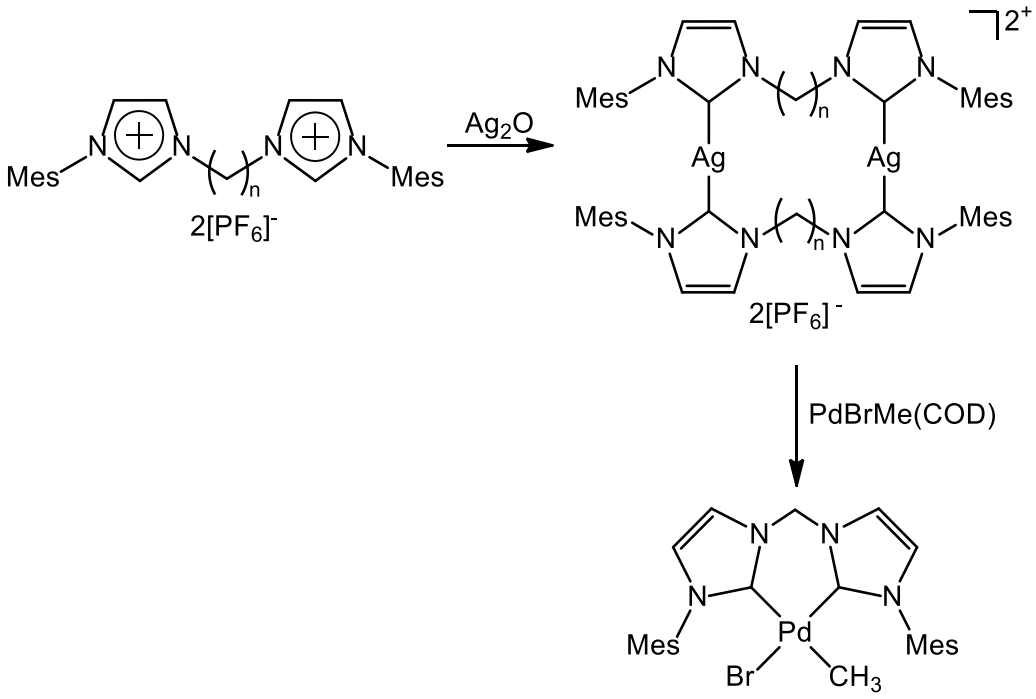

Scheme 4.10. Synthesis of unsaturated bis(NHC) disilver complex and subsequent transmetallation to form chelating bis(NHC) palladium bromomethyl complex.[16]

There have been previous reports of silver NHC complexes which contain variable $(Ag_xBr_y)^{n-}$ counteranions,[19,21] which impede stoichiometric transmetallation reactions. Thus we exchanged the imidazolinium salt halide counteranions by dissolution of the dibromide salts **17a** and **17c** in water, followed by the addition of excess potassium hexafluorophosphate. After approximately one minute the respective imidazolinium dihexafluorophosphate salts **17d** and **17e** precipitated as white solids, which were collected by filtration and dried *in vacuo* in essentially quantitative yield.

The disilver complexes $[\{(^{S}MesIm)_2CH_2\}_2Ag_2][PF_6]_2$ **23a** and $[\{(^{S}MesIm)_2C_3H_6\}_2Ag_2][PF_6]_2$ **23c** were prepared using a modified literature procedure.[20] The relevant imidazolinium salts **17d** and **17e** were dissolved in acetonitrile with 1.25 equivalents of silver oxide and the resulting suspensions were

heated at 55 °C for 18 hours with the exclusion of light. The cooled suspensions were filtered through Celite and the filtrates concentrated. Diethyl ether was added to precipitate the products as white solids which were collected by filtration and washed with diethyl ether (Scheme 4.11). Attempts to prepare the ethylene-linked analogue under these conditions resulted in an impure product which was not successfully isolated for NMR or X-ray crystallographic analysis.

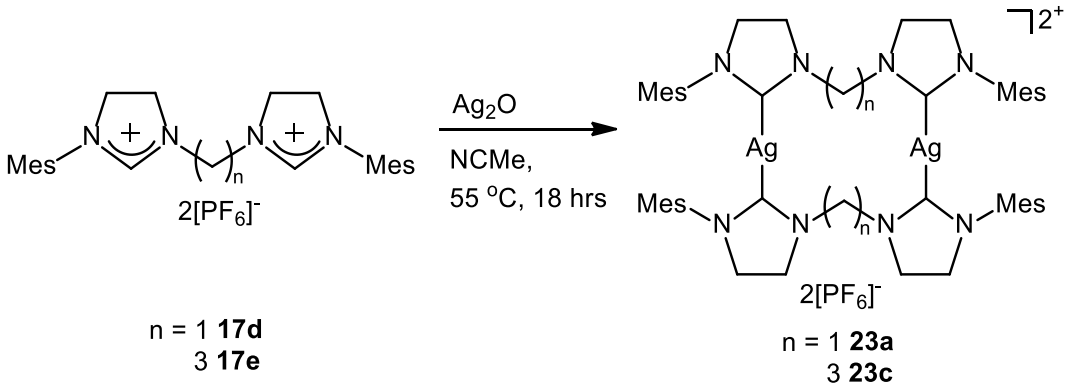

Scheme 4.11. Synthesis of disilver bis(NHC) complexes **22a** and **22c**.

Crystals of the silver complexes **23a** and **23c** suitable for X-ray diffraction were produced by slow diffusion of diethyl ether into saturated acetonitrile solutions as colourless needles. Complex **23a** (Figure 4.10) showed the expected $P\bar{1}$ structure similar to that previously observed for the unsaturated *N*-mesityl bis(NHC) methylene linked disilver complex reported by Slaughter and coworkers.[21] The Ag-C bond lengths (2.084(4)-2.109(4) Å) of complex **23a** are similar to those of the unsaturated NHC disilver analogue and within the normal range of other published silver NHC structures.[16,21,22] It also shares the relatively short Ag···Ag distance (3.1992(12) Å) with its unsaturated analogue.[21] Weak silver-hydrogen interactions between the methylene-linker protons and the silver centres were observed, ranging from *ca.* 2.88-3.07 Å.

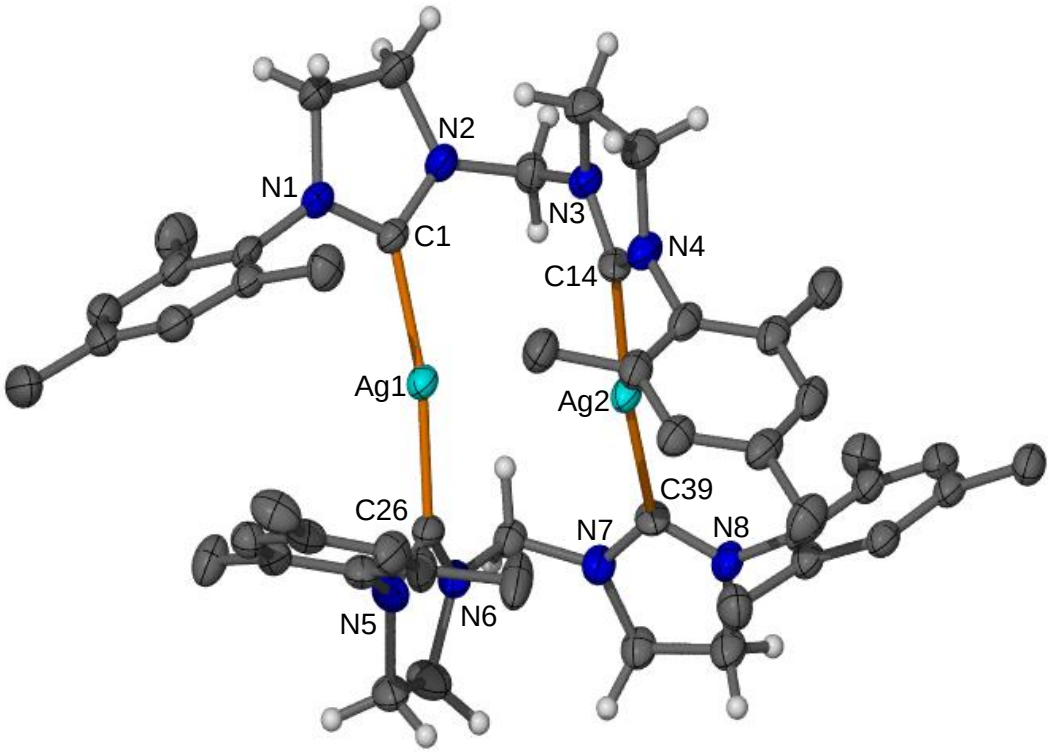

Figure 4.10. Molecular structure of the cation of $[\{(^{S}MesIm)_2CH_2\}_2Ag_2][PF_6]_2$ **23a**. Displacement ellipsoids are shown at the 50 % probability level. All *N*-substituent hydrogen atoms, $[PF_6]^-$ counteranions and lattice acetonitrile solvent molecules are omitted for clarity. Selected bond lengths (Å) and angles (°): Ag1-Ag2 3.1992(12), Ag1-C1,C26 2.085(4),2.084(4), Ag2-C14,C39 2.100(4),2.109(4), C1-Ag1-C26 168.38(15), C14-Ag2-C39 173.35(16), Ag1-C1-N1,N2 124.7(3),127.1(3), Ag1-C26-N5,N6 123.4(3),127.3(3), Ag2-C14-N3,N4 126.2(3),124.6(3), Ag2-C39-N7,N8 127.3(3),123.3(3).

The propylene-linked disilver complex **23c** contained two molecules in the asymmetric unit, each with a C_2 symmetric centre. Similar to previously reported propylene-linked disilver carbene complexes, there was no silver-silver interaction and the Ag-Ag distance of 5.858 (5.942(2)) Å was similar to those reported by Liu and co-workers for *N*-ethyl (5.735(3) Å) and *N*-benzyl (5.578(2) Å) analogues.[22] The Ag-C distances (2.106(3) (2.093(3)) Å, 2.106(3) (2.100(3)) Å) and relatively linear

C-Ag-C angles (177.39(11) (175.96(12)) °) are similar to those in complex **23a** and with other literature silver NHC complexes.[21,22]

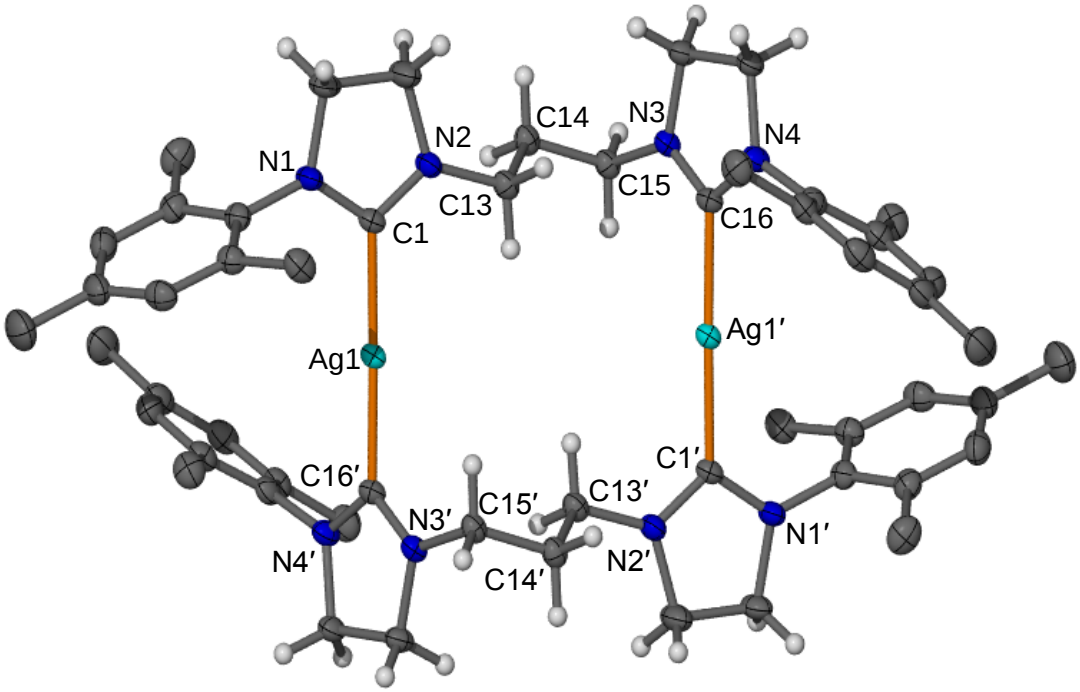

Figure 4.11. Molecular structure of one dication of $[\{(^{S}MesIm)_2(C_3H_6)\}_2Ag_2][PF_6]_2$ **23c**. Displacement ellipsoids are shown at the 50 % probability level. All *N*-substituent hydrogen atoms, $[PF_6]^-$ counteranions and lattice acetonitrile solvent molecules are omitted for clarity. Selected bond lengths (Å) and angles (°) (values for the second molecule provided in brackets): Ag1-Ag1′ 5.858(2) (5.949(2)), Ag1-C1,C16, 2.105(3) (2.092(3)),2.104(3) (2.101(3)), C1-Ag1-C16 177.39(10) (175.99(11)), Ag1-C1-N1,N2 109.2(2) (122.2(2)),128.3(2) (128.7(2)), Ag1-C16-N3,N4 127.0(2) (130.8(2)),123.0(2) (119.7(2)).

^{1}H and ^{13}C NMR spectroscopy were also consistent with the proposed structures of **23a** and **23c**. The methylene-linked bridging bis(NHC) disilver complex **23a** displayed a single *N*-Mes ring environment with restricted N-C bond rotation, showing distinct resonances for the *ortho*-methyl protons on each ring at 1.65 and

1.75 ppm, while the mesityl *meta*-CH proton resonances were singlets at 6.87 and 7.01 ppm. Thus the twisted nature of the C-Ag-C coordination geometries seen in the solid state structure appeared to interconvert. The methylene linker protons appeared as an AB spin system, with the two separate doublets at 4.85 and 6.08 ppm, consistent with the silver-hydrogen interactions observed by X-ray crystallography, similar to those seen in the unsaturated dipalladium hydride complex **5a** discussed in Chapter 2. The ^{13}C NMR spectroscopy showed the Ag-C carbenes as a doublet at 203.7 ppm, though no ^{107,109}Ag-^{13}C coupling was observed. This is common for silver-NHC complexes, and is a sign of labile Ag-C bonds.[23]

The propylene-linked bridging bis(NHC) disilver complex **23c** appeared to have higher symmetry by ^{1}H and ^{13}C NMR spectra, consistent with X-ray crystallographic analysis. The mesityl *ortho*- and *para*-CH_3 protons appeared as singlets at 1.86 and 2.34 ppm respectively, while the linker *N*-CH_2 protons appeared as a triplet at 3.57 ppm. The central linker CH_2 group was observed as a triplet at 1.94 ppm. The Ag-C carbene resonance was observed with ^{13}C NMR spectroscopy as a doublet at 202.7 ppm. Again, no ^{107,109}Ag-^{13}C coupling was observed.

Transmetallation reactions similar to those reported by Slaughter[21] were attempted with complexes **23a** and **23c** using $PdBr_2$(COD) and PdBrMe(COD). In all cases the silver complex was dissolved in acetonitrile and 1-2 equivalents of the relevant palladium complex added. The solution was stirred with exclusion from light for 3 hours and the resultant silver halide precipitate removed by filtration through Celite (Scheme 4.12). The resultant yellow precipitate from each reaction was examined by ^{1}H NMR spectroscopy.

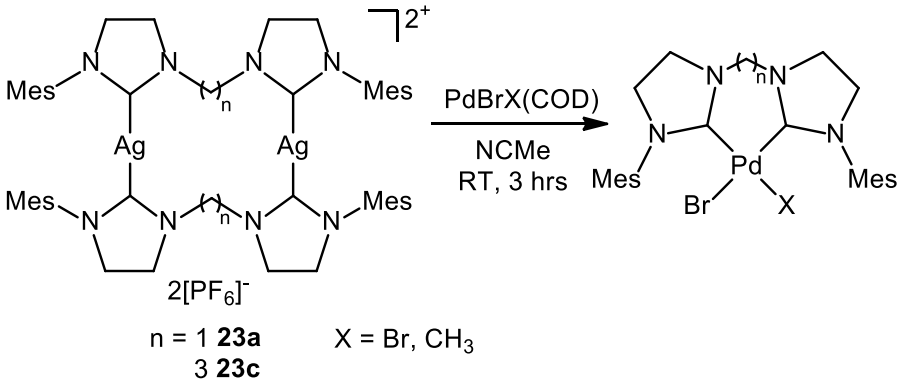

Scheme 4.12. Proposed transmetallation scheme for the synthesis of chelated bis(NHC) palladium complexes from disilver complexes **23a** and **23c**.

The reaction of the methylene-linked bridging bis(NHC) disilver complex **23a** with 2 equivalents of $PdBr_2(COD)$ did produce the chelated dibromide complex **18a** as an impure product (determined by ^{1}H NMR spectroscopy). However there was no success in forming the chelated bis(NHC) palladium bromomethyl complex from **23a**, with ^{1}H NMR spectroscopic analysis indicating a mixture of impure products, all of which lacked the characteristic resonance in the 4-7 ppm range for the methylene linker protons.

The transmetallation reaction of the propylene-linked bridging bis(NHC) disilver complex **23c** with $PdBr_2(COD)$ was also unsuccessful by ^{1}H NMR spectroscopic analysis, with a mixture of products observed.

4.2.5 **Attempted Synthesis of Asymmetric Saturated/Unsaturated Complex**

The catalytic properties and reactivity of the unsaturated *N*-mesityl bis(NHC)palladium(II) complexes has been explored previously.[13,14] We sought to prepare an asymmetric diimidazolium/inium salt to explore the difference in ligand electronic effects for catalytic applications. We also wished to examine the possible

formation of palladium(I) species by reduction under basic conditions, as was observed for the unsaturated analogue **5a** (see Chapter 2).

The selective synthesis of *N*,*N*′-asymmetrically substituted diimidazolium salts has been previously reported, in which a monoimidazolium alkylhalide such as *N*-mesityl-*N*′-methylhalide imidazolium halide **24**, was prepared and reacted with a different imidazole (Scheme 4.13).[24]

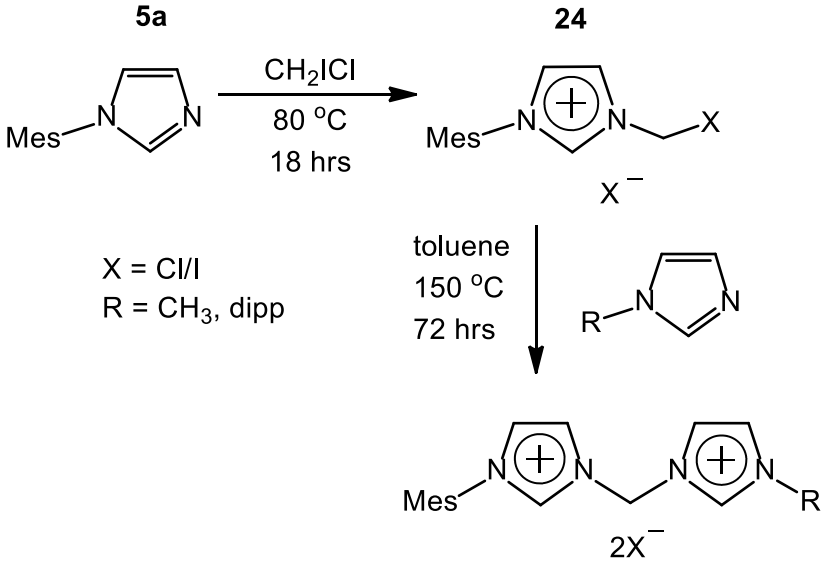

Scheme 4.13. Synthesis of asymmetric imidazolium salts *via* a monoimidazolium alkylhalide.[24]

The synthesis of asymmetrically substituted monoimidazolinium alkyl halide salts has been reported by Straub and co-workers. They describe difficulties with the more reactive imidazoline species in these conditions,[10] showing that the reaction of saturated *N*-diisopropylphenyl imidazole and 1,3-dibromopropane produced the *N*-diisopropylphenyl-*N*′-propylbromide imidazolinium bromide salt as a major product inseparable from the diimidazolinium dibromide salt, which they used impure for further reactions (Scheme 4.14)

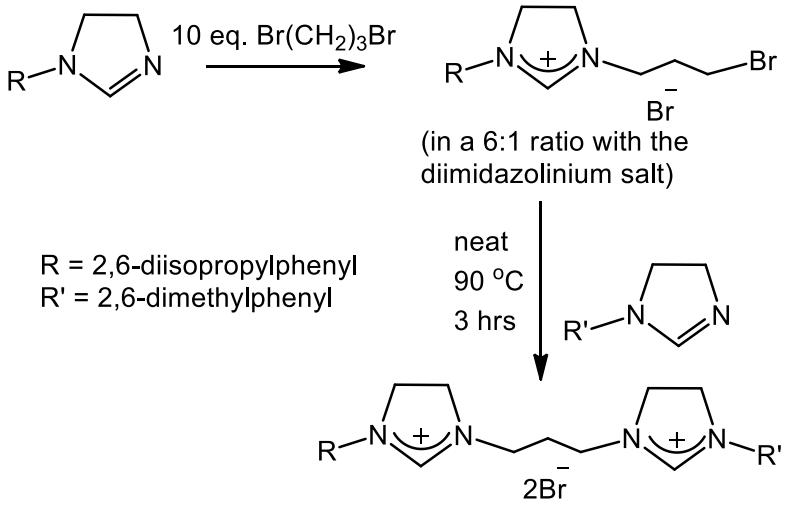

Scheme 4.14. Synthesis of asymmetrically substituted diimidazolinium salt reported by Straub.[10]

In a modified literature procedure,[24] *N*-mesityl imidazoline **16** was dissolved in neat chloroiodomethane and heated at 80 °C for 18 hours (Scheme 4.15). The resultant white precipitate was collected by filtration and dried *in vacuo*. ^{1}H NMR spectroscopic analysis of the product showed it was identical to the diimidazolinium salt **17a**, however. The reaction was repeated at room temperature and the resultant white precipitate was shown by ^{1}H NMR spectroscopic analysis to be the hydrohalide salt of the imidazoline **16a**, observed previously observed as a by-product in the synthesis of imidazolinium **17a**. This hydrohalide salt **16a** was also obtained from a room temperature reaction of imidazoline **16** and dibromomethane under the conditions used by Straub and co-workers.[10]

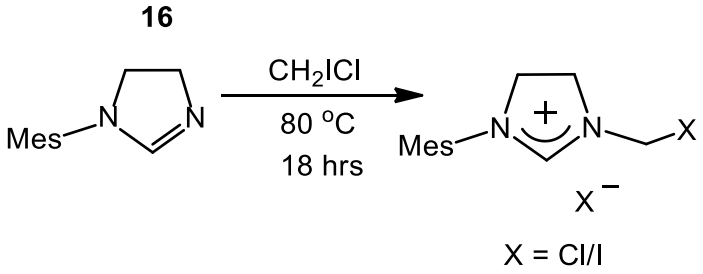

Scheme 4.15. Proposed synthesis of saturated methylhalide monoimidazolinium halide salt.

An alternative pathway was pursued, in which the unsaturated imidazolium methyl halide salt was prepared according to literature methods.[24] This was suspended in toluene with the imidazoline **16** and heated at 140 °C for 72 hours as per the modified literature procedure used to prepare asymmetrically substituted diimidazolium salts (Scheme 4.16).[24] The off-white precipitate was collected by filtration and examined by ^{1}H NMR spectroscopic analysis, which indicated that there was a mixture of products. Comparison with previously obtained spectroscopic data allowed us to identify the two major products as remaining unsaturated imidazolium methyl halide salt alongside the saturated diimidazolinium dihalide salt **17a**.

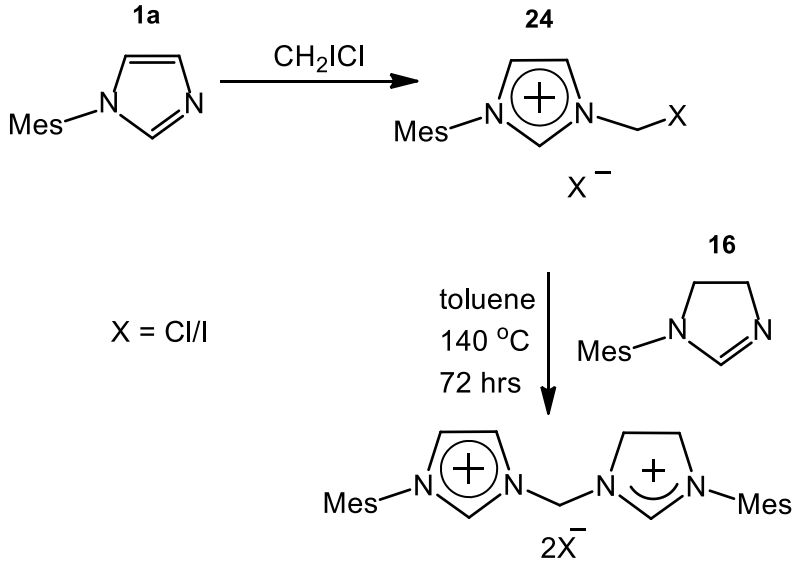

Scheme 4.16. Proposed synthesis of saturated/unsaturated mixed diimidazolium salt *via* the unsaturated imidazolium methyl halide precursor **24**.

We hypothesise that this occurs during the intended substitution reaction, where the imidazole is a better leaving group than the halide, thus the imidazolinium methyl halide is formed instead. This species, as we have previously established, reacts rapidly with a second equivalent of imidazoline **16** to form the diimidazolinium salt.

The tendency of the imidazole to act as a good leaving group likely contributed to the formation of the coordination complex **19**, especially in the case of recrystallisations of the pendant complexes **22a-c**, where ^{1}H NMR spectroscopy confirmed pure products prior to recrystallisation. As we have been unsuccessful to date in preparing the mixed saturated/unsaturated bis(NHC) ligand precursor, we have not been able to examine this analogue further.

4.3 Conclusion

We have prepared the first isolated and structurally characterised saturated chelated bis(NHC) palladium complex [{(^{S}MesIm)$_2$CH$_2$}PdBr$_2$] **18a**. We also observed a

secondary decomposition product, the coordination complex $[(^{S}MesImH)_2PdBr_2]$ **19a**. Complex **18a** was similar to its unsaturated analogue, and underwent the same reactivity with sodium hexafluorophosphate to form the dicationic acetonitrile adduct $[\{(^{S}MesIm)_2CH_2\}Pd(NCMe)_2][PF_6]_2$ **20a**. This complex was studied for catalytic activity in the copolymerisation of ethylene and carbon monoxide, but was found to have less activity than the previously examined unsaturated analogue. It is possible that this reduced activity could be due to increased reactivity towards the formation of decomposition products such as dipalladium(I) hydride species similar to that observed for the unsaturated analogue.

Complex **20a** was reacted with sodium carbonate to examine whether it showed similar reactivity to the unsaturated analogue in the formation of a dipalladium(I) hydride species. Solution colour change was potentially indicative of this oxidation state being present, however we have been unsuccessful to date in isolating or confirming the presence of $[\{\mu\text{-}(^{S}MesIm)_2CH_2\}_2Pd_2H][PF_6]$ **21a**.

Extended linker analogues of the imidazolinium salts $[(^{S}MesIm)_2C_2H_4]Br_2$ **17b** and $[(^{S}MesIm)_2C_3H_6]Br_2$ **17c** were prepared with ethylene and propylene linkers. Reaction of these with palladium acetate was found to produce the monocarbene pendant imidazolinium palladium tribromide complexes $[\{(^{S}MesIm)(^{S}MesImH)C_2H_4\}PdBr_3]$ **22b** and $[\{(^{S}MesIm)(^{S}MesImH)C_3H_6\}PdBr_3]$ **22c**. The proposed structures were consistent with NMR spectroscopic and elemental microanalysis, though to date no X-ray crystal structure has been obtained. These complexes showed particular sensitivity during recrystallisation and partially decomposed to form the coordination complex **19a**. The methylene-linked monocarbene pendant imidazolium palladium triiodide complex was also prepared and examined by NMR spectroscopy and X-ray crystallography.

The methylene- and propylene-linked bridging bis(NHC) disilver complexes $[\{(^{S}MesIm)_2CH_2\}_2Ag_2][PF_6]_2$ **23a** and $[\{(^{S}MesIm)_2C_3H_6\}_2Ag_2][PF_6]_2$ **23c** were prepared and structurally characterised. Transmetallation reactions with $PdBr_2(COD)$ and PdBrMe(COD) to form the chelated bis(NHC) palladium dibromide or bromomethyl complexes were trialled and, to date, have been unsuccessful.

The synthesis of an asymmetric saturated/unsaturated imidazolium/inium salt was attempted. Attempts to isolate the necessary imidazolinium methylhalide compound were unsuccessful, with various reaction conditions only producing the diimidazolinium salt **17a** or the hydrobromide salt of imidazoline **16, 16a**. Attempts to react imidazoline **16** with the reported imidazolium methyl halide salt **24** produced a mixture of products including the diimidazolinium salt **17a** and unreacted starting materials.

4.4 Experimental

4.4.1 General Conditions

All syntheses of imidazolium salts, silver transmetallation reactions and halide ligand exchange reactions were carried out in air, while the syntheses of the palladium complexes were conducted under an inert atmosphere of high purity argon (BOC gases) using standard Schlenk techniques. Anhydrous DMSO, methanol and acetonitrile were purchased from Sigma-Aldrich and stored over activated 3 Å molecular sieves. Other anhydrous solvents used were obtained by passage through columns on an Innovative Technologies Solvent Purifier.

Palladium(II) acetate was purchased from Precious Metals Online and used as received. Imidazoline **16**,[10] the propylene linked diimidazolinium dibromide salt **17c**[10] and *N*-mesityl-*N*′-methylhalide imidazolium halide **24**[24] were prepared

according to literature procedures. All other reagents were purchased from Sigma-Aldrich and used as received. For non-air-sensitive syntheses, solvents were analytical grade and used as received.

4.4.2 Instrumentation

NMR spectroscopic studies were carried out on a Bruker Avance 3 HD 400 MHz Wide Bore spectrometer with a 5 mm BBFO probe in $CDCl_3$ and DMSO-d_6. NMR spectral data was obtained at room temperature (293 K) unless specified otherwise. $CDCl_3$ was used as received. DMSO-d_6 was distilled over CaH_2 and stored over 4 Å molecular sieves.

^{1}H NMR spectra were obtained at 399.58 MHz while ^{13}C NMR spectra were recorded at 100.47 MHz. ^{1}H NMR spectra were referenced to the ^{1}H resonance of the residual solvent peaks, while ^{13}C NMR spectra were referenced to the deuterated ^{13}C resonance. Elemental analyses were conducted by the Central Science Laboratory at the University of Tasmania using a Carlo Erba EA1108 Elemental Analyser. X-ray crystallography studies were conducted at the Australian Synchrotron using the MX1 and MX2 beamlines.

4.4.3 Carbon monoxide/ethylene Copolymerisation Trial

20 mg of catalyst complex **20a** was dissolved in methanol (50 mL) under argon atmosphere and transferred to a 0.3 L stainless steel Parr 5500 Compact Mini Reactor also under an argon atmosphere. The autoclave was charged in turn with 10 bar of ethylene and 10 bar of carbon monoxide, heated to 70 °C and stirred for two hours. The autoclave was cooled to room temperature and the black precipitate collected by filtration.

4.4.4 X-ray Crystallography

Data for **17a-23c** were collected at -173 °C on crystal mounted on a Hampton Scientific cryoloop at the MX1 or MX2 beamline of the Australian Synchrotron.[25,26] Data completeness is limited by the single axis goniometer on the MX beamlines at the Australian Synchrotron. The structures were solved by direct methods with SHELXS-97,[27] refined using full-matrix least-squares routines against F^2 with SHELXL-97, and visualised using X-SEED or OLEX2.[28,29] All non-hydrogen atoms were refined anisotropically. All hydrogen atoms were placed in calculated positions and refined using a riding model with fixed C-H distances of 0.95 Å (sp^2CH), 0.99 Å (CH_2), 0.98 Å (CH_3). The thermal parameters of all hydrogen atoms were estimated as $U_{iso}(H) = 1.2U_{eq}(C)$ except for CH_3 where $U_{iso}(H) = 1.5U_{eq}(C)$. CIF files for X-ray crystallographic analysis can be provided upon request.

4.4.5 Synthesis

Preparation of [(^{S}MesIm)$_2$CH$_2$]Br$_2$ 17a

Imidazoline **16** (0.38 g, 2.0 mmol) and dibromomethane (0.53 g, 3.0 mmol) were dissolved in toluene (8 mL) and heated at 130 °C in a sealed pressure tube for 24 hours. The resultant white precipitate was collected by filtration, washed with chloroform (2 x 10 mL) and dried in vacuo as pure **17a** (0.44 g, 40 % yield). m.p. 304 °C.

^{1}H NMR (399.58 MHz, DMSO-d_6): δ 2.29 (6H, s, *p*-CH_3), 2.34 (12H, s, *o*-CH_3), 4.31 (8H, s, ImCH_2), 5.50 (2H, s, CH_2), 7.08 (4H , s, *m*-CH), 9.24 (2H, s, ImCH).

^{13}C NMR (100.48 MHz, DMSO-d_6): δ 17.4 (CH_3), 20.5 (CH_3), 47.4 ($ImCH_2$), 51.4 ($ImCH_2$), 59.0 (CH_2), 129.4 (*m*-CH), 130.7 (C), 135.3 (C), 139.6 (C), 160.4 (ImCH).

Found: C, 52.84; N, 9.95; H, 6.63. Calc. for $C_{25}H_{34}N_4Br_2.H_2O$: C, 52.83; N, 9.86; H, 6.38.

Preparation of [(^{S}MesIm)$_2$C$_2$H$_4$]Br$_2$ 17b

In a modified literature procedure[10] **16** (676.2 mg, 3.60 mmol) 1,2-dibromoethane (338.9 mg, 1.80 mmol) were heated at 100 °C for 2 hours. The resultant orange glass was dissolved in dichloromethane (5 mL) and diethyl ether (2 mL) was added to precipitate out pure **17b** as an off white solid which was collected by filtration, washed with diethyl ether (10 mL) and dried *in vacuo* (0.26 g, 24% yield). m.p. 269 °C.

^{1}H NMR (399.58 MHz, $CDCl_3$): δ 2.28 (12H, s, *o*-CH_3), 2.29 (6H, s, *p*-CH_3), 4.26 (4H, t, *J* = 10.6 Hz, $ImCH_2$), 4.48 (4H, s, CH_2), 4.79 (4H, t, *J* = 10.7 Hz, $ImCH_2$), 6.92 (4H, s, *m*-CH), 10.34 (2H, s, ImCH).

^{13}C NMR (100.48 MHz, $CDCl_3$): δ 18.4 (CH_3), 21.1 (CH_3), 45.7 (CH_2), 50.8 ($ImCH_2$), 51.4 ($ImCH_2$), 130.1 (C), 135.1 (C), 140.5 (C), 159.9 (ImCH).

Preparation of [(^{S}MesIm)$_2$C$_3$H$_6$]Br$_2$ 17c

In a modified literature procedure[10] a neat mixture of **16** (1.04 g, 5.5 mmol), 1,3-dibromopropane (0.56 g, 2.8 mmol) were heated at 100 °C for 2 hours. The resultant orange glass was dissolved in dichloromethane (5 mL) and diethyl ether (2 mL) was added to precipitate out pure **17c** as an off white solid which was dried *in vacuo* and determined by ^{1}H NMR spectroscopy to be identical to literature (1.36 g, 85 % yield). m.p. 288 °C.

^{1}H NMR (399.58 MHz, DMSO-d_6): δ 2.15 (2H, quin, J = 6.9 Hz, CH_2), 2.27 (18H, s, *o*-CH_3, *p*-CH_3), 3.66 (4H, t, J = 6.9 Hz, *N*-CH_2), 4.20 (8H, s, ImCH_2), 7.04 (4H, s, *m*-CH), 8.88 (2H, s, ImCH).

Found: C, 54.38; N, 9.37; H, 6.84. Calc. for $C_{27}H_{38}N_4Br_2.(H_2O)$: C, 54.32; N, 9.39; H, 6.76.

Preparation of diimidazolium dihexafluorophosphate salts

Conversion of the dihalide diimidazolinium salts **17a** and **17c** to dihexafluorophosphate salts **17d** and **17e** was achieved by dissolving the respective diimidazolinium salt in water and treating it with a saturated aqueous solution of potassium hexafluorophosphate. The resultant white precipitate was collected by filtration and dried *in vacuo* in essentially quantitative yield and used directly without further characterisation.

Preparation of [{(^{S}MesIm)$_2$CH$_2$}PdBr$_2$] 18a

This is a modified literature procedure.[13] In a pre-dried Schlenk flask, the imidazolinium **17a** (151.4 mg, 0.28 mmol) and $Pd(OAc)_2$ (61.9 mg, 0.28 mmol) were dried by heating at *ca.* 70 °C *in vacuo* prior to the addition of DMSO (8 mL). The resulting orange solution was stirred at 50 °C for 3 hours and 110 °C for 2 hours, whereupon the orange-yellow solution paled slightly. The solvent was removed *in vacuo* and dichloromethane (15 mL) was added. The product precipitated from the filtrate within 5 minutes as an off-white solid which was collected by filtration and washed with a further 10 mL of dichloromethane (104.8 mg, 58 % yield). m.p. 294 °C(dec).

^{1}H NMR (399.58 MHz, DMSO-d_6): δ 2.24 (18H, bs, *o*-CH_3, *p*-CH_3), 3.70-4.18 (8H, m, ImCH_2 x4), 4.89 (1H, bs, CH_2), 5.34 (1H, bs, CH_2), 6.90 (4H, s, *m*-CH).

^{13}C NMR (100.48 MHz, DMSO-d_6): δ 19.4 (CH_3), 20.5 (CH_3), 48.8 (ImCH_2), 53.3 (ImCH_2), 60.8 (CH_2), 128.8 (CH), 134.2 (C), 136.8 (C), 137.1 (C), 167.7 (Pd-C).

Found: C, 45.93; N, 8.65; H, 4.85. Calc. for $C_{25}H_{32}N_4PdBr_2$: C, 45.86; N, 8.56; H, 4.93.

Preparation of [(^{S}MesImH)$_2$PdBr$_2$] 19

N-mesityl imidazoline **16** (141.7 mg, 0.38 mmol) and $PdBr_2$(COD) (140.9 mg, 0.38 mmol) were dissolved in tetrahydrofuran (35 mL) and stirred for 16 hours. The solvent was removed *in vacuo* and the orange residue redissolved in acetonitrile whereupon compound **19** precipitated out as an orange crystalline solid which was collected by filtration (226.1 mg, 0.35 mmol, 93 % yield). m.p. 220 °C(dec). Accurate elemental microanalysis not obtained due to an unidentified inorganic impurity which appeared inseparable from the complex.

^{1}H NMR (399.58 MHz, DMSO-d_6): δ 2.14 (12H, s, *o*-CH_3), 2.22 (6H, s, *p*-CH_3), 3.57 (4H, t, *J* = 10.5 Hz, ImCH_2), 3.86 (4H, t, *J* = 10.6 Hz, ImCH_2), 6.94 (4H, s, *m*-CH), 7.41 (2H, s, ImCH).

^{13}C NMR (100.48 MHz, DMSO-d_6): δ 17.5 (*o*-CH_3), 20.5 (*p*-CH_3), 48.2 (CH_2), 55.1 (CH_2), 129.2 (*m*-CH), 133.5(C), 135.9 (*N*-C), 137.6 (C), 160.8 (CH).

Preparation of [{(^{S}MesIm)$_2$CH$_2$}Pd(NCMe)$_2$][PF$_6$]$_2$ 20a

In a modified literature procedure,[13] palladium complex **18a** (112.5 mg, 0.17 mmol) and $NaPF_6$ (0.77 g, 4.58 mmol) were dissolved in a 1:1 mixture of acetonitrile and

water (30 mL each) and stirred for 2 hours at 80 °C. The solution was cooled and the acetonitrile removed in vacuo with the resultant white precipitate collected by filtration. The solid was dried and recrystallised by slow diffusion of diethyl ether into a saturated acetonitrile solution to afford the product **20a** overnight as a colourless crystalline solid (102.5 mg, 0.12 mmol, 69 %). m.p. 224 °C (dec).

^{1}H NMR (399.58 MHz, DMSO-d_6): δ 2.07 (6H s, 2 x NCCH_3), 2.26 (6H, s, *p*-CH_3), 2.28 (12H, s, *o*-CH_3), 3.92-4.03 (4H, m, ImCH_2), 4.06-4.16 (4H, m, ImCH_2), 5.21 (2H, bs, CH_2), 7.00 (4H, s, *m*-CH).

^{13}C NMR (100.48 MHz, DMSO-d_6): δ 1.1 (NC*C*H_3), 18.5 (CH_3), 20.5 (CH_3), 49.2 (ImCH_2), 53.2 (ImCH_2), 60.4 (CH_2), 118.0 (N*C*CH_3), 129.0 (CH), 134.3 (C), 135.6 (*N*-C), 138.1 (C), 175.3 (Pd-C).

Found: C, 40.87; N, 10.76; H, 4.48. Calc. for $C_{25}H_{32}N_4PdBr_2$.NCMe: C, 41.00; N, 10.80; H, 4.55.

Attempted preparation of [{μ-(^{S}MesIm)$_2$CH$_2$}$_2$Pd$_2$H][PF$_6$] 21a

In a modified literature procedure,[14] **20a** (10 mg, 0.01 mmol) was dissolved in deuterated methanol in a Young's NMR tube. Sodium carbonate (5 mg, 0.05 mmol) was added and the suspension was heated at 60 °C. ^{1}H NMR spectroscopic data was collected prior to and immediately after the addition of sodium carbonate, and after 2 and 4.5 hours of heating, during which time the solution turned orange and a change was observed in the ^{1}H NMR spectrum. Isolation of **21a** was not successful and NMR spectra were recorded *in situ*. Elemental microanalysis was not obtained as no pure product was isolated.

^{1}H NMR (399.58 MHz, CD_3OD): δ 2.20-2.25 (36H, m, *p*-CH_3, *o*-CH_3), 3.91-3.99 (8H, m, ImCH_2), 4.05-4.12 (8H, m, ImCH_2), 5.02 (4H, s, CH_2), 6.86 (8H, s, *m*-CH).

^{13}C NMR (100.48 MHz, CD_3OD): δ 18.1 (CH_3), 21.1 (CH_3), 50.3 (ImCH_2), 53.9 (ImCH_2), 62.0 (CH_2), 130.2 (CH), 135.3 (C), 137.1 (C), 139.5 (C), 161.5 (Pd-C).

Preparation of [{(^{S}MesIm)(^{S}MesImH)CH_2}PdI_3] 22a

In a pre-dried Schlenk flask imidazolinium **17a** (98.5 mg, 0.18 mmol), $PdBr_2$(COD) (66.9 mg, 0.18 mmol) and sodium acetate (14.8 mg, 0.18 mmol) were dissolved in DMSO (5 mL) and heated at 50 °C for 4 hours. Sodium iodide (549.4 mg, 3.67 mmol) was added and the solution heated for an additional 50 minutes. The solvent was removed *in vacuo* and the red-brown glass redissolved in a 1:1 mixture of acetonitrile and water (20 mL/ 20mL) and heated at 80 °C for 10 minutes. The acetonitrile was removed in vacuo to produce **22a** as a dark red precipitate which was collected by filtration (92.7 mg, 0.11 mmol, 68 % yield). m.p. 232 °C(dec).

^{1}H NMR (399.58 MHz, DMSO-d_6): δ 2.28 (6H, s, *o*-CH_3), 2.30 (6H, s, *o*-CH_3), 2.44 (6H, s, *p*-CH_3 x2), 3.94 (4H, m, ImCH_2), 4.32 (4H, m, ImCH_2), 5.80 (2H, bs, CH_2), 6.98 (2H, s, *m*-CH), 7.06 (2H, s, *m*-CH), 8.92 (1H, s, ImCH).

^{13}C NMR (100.48 MHz, DMSO-d_6): δ 17.7 (CH_3), 21.00 (CH_3), 21.02 (CH_3), 21.7 (CH_3), 46.9 (ImCH_2), 49.2 (ImCH_2), 51.8 (ImCH_2), 52.6 (ImCH_2), 64.4 (CH_2), 129.8 (*m*-CH), 129.9 (*m*-CH), 131.3(C), 134.2 (C), 135.9 (C), 136.8 (C), 138.7 (C), 140.1 (Pd-C), 160.5 (ImCH).

Found: C, 40.44; N, 7.77; H, 4.43. Calc. for $C_{25}H_{33}N_4PdBr_3$: C, 40.81; N, 7.62; H, 4.52.

Preparation of [{(^{S}MesIm)(^{S}MesImH)C_2H_4}$PdBr_3$] 22b

In a pre-dried Schlenk flask, imidazolinium **17b** (133.1 mg, 0.24 mmol), $PdBr_2$(COD) (88.8 mg, 0.24 mmol) and sodium acetate (19.4 mg, 0.24 mmol) were dried by heating at *ca.* 70 °C *in vacuo* prior to the addition of DMSO (10 mL). The resulting orange solution was heated at 50 °C for 4 hours. The solvent was removed *in vacuo* and the brown residue was dissolved in dichloromethane (25 mL) and filtered through Celite. The product precipitated from the filtrate after partial evaporation over 16 hours as a yellow powder which was collected by filtration as pure **22b** (10.9 mg, 6 % yield). m.p. 245 °C(dec).

^{1}H NMR (399.58 MHz, DMSO-d_6): δ 2.30 (12H, m, *o*-CH_3 x2), 2.36 (6H, s, *p*-CH_3 x2), 3.87 (4H, bs, ImCH_2 x2), 4.05 (2H, bs, CH_2), 4.21 (2H, m, CH_2), 4.46 (4H, bs, ImCH_2 x2), 6.97 (2H, s, *m*-CH), 7.05 (2H, s, *m*-CH), 8.87 (1H, s, CH).

^{13}C NMR (100.48 MHz, DMSO-d_6): δ 17.6 (CH_3), 19.6 (CH_3), 20.5 (CH_3), 20.6 (CH_3), 45.1 (CH_2), 47.5 (ImCH_2), 48.2 (ImCH_2), 49.0 (ImCH_2), 50.8 (CH_2) 51.2 (ImCH_2), 129.1 (*m*-CH), 129.4 (*m*-CH), 131.1 (C), 134.2 (C), 135.5 (C), 135.8 (C), 136.9 (C), 137.9 (Pd-C), 139.3 (C), 159.5 (ImCH).

Found: C, 41.52; N, 7.50; H, 4.63. Calc. for $C_{26}H_{35}N_4PdBr_3$: C, 41.65; N, 7.47; H, 4.71.

Preparation of [{(^{S}MesIm)(^{S}MesImH)C_3H_6}$PdBr_3$] 22c

In a pre-dried schlenk flask, imidazoliunium **17c** (193.0 mg, 0.33 mmol) and palladium acetate (74.8 mg, 0.33 mmol) were dried by heating at *ca.* 70 °C *in vacuo* prior to the addition of DMSO (10 mL). The resulting orange solution was heated at 50 °C for 3 hours, then 110 °C for 2 hours, resulting in a pale orange solution. The

solvent was removed *in vacuo* and the orange residue was dissolved in dichloromethane (15 mL) and filtered through Celite. The product precipitated from the filtrate after partial evaporation over 16 hours as a yellow powder which was collected by filtration as pure **22c** (21.7 mg, 9 % yield). m.p. 264 °C(dec).

^{1}H NMR (399.58 MHz, DMSO-d_6): δ 2.26 (3H, s, *p*-CH_3), 2.27 (3H, s, *p*-CH_3), 2.30 (8H, bs, 2 x *o*-CH_3, 1 x CH_2), 2.37 (6H, s, *o*-CH_3), 3.73-3.79 (2H, m, CH_2), 3.86 (4H, bs, 2 x ImCH_2), 4.10-4.27 (4H, m, 2 x ImCH_2), 4.30-4.39 (2H, m, CH_2), 6.96 (2H, s, *m*-CH), 7.04 (2H, s, *m*-CH), 8.88 (1H, s, ImCH).

^{13}C NMR (100.48 MHz, DMSO-d_6): δ 17.5 (*o*-CH_3), 19.5 (*o*-CH_3), 20.51 (*p*-CH_3), 20.54 (*p*-CH_3), 24.2 (CH_2), 45.4 (ImCH_2), 47.4 (ImCH_2), 48.0 (ImCH_2), 48.4 (ImCH_2), 50.5 (CH_2), 51.0 (CH_2), 129.0 (*m*-CH), 129.3 (*m*-CH), 131.2 (C), 134.3 (C), 135.6 (C), 137.0 (C), 137.7 (C), 139.2 (C), 158.9 (ImCH) (Pd-C not observed due to low concentration).

Found: C, 40.19; N, 6.67; H, 4.78. Calc. for $C_{27}H_{37}N_4PdBr_3.(CH_2Cl_2)$: C, 39.63; N, 6.60; H, 4.63.

Preparation of silver complexes

General procedure

In a modified literature procedure,[20] the appropriate imidazolinium salt was dissolved in acetonitrile with 1.25 eq. silver oxide. The resulting suspension was heated at 55 °C for 18 hours excluded from light. The cooled suspension was filtered through Celite and the solvent reduced to *ca.* 5 mL. Diethyl ether (20 mL) was added to precipitate the product as a white solid which was collected by filtration and washed with diethyl ether (2 x 5 mL) and dried *in vacuo*. Pure disilver complexes

were collected by filtration and crystals suitable for X-ray diffraction were produced by vapour diffusion of diethyl ether into saturated acetonitrile solutions.

Preparation of [{(^{S}MesIm)$_2$CH$_2$}$_2$Ag$_2$][PF$_6$]$_2$ 23a

With **17e** (448.6 mg, 0.66 mmol) and silver oxide (200.8 mg, 0.87 mmol) in acetonitrile (50 mL) to produce pure **23a** as a white solid (312.4 mg, 37% yield). m.p. 260 °C(dec).

^{1}H NMR (399.58 MHz, DMSO-d_6): δ 1.65 (12H, s, *o*-CH_3), 1.75 (12H, s, *o*-CH_3), 2.40 (12H, s, *p*-CH_3), 3.69-3.79 (4H, m, 2 x ImCH_2), 3.79-3.88 (4H, m, 2 x ImCH_2), 3.92-4.04 (8H, m, 4 x ImCH_2), 4.85 (2H, d, *J* = 14.3 Hz, CH_2), 6.08 (2H, d, *J* = 14.2 Hz, CH_2), 6.87 (4H, s, *m*-CH), 7.01 (4H, s, *m*-CH).

^{13}C NMR (100.48 MHz, DMSO-d_6): δ 16.9 (*o*-CH_3), 17.5 (*o*-CH_3), 20.7 (*p*-CH_3), 49.5 (ImCH_2), 51.7 (ImCH_2), 63.5 (*N*-CH_2), 64.9 (*N*-CH_2), 129.2 (*m*-CH), 129.5 (*m*-CH), 134.8 (C), 134.9 (C), 135.0 (C), 137.8 (N-C), 203.7 (d, *J* = 12.6 Hz, C-Ag).

Found: C, 46.92; N, 9.41; H, 5.20. Calc. for $C_{54}H_{72}N_8Ag_2P_2F_{12}.CH_3CN$: C, 47.18; N, 9.52; H, 5.10.

Preparation of [{(^{S}MesIm)$_2$(C$_3$H$_6$)}$_2$Ag$_2$][PF$_6$]$_2$ 23c

With **17e** (106.2 mg, 0.15 mmol) and silver oxide (42.9 mg, 0.19 mmol) in acetonitrile (20 mL) to produce pure **23c** as a white solid (83.4 mg, 42% yield). m.p. 256 °C(dec).

^{1}H NMR (399.58 MHz, DMSO-d_6): δ 1.86 (24H, s, *o*-CH_3), 1.94 (4H, t, *J* = 6.4 Hz, CH_2), 2.34 (12H, s, *p*-CH_3), 3.57 (8H, t, *J* = 7.4 Hz, 2x *N*-CH_2), 3.71-3.88 (16H, m, 4x Im-CH_2), 6.88 (8H, s, *m*-CH).

^{13}C NMR (100.48 MHz, DMSO-d_6): δ 17.2 (*o*-CH_3), 20.6 (*p*-CH_3), 26.3 (CH_2), 48.0 (*N*-CH_2), 48.3 (Im-CH_2), 50.8 (Im-CH_2), 129.1 (*m*-CH), 135.2 (*p*-*C*(CH_3)), 135.2 (*o*-*C*(CH_3)), 137.4 (*N*-C), 202.7 (d, *J* = 12.6 Hz, C-Ag).

Found: C, 46.64; N, 8.33; H, 5.48. Calc. for $C_{54}H_{72}N_8Ag_2P_2F_{12}.CH_3CN.(H_2O)_3$: C, 46.90; N, 8.79; H, 5.69.

4.5 References

[1] Nelson, D. J.; Nolan, S. P. *Chem. Soc. Rev.* **2013**, *42*, 6723.

[2] Hopkinson, M. N.; Richter, C.; Schedler, M.; Glorius, F. *Nature* **2014**, *510*, 485.

[3] Droge, T.; Glorius, F. *Angew. Chem. Int. Ed.* **2010**, *49*, 6940.

[4] Kuo, H.-Y.; Liu, Y.-H.; Peng, S.-M.; Liu, S.-T. *Organometallics* **2012**, *31*, 7248.

[5] Arnold, P. L.; Casely, I. J.; Turner, Z. R.; Bellabarba, R.; Tooze, R. B. *Dalton Trans.* **2009**, 7236.

[6] Lord, R. L.; Wang, H.; Vieweger, M.; Baik, M.-H. *J. Organomet. Chem.* **2006**, *691*, 5505.

[7] Vehlow, K.; Maechling, S.; Blechert, S. *Organometallics* **2006**, *25*, 28.

[8] Hillier, A. C.; Sommer, W. J.; Yong, B. S.; Petersen, J. L.; Cavallo, L.; Nolan, S. P. *Organometallics* **2003**, *22*, 4322.

[9] Fu, C. F.; Lee, C. C.; Liu, Y. H.; Peng, S. M.; Warsink, S.; Elsevier, C. J.; Chen, J. T.; Liu, S. T. *Inorg. Chem.* **2010**, *49*, 3011.

[10] Straub, B.; Bessel, M.; Rominger, F. *Synthesis* **2010**, *2010*, 1459.

[11] Ozdemir, I.; Cetinkaya, B.; Demir, S.; Gurbuz, N. *Catal. Lett.* **2004**, *97*, 37.

[12] Xiao, X.-Q.; Jia, A.-Q.; Lin, Y.-J.; Jin, G.-X. *Organometallics* **2010**, *29*, 4842.

[13] Gardiner, M. G.; Herrmann, W. A.; Reisinger, C.-P.; Schwarz, J.; Spiegler, M. *J. Organomet. Chem.* **1999**, *572*, 239.

[14] Boyd, P. D. W.; Edwards, A. J.; Gardiner, M. G.; Ho, C. C.; Lemee-Cailleau, M.-H.; McGuinness, D. S.; Riapanitra, A.; Steed, J. W.; Stringer, D. N.; Yates, B. F. *Angew. Chem. Int. Ed.* **2010**, *49*, 6315

[15] Marshall, C.; Ward, M. F.; Skakle, J. M. *Synthesis* **2006**, 1040.

[16] Ho, C. C. Structural and Mechanistic Investigations of Systematically Modified Bis(NHC) Palladium Complexes (PhD Thesis), University of Tasmania, Hobart, **2015**.

[17] Scherg, T.; Schneider, S. K.; Frey, G. D.; Schwarz, J.; Herdweck, E.; Herrmann, W. A. *Synlett* **2006**, *18*, 2894.

[18] McGuinness, D. S.; Cavell, K. J. *Organometallics* **2000**, *19*, 741.

[19] Sluijter, S. N.; Warsink, S.; Lutz, M.; Elsevier, C. J. *Dalton Trans.* **2013**, *42*, 7365.

[20] Han, Y. F.; Jin, G. X.; Daniliuc, C. G.; Hahn, F. E. *Angew. Chem. Int. Ed.* **2015**, *54*, 4958.

[21] Wanniarachchi, Y. A.; Khan, M. A.; Slaughter, L. M. *Organometallics* **2004**, *23*, 5881.

[22] Liu, Q.-X.; Yang, X.-Q.; Zhao, X.-J.; Ge, S.-S.; Liu, S.-W.; Zang, Y.; Song, H.-b.; Guo, J.-H.; Wang, X.-G. *CrystEngComm* **2010**, *12*, 2245.

[23] Lee, K. M.; Wang, H. M. J.; Lin, I. J. B. *J. Chem. Soc., Dalton Trans.* **2002**, 2852.

[24] Gardiner, M. G.; Ho, C. C.; Mackay, F. M.; McGuinness, D. S.; Tucker, M. *Dalton Trans.* **2013**, *42*, 7447.

[25] Cowieson, N. P.; Aragao, D.; Clift, M.; Ericsson, D. J.; Gee, C.; Harrop, S. J.; Mudie, N.; Panjikar, S.; Price, J. R.; Riboldi-Tunnicliffe, A.; Williamson, R.; Caradoc-Davies, T. *J. Synchrotron Radiat.* **2015**, *22*, 187.

[26] Kuhn, P.; McPhillips, T. M.; McPhillips, S. E.; Chiu, H.-J.; Cohen, A. E.; Deacon, A. M.; Ellis, P. J.; Garman, E.; Gonzalez, A.; N. K. Sauter; 2002 *J. Synchrotron Radiat.* **2002**, *179*, 401.

[27] Sheldrick, G. M., *SHELX97*, Programs for Crystal Structure Analysis, Universität Göttingen, Germany, **1998**.

[28] Barbour, L. J. *J. Supramol. Chem.* **2001**, *1*, 189.

[29] Dolomanov, O. V.; Bourhis, L. J.; Gildea, R. J.; Howard, J. A. K.; Puschmann, H. *J. Appl. Cryst.* **2009**, *42*, 339.

Chapter 5: Abnormal Palladium(II) Carbene Complexes with a Strong Electron Withdrawing Substituent.

5.1 Introduction

Abnormal and remote carbenes (aNHCs and rNHCs, respectively) are of great interest for their significantly different electronic effects compared to normal NHCs (nNHCs) and interesting potential for catalytic applications.[1] Abnormal carbenes are notable for their mesoionic character; unlike nNHCs it is not possible to draw a reasonable neutral resonance form (Figure 5.1).[2] The increased charge separation results in a stronger anionic character of the carbene, which in turn enhances the donor ability.

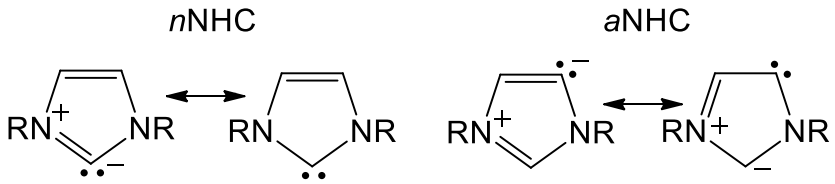

Figure 5.1. Example resonance forms of normal NHCs and abnormal NHCs.

The stability of the free ligand is reduced, however, due to the decreased number of heteroatoms adjacent to the carbene carbon, although the inductive effects of the heteroatoms are less pronounced which also enhances the donor ability of the ligand and increases the electron density on a coordinated metal centre.[3]

rNHCs are defined as having the carbene carbon not adjacent to any heteroatoms. This does not require that they fall into the aNHC definition of the free carbene

being mesoionic. The majority of studies into these interesting and important carbenes have occurred in the last 15 years.

The earliest example of a mesoionic NHC complex was reported by Araki and co-workers in 1993, in which a diaryltetraazolium salt was reacted with mercury or palladium to produce the complexes shown in Figure 5.2.[4]

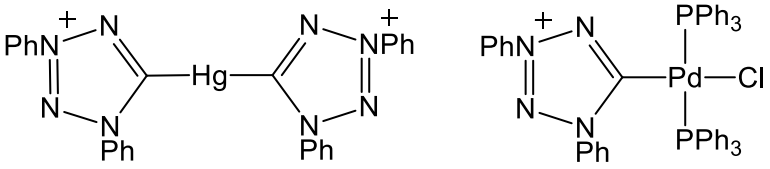

Figure 5.2. Mesoionic carbene complexes reported by Araki.[4]

The first true aNHC metal complex was serendipitously accessed by Crabtree and co-workers from the reaction of a 2-pyridylmethylimidazolium salt and an iridium hydride precursor to produce a mixture of the nNHC and aNHC products.[5]

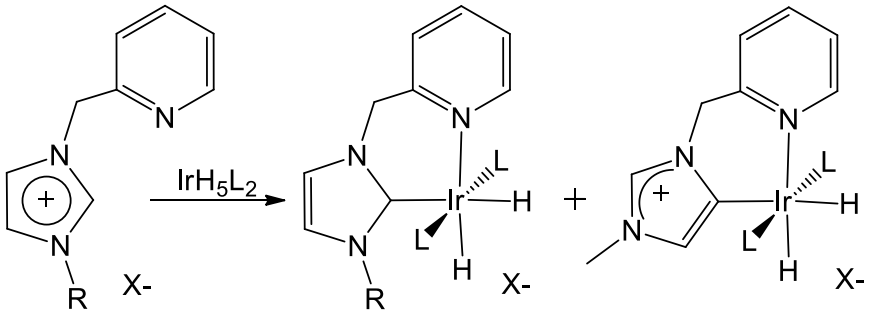

Scheme 5.1. Synthesis of nNHC- and aNHC-iridium complexes reported by Crabtree. [5]

The complexes were described as stable, showing no interconversion and it was noted that the aNHC analogue was favoured. This showed that the common assumption that the C-2 position would be more reactive than C-5 is not necessarily true for all azolium systems.

The first free abnormal carbene was isolated by Bertrand and co-workers in 2009, who achieved this by blocking the C-2 and C-4 sites with bulky phenyl substituents.[6] Deprotonation with a suitable base resulted in the free carbene, which was structurally authenticated *via* X-ray crystallography. The free carbene was then used for further synthesis, forming an aNHC-Au complex and for carboxylation at the carbene site.

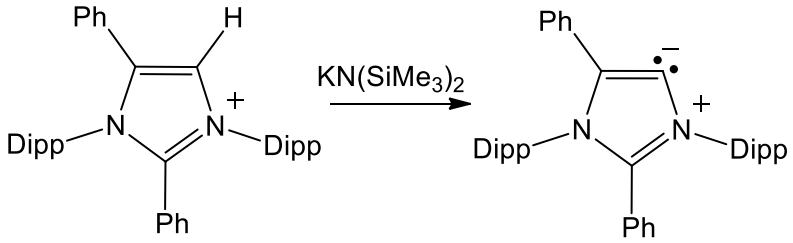

Scheme 5.2. Preparation of a free aNHC reported by Bertrand.[6]

Synthesis of metal complexes of aNHCs/rNHCs can be achieved through a range of methods. Deprotonation of the C-4/5 proton and subsequent coordination similar to the synthesis of nNHCs can be effective in cases where the "abnormal" position is more active or if the "normal" C-2 position is blocked. This blocking group can take the form of a substituent in the C-2 position such as those reported by Albrecht and co-workers, or through steric hindrance of the adjacent *N*-substituents restricting accessibility of the "normal" carbene site.[7] Both Li and Esteruelas provided examples of the latter case in 2008 as shown in Figure 5.3.[8,9]

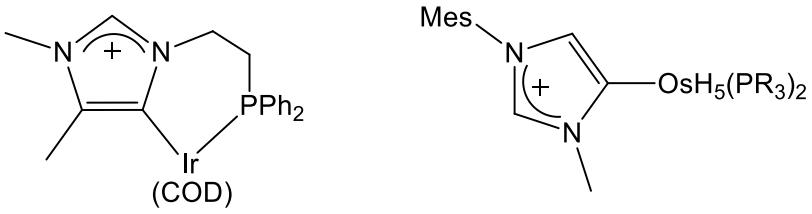

Figure 5.3. Examples of aNHC-M complexes where the aNHC species was selectively formed, aided by steric hindrance of the *N*-substituents.[8,9]

There have been some reports of transmetallation *via* a silver salt to form various aNHC-transition metal complexes.[10] This has been shown to be an unreliable method, however, even when the C-2 position is blocked. C-C bond cleavage in an aNHC precursor with a methyl substituent at C-2 was observed upon reaction with silver oxide to form the nNHC-rhodium complex (Scheme 5.3).[11]

Scheme 5.3. C-C cleavage occurring during transmetallation of an aNHC precursor.

The synthesis of aNHC-Pd complexes *via* oxidative addition of halogenated aNHC precursors with various palladium(0) sources has been reported. Examples reported by Huynh[12] and Albrecht[3,13] are shown in Scheme 5.4. However this method does require the halogenation of the appropriate position on the aNHC/rNHC ligand precursor.

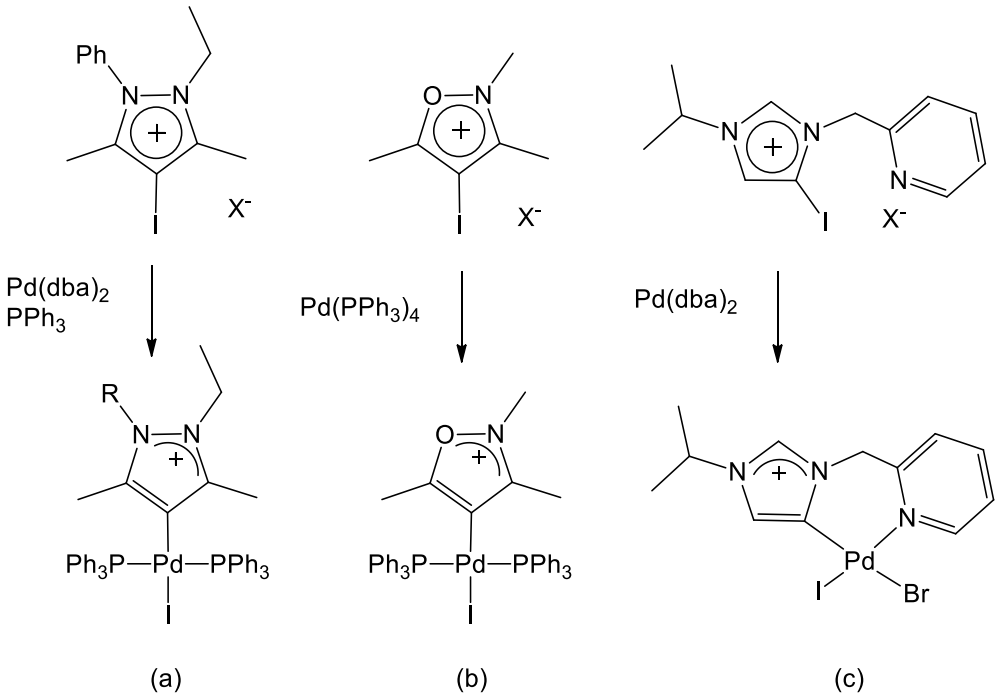

Scheme 5.4. Examples of aNHC/rNHC-Pd complexes formed by oxidative addition of halogenated precursors with Pd(0).

Huynh and co-workers described a useful measure of nNHC, aNHC and rNHC ligand donor ability by using a carbene probe palladium(II) NHC complex shown in Figure 5.4.[14] Various ligands were coordinated and the ^{13}C NMR shift of C1 was used as a measure of the *trans* influence and therefore relative donor strength of the other NHC ligand. This scale provides an alternative measure to common methods of gauging ligand donor strength such as Tolman electronic parameters (TEP) or Lever electron parameters.[15]

In the case of TEP, there are very few Pd-carbonyl complexes which with to compare the determined values, limiting good comparison. Additionally, as discussed in Chapter 1, the range of TEP values is quite small for NHC species, which further limits differentiation.[15] LEP are calculated from electrochemistry,[15] and while useful for some transition metal complexes, are generally not suitable for

palladium(II) species as the redox potential of these complexes is often beyond the practical range for common solvents. Direct comparison of the ^{13}C NMR shift of NHC carbenes in Pd-NHC complexes is not necessarily valid either as different steric and electronic environments can have large effects on the NMR shift, limiting these comparisons to isostructural species.

The one major disadvantage to the scale proposed by Huynh and co-workers is that it does require the synthesis of the benzimidazol-2-ylidine palladium dibromide complex of the desired NHC species. Such complexes can be difficult to prepare, or inaccessible however, as many NHC ligand precursors require specific reaction conditions for coordination to metal. The steric bulk of the *N*-substituents on the NHC probe can also hinder coordination of the secondary NHC species of interest.

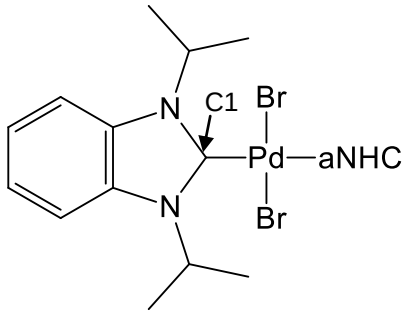

Figure 5.4. Palladium nNHC/aNHC complex used by Huynh to probe aNHC ligand donor ability.

Another possible measure of donor ability was proposed, where the synthesis of NHC-Pd$(PPh_3)_2$ complexes allowed the use of ^{31}P NMR spectroscopy to compare the effect of the carbene ligand. Albrecht and co-workers produced a series of isostructural complexes of this motif (an example of such is shown in Scheme 5.4(b)) and compared the ^{31}P NMR and ^{13}C NMR shifts as well as the calculated TEP for the ligands.[3] They noted that their ^{31}P NMR shift scale was

consistent with the ordering of ligand donating ability implied by the other scales. They were also able to compare the catalytic activity of the series for the Suzuki-Miyaura coupling of aryl bromides, where they observed a slight correlation between ligand donor ability and catalytic activity.

This observation was consistent with numerous attributions of greater catalytic activity for aNHC complexes, though there is some debate in many of these cases whether the difference is due to the increased donor properties or an altered steric environment around the metal centre.[16] As with Albrecht's study discussed above, others have probed this using carefully constructed ligands which share identical substituent arrangements around the metal (Figure 5.5). Both Hong[17] and Lee[18] report that there was increased catalytic activity from the aNHC species compared to their nNHC analogues for Suzuki-Miyaura cross coupling of aryl halides with arylboronic acids (Figure 5.5(a)) and Mizoroki-Heck cross coupling, direct C-H arylation and decarboxylative coupling reactions (Figure 5.5(b)), respectively.

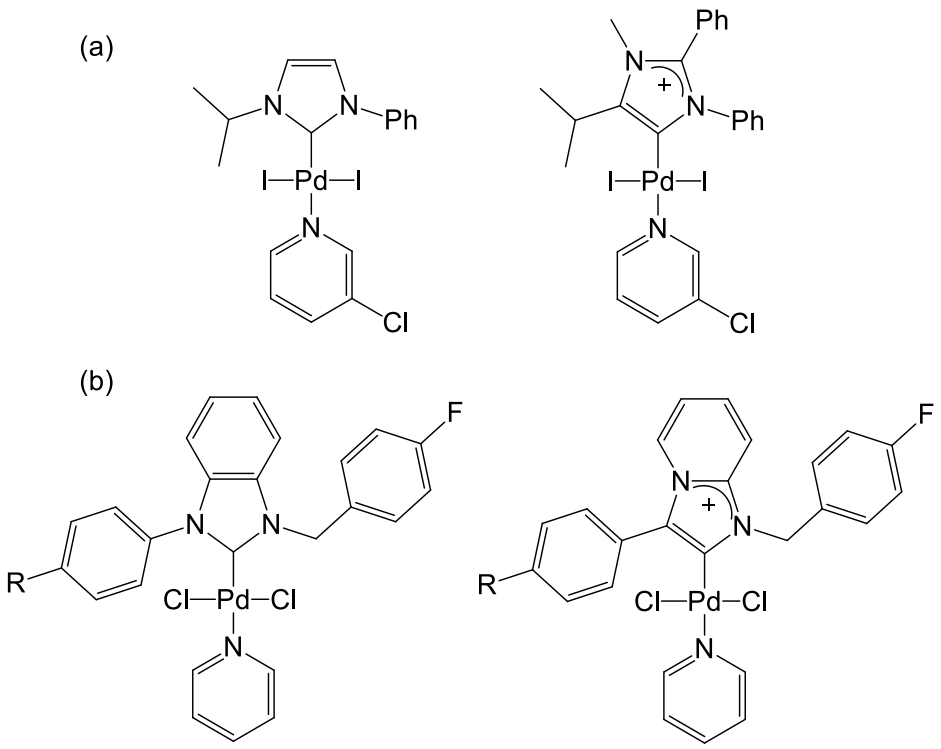

Figure 5.5. Examples of sterically similar NHC-Pd analogues produced by Hong (a) and Lee (b) to compare catalytic activity of nNHC and aNHC complexes.

In a review of mesoionic carbenes Crabtree discusses the ambiguity in terminology of abnormal versus normal carbenes with an interesting thought experiment.[2] He suggested that an arrangement such as that shown in Figure 5.6, would be considered a normal carbene with a neutral resonance form when the rings are planar as in (a). Should the pyridinium ring be rotated 90 ° out of the plane the resonance form through conjugation would no longer be possible and therefore there would no longer be a neutral arrangement. Thus (b) could be considered an abnormal carbene. At intermediate dihedral angles this biaryl ligand arrangement would therefore not be able to be classed as either an nNHC or aNHC, as the character would fall between these two definitions. It was suggested by Crabtree that a new definition might be necessary for this class of compound; we suggest describing this arrangement as a "partially normalised" abnormal carbene.

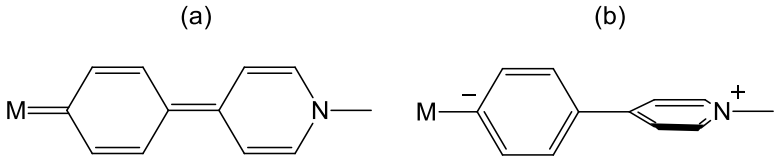

Figure 5.6. Resonance structures of a biaryl system which could be defined as an nNHC or aNHC.

We have observed a system in which a scenario such as this might be considered. The unusual tricyclic product **I** produced from the reaction of $[(MesIm)_2C_2H_4]Br_2$ with palladium acetate was discussed previously in Chapter 3 (Scheme 3.3). Scheme 5.5 shows the possible resonance forms of **I** in which this conjugation could be considered to occur between the two aryl rings. The C-5 proton of the palladium-bound NHC was not observed by ^{1}H NMR spectroscopy,[19] presumably undergoing rapid exchange with the deuterated solvent, indicative of high lability at that position, to give an aNHC at this position.

I

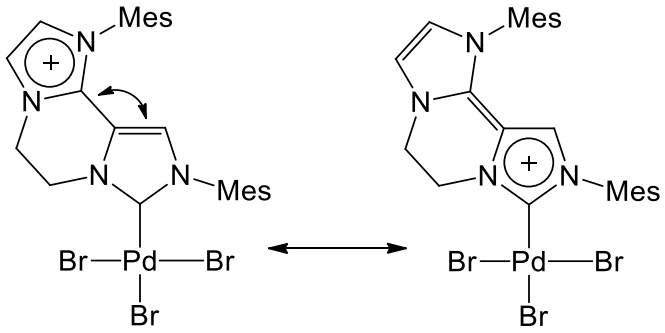

Scheme 5.5. Possible resonance forms of the rearranged dicarbene palladium tribromide **I**.

Preparation of complex **I** for investigation into the possible aNHC character of the deprotonated form is difficult due to the low reaction yield and the potential formation of the alternative chelated bis(NHC) palladium dibromide species (See

Chapter 3). Thus we sought to explore a more convenient conjugated biaryl ligand motif using a suitably substituted aNHC system approximating this arrangement (Figure 5.7). This would allow us to probe the structural effects of an abnormal carbene which, assuming the desired coplanar ring arrangement and electron migration occurred, could be considered a "partially normalised" aNHC.

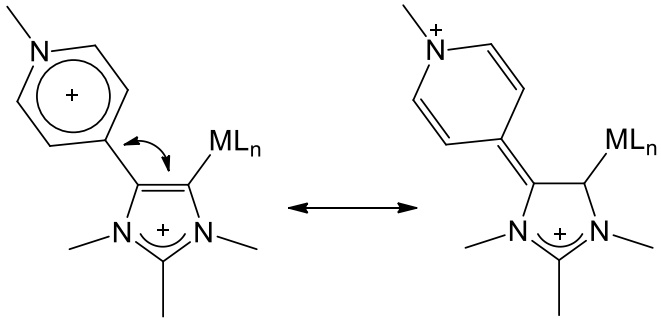

Figure 5.7. Proposed resonance forms of the target aNHC ligand.

5.2 Results and Discussion

5.2.1 **Synthesis of Methylated aNHC Ligand Precursor**

1,2-dimethyl-5-(4-pyridine)imidazole **25** was prepared by a Mizoroki-Heck coupling of 1,2-dimethylimidazole and 4-bromopyridine under basic conditions, as per a modified literature method with significantly increased reaction scale.[20] Methylation of **25** with an excess of methyl iodide was found by ^{1}H NMR spectroscopy to produce 1,2,3-trimethyl-5-(4-pyridine) imidazolium iodide **26** and 1,2-dimethyl-5-(4-*N*-methylpyridinium) imidazole iodide **27** as the two major products (Scheme 5.6.). This was determined by two sets of signals, each set containing three methyl resonances at 2.70, 3.78 and 3.80 ppm for **26** and 2.45, 3.76 and 4.27 ppm for **27**. Small downfield shifts of the pyridine protons and a larger downfield shift of the imidazolium C-4 proton to 8.04 ppm were observed in **26** as

expected. Likewise, the expected small downfield shift of the imidazolium C-4 proton to 7.80 ppm and the significantly larger downfield shifts of the pyridinium *meta*- and *ortho*- protons to 8.18 and 8.84 ppm, respectively, were observed for **27**. Interestingly, there was essentially no formation of the tetramethylated product 1,2,3-trimethyl-5-(4-*N*-methylpyridinium) imidazolium diiodide **28** observed under these conditions, which indicates that the electron withdrawing effect of the methylation at either of the nitrogen positions was sufficient to prevent reactivity at the other. The two products could be easily separated by washing the mixture with DCM, in which **26** was essentially insoluble, while **27** displayed moderate solubility.

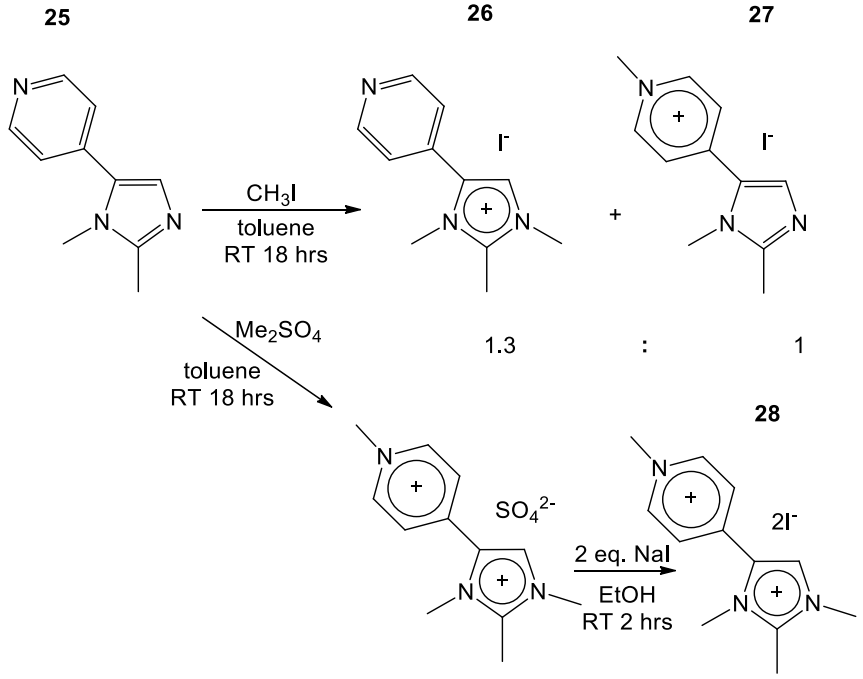

Scheme 5.6. Synthesis of various cationic imidazolium aNHC ligand precursors.

Crystals of **26** and **27** suitable for single crystal X-ray diffraction were prepared by slow diffusion of diethyl ether into saturated acetonitrile solutions of the respective compounds. From the crystal structures we gain information about the nature of the bonding. The presence of the dominant resonance form of the biaryl ring system

(Figure 5.7) would be evidenced by a relatively short (*ca*. 1.34 Å) C2-C7 bond length and a decrease in the C8-C10/C9-C11 bond lengths compared to typical aromatic bonds in pyridine (< *ca*. 1.39 Å), indicative of double bond character. In addition the angle between the imidazolium/NHC ring plane and the pyridine ring plane can be measured; in the biaryl aNHC resonance form the rings would be near-coplanar.

The C2-C7 bond length of 1.470(5) Å in **26** is indicative of typical single-bond character between sp^2 hybridised carbon centres, and the essentially identical (within error) C-C bonds measuring > 1.39 Å in the pyridinium substituent suggested that there was no contribution from the nNHC resonance form in this compound. The angle between the ring planes of 38.5(2) ° was also consistent with this observation. This is unsurprising as the lack of pyridine *N*-substituent would prevent the electron transfer necessary to the nNHC resonance form.

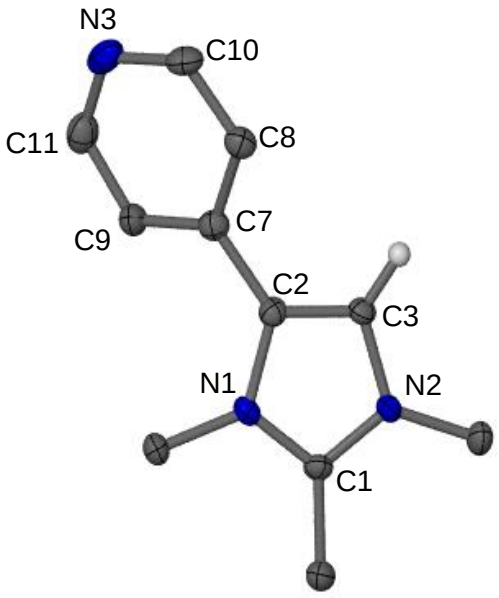

Figure 5.8. Molecular structure of the cation of 1,2,3-trimethyl-5-(4-pyridine) imidazolium iodide **26**. Displacement ellipsoids are shown at the 50 % probability level. All pyridinium and methyl hydrogens and iodide counteranion were omitted for clarity. Selected bond lengths (Å) and angles (°): C2-C7 1.470(5), C7-C8,C9 1.399(5),1.398(5), C8-C10 1.388(5), C9-C11 1.402(5), N3-C10,C11 1.360(5),1.292(6), C2-C3-N2 107.5(3).

The C2-C6 bond length appeared increased in **27** compared to imidazolium **26** (Δ 0.025Å), though there was some shortening of the pyridinium C7-C9/C8-C10 bonds in **27** relative to **26** and the angle between the imidazolium and pyridine ring planes was measured to be 8.9(1) °. The resonance forms discussed above (Figure 5.7) are not valid for imidazole **27**, however, as the C-4 proton is not suitable for abstraction.

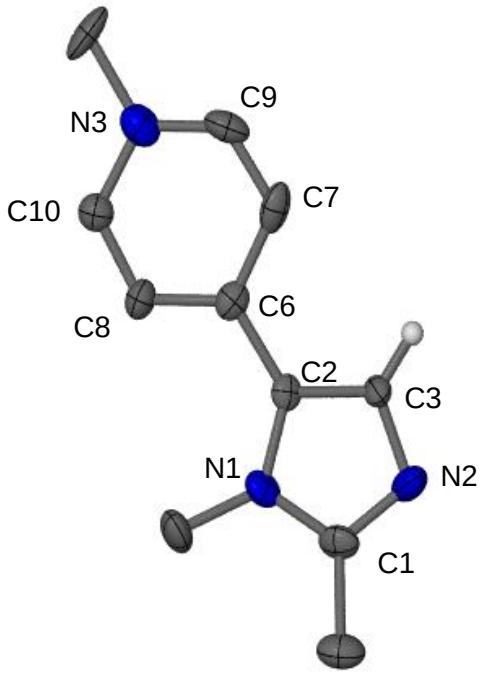

Figure 5.9. Molecular structure of the cation of 1,2-dimethyl-5-(4-N-methylpyridinium) imidazole iodide **27**. The structure was refined isotropically with displacement ellipsoids shown at the 50 % probability level. All pyridinium and methyl hydrogens and iodide counteranion were omitted for clarity. Selected bond lengths (Å) and angles (°): C2-C6 1.50(1), C6-C7,C8 1.43(1),1.41(1), C7-C9 1.32(1), C8-C10 1.36(1), N3-C9,C10 1.32(1),1.36(1), C2-C3-N2 110.3(7).

The tetramethylated product **28** was prepared by stirring the imidazole **25** with an excess of dimethyl sulfate for 18 hours in toluene. The resultant red oil was dissolved in ethanol and reacted with 2 equivalents of sodium iodide to precipitate sodium sulfate and allow isolation of the tetramethylated imidazolium **28** after the filtrate was removed *in vacuo* as a yellow solid. The successful methylation of all sites was confirmed with ^{1}H NMR spectroscopy by the presence of four methyl signals at 2.73, 3.88, 3.89 and 4.39 ppm. There was also a significant downfield shift of the imidazolium proton from 7.12 ppm in the unsubstituted imidazole **25** to 8.41 ppm in **28** and the expected downfield shifts of the pyridinium *ortho*- and

meta-protons to 8.34 and 9.13 ppm, respectively. Crystals of **28** suitable for X-ray diffraction were grown from slow diffusion of diethyl ether into a saturated methanol solution (Figure 5.10).

The C2-C7 distance of 1.456(3) Å, while decreased in comparison to imidazolium **26**, was not indicative of a typical sp^2 hybridised C-C double bond. There was a slight decrease in the C8-C10/C9-C11 bonds in the *N*-methylpyridinium substituent as would be expected in comparison to imidazolium **26**, similar to that seen in **27**. A reduction in the angle between the ring planes to 22.1(2) ° compared to imidazolium **26** was also observed.

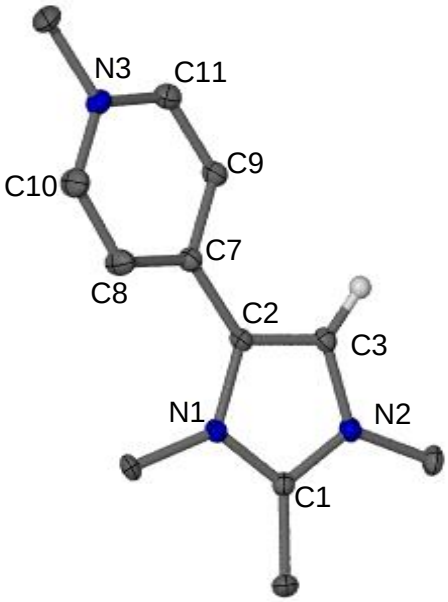

Figure 5.10. Molecular structure of the dication of 1,2,3-trimethyl-5-(4-*N*-methylpyridinium) imidazolium diiodide **28**. Displacement ellipsoids are shown at the 50 % probability level. All pyridinium and methyl hydrogens, iodide counteranions and lattice solvent water molecule are omitted for clarity. Selected bond lengths (Å) and angles (°): C2-C7 1.456(3), C7-C8,C9 1.401(3),1.402(3), C8-C10 1.381(4), C9-C11 1.381(3), N3-C10,C11 1.341(4),1.348(4), C2-C3-N2 107.4(2).

5.2.2 **Attempted Synthesis of aNHC Palladium(II) Complexes *via* C-H Metallation Methods**

Synthesis of a palladium complex with imidazolium salt **28** was attempted using a variety of literature methods (Scheme 5.7). The synthesis of palladium-NHC complexes *via in situ* deprotonation with palladium acetate is well established in the literature for both mono- and bis-NHCs.[7,17,21] A similar method was reported by Mandal and co-workers using palladium acetate in dioxane to produce a sterically bulky dinuclear aNHC-Pd complex which showed good activity in Suzuki-Miyaura

cross-coupling reactions of aryl chlorides.[1] Reaction of imidazolium **28** under these conditions produced only decomposition products and moderate amounts of starting material (by ^{1}H NMR spectroscopy) however.

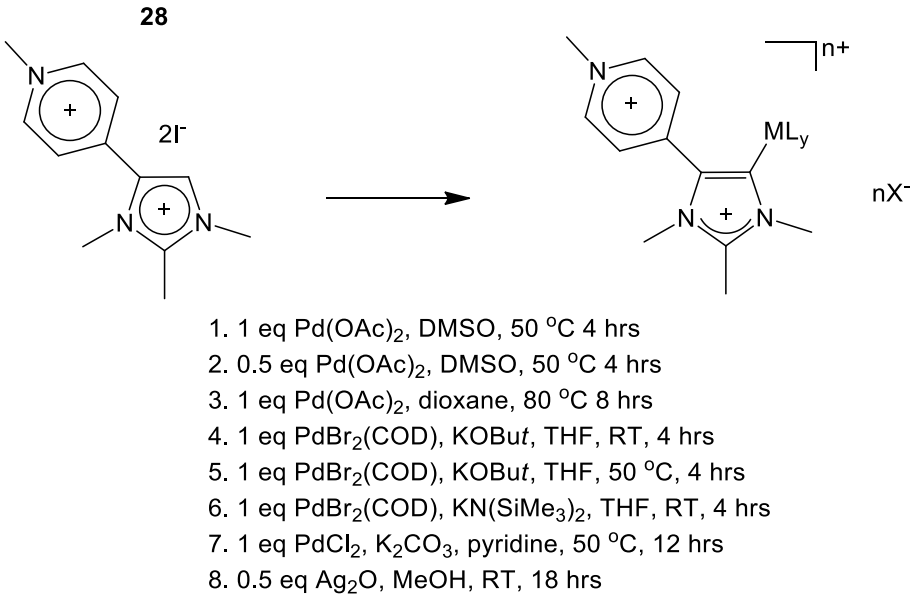

Scheme 5.7. Some of the reaction conditions used to attempt the C-H metallation of **28**.

Direct deprotonation of NHCs *via* a strong base to form the free carbene *in situ*, followed by subsequent coordination of a metal is also well established in the literature.[21,22] However this method also proved to be ineffective with essentially pure starting material **28** being retrieved as the only product from the synthesis. A study of the *in situ* deprotonation was conducted under inert conditions in a Young's tube with ^{1}H NMR spectroscopic analysis showing no decrease in the imidazolium C-H signal upon addition of potassium *tert*-butoxide, nor with subsequent heating.

Ghosh and co-workers report a similar method of base deprotonation using potassium carbonate followed by coordination to palladium chloride to access an aNHC-Pd complex with similar substitution to our ligand.[23] The reaction was

conducted in pyridine, a basic solution which can serve as a coordinating ligand that was aimed to aid complex formation. Again, the reaction of **28** under these conditions produced only starting material and some decomposition products.

As described previously, transmetallation *via* silver complexes has not been widely used to access aNHC metal complexes, though Huynh and co-workers report using the method for the preparation of several rNHC palladium complexes with good success.[10] Under similar conditions with **28** however, no reaction was observed. The above synthetic methods were also trialled with imidazolium **26** as an attempt to understand the effect of *N*-methylation of the pyridine substituent and a similar lack of reactivity was observed.

It is worth noting that these literature methods used monocationic ligand species without a strong electron withdrawing group affecting the electronic properties of the NHC. It is clear that the electron withdrawing nature of both the pyridine and pyridinium group have a significant effect on the acidity of the imidazolium proton.

5.2.3 **aNHC Palladium(II) Complexes *via* Oxidative Addition**

Albrecht and co-workers have reported the synthesis of various aNHC and rNHC palladium complexes *via* oxidative addition.[3,13] We sought to emulate some of their methodology to prepare complexes using our ligand system.

Imidazole **25** was brominated by stirring it with 1 equivalent of *N*-bromosuccinnimide in THF for 18 hours. After washing with water the product **29** precipitated as a pure off-white solid in modest yield. Bromination of the C-4 position was confirmed by the disappearance of the resonance at 7.12 ppm in the ^{1}H NMR spectrum, corresponding to the C-4 proton and the upfield shift of the C-4 carbon to 114.8 ppm in the ^{13}C NMR spectrum.

Methylation of the brominated imidazole **29** was attempted using methyl iodide. However the increased steric hindrance adjacent to the unsubstituted imidazole nitrogen prevented favourable methylation at that site, resulting in an inseparable mixture of the *N*-Me-pyridinium imidazole (major product) and a small amount of the trimethylated imidazolium salt, determined by ^{1}H NMR spectroscopy (Scheme 5.8).

Clean trimethylation of the brominated imidazole **29** was achieved by reaction with an excess of dimethyl sulfate in toluene at 120 °C in a sealed tube. The resultant brown oil was determined by ^{1}H NMR spectroscopy to be essentially pure imidazolium, theorised as the sulfate salt. Subsequent reaction with sodium iodide to obtain the imidazolium dihalide by precipitation of sodium sulfate was unsuccessful, producing only decomposition products. Thus the imidazolium was converted to the hexafluorophosphate salt **30** by dissolving the imidazolium sulfate salt in water and adding an excess of potassium hexafluorophosphate.

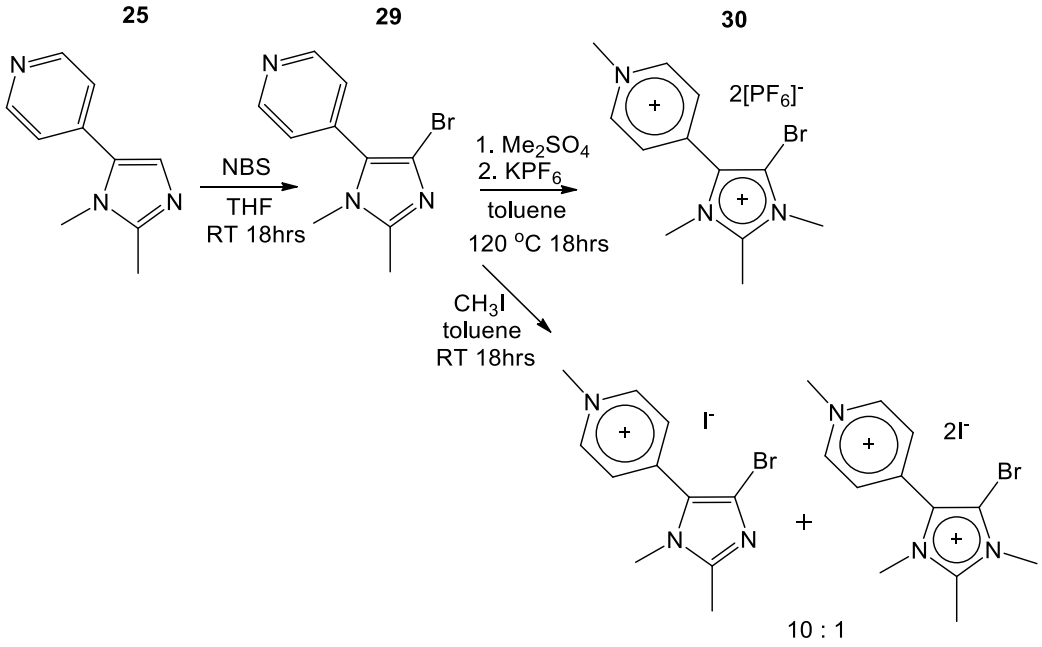

Scheme 5.8. Synthesis of methylated imidazolium product **30** from the brominated imidazole **29**.

The resultant off-white precipitate was confirmed by ^{1}H and ^{13}C NMR spectroscopy and X-ray crystallography to be the desired product **30** with the C-4 position substituted as expected (Figure 5.11). The increased bulk of the bromide substituent does result in an increased angle between the imidazolium ring plane and pyridinium ring plane, with an angle of 27.2(1) ° (compared to 22.1(2)) and a near-equal (Δ 0.010 Å) C2-C7 bond compared to the non-halogenated analogue **28**. The pyridinium C-C bond lengths were identical within error, however.

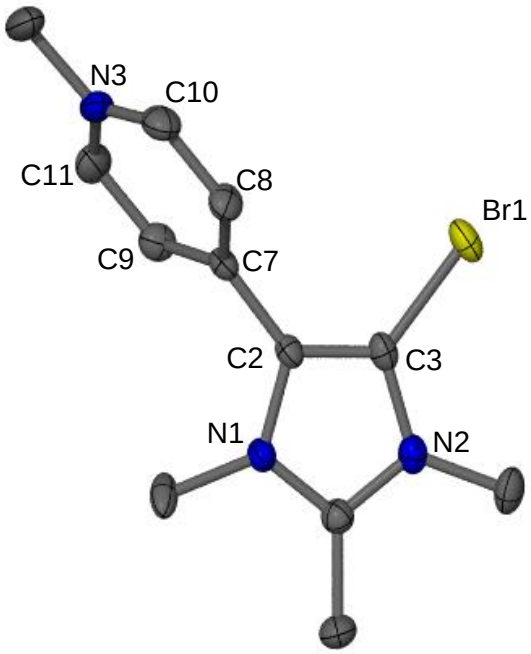

Figure 5.11. Molecular structure of the dication of [1,2,3-trimethyl-4-bromo-5-(4-*N*-methylpyridinium)Im][PF_6]$_2$ **30**. Displacement ellipsoids are shown at the 50 % probability level. All hydrogen atoms and [PF_6]$^-$ counteranions are omitted for clarity. Selected bond lengths (Å) and angles (°): C3-Br1 1.847(3), C2-C3 1.349(4), C2-C7 1.466(4), C7-C8,C9 1.388(4),1.388(5), C8-C10 1.380(5), C9-C11 1.379(5), N3-C10,C11 1.330(5),1.337(6), C2-C3-N2 108.2(3),1.388(5), C8-C10 1.380(5), C9-C11 1.379(5), N3-C10,C11 1.330(5),1.337(6), C2-C3-N2 108.2(3).

Palladium aNHC complexes were formed by oxidative addition of **30** with a slight excess of Pd(dba)$_2$ in pyridine at 75 °C. After heating for 1.5 hours a second coordinating ligand was added to form complexes **31-33** (Scheme 5.9). Exchange of the reaction solvent to acetonitrile or DMSO under these conditions resulted in only partial conversion of **30** to the metallated product. This suggested that the basic pyridine played some role in promoting the oxidative addition.

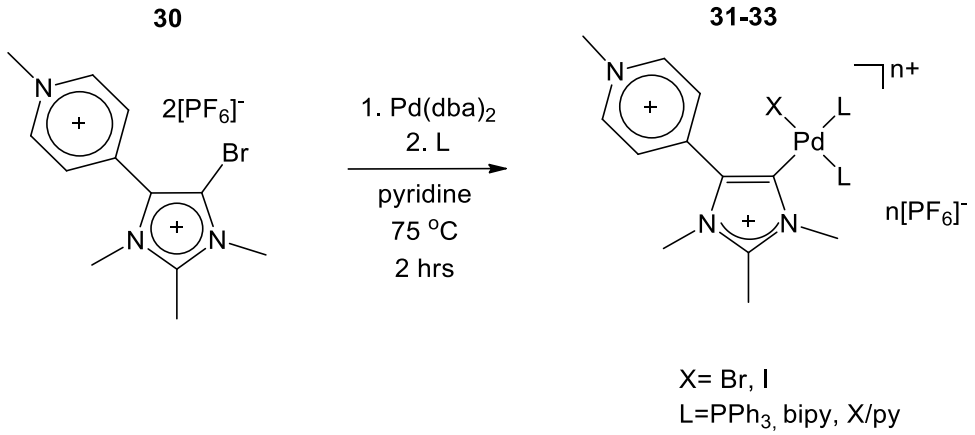

Scheme 5.9. General reaction scheme for the synthesis of aNHC-Pd complexes utilising **30**.

Addition of 1 equivalent of 2,2′-bipyridine (bipy) to the oxidative addition reaction produced the complex [{1,2,3-trimethyl-5-(4-*N*-methylpyridinium)Im}PdBr(bipy)][PF_6]$_2$ **31** as a pale brown solid in moderate yield. Successful coordination was indicated by the desymmetrisation of the bipyridine ligand in the ^{1}H NMR spectrum and the significant downfield shift of the C-4 carbon from 110.4 ppm in **30** to 139.1 ppm in the ^{13}C NMR spectrum. Crystals suitable for X-ray diffraction were grown by slow evaporation of diethyl ether into a saturated THF solution (Figure 5.12).

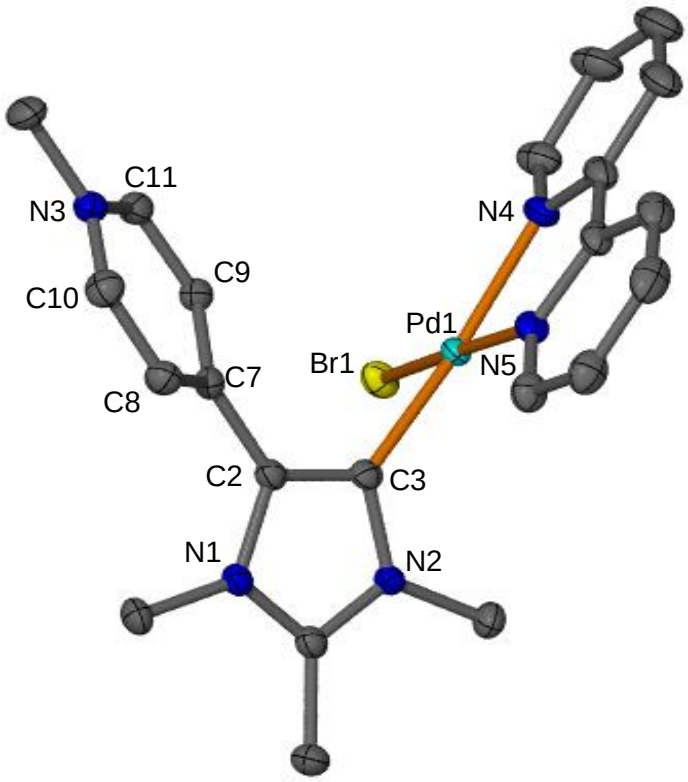

Figure 5.12. Molecular structure of the dication of [{1,2,3-trimethyl-5-(4-*N*-methylpyridinium)Im}PdBr(bipy)][PF_6]$_2$ **31**. Displacement ellipsoids are shown at the 50 % probability level. All hydrogen atoms and [PF_6]$^-$ counteranions are omitted for clarity. Selected bond lengths (Å) and angles (°): Pd1-C3 1.979(3), Pd1-Br1 2.4249(8), Pd-N4,N5 2.083(2),2.034(2), C2-C7 1.460(3), C7-C8,C9 1.400(4),1.398(4), C8-C10 1.382(4), C9-C11 1.381(4), N3-C10,C11 1.339(4),1.340(4), C3-Pd1-Br1 87.66(7), Br1-Pd1-N4 97.02(7), N4-Pd1-N5 80.46(9), N5-Pd1-C3 95.2(1), Pd1-C3-N2 126.7(2), Pd1-C3-C2 128.2(2).

The metal coordination geometery in complex **31** was square planar, with the aNHC ligand bound at an angle of 76.02(7) ° to the metal coordination plane. Markies and co-workers report observing a similar effect in a (bipy)PdIPh complex (Figure 5.13(a)) where the phenyl ligand was rotated 75.7(2) ° from the Pd-bipy

plane.[24] The *trans* effect of the aNHC ligand in **31** was observed in the 0.049 Å increase in Pd-N4 compared to Pd-N5. This change was consistent with other literature (bipy)PdXL complexes, where X here represents any halide (Table 1). Complexes (a)-(c) do show a greater magnitude of *trans*-effect compared to **31**, with $\Delta_{N\text{-}Pd}$ ranging 0.056-0.078 Å. However the aNHC complex **31** does have comparatively shorter Pd-N bond distances in general, though the dicationic nature of **31** may contribute to this. It is difficult to make any direct comparisons as the Cambridge crystal structure database (CCSD) contains no examples of (bipy)PdXNHC complexes.

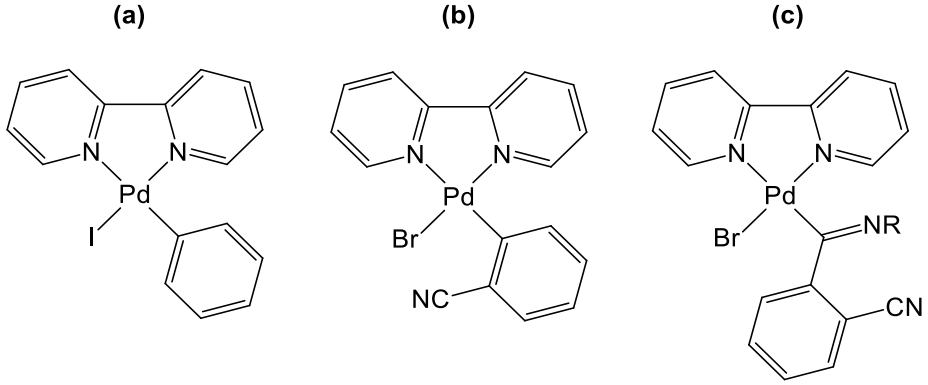

Figure 5.13. Examples of (bipy)PdXL complexes **(a)**[24] , **(b)**[25], and **(c)**[26] showing the increased Pd-N bond length *trans* to L.

Table 1. Comparison of bond lengths in (bipy)PdXL complexes (Figure 5.12 and Figure 5.13)

Dist(Å)	Pd-C	Pd-X	Pd-N *trans* to C	Pd-N *trans* to X	Δ Pd-N
31	1.979(3)	2.4249(8)	2.083(2)	2.034(2)	0.049(2)
(a)	2.00(1)	2.575(1)	2.144(8)	2.070(8)	0.074(8)
(b)	1.986(4)	2.4127(6)	2.112(3)	2.056(3)	0.056(3)
(c)	1.988(2)	2.4255(3)	2.144(2)	2.066(2)	0.078(2)

The C2-C7 bond length of 1.460(3) Å was consistent with sp^2 hybridised C-C single bond character and the pyridinium C-C bond lengths were similar (within error) and within the expected ranges for the delocalised aromatic bonds, suggesting that there was little contribution from the postulated partially normalised resonance form. The angle between the pyridinium ring plane and the NHC ring plane was measured to be 42.31(11) °, a significant increase compared to the uncoordinated species **28** and **30**, consistent with the observation that no significant contribution from the conjugated ring resonance form was observed.

Addition of 20-30 equivalents of sodium bromide to the oxidative addition reaction of **30** to $Pd(dba)_2$ produced complex [{1,2,3-trimethyl-5-(4-*N*-methylpyridinium)Im}$PdBr_2$Py][PF_6] **32a** as a yellow solid, which was washed with water to remove any excess salt. The iodide analogue was also prepared for structural comparison to a similarly sterically hindered literature example *via* addition of sodium iodide under otherwise identical conditions. This produced the complex [{1,2,3-trimethyl-5-(4-*N*-methylpyridinium)Im}PdI_2Py][PF_6] **32b**. Successful synthesis was indicated by NMR spectroscopy with the downfield shifts

of the pyridinium proton signals compared to the imidazolium precursor **30**, and the significant downfield shift of the C-4 carbon from 110.4 ppm to 136.0 ppm (**32a**) and 133.1 ppm (**32b**), respectively, in the ^{13}C NMR spectrum associated with the formation of the carbene. Crystals of each suitable for X-ray diffraction were grown by slow evaporation of diethyl ether into a saturated acetonitrile solution (Figure 5.14 and Figure 5.15).

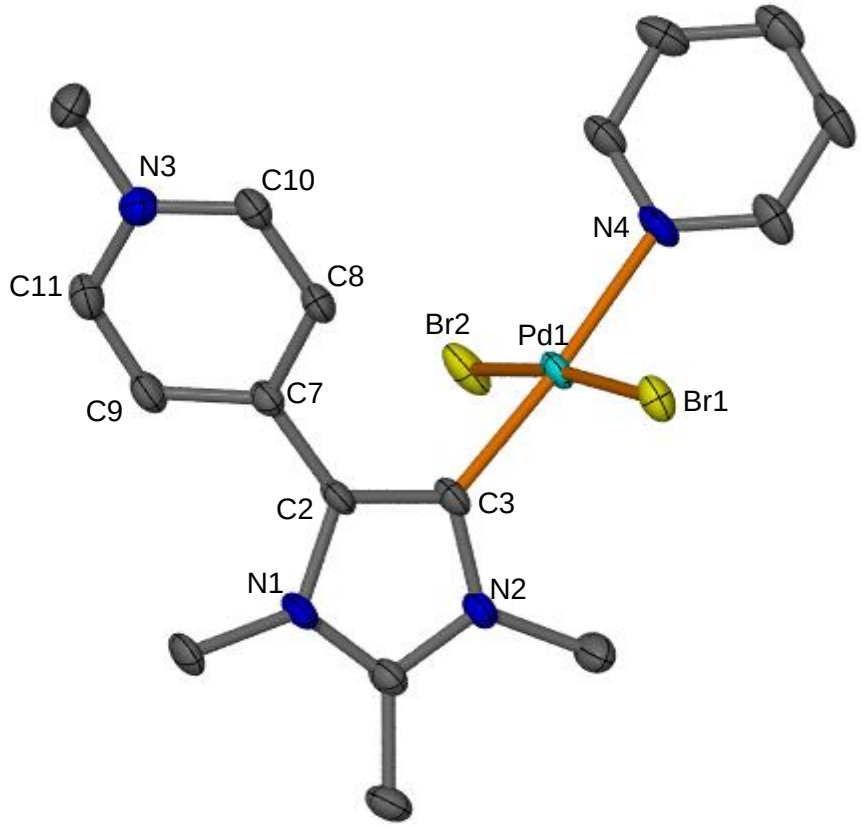

Figure 5.14. Molecular structure of the cation of [{1,2,3-trimethyl-5-(4-*N*-methylpyridinium)Im}$PdBr_2$Py)][PF_6] **32a**. Displacement ellipsoids are shown at the 50 % probability level. All hydrogen atoms and $[PF_6]^-$ counteranion are omitted for clarity. Selected bond lengths (Å) and angles (°): Pd1-C3 1.964(4), Pd1-Br1,Br2 2.4362(6),2.4214(7), Pd-N4 2.110(3), C2-C7 1.448(5), C7-C8,C9 1.406(5),1.398(5), C8-C10 1.371(6), C9-C11 1.371(6), N3-C10,C11 1.351(5),1.352(5), C3-Pd1-Br1,Br2 89.7(1),86.2(1), N4-Pd1-Br1,Br2 92.6(1),91.9(1), Pd1-C3-N2 123.5(3), Pd1-C3-C2 130.8(3), C2-C3-N2 105.3(4).

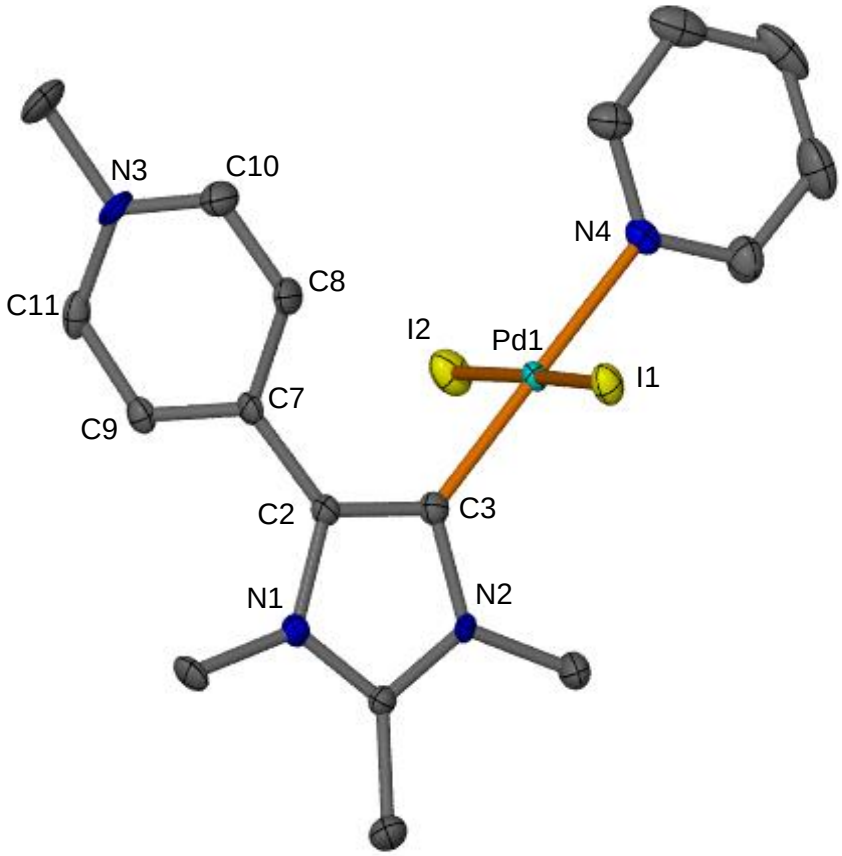

Figure 5.15. Molecular structure of one cation of [{1,2,3-trimethyl-5-(4-*N*-methylpyridinium)Im}PdI_2Py)][PF_6] **32b**. Displacement ellipsoids are shown at the 50 % probability level. All hydrogen atoms and $[PF_6]^-$ counteranion are omitted for clarity. Selected bond lengths (Å) and angles (°) (values for second molecule provided in brackets): Pd1-C3 1.968(5) (1.972(5)), Pd1-I1,I2 2.5956(5) (2.6122(5)),2.5942(5) (2.5855(5)), Pd-N4 2.092(4) (2.092(4)), C2-C7 1.452(7) (1.475(7)), C7-C8,C9 1.401(7) (1.392(7)),1.394(7) (1.390(8)), C8-C10 1.363(8) (1.362(8)), C9-C11 1.366(7) (1.370(8)), N3-C10,C11 1.341(7) (1.348(7)),1.343(7) (1.344(7)), C3-Pd1-I1,I2 86.3(2),91.4(2), N4-Pd1-I1,I2 91.8(1),91.5(1), Pd1-C3-N2 122.9(4), Pd1-C3-C2 131.8(4), C2-C3-N2 104.4(4).

The complexes **32a-b** were isostructural, with the palladium centres displaying the expected square planar geometries. The iodide analogue **32b** contained two molecules in the asymmetric unit. The aNHC ligands were *trans* to the coordinated pyridine solvent, with the remaining two sites filled by the relevant halide. This arrangement was observed regardless of the excess qunantaties of sodium halide added to the reaction mixture and was retained even when the isolated complex was reacted with a further excess of sodium halide in acetonitrile.

The aNHC was oriented near-perpendicular to the palladium coordination plane (81.8(1) ° and 82.8(1) (89.2(1) ° for **32a** and **32b**, respectively). The reduced steric bulk and rigidity in the ancillary ligands around the palladium may have resulted in a slight decrease in the Pd-C bond length of 0.015(4) and, *ca.* 0.010(5) Å (average) for **32a** and **32b**, respectively, compared to the bipy analogue **31**. The C2-C7 bond lengths were identical, within error, and consistent with no typical sp^2 hybridised C-C double bond character. There was a slight decrease in the C8-C10/C9-C11 bond lengths from those expected for the delocalised pyridine bond arrangement in the aNHC resonance form, and the angle between the pyridinium ring plane and NHC ring plane was measured at 32.8(2) ° and 38.8(2) (41.7(3)) ° respectively. This suggested that there was little contribution from the normalised resonance form containing coplanar ring systems.

We were able to compare these compounds to several literature examples that shared a similarly bulky aNHC ligand and *trans*-PdX_2Py centre, where X represented any halide. Ghosh and Lee both reported on aNHC-Pd complexes of interest in various C-C coupling reactions.[18,22]

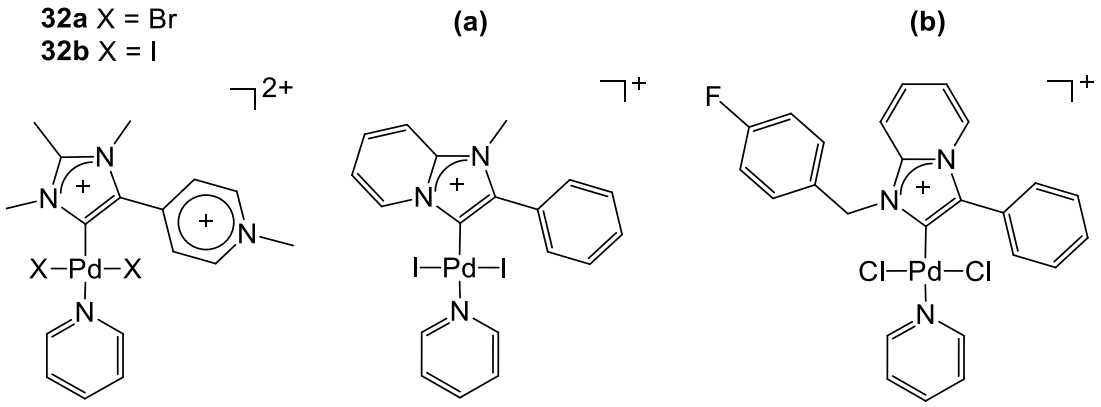

Figure 5.16. Examples of similarly sterically hindered aNHCPdX_2Py complexes **32a**, **32b**, **(a)**[23] and **(b)**.[18]

Table 2. Comparison of bond lengths in aNHCPdX_2Py complexes (Figure 5.16). Bond lengths from both molecules of **32b** are provided.

Dist(Å)	Pd-C	Pd-X		Pd-N
32a	1.964(4)	2.4362(6)	2.4214(7)	2.110(3)
32b	1.968(5)	2.5956(5)	2.5942(5)	2.092(4)
	1.972(5)	2.6122(5)	2.5855(5)	2.092(4)
(a)	1.98(2)	2.596(2)	2.607(1)	2.13(1)
(b)	1.960(8)	2.298(2)	2.309(2)	2.103(7)

Ghosh and co-workers provide significant analysis of the *trans* effect of the strongly σ-donating aNHC ligand in **(a)**, which results in the greatly weakened Pd-py interaction, causing the pyridine to essentially be considered a "throw-away" ligand in catalytic conditions.[22] They note an effective measure of this σ-donating power is to compare the Pd-C and Pd-N distances to the sum of the individual covalent radii of the atoms (Pd-C 2.055 Å, Pd-N 1.983 Å).[27] All of the above complexes indeed

show Pd-C bond lengths shorter than, and Pd-N bond lengths greater than these values, providing good agreement for the strong σ-donating power of these aNHC ligands. In particular, comparison can be made between complexes **32b** and **(a)** which share a similar coordination environment and ligand steric bulk. The Pd-C distances in these two complexes are identical within error, though the Pd-N distances were decreased in complex **32b**. This is consistent with the reduced electron donating power of our ligand due to the electron withdrawing substituent decreasing the *trans* effect of the aNHC ligand.

Another possible measure of the electronic environment at the carbene carbon is the ^{13}C NMR spectroscopic chemical shift. However different steric environments can affect the chemical shift so comparisons are limited to complexes with similar coordination environments.[15] Complex **(a)** had a Pd-C ^{13}C NMR spectroscopic signal at 130.2 ppm. Pd-C signal observed for **32b** at 133.1 ppm, the downfield shift presumably due in part to the electron-withdrawing substituent reducing the shielding on the carbon nucleus.

Complex [{1,2,3-trimethyl-5-(4-*N*-methylpyridinium)Im}PdBr(PPh_3)$_2$)][PF_6]$_2$ **33** was formed by extracting the oxidative addition product of **30** with Pd(dba)$_2$ as a pyridine adduct and exchanging the ligands of the partially purified compound with an excess of triphenylphosphine in acetonitrile at 50 °C. The solvent was removed and the resultant yellow solid washed with diethyl ether to remove all remaining triphenylphosphine. This alternative synthesis was required due to the high solubility of **33** in dichloromethane, a necessary component in the removal of residual dba from the oxidative addition reaction. Successful synthesis was indicated by the significant downfield shift of the C-4 carbon from 110.4 ppm to 133.2 ppm in the ^{13}C NMR spectrum. The complex formed the *trans* Pd-Br isomer, indicated by the

single phosphorous signal in the appropriate region of the ^{31}P NMR spectrum. NMR spectroscopy also revealed a small amount of triphenylphosphine oxide present, presumably a minor byproduct of the synthesis which was not separable from **33**. Attempts to isolate the iodide analogue of **33** for direct comparison to literature examples are ongoing. Crystals of **33** suitable for X-ray diffraction were produced from slow evaporation of diethyl ether into a saturated methanol solution (Figure 5.17).

The palladium centre displayed a distorted square planar coordination geometry with a *trans* arrangement of the triphenylphosphine ligands to reduce steric interactions. As with the other complexes in this chapter the aNHC was oriented near-perpendicular to the palladium coordination plane (82.5(1) °), with a significantly larger (in comparison to the previous aNHC compounds) angle between the pyridinium and NHC rings of 44.9(1) °. The C2-C7 bond length of 1.466(4) Å is not indicative of typical sp^2 hybridised C-C double bond character and the pyridinium C-C bonds are not significantly altered from the typical bond lengths expected from the delocalised arrangement. This again suggests that there is essentially no contribution from the partially normalised ligand resonance form.

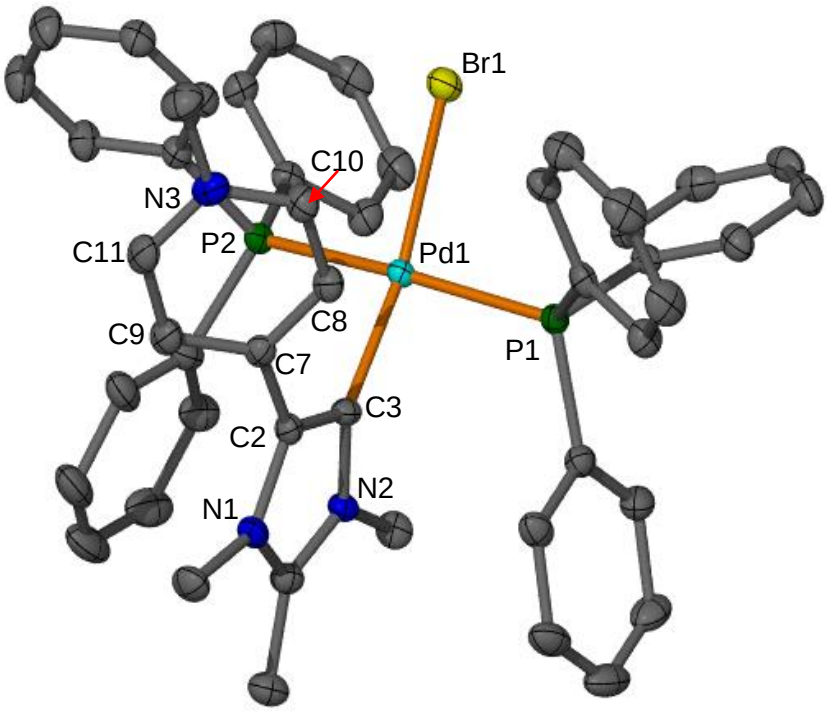

Figure 5.17. Molecular structure of [{1,2,3-trimethyl-5-(4-*N*-methylpyridinium)Im}PdBr(PPh_3)$_2$][PF_6]$_2$ **33**. Displacement ellipsoids are shown at the 50 % probability level. All hydrogen atoms, lattice MeOH solvent molecule and [PF_6]$^-$ counteranions are omitted for clarity. Selected bond lengths (Å) and angles (°): Pd1-C3 1.998(3), Pd1-Br1 2.475(1), Pd1-P1,P2 2.352(1),2.329(1), C2-C7 1.466(4), C7-C8,C9 1.394(4),1.398(5), C8-C10 1.380(5), C9-C11 1.374(5), N3-C10,C11 1.347(5),1.346(5), C3-Pd1-P1,P2 93.31(9),88.03(9), Br1-Pd1-P1,P2 92.89(3),87.99(3) Pd1-C3-N2 128.1(2), Pd1-C3-C2 126.8(2).

Albrecht has reported a range of similar aNHC/rNHC complexes sharing the LPd(PPh_3)$_2$X core. Examples of these with X-ray crystallographic data are shown in Figure 5.18 with the key bond lengths compared in Table 3.[3]

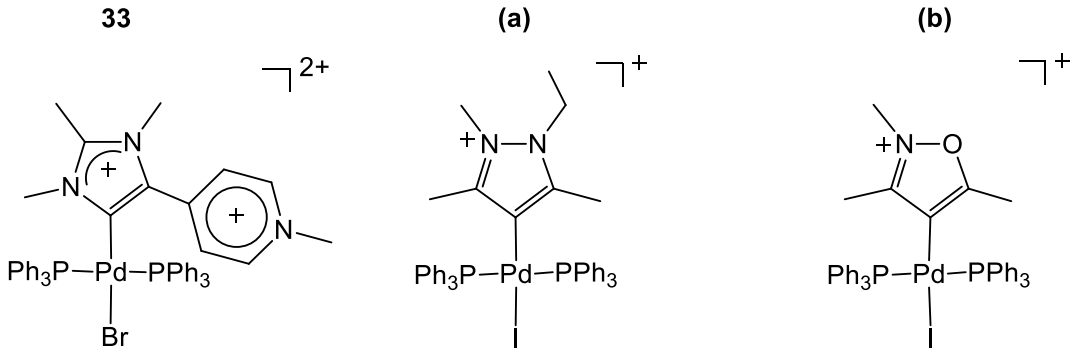

Figure 5.18. Examples of aNHC- or rNHCPdX(PPh_3)$_2$ complexes **33**, **(a)**[12] and **(b)**[3]

Table 3. Comparison of bond lengths (Å) in aNHCPdX(PPh_3)$_2$ complexes (Figure 5.18).

Å	Pd-C	Pd-P		Pd-X
33	1.998(3)	2.329(1)	2.353(1)	2.475(1)
(a)	2.020(5)	2.327(1)	2.330(1)	2.6727(5)
(b)	2.04(2)	2.330(5)	2.339(5)	2.647(2)

The Pd-C and Pd-P bond lengths are similar between these complexes, though direct comparison is not possible due to the unavailability of literature examples containing an ancillary bromide ligand.

Albrecht also reported an extensive study of the correlation between ^{31}P NMR chemical shifts and donor strengths of the ligands. The ^{13}C and ^{31}P NMR chemical shifts of the compounds shown in Figure 5.18 and Figure 5.19 were compiled in Table 4, though again the variation of the halide from bromide to iodide limits more detailed comparison.

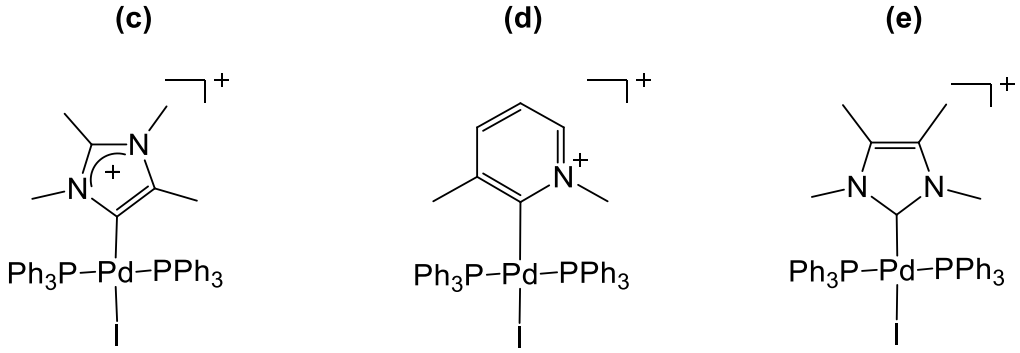

Figure 5.19. A selection of other NHC-Pd(PPh_3)$_2$I complexes reported by Albrecht.[3]

Table 4. NMR chemical shifts of compounds shown in Figure 5.18 and Figure 5.19.

Ppm	**33**	**(a)**	**(b)**	**(c)**	**(d)**	**(e)**
^{31}P Pd-P	20.08	22.80	21.28	20.48	18.96	18.76
^{13}C Pd-C	150.0	127.8	168.0	137.4	193.7	162.3

The ^{13}C and ^{31}P NMR spectroscopic chemical shifts of complex **33** fall within the range of values for the normal and abnormal NHC complexes **(c)** and **(e)**, though again there is likely some effect from the different halide and the electron withdrawing pyridinium group.

5.2.4 **nNHC Palladium(II) Analogue of I**

Consideration of the original complex **I** which inspired this series of abnormal carbene complexes suggested that the acidity of the imidazolium proton might be increased with a more direct analogue to the tricyclic palladium tribromide.

N-methyl-5-(4-pyridine)imidazole **34** was prepared *via* a modified literature procedure using *N*-methylimidazole in place of the 1,2-dimethyl imidazole.[20] Methylation of the remaining nitrogen positions was achieved by heating the

substituted imidazole **34** with excess methyl iodide in a sealed tube at 120 °C for 18 hours. All other methylation methods attempted gave a mixture of partially methylated products in poor yield. The imidazolium **35** was deprotonated with sodium acetate and reacted with palladium iodide to form the nNHC palladium triiodide complex **36**, analogous to the tricyclic rearranged dicarbene palladium tribromide **I**, as a dark red solid in moderate yield (Scheme 5.10).

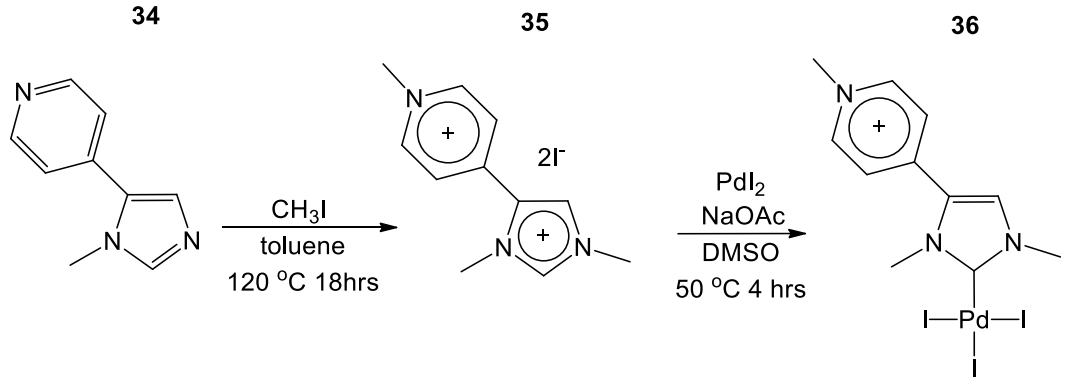

Scheme 5.10. Synthesis of **36**, an nNHC analogue of **I**.

Characterisation with ^{1}H and ^{13}C NMR spectroscopy indicated successful formation of complex **36** by the disappearance of the C-2 proton at 9.37 ppm and the downfield shift of the C-2 ^{13}C signal from 140.7 ppm to 149.2 ppm. Comparison of this carbene resonance to mono(NHC) palladium(II) trihalide complexes bearing a positive charge on the NHC ligand such as **10a** (136.6 ppm) and **12a-b** (138.4 and 138.8 ppm, respectively) discussed in Chapter 3 showed the deshielding effect of the electron-withdrawing pyridinium substituent on the carbene centre. This lends some validity to our proposed ligand system having some of the intended electronic effects. Direct comparison cannot be made, however, due to variation in the *N*-substituent steric bulk and a lack of other similar complexes in the literature.

Complex **I** was shown to have high lability of the C-4 proton, determined by the lack of the ^{1}H NMR resonance for this proton, suggesting the site may be amenable for reaction. Metallation of the C-4 position of analogue **36** was attempted *via* deprotonation with sodium acetate and subsequent coordination of palladium iodide, though no reaction was observed by ^{1}H NMR spectroscopy. It is worth noting that there are very few examples of 2,4-dimetallated NHC complexes, however. The C-4 proton resonance in **36** at 8.37 ppm is comparatively low for an imidazolium was unexpected from the observations of **I**.

Recrystallisation of **36** from diffusion of diethyl ether into an acetonitrile solution yielded red crystals suitable for X-ray crystallography (Figure 5.20). The palladium displayed distorted square planar geometry with the carbene ligand close to orthogonal to the metal coordination plane and a "see-saw" geometric distortion effect around the palladium centre, with pronounced deviations in the ligands from a flat square planar arrangement of 0.196(1)-0.198(1) Å for the *trans* iodides, and 0.159(2)-0.251(2) Å for the *trans* carbene/iodide.

The C2-C6 bond length of 1.468(8) Å and the identical (within error) pyridinium C-C bond lengths were indicative of little contribution from a normalised resonance form. The angle between the NHC ring plane and the pyridinium ring plane in **36** was measured as 35.9(3) °, consistent with this observation.

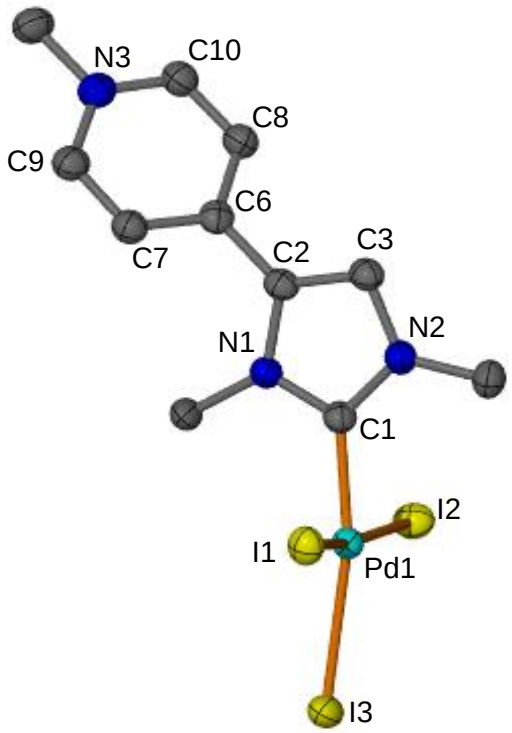

Figure 5.20. Molecular structure of [{1,3-dimethyl-5-(4-*N*-methylpyridinium)Im}PdI_3], **36**. Displacement ellipsoids are shown at the 50 % probability level. All hydrogen atoms are omitted for clarity. Selected bond lengths (Å) and angles (°): Pd1-C1 1.961(5), Pd1-I1,I2,I3 2.5949(7),2.6198(7),2.6560(7), C2-C6 1.468(8), C6-C7,C8 1.394(8),1.387(8), C7-C9 1.379(9), C8-C10 1.376(9), N3-C9,C10 1.342(9),1.332(9), C1-Pd1-I1, I2 86.1(2),87.59(16), I1,I2-Pd1-I3 94.79(2),93.15(2), Pd1-C1-N1,N2 123.3(4),130.8(4).

5.3 Conclusion

In conclusion, we have prepared a range of 5-pyridinium substituted imidazolium systems to examine whether conjugation between the rings can lead to a "partially normalised" abnormal carbene. We have shown that the strong electron withdrawing

nature of the C-4 substituent in imidazolium salts **26** and **28** prevented the synthesis of aNHC metal complexes *via* a range of literature C-H metallation methods.

The biaryl imidazole **25** was brominated using NBS and methylated to produce imidazolium **30**, which was used in the synthesis of aNHC-palladium complexes **31-33**. This was achieved *via* oxidative addition of the brominated ligand precursor **30** with $Pd(dba)_2$. The complexes displayed varying degrees of torsion between the NHC and pyridinium ring systems, though none of the complexes showed C-C bond lengths consistent with any significant contribution of the partially normalised resonance form containing coplanar rings. We have also established that the more direct analogue to our self-coupled product **I**, the nNHC-palladium complex **36**, does not enhance the reactivity of the C-4 proton to form a new aNHC ligand.

At this stage our ability to establish the influence of the electron withdrawing C-5 substituent on aNHC donor strength is limited. We hope to modify the ligand system for future work to help force the necessary coplanar ring arrangement. Options for this include a ligand system containing a suitably placed unsubstituted heteroatom for metal coordination or a rigid linker between the two rings to help hold the planar arrangement, though this would likely increase the difficulty of coordination to palladium further.

Another avenue to explore in future work would be the protection of the pyridine nitrogen group to allow selective methylation of the imidazolium nitrogen. This would allow us more control over the electron withdrawing effects of the pyridine substituent. It would also potentially allow imidazole coupling to form bis(aNHC) ligand precursors similar to those reported in the literature.[7]

5.4 Experimental

5.4.1 General Conditions

All syntheses of halogenated imidazoles, imidazolium salts and anion exchange reactions of metal complexes were carried out in air, while the syntheses of the imidazoles and palladium complexes were conducted under an inert atmosphere of high purity argon (BOC gases) using standard Schlenk techniques. Some analyses were performed in a dry glove box (Innovative Technologies) under a nitrogen atmosphere. Anhydrous DMSO was purchased from Sigma-Aldrich and stored over activated 3 Å molecular sieves. Other anhydrous solvents used were obtained by passage through columns on an Innovative Technologies Solvent Purifier.

Palladium(II) acetate was purchased from Precious Metals Online and used as received. Palladium dibenzylideneacetone was prepared from literature procedure[28] and used in the $Pd(dba)_2$ form. All other reagents were purchased from Sigma-Aldrich and used as received. For non-air-sensitive syntheses, solvents were analytical grade and used as received.

5.4.2 Instrumentation

^1H NMR spectroscopic studies were carried out on a 400 MHz Bruker Avance 3 HD Wide Bore spectrometer with a 5 mm BBFO probe in $CDCl_3$ and DMSO-d_6. NMR spectral data was obtained at room temperature (293 K) unless specified otherwise. $CDCl_3$ was used as received. DMSO-d_6 was distilled over CaH_2 and stored over 4 Å molecular sieves.

^1H NMR spectra were obtained at 399.58 MHz while ^{13}C NMR spectra were recorded at 100.47 MHz. ^1H NMR spectra were referenced to the ^1H resonance of the residual solvent peaks, while ^{13}C NMR spectra were referenced to the deuterated

^{13}C resonance. Elemental analyses were conducted by the Central Science Laboratory at the University of Tasmania using a Carlo Erba EA1108 Elemental Analyser. X-ray crystallography studies were conducted at the Australian Synchrotron using the MX1 and MX2 beamlines or at the University of Tasmania or at the University of Tasmania using a Bruker D8 Quest diffractometer.

5.4.3 **X-ray Crystallography**

Data for **26-32a** and **33-36** were collected at -173 °C on crystals mounted on Hampton Scientific cryoloops at the MX1 or MX2 beamline of the Australian Synchrotron. Data completeness was limited by the single axis goniometer on the MX beamlines at the Australian Synchrotron.[29] Data for **32b** was collected at -173 °C on a crystal mounted on a Hampton Scientific cryoloop using a Bruker D8 Quest diffractometer with copper microfocused tube (λ= 1.54178 Å) with a nominal crystal to detector distance of 40 mm. The structures were solved by direct methods with SHELXS-97,[30] refined using full-matrix least-squares routines against F^2 with SHELXL-97, and visualised using X-SEED or OLEX2.[31,32] All non-hydrogen atoms were refined anisotropically. All hydrogen atoms were placed in calculated positions and refined using a riding model with fixed C-H distances of 0.95 Å (sp^2CH), 0.99 Å (CH_2), 0.98 Å (CH_3). The thermal parameters of all hydrogen atoms were estimated as $U_{iso}(H) = 1.2U_{eq}(C)$ except for CH_3 where $U_{iso}(H) = 1.5U_{eq}(C)$. Disorder in the $[PF_6]^-$ counteranions was modelled using atom splitting in OLEX2. CIF files for X-ray crystallographic analysis can be provided upon request.

5.4.4 **Synthesis**

Preparation of 1,2-dimethyl-5-(4-pyridine)imidazole 25

This procedure is modified from literature.[20] A Schlenk flask was loaded with 4-bromopyridine hydrochloride (5.00 g, 26 mmol), potassium acetate (7.57 g, 77 mmol), 1,2-dimethyl imidazole (2.45 g, 26 mmol) and palladium acetate (32.1 mg, 0.14 mmol) and dried *in vacuo* at 70 °C. *N*,*N*-dimethylacetamide (50 mL) was added and the resulting mixture stirred at 150 °C for 2.5 days. The solvent was removed *in vacuo* and the resultant brown glass was redissolved with 40% aq. potassium hydroxide solution until pH > 9. This was extracted with dichloromethane (2 x 30 mL, 1 x 10 mL). The combined extracts were washed with water, dried over magnesium sulfate, filtered and the solvent removed *in vacuo* to obtain a brown solid. This solid was heated under vacuum to remove any residual 1,2-dimethylimidazole and collected once cooled as pure **25** which was spectroscopically identical to literature (1.15 g, 26 % yield).

^{1}H NMR (399.58 MHz, $CDCl_3$): δ 2.46 (3H, s, CH_3), 3.61 (3H, s, *N*-CH_3), 7.12 (1H, s, CH(Im)), 7.27 (2H, d, *J*= 5.9 Hz, *m*-CH(py)), 8.62 (2H, d, *J*= 5.8 Hz, *o*-CH(py)).

Preparation of 1,2,3-trimethyl-5-(4-pyridine) imidazolium iodide 26 and 1,2-dimethyl-5-(4-*N*-methylpyridinium) imidazole iodide 27

Imidazole **25** (0.4017 g, 2.32 mmol) was dissolved in toluene (15 mL). An excess of methyl iodide (0.43 mL, 6.91 mmol) was added and the solution was stirred for 18 hours at room temperature. The resultant yellow precipitate was collected by filtration as a mixture of **26** and **27**. Dichloromethane was added to the mixture and the undissolved solid was collected by filtration as **26** (0.1552 g, 21 % yield). The filtrate solvent was removed *in vacuo* to give **27** (0.0940 g, 13 % yield).

1,2,3-trimethyl-5-(4-pyridine) imidazolium iodide 26

m.p. 180 °C.

^{1}H NMR (399.58 MHz, DMSO-d_6): δ 2.70 (3H, s, CH_3), 3.78 (3H, s, *N*-CH_3), 3.80 (3H, s, *N*-CH_3), 7.60 (2H, d, *J* = 5.4 Hz, py *m*-CH), 8.04 (1H, s, ImCH), 8.78 (2H, d, *J* = 5.8 Hz, py *o*-CH).

^{13}C NMR (100.48 MHz, DMSO-d_6): δ 10.0 (CH_3), 33.5 (*N*-CH_3), 35.0 (*N*-CH_3), 121.6 (py-CH), 123.0 (py-CH), 130.5 (C), 136.4 (C), 146.7 (C), 150.5 (ImCH).

Found: C, 41.53; N, 13.06; H, 4.20. Calc. for $C_{11}H_{14}N_3I$: C, 41.92; N, 13.33; H, 4.48.

1,2-dimethyl-5-(4-*N*-methylpyridinium) imidazole iodide 27

m.p. 193 °C(dec).

^{1}H NMR (399.58 MHz, DMSO-d_6): δ 2.45 (3H, s, CH_3), 3.76 (3H, s, *N*-CH_3), 4.27 (3H, s, py *N*-CH_3), 7.80 (1H, s, ImCH), 8.18 (2H, d, *J* = 6.8 Hz, py *m*-CH), 8.84 (2H, d, *J* = 6.7 Hz, py *o*-CH).

^{13}C NMR (100.48 MHz, DMSO-d_6): δ 11.1 (CH_3), 34.0 (*N*-CH_3), 46.8 (py *N*-CH_3), 122.1 (CH), 127.7 (CH), 136.0 (C), 143.8 (C), 145.1 (CH).

Found: C, 41.62; N, 13.47; H, 4.20. Calc. for $C_{11}H_{14}N_3I$: C, 41.92; N, 13.33; H, 4.48.

Preparation of 1,2,3-trimethyl-5-(4-*N*-methylpyridinium)imidazolium diiodide 28

Imidazole **25** (0.75 g, 4.3 mmol) was dissolved in toluene (10 mL). An excess of dimethylsulfate (1 mL, 10.5 mmol) was added and the solution was stirred for 18 hours at room temperature. The toluene was decanted and the red-brown residue

was dissolved in ethanol (25 mL). Sodium iodide (1.28 g, 8.5 mmol) was added and the solution stirred for 2 hours where an off-white precipitate was formed. The solution was filtered through celite and the solvent removed *in vacuo* to produce **28** as a yellow solid (0.59 g, 30 % yield). Crystals suitable for X-ray diffraction were grown from slow diffusion of diethyl ether into a saturated methanol solution. m.p. 291 °C(dec).

^{1}H NMR (399.58 MHz, DMSO-d_6): δ 2.73 (3H, s, CH_3), 3.88 (3H, s, *N*-CH_3), 3.89 (3H, s, *N*-CH_3), 4.39 (3H, s, pyridine-*N*-CH_3) 8.34 (2H, d, *J* = 6.9 Hz, CH(*m*-pyridinium)), 8.41 (1H, s, CH(Im)), 9.13 (2H, d, *J* = 6.8 Hz, CH(*o*-pyridinium)).

^{13}C NMR (100.48 MHz, DMSO-d_6): δ 10.21 (CH_3), 34.2 (*N*-CH_3), 35.4 (*N*-CH_3), 47.8 (py *N*-CH_3), 125.1 (ImCH), 125.9 (py *m*-CH), 128.1 (*o*-CH), 141.4 (C), 146.2 (C), 148.9 (C).

Found: C, 31.53; N, 8.94; H, 4.07. Calc. for $C_{12}H_{17}N_3I_2$: C, 31.53; N, 8.94; H, 3.75.

Preparation of 1,2-dimethyl-4-bromo-5-(4-pyridine) imidazole 29

Imidazole **25** (1.35 g, 7.8 mmol) was dissolved in THF (20 mL) under an inert atmosphere. *N*-bromosuccinimide (1.38 g, 7.8 mmol) was added and the reaction was stirred for 18 hours. The brown precipitate was removed by filtration through celite, and the solvent removed by rotary evaporation to produce a golden brown oil. Water (25 mL) was added and the mixture stirred until the product precipitated as a white solid. This was collected and dried under vacuum. (1.42 g, 73 % yield). m.p. 117 °C.

^{1}H NMR (399.58 MHz, $CDCl_3$): δ 2.45 (3H, s, CH_3), 3.53 (3H, s, *N*-CH_3), 7.34 (2H, d, *J* = 6.0 Hz, CH(*m*-pyridine)), 8.71 (2H, d, *J* = 6.0 Hz, CH(*o*-pyridine)).

^{13}C NMR (100.48 MHz, $CDCl_3$): δ 13.8 (C-CH_3), 32.5 (*N*-CH_3), 114.8 (C-Br), 124.0 (*m*-CH), 137.0 (C), 146.9 (C), 150.1 (*o*-CH).

Found: C, 47.30; N, 16.45; H, 4.00. Calc. for $C_{10}H_{10}N_3Br$: C, 47.64; N, 16.67; H, 4.00.

Preparation of 1,2,3-trimethyl-4-bromo-5-(4-*N*-methylpyridinium) imidazolium 2[PF6]$^-$ 30

Imidazole **29** (0.252 g, 1.00 mmol) was dissolved in toluene (5 mL). An excess of dimethylsulfate (0.5 mL, 5.27 mmol) was added and the solution heated at 120 °C for 18 hours in a sealed pressure vessel. After cooling the toluene was decanted and the red-brown residue was dissolved in water (10 mL). Potassium hexafluorophosphate (2.00 g, 10.9 mmol) was added and the resulting off-white precipitate was collected by filtration, washed with additional water and dried *in vacuo* to produce **30** (1.119 g, 51 % yield). m.p. 278 °C.

^{1}H NMR (399.58 MHz, DMSO-d_6): δ 2.80 (3H, s, CH_3), 3.76 (3H, s, *N*-CH_3), 3.85 (3H, s, *N*-CH_3), 4.43 (3H, s, pyridine-*N*-CH_3) 8.33 (2H, d, *J* = 6.8 Hz, CH(*m*-pyridinium)), 9.19 (2H, d, *J* = 6.8 Hz,, CH(*o*-pyridinium)).

^{13}C NMR (100.48 MHz, DMSO-d_6): δ 11.1 (CH_3), 34.5 (*N*-CH_3), 34.6 (*N*-CH_3), 48.1(Py *N*-CH_3), 110.4 (Br-C), 127.1 (*p*-Py C), 128.1 (*m*-Py CH), 140.3 (C-5), 146.5 (*o*-Py CH), 148.8 (C-2).

Found: C, 25.16; N, 7.26; H, 2.81. Calc. for $C_{12}H_{16}N_3BrP_2F_{12}$: C, 25.19; N, 7.34; H, 2.82.

Preparation of palladium complexes by oxidative addition

General procedure

A Schlenk flask was loaded with imidazolium **30** and $Pd(dba)_2$, and dried *in vacuo* at 70 °C. Pyridine was added and the solution was heated at 75 °C for 1.5 hours. The appropriate ligand was added and the solution was heated for a further time. The solvent was removed *in vacuo* and the resultant green residue redissolved in acetonitrile, filtered through celite and removed *in vacuo* to obtain a yellow solid. This was washed with dichloromethane (2 x 10 mL, 2 x 5 mL) and the remaining solid dried to obtain the metal complexes **31-33**.

Preparation of [{1,2,3-trimethyl-5-(4-*N*-methylpyridinium)Im}PdBr(bipy)] 2[PF_6]$^-$ 31

From **30** (148.5 mg, 0.26 mmol) and $Pd(dba)_2$ (164.3 mg, 0.29 mmol) in 10 mL pyridine. Bipyridine (40.5 mg, 0.26 mmol) was added after 1.5 hours and the solution heated at 75 °C for an additional 30 minutes. The compound was treated as described in the general conditions, with complex **31** produced as a pale brown solid with crystals suitable for X-ray crystallography produced by slow diffusion of diethyl ether into a solution of **31** in THF (57.4 mg, 26% yield). m.p. 224 °C(dec).

^{1}H NMR (399.58 MHz, DMSO-d_6): δ 2.75 (3H, s, CH_3), 3.85 (3H, s, *N*-CH_3), 4.08 (3H, s, *N*-CH_3), 4.25 (3H, s, pyridine-*N*-CH_3), 7.55 (1H, m, bipy), 7.89 (2 x 1H, m, bipy), 8.33 (1H, t, *J* = 7.9 Hz, bipy), 8.39 (1H, t, *J* = 7.9 Hz, bipy) 8.59 (2 x 1H, d, *J* = 6.8 Hz, CH(*m*-pyridinium)), 8.67 (2 x 1H, bd, *J* = 7.4 Hz, bipy), 8.89 (2H, d, *J* = 7.2 Hz, CH(*o*-pyridinium)), 9.18 (1H, d, *J* = 6.8 Hz, bipy).

^{13}C NMR (100.48 MHz, DMSO-d_6): δ 10.9 (CH_3), 34.3 (*N*-CH_3), 38.4 (*N*-CH_3), 47.3 (pyridinium *N*-CH_3), 123.6 (bipy CH), 124.2 (bipy CH), 125.6 (*m*-pyridinium CH), 127.7 (bipy CH), 128.1 (bipy CH), 129.1(Im C5), 139.1 (C-Pd), 141.2 (bipy CH), 141.3 (bipy CH), 145.2 (*o*-pyridinium CH), 149.1 (bipy CH), 149.8 (Im C2), 151.1 (bipy CH), 155.0 (bipy C-C), 156.4 (bipy C-C).

Found: C, 31.85; N, 8.27; H, 2.91. Calc. for $C_{22}H_{24}N_5PdBrP_2F_{12}$: C, 31.66; N, 8.39; H, 2.90.

Preparation of [{1,2,3-trimethyl-5-(4-*N*-methylpyridinium)Im}PdBr$_2$(py)][PF$_6$]$^-$ 32a

From **30** (97.1 mg, 0.17 mmol) and Pd(dba)$_2$ (107.5 mg, 0.19 mmol) in 8 mL pyridine. Sodium bromide (502.9 mg, 4.89 mmol) was added after 1.5 hours and the solution heated at 75 °C for an additional hour. The compound was treated as described in the general conditions, with complex **32a** was produced as a yellow solid with crystals suitable for X-ray crystallography produced by slow diffusion of diethyl ether into a solution of **32a** in acetonitrile. (61.6 mg, 52 % yield). m.p. 241 °C(dec).

^{1}H NMR (399.58 MHz, DMSO-d_6): δ 2.69 (3H, s, CH_3), 3.80 (3H, s, *N*-CH_3), 4.19 (3H, s, *N*-CH_3), 4.34 (3H, s, pyridinium-*N*-CH_3), 7.52 (2H, t, *J* = 6.6 Hz, *m*-py), 7.96 (1H, t, *J* = 7.5 Hz, *p*-py), 8.87 (2H, d, *J* = 4.9 Hz, *o*-py), 8.94 (2H, d, *J* = 6.5 Hz, CH(*m*-pyridinium)), 9.03 (2H, d, *J* = 6.8 Hz, CH(*o*-pyridinium)).

^{13}C NMR (100.48 MHz, DMSO-d_6): δ 10.6 (CH_3), 34.3 (*N*-CH_3), 38.7 (*N*-CH_3), 47.1 (pyridinium-*N*-CH_3), 124.8 (py *m*-CH), 125.0 (pyridinium *m*-CH), 128.2 (Im-

C5), 136.0 (C-Pd), 138.5 (py *p*-CH), 144.6 (pyridinium *o*-CH), 146.0 (pyridinium-C), 148.1 (Im-C2), 152.0 (py *o*-CH).

Found: C, 29.44; N, 8.00; H, 2.80. Calc. for $C_{17}H_{21}N_4PdBr_2PF_6$: C, 29.48; N, 8.09; H, 3.06.

Preparation of [{1,2,3-trimethyl-5-(4-*N*-methylpyridinium)Im}PdI_2(py)][PF_6]$^-$ 32b

From **30** (103.3 mg, 0.18 mmol) and $Pd(dba)_2$ (135.5 mg, 0.23 mmol) in 8 mL pyridine. Sodium iodide (219.3 mg, 1.46 mmol) was added after 1.5 hours and the solution heated at 75 °C for an additional hour. The compound was treated as described in the general conditions with an additional final wash of water (2 x 10 mL) to remove any remaining sodium iodide, with complex **32b** produced as a yellow solid with crystals suitable for X-ray crystallography produced by slow diffusion of diethyl ether into a solution of **32b** in acetonitrile (31.9 mg, 22 % yield). m.p. 232 °C(dec).

^{1}H NMR (399.58 MHz, DMSO-d_6): δ 2.71 (3H, s, CH_3), 3.82 (3H, s, *N*-CH_3), 4.13 (3H, s, *N*-CH_3), 4.34 (3H, s, pyridinium-*N*-CH_3), 7.51 (2H, t, *J* = 6.2 Hz , *m*-py), 7.93 (1H, t, *J* = 6.2 Hz, *p*-py), 8.91 (4H, m, 2 x CH(*m*-pyridinium) , 2 x *o*-Py), 9.02 (2H, d, *J* = 5.8 Hz, CH(*o*-pyridinium)).

^{13}C NMR (100.48 MHz, DMSO-d_6): δ 10.7 (CH_3), 34.5 (*N*-CH_3), 39.7 (*N*-CH_3), 47.1 (pyridinium-*N*-CH_3), 124.6 (py *m*-CH), 124.7 (pyridinium *m*-CH), 128.6 (Im-C5), 133.1 (C-Pd), 138.3 (py *p*-CH), 144.4 (pyridinium *o*-CH), 146.1 (pyridinium-C), 148.4 (Im-C2), 153.1 (py *o*-CH).

Found: C, 26.30; N, 7.04; H, 2.63. Calc. for $C_{17}H_{21}N_4PdI_2PF_6$: C, 25.96; N, 7.12; H, 2.69.

Preparation of [{1,2,3-trimethyl-5-(4-*N*-methylpyridinium)Im}PdBr(PPh_3)$_2$)] 2[PF_6]$^-$ 33

A Schlenk flask was loaded with imidazolium **30** (62.7 mg, 0.11 mmol) and $Pd(dba)_2$ (69.1 mg, 0.12 mmol) and dried *in vacuo* at 70 °C. Pyridine (10 mL) was added and the solution was heated at 75 °C for 1.5 hours. The solvent was removed *in vacuo* and the resultant green residue redissolved in acetonitrile (5 mL), filtered through celite and removed *in vacuo* to obtain a yellow solid. This was washed with dichloromethane (2 x 10 mL, 2 x 5 mL) and the remaining solid was redissolved in acetonitrile (15 mL). Triphenylphosphine (100.7 mg, 0.38 mmol) was added and the solution heated for a further 1 hour at 80 °C. The acetonitrile was removed *in vacuo* and the resultant solid was washed with diethyl ether (2 x 15 mL) to remove excess triphenylphosphine. The remaining yellow product was dried and collected (42.0 mg, 32 % yield). Crystals of **33** suitable for X-ray diffraction were produced by slow evaporation of diethyl ether into a saturated acetonitrile solution. m.p. 236 °C(dec). Elemental microanalysis was not obtained due to inseparable co-crystallisation of an irregular amount of triphenylphosphine oxide.

^{1}H NMR (399.58 MHz, DMSO-d_6): δ 2.03 (3H, s, CH_3), 2.94 (3H, s, *N*-CH_3), 3.53 (3H, s, *N*-CH_3), 4.36 (3H, s, pyridinium-*N*-CH_3), 7.21-7.66 (30H, m, 6 x P-Ph), 8.12 (2H, d, *J* = 6.6 Hz, CH(*m*-pyridinium)), 8.86 (2H, d, *J* = 6.6 Hz, CH(*o*-pyridinium)).

^{13}C NMR (100.48 MHz, DMSO-d_6): δ 10.4 (CH_3), 34.4 (*N*-CH_3), 38.1 (*N*-CH_3), 47.1 (py *N*-CH_3), 124.5 (*m*-py CH), 127.9 (C-P), 128.3 (C-P), 128.6 (C-P), 128.7 (2 x *m*-Ph CH), 128.8 (*m*-Ph CH), 131.4 (*o*-Ph CH), 131.5 (*o*-Ph CH), 132.0 (*o*-Ph CH),

132.2 (C), 133.1 (*p*-Ph CH), 133.3 (*p*-Ph CH), 134.0 (*p*-Ph CH), 143.8 (C), 144.7(*o*-py CH), 148.5 (C), 150.0 (C, Pd-C overlapped).

^{31}P NMR (161.7 MHz, DMSO-d_6): δ -143.23 (quint, J = 711 Hz, PF_6), 20.08 (s, PPh_3), 26.45 (inseparable contaminant $OPPh_3$).

Preparation of 1-methyl-5-(4-pyridine) imidazole 34

This procedure is modified from literature.[20] A Schlenk flask was loaded with 4-bromopyridine hydrochloride (6.00 g, 30 mmol), potassium acetate (9.22 g, 93 mmol), 1-methylimidazole (6.00 g, 73 mmol) and palladium acetate (0.04 g, 0.17 mmol) and dried *in vacuo* at 70 °C. *N*,*N*-dimethylacetamide (50 mL) was added and the resulting mixture stirred at 150 °C for 2 days. The solvent was removed *in vacuo* and the resultant brown glass was redissolved with 40% aq. potassium hydroxide solution until pH > 9. This was extracted with dichloromethane (3 x 100 mL). The combined extracts were washed with water, dried over magnesium sulfate, filtered and the solvent removed *in vacuo* to obtain a brown solid. This solid was heated under vacuum to remove any residual 1-methylimidazole and collected once cooled as pure **34** which was spectroscopically identical to literature[33] (1.83 g, 37 % yield).

^{1}H NMR (399.58 MHz, $CDCl_3$): δ 3.76 (3H, s, *N*-CH_3), 7.27 (1H, s, CH), 7.31 (2H, d, J = 4.6 Hz, *m*-CH), 7.58 (1H, s, CH), 8.64 (2H, d, J = 4.4 Hz, *o*-CH).

Preparation of 1,3-dimethyl-5-(4-*N*-methylpyridinium) imidazolium diiodide 35

Imidazole **34** (0.637 g, 4.0 mmol) was dissolved in toluene (5 mL). An excess of methyl iodide (1 mL, 16 mmol) was added and the solution heated at reflux for 2.5 days in a sealed pressure vessel. The resulting yellow precipitate was collected

by filtration, washed with diethyl ether and dried *in vacuo* to produce **35** (1.2544 g, 71 % yield). m.p. 228 °C(dec).

^{1}H NMR (399.58 MHz, DMSO-d_6): δ 3.96 (3H, s, *N*-CH_3), 4.05 (3H, s, *N*-CH_3), 4.40 (3H, s, pyridine-*N*-CH_3) 8.39 (2H, d, *J* = 6.7 Hz, CH(*m*-pyridinium)), 8.52 (1H, s, CH), 9.15 (2H, d, *J* = 6.8 Hz, CH(*o*-pyridinium)), 9.40 (1H, s, CH).

^{13}C NMR (100.48 MHz, DMSO-d_6): δ 35.7 (*N*-CH_3), 36.3 (*N*-CH_3), 47.8 (py *N*-CH_3), 125.5 (py *m*-CH), 126.2 (Im C-4 CH), 129.1 (Im C5), 140.7 (Im C-2 CH), 140.8 (py *p*-C), 146.1 (py *o*-CH).

Found: C, 29.89; N, 9.41; H, 3.35. Calc. for $C_{11}H_{15}N_3I_2$: C, 29.82; N, 9.48; H, 3.41.

Preparation of [{1,3-dimethyl-5-(4-*N*-methylpyridinium)Im}PdI_3] 36

A Schlenk flask was loaded with imidazolium **35** (132.1 mg, 0.30 mmol), palladium iodide (107.5 mg, 0.30 mmol) and sodium acetate (25.8 mg, 0.31 mmol), and dried *in vacuo* at 70 ^{o}C. DMSO (5 mL) was added and the solution was heated at 50 °C for 4 hours. The solvent was removed *in vacuo* at elevated temperature and the red-brown residue redissolved in a 1:1 mixture of acetonitrile and water (25 mL each) and heated at 80 °C for 20 minutes. The mixture was placed under reduced pressure to remove the acetonitrile and the resultant red precipitate was collected by filtration and washed with additional water (10 mL). The product was dried *in vacuo* to produce a dark red solid which was pure **36** (114.0 mg, 57% yield). Crystals suitable for X-ray diffraction were produced by slow diffusion of diethyl ether into an acetonitrile solution. m.p. 283 °C(dec).

^{1}H NMR (399.58 MHz, DMSO-d_6): δ 3.89 (3H, s, *N*-CH_3), 4.10 (3H, s, *N*-CH_3), 4.33 (3H, s, pyridine-*N*-CH_3) 8.26 (2H, d, *J* = 6.8 Hz, CH(*m*-pyridinium)), 8.37 (1H, s, CH), 9.00 (2H, d, *J* = 6.8 Hz, CH(*o*-pyridinium)).

^{13}C NMR (100.48 MHz, DMSO-d_6): δ 38.1 (CH_3), 40.4 (CH_3), 47.3 (CH_3), 124.0 (CH), 128.3 (CH), 130.0 (C), 141.8 (C), 145.7 (CH), 149.2 (Pd-C).

Found: C, 19.02; N, 6.04; H, 1.92. Calc. for $C_{11}H_{14}N_3PdI_3$.(H_2O): C, 19.05; N, 6.06; H, 2.33.

5.5 References

[1] Sau, S. C.; Santra, S.; Sen, T. K.; Mandal, S. K.; Koley, D. *Chem. Commun.* **2012**, *48*, 555.

[2] Crabtree, R. H. *Coord. Chem. Rev.* **2013**, *257*, 755.

[3] Iglesias, M.; Albrecht, M. *Dalton Trans.* **2010**, *39*, 5213.

[4] Araki, S.; Wanibe, Y.; Uno, F.; Morikawa, A.; Yamamoto, K.; Chiba, K.; Butsugan, Y. *Chem. Ber.* **1993**, *126*, 1149.

[5] Gründemann, S.; Kovacevic, A.; Albrecht, M.; Faller Robert, J. W.; Crabtree, H. *Chem. Commun.* **2001**, 2274.

[6] Aldeco-Perez, E.; Rosenthal, A. J.; Donnadieu, B.; Parameswaran, P.; Frenking, G.; Bertrand, G. *Science* **2009**, *326*, 556.

[7] Heckenroth, M.; Kluser, E.; Neels, A.; Albrecht, M. *Angew. Chem. Int. Ed.* **2007**, *46*, 6293.

[8] Song, G.; Wang, X.; Li, Y.; Li, X. *Organometallics* **2008**, *27*, 1187.

[9] Eguillor, B.; Esteruelas, M. A.; Oliván, M.; Puerta, M. *Organometallics* **2008**, *27*, 445.

[10] Bernhammer, J. C.; Huynh, H. V. *Organometallics* **2012**, *31*, 5121.

[11] Chianese, A. R.; Zeglis, B. M.; Crabtree, R. H. *Chem. Commun.* **2004**, 2176.

[12] Han, Y.; Huynh, H. V.; Tan, G. K. *Organometallics* **2007**, *26*, 6581.

[13] Krüger, A.; Kluser, E.; Müller-Bunz, H.; Neels, A.; Albrecht, M. *Eur. J. Inorg. Chem.* **2012**, 1394.

[14] Huynh, H. V.; Han, Y.; Jothibasu, R.; Yang, J. A. *Organometallics* **2009**, *28*, 5395.

[15] Nelson, D. J.; Nolan, S. P. *Chem. Soc. Rev.* **2013**, *42*, 6723.

[16] Poulain, A.; Iglesias, M.; Albrecht, M. *Curr. Org. Chem.* **2011**, *15*, 3325.

[17] Xu, X.; Xu, B.; Li, Y.; Hong, S. H. *Organometallics* **2010**, *29*, 6343.

[18] Ke, C.-H.; Kuo, B.-C.; Nandi, D.; Lee, H. M. *Organometallics* **2013**, *32*, 4775.

[19] Ho, C. C. Structural and Mechanistic Investigations of Systematically Modified Bis(NHC) Palladium Complexes (PhD Thesis), University of Tasmania, Hobart, **2015**.

[20] Roger, J.; Doucet, H. *Tetrahedron* **2009**, *65*, 9772.

[21] Hahn, F. E.; Jahnke, M. C. *Angew. Chem. Int. Ed.* **2008**, *47*, 3122.

[22] John, A.; Modak, S.; Madasu, M.; Katari, M.; Ghosh, P. *Polyhedron* **2013**, *64*, 20.

[23] John, A.; Shaikh, M. M.; Ghosh, P. *Dalton Trans.* **2009**, 10581.

[24] Markies, B. A.; Canty, A. J.; Graaf, W. d.; Boersma, J.; Janssen, M. D.; Hogerheide, M. P.; Smeets, W. J. J.; Spek, A. L.; Koten, G. v. *J. Organomet. Chem.* **1994**, *482*, 191.

[25] Vicente, J.; Abad, J.-A.; Martínez-Viviente, E.; Ramírez de Arellano, M. C.; Jones, P. G. *Organometallics* **2000**, *19*, 752.

[26] Vicente, J.; Abad, J.-A.; Martínez-Viviente, E.; Jones, P. G. *Organometallics* **2002**, *21*, 4454.

[27] Pauling, L., in *The Nature of the Chemical Bond, third ed., Vol.* Cornell University Press, Ithaca, NY, **1960**, pp. 224-228, 256-258.

[28] Rettig, M. F.; Maitlis, P. M.; Cotton, F. A.; Webb, T. R. *Inorg. Synth.* **2007**, *17*, 134.

[29] Cowieson, N. P.; Aragao, D.; Clift, M.; Ericsson, D. J.; Gee, C.; Harrop, S. J.; Mudie, N.; Panjikar, S.; Price, J. R.; Riboldi-Tunnicliffe, A.; Williamson, R.; Caradoc-Davies, T. *J. Synchrotron Radiat.* **2015**, *22*, 187.

[30] Sheldrick, G. M., *SHELX97*, Programs for Crystal Structure Analysis, Universität Göttingen, Germany, **1998**.

[31] Barbour, L. J. *J. Supramol. Chem.* **2001**, *1*, 189.

[32] Dolomanov, O. V.; Bourhis, L. J.; Gildea, R. J.; Howard, J. A. K.; Puschmann, H. *J. Appl. Cryst.* **2009**, *42*, 339.

[33] Seerden, J.-P. G.; Leusink-Ionescu, G.; Leguijt, R.; Saccavini, C.; Gelens, E.; Dros, B.; Woudenberg-Vrenken, T.; Molema, G.; Kamps, J. A. A. M.; Kellogg, R. M. *Bioorg. Med. Chem. Lett.* **2014**, *24*, 1352.

Chapter 6: Conclusions

6.1 General Summary

This research project has incorporated a number of investigations into palladium complexes bearing NHC ligands.

In Chapter 2 the possible solid state hydride dynamics of a lattice THF solvated dipalladium(I) hydride complex [μ-{$(MesIm)_2CH_2$}$_2$$Pd_2H$][$PF_6$] **5a** were examined by two neutron techniques. IINS was employed alongside DFT-MD simulations to examine the barrier for hydride migration across the Pd-Pd bond. To enhance identification of the normal modes of vibration attributed to the hydride, chemical deuteration of the ligand system was undertaken in collaboration with the NDF to produce isotopomers of **5a**, [μ-{$(^{D}MesIm)_2CD_2$}$_2$$Pd_2H$][$PF_6$] **5b** and [μ-{$(^{D}MesIm)_2CD_2$}$_2$$Pd_2D$][$PF_6$] **5c**. Neutron scattering experiments were undertaken on these deuterated isotopomers and the experimental spectra were used to validate the MD model of the simulation of the hydride transfer, where the hydride was shown to display an unexpectedly high degree of anharmonicity.

Single crystal Laue neutron diffraction studies on the lattice unsolvated form of **5a** indicated that there was no observed hydride migration or alteration in the metal-metal interactions in the complex over a range of 100-300 K. Agostic and anagostic interactions between the non-hydridic palladium centre and spatially adjacent ligand methyl and methylene protons appeared to influence the complex against any hydride transfer in this form.

Single crystal Laue neutron diffraction studies were also undertaken for complete structural characterisation of an extended linker analogue of **5a**, the propylene-linked bis(NHC) dipalladium(I) hydride complex [μ-{$(MesIm)_2(CH_2)_3$}$_2$$Pd_2H$][$PF_6$] **7**, and on a trapped intermediate formed during the preparation of **7**, the dinuclear tris(NHC) palladium(II) hydride complex [μ-{$(MesIm)_2(CH_2)_3$}{$(PdH)(MesIm)_2(CH_2)_3$}$_2$][PF_6]$_2$ **8**. Complex **7** was observed to have similar agostic and anagostic interactions between the non-hydridic palladium centre and ligand methyl and methylene protons to that of **5a** and a decreased Pd-Pd bond length enabled by increased ligand flexibility. There were no indications of hydride dynamics in **7**.

A study on the *N*-*t*-butyl pendant imidazolium mono(NHC) palladium(II) dihalide acetate intermediates formed in the synthesis of chelated bis(NHC) palladium(II) dihalide species was described in Chapter 3. Alterations to the halide and to the basicity of the acetate group were made to form complexes [{(tBuIm)(tBuImH)CH_2}PdX_2CO_2R] **11a-f**, and the effect on the hydrogen bonding was examined in solution (^{1}H NMR spectroscopy) and in the solid state (single crystal X-ray and neutron crystallography). A trend was observed in solution consistent with expected halide size and acetate basicity, however no obvious trend was observed in the solid state. The methylene-linked *N*-mesityl pendant imidazolum mono(NHC) palladium(II) trihalide complexes [{(MesIm)(MesImH)CH_2}PdX_3] **12a-b** were prepared and the pendant imidazolium mono(NHC) palladium(II) dibromide trifluoroacetate complex [{(MesIm)(MesImH)CH_2}$PdBr_2CF_3$] **13** was obtained and structurally characterised for comparison of hydrogen bonding to the less bulky *N*-*t*-butyl substituent analogues. The ethylene-linked *N*-mesityl pendant imidazolium mono(NHC) palladium(II) dibromide acetate complex

[{(MesIm)(MesImH)C_2H_4}$PdBr_2CO_2CH_3$] **15** was observed *in situ* by ^{1}H NMR spectroscopy, though has not yet been isolated.

Chapter 4 describes the preparation of the *N*-mesityl diimidazolinium dibromide salt [(^{S}MesIm)$_2CH_2$]Br_2 **17a**, and the bis(NHC) palladium(II) dibromide and bis(acetonitrile) complexes [{(^{S}MesIm)$_2CH_2$}$PdBr_2$] **18a** and [{(^{S}MesIm)$_2CH_2$}$Pd(NCMe)_2$][PF_6]$_2$ **20a**, respectively. Complex **20a** was tested for catalytic activity in the copolymerisation of carbon monoxide and ethylene, under conditions identical to those reported for the unsaturated analogue, though was found to have less activity for this reaction than the previously reported unsaturated species. This was potentially due to increased reactivity of the saturated complex **20a** towards decomposition products such as dipalladium(I) hydride species, in comparison to the unsaturated analogue **4a**, though we have not yet isolated any saturated bis(NHC) palladium hydride complexes.

Extended linker bis(imidazolinium) salts containing ethylene and propylene alkyl linkers (**17b-c**) were also prepared, though attempted conversion to the bis(NHC) palladium(II) dibromide complexes proceeded only to the formation of the pendant imidazolinium mono(NHC) palladium(II) tribromide species [{(^{S}MesIm)(^{S}MesImH)$(CH_2)_n$}$PdBr_3$] **22b-22c**. The bis(NHC) disilver(I) complexes [{(^{S}MesIm)$_2(CH_2)_n$}$_2Ag_2$][PF_6]$_2$ **23a** and **23c** were prepared, though transmetallation reactions with PdBrMe(COD) to form chelated bis(NHC) palladium(II) bromomethyl complexes were unsuccessful. Attempts to prepare an asymmetrically substituted diimidazolium/inium salt *via* various imidazolium/inium haloalkyl halide salts were also unsuccessful.

The preparation of an unusual aNHC ligand precursor 1,2,3-trimethyl-5-(4-*N*-methylpyridinium)imidazolium diiodide **28**, which contained a substituent with high electron withdrawing ability, was discussed in Chapter 5. This arrangement was designed to allow conjugation between the ligand carbene and pyridinium rings, assuming ring coplanarity. Synthesis of a series of aNHC metal complexes [{1,2,3-trimethyl-5-(4-*N*-methylpyridinium)Im}PdL_n][PF_6]$_y$ **31-33** was achieved by oxidative addition of the brominated ligand precursor 1,2,3-trimethyl-4-bromo-5-(*N*-methylpyridinium)imidazolium [PF_6]$_2$ **30** to $Pd(dba)_2$. Structural characterisation revealed that though steric interference from the carbene *N*-methyl, and from the various ancillary ligands employed to fill the palladium coordination plane prevented the desired coplanar ring conjugation arrangement from occurring. Comparison of key C-C bond lengths in these complexes was consistent with this observation. Comparison of the trends in ^{13}C NMR spectroscopic shifts to pendant imidazolium mono(NHC) complexes did suggest that the electron withdrawing substituent did have some effect on the ligand electronics.

6.2 Future Outlooks

In this project we have used Laue single crystal neutron diffraction to determine the location of hydride ligands in several palladium hydride complexes. Future efforts may involve using this technique to investigate other palladium hydride complexes which have been obtained in our group such as the *N*,*N*′-asymmetrically substituted dipalladium(I) hydride complex [μ-{(MesIm)[2,6-(*i*-Pr)$_2$PhIm]CH_2}$_2$$Pd_2H$][$PF_6$] and the tetranuclear palladium hydride cluster currently posited to have the formula [μ-{(MesIm)C_2H_4}$_3$$Pd_4H_2$][$PF_6$]$_2$.

Further studies may also be warranted on the pendant imidazolium mono(NHC) palladium(II) dihalide acetate complexes discussed in Chapter 3. We have yet been unable to prepare samples of most of the *N*-*t*-butyl complexes suitable for Laue single crystal neutron diffraction studies. Future efforts may involve alterations to the recrystallisation methods employed, or the use of alternative acetate substituents to provide suitable crystals for further examination of hydrogen bonding between the pendant imidazolium C-2 proton and the acetate ligand.

We also hope to isolate the *N*-mesityl ethylene-linked pendant imidazolium mono(NHC) palladium(II) dihalide acetate complex [{(MesIm)(MesImH)$(CH_2)_2$}$PdBr_2CO_2CH_3$] **15** for structural characterisation by X-ray crystallography. This complex would provide evidence consistent with proposed DFT mechanistic studies into the reaction pathways of this ligand system with palladium, potentially allowing better control of this reaction pathway and providing increased scope for ligand modifications for this class of bis(NHC) complexes.

Our initial investigations in the novel area of saturated chelated bis(NHC) palladium(II) complexes have potential scope for further inquiry. A preliminary catalysis study using [{(^{S}MesIm)$_2CH_2$}$Pd(NCMe)_2][PF_6]_2$ **20a** to promote the copolymerisation of ethylene and carbon monoxide was undertaken. Avenues which may be explored include repetitions and modification of this catalytic procedure and examination of other potential applications such as C-C cross-coupling reactions. Structural modifications of the complex motif such as variation of the *N*-substituents and variation of the alkyl linker group may also be pursued. Further investigation into the reactivity of complex **20a** under basic conditions towards the formation of

an analogous dipalladium(I) hydride species [{μ-(^{S}MesIm)$_2$CH$_2$}$_2$Pd$_2$H][PF$_6$] **21a** is also warranted.

The synthesis of the aNHC palladium(II) complexes [{1,2,3-trimethyl-5-(*N*-methylpyridinium)Im}PdL$_n$][PF$_6$]$_y$ **33-35** was successful, however the complexes did not display the desired ligand biaryl conjugation that we hypothesised. Modification to this ligand motif to maximise NHC and pyridine ring coplanarity is an ongoing effort in our group. Investigation into the catalytic activity of these aNHC palladium(II) complexes may also be pursued.